MIT - 2073-5
(MITNE - 77)

A GENERALIZED STUDY OF THE BREEDING POTENTIAL OF LARGE HEAVY WATER MODERATED POWER REACTORS FUELED WITH THORIA AND URANIA

MAX C. RICHARDSON
MANSON BENEDICT
EDWARD A. MASON

JANUARY 1967

DEPARTMENT OF NUCLEAR ENGINEERING
MASSACHUSETTS INSTITUTE OF TECHNOLOGY
CAMBRIDGE, MASSACHUSETTS, 02139

FOR THE
U.S. ATOMIC ENERGY COMMISSION
UNDER CONTRACT AT(30-1)-2073

MIT-2073-5
MITNE-77

MASSACHUSETTS INSTITUTE OF TECHNOLOGY

DEPARTMENT OF NUCLEAR ENGINEERING

Cambridge, Massachusetts 02139

A GENERALIZED STUDY OF THE BREEDING POTENTIAL OF LARGE HEAVY WATER MODERATED POWER REACTORS FUELED WITH THORIA AND URANIA

by

M. C. Richardson, M. Benedict and E. A. Mason

January, 1967

CONTRACT AT(30-1)-2073

U. S. Atomic Energy Commission

ACKNOWLEDGMENTS

This report is based largely on a thesis of the same title submitted by Mr. Max C. Richardson in partial fulfillment of the requirements for the degree of Doctor of Philosophy in Nuclear Engineering at Massachusetts Institute of Technology. Supplementary calculations were made by Richard J. Weader. All calculations were performed at the MIT Computation Center.

Financial support from the U.S. Atomic Energy Commission under Contract AT(30-1)-2073 and in the form of Mr. Richardson's AEC Fellowship is gratefully acknowledged.

The authors wish to thank the following men for furnishing nuclear data used in the course of this work: Dr. H. B. Stewart of General Atomic, Dr. W. H. Walker of the Chalk River Laboratory of Atomic Energy of Canada Ltd., Dr. W. A. Wittkopf of Babcock and Wilcox, and Mr. E. H. Gift of Oak Ridge National Laboratory.

TABLE OF CONTENTS

TABLE OF CONTENTS

APPENDICES

LIST OF FIGURES

LIST OF TABLES

A GENERALIZED STUDY OF THE BREEDING POTENTIAL OF LARGE HEAVY WATER MODERATED POWER REACTORS FUELED WITH THORIA AND URANIA

BY

M. C. Richardson, M. Benedict and E. A. Mason

I. ABSTRACT

This report presents a generalized study of the conversion ratio obtainable in large D_2O moderated power reactors fueled with ThO_2 and UO_2. From the results of this report, it is possible to estimate the conversion ratios of other reactors having any combination of values of seven principal design variables. The main objective of this work has been to find the range of design variables for a large, thermal, heterogeneous reactor in which breeding is possible.

The adjective "generalized" means that many design details, such as fuel bundle design, have been disregarded so that the effect on the conversion ratio of wide ranges of design variables with greater effect on conversion ratio can be studied. The Th232-U233 system is studied because U233 has the highest value of η of any of the fissile nuclides in the thermal neutron energy range. Moderation by D_2O is studied because of the low thermal absorption cross section of ^2D_2O. Large power reactors of the size suggested by the work on the desalination of sea water are studied.

The following reactor characteristics are fixed throughout this study: core height/core radius of 1.845; radial and axial blankets of two foot thickness; continuous steady state bidirectional fueling with recycle in the core and without recycle in the blankets; reactor lattice consisting of uniformly spaced zircaloy clad cylindrical rods surrounded by D_2O moderator.

The seven variables whose effects on the conversion ratio are studied are as follows:

Primary variables

Feed burnup, megawatt days/metric tonne of uranium plus thorium fed
Volume of moderator/volume of fuel
Fuel rod diameter

The effect on the conversion ratio of changing the primary variables is determined by direct calculation.

Secondary variables

Average specific thermal power in the core, kw/kg fissile
Volume of zircaloy/volume of fuel
Fraction of core and blanket discharge lost in reprocessing
Total thermal power in the core

The values of volume of moderator/volume of fuel and fuel rod diameter which give nearly the maximum conversion ratio for each feed burnup are selected. Each of the secondary variables is then varied independently of the others to determine its effects on the conversion ratio and the components of the conversion ratio. The behavior of the conversion ratio and its components in these cases can then be used to estimate the changes in the conversion ratio and its components with changing values of the secondary variables starting with other values of the primary variables.

The neutron behavior model used is two-energy-group diffusion theory in two dimensions of cylindrical coordinates and in two regions. This model is similar to that used in other MIT fuel cycle studies.

Highest values of the conversion ratio were found at the lowest burnup studied (10,000 mwd/t), the smallest rod diameter (0.1 inch), the lowest average specific power (1000 kw/kg fissile), the lowest zircaloy to fissile absorption ratio (zero), the lowest reprocessing loss (zero) and the largest power (8333 MW(th)). The conversion ratio had a maximum value of about 1.13 at a moderator to fuel volume ratio of about 30. Such a reactor would not be practical.

Detailed discussions are given of the way each variable affects the neutron balance and the conversion ratio, and approximate procedures are developed from which estimates can be made of the conversion ratio for other combinations of the seven principal design variables than those for which calculations were made in this report.

One such estimate was made of the conversion ratio of a practical reactor similar to the CANDU reactor with thorium fuel. This reactor had a burnup of 20,000 mwd/t, a moderator to fuel volume ratio of 20, a rod diameter of 1 inch, an average specific power of 3000 kw/kg fissile, a zircaloy to fissile absorption ratio of 0.05, and a reprocessing loss of 2% of the fuel discharged from the reactor. The conversion ratio was estimated to be about 0.95. The conversion ratio does not vary appreciably with total power, in the range 500 to 8333 MW(th), because of the blanket 2 feet thick assumed.

Another estimate of the conversion ratio was made for a second practical reactor with the seven design variables set at values found by Oak Ridge National Laboratory to be near those leading to minimum power cost. At a burnup of 28,800 Mwd/t, a moderator to fuel volume ratio of 16.6, a rod diameter of 1 inch, an average specific power of 2700 kw/kg fissile, a zircaloy to fissile absorption ratio of 0.07, a neutron leakage to fissile absorption ratio of 0.025 and zero reprocessing loss, a conversion ratio of 0.8476 was found by computer calculation. This may be compared with Oak Ridge's value of 0.8255 for a similar reactor and with estimates of 0.87-0.88 obtained by the approximate procedures developed in this report.

CHAPTER II

INTRODUCTION

A. Motivation

The interest in thermal reactors with high conversion ratios is well established (C2, D1, R1). One type of thermal reactor whose technology is well developed which has a good prospect of breeding is a heterogeneous reactor moderated by heavy water and operating on the thorium-uranium 233 fuel cycle. The object of this report is to present calculations of the conversion ratios obtainable in this type of reactor for a number of combinations of seven principal design variables and to present means for estimating conversion ratios for other combinations of these variables.

This study is a generalized one, in the sense that consideration of many design details with only a minor effect on conversion ratio, such as fuel bundle details, have been subordinated to variables with greater effect. Some unrealistic values of these more important variables are studied to determine just how high a conversion ratio can be obtained with the reactor type under consideration. No consideration is given to cost or feasibility of the reactor system.

The Th232-U233 system is studied because U233 has the highest value of η, the number of fast neutrons produced per absorption is a fissile nucleus, of any of the fissile nuclides in the thermal neutron energy range. Moderation by D_2O is studied because D_2O has the smallest thermal absorption cross section of the moderators normally considered. Large, 8333 thermal megawatt power reactors are studied because it was expected that large reactors would have the highest conversion ratio and this size has been suggested for the desalination of sea water (B3).

B. Fixed reactor characteristics

The following reactor characteristics are fixed throughout this work:

1. The ratio core height/core radius is held constant at 1.845. This corresponds to the minimum critical volume for a finite cylinder (G4). The core volume is adjusted to give the desired total thermal power.

2. The reactor lattice consists of a cylindrical rod of mixed UO_2-ThO_2 fuel surrounded by a zircaloy sheath and D_2O moderator. The zircaloy sheath represents the effect of the cladding and any other zircaloy structural material that might be used in a practical reactor.

3. Radial and axial blankets of two foot thickness are used throughout this study. The volume of moderator/volume of fuel in the blankets is the same as in the core and the blanket feed is pure ThO_2. The blanket discharge is irradiated to a given thermal flux time.

4. The fueling technique used in both the core and blanket is continuous steady state bidirectional fuel movement. The fuel is moved axially in opposite directions in adjacent channels at a velocity such that the reactor is just critical without control poison. This procedure is similar to the fueling technique used in the CANDU reactor (A2, H2, S3). The fuel in the core travels at a radially uniform axial velocity and is irradiated to a given average burnup. The steady state condition is that in which the composition of the core feed does not change with time and the composition of the core discharge does not change with time. If the conversion ratio of the system is greater than 1.0, only that fraction of the reprocessed core discharge necessary to maintain criticality is recycled into the core feed. If the conversion ratio is less than 1.0,

the entire reprocessed core discharge is recycled into the feed and pure U235 is added as makeup. The entire reprocessed discharge from the blanket is recycled into the core feed at all times. The radial blanket discharge is irradiated to a thermal flux time of 0.05 n/kb and the axial blanket discharge is irradiated to a thermal flux time of 0.001 n/kb.

C. Variables

1. Primary variables

The effect on conversion ratio of a number of combinations of the three following primary variables was first calculated, with results described in chapter V:

a. Feed burnup, megawatt days/metric tonne of uranium plus thorium fed.
b. Volume of moderator/volume of fuel
c. Fuel rod diameter

2. Secondary variables

The values of volume of moderator/volume of fuel and fuel rod diameter which gave nearly the maximum conversion ratio for each feed burnup were selected. Each of the following secondary variables was then varied independently to determine its effect on the conversion ratio and the components of the conversion ratio, with results described in chapter VI:

a. Average specific thermal power in the core, kw/kg fissile
b. Volume of zircaloy cladding and structural material/volume of fuel
c. Fraction of core and blanket discharge lost in reprocessing
d. Total thermal power in the core or geometric buckling

In chapter VII approximate procedures are described for using the detailed calculations of the conversion ratio and its components in

chapters V and VI to estimate the effect of changing several secondary variables together or starting from values of the primary variables other than those used in chapter VI. With these procedures, values of the conversion ratio can be estimated for all possible combinations of the seven primary and secondary variables, within the ranges studied.

D. Nuclear model

The neutron behavior model used in this work is two-energy-group diffusion theory applied in the r-z directions of cylindrical coordinates in a maximum of three regions. This nuclear model is basically the same as that used in other MIT fuel cycle studies (M3). The basic computer code used is due to Hofmann (H2, S3) although extensive improvements have been made in the course of this work.

E. Improvements over other MIT fuel cycle codes

The following improvements over other MIT fuel cycle codes have been made in this work:

1. More recent thermal absorption and resonance absorption data are used (G1, G2, G3).

2. The theory of equivalence between homogeneous and heterogeneous effective resonance integrals is used (D2).

3. More recent nonsaturating fission product data are used, and the variation of the microscopic absorption cross section of the nonsaturating fission products with the Westcott r factor is considered (W1, W2).

4. Both axial and radial blankets are considered. The code is equipped to also consider both axial and radial reflectors.

5. The two-energy-group diffusion equations are solved directly for the fluxes rather than by eliminating the fast flux between the two equations and then solving the resulting equation for the thermal flux as was done in previous MIT fuel cycle codes. This makes the calculational procedure used here more stable than previous MIT fuel cycle codes, but slower.

6. Neutron balances are calculated for the reactors in their steady state conditions.

CHAPTER III

SUMMARY OF PRINCIPAL RESULTS

A. Definitions of the conversion ratio

In this thesis, two conversion ratios are considered. These are the internal conversion ratio and the conversion ratio with reprocessing loss. The internal conversion ratio can be defined in three ways, all of which are equivalent. Each definition is discussed in detail below.

(1) The first definition of the conversion ratio is given by equation (3A1), with reference to figure 3.1A:

$$CR_L = \frac{\text{Total fissile atom source}}{\text{Total fissile atom sink}} = \frac{Q_R}{S_R + B \cdot O_R} \qquad (3A1)$$

where

CR_L = conversion ratio with reprocessing loss

Q_R = source of fissile atoms in the reactor

S_R = sink of fissile atoms in the reactor

O_R = fissile atoms leaving the reactor

B = fraction of reactor discharge which is lost in reprocessing and fabrication

and in figure 3.1A

I_R = fissile atoms entering the reactor

The internal conversion ratio is obtained by deleting from equation (3A1) the contribution to the total fissile atom sink of the reprocessing loss:

$$CR_o = \frac{Q_R}{S_R} \qquad (3A2)$$

where

CR_o = internal conversion ratio

The conversion ratio considered from the point of view described in this paragraph is used in this work only in calculating the conversion ratio with reprocessing loss with equation (3A1).

(2) The second definition of the internal conversion ratio is given by equation (3A3):

$$CR_o = \left\{[(\bar{\eta})] - [(1) + (PAPL) + (D_2O) + (Zr) + (Pa233)]\right\} - \left\{(Pa233)\right\} \qquad (3A3)$$

where

$(\bar{\eta})$ = number of fast neutrons produced by fission per absorption (resonance plus thermal) in a fissile nucleus (U233 plus U235).

(1) = absorption (resonance plus thermal) in a fissile nucleus (U233 plus U235) required to maintain the chain reaction.

(PAPL) = Parasitic Absorptions Plus Leakage per fissile absorption. The parasitic absorbers included in (PAPL) are U236, Np237, Xe135, the "Sm" group and nonsaturating fission products. The leakages are overall fast and thermal leakages from the reactor.

(D_2O) = absorption in heavy water per fissile absorption.

(Zr) = absorption in zircaloy (or other structural materials) per fissile absorption.

(Pa233) = absorption in Pa233 per fissile absorption.

It is seen that the quantities in the second set of brackets, i.e., $[(1) + \cdots\cdots\cdots]$, include the overall leakages and absorptions in all nuclides in the reactor other than the fertile nuclides, Th232 and U234. Therefore, when this quantity is subtracted from $\bar{\eta}$, the total number of fast neutrons per fissile absorption with which one has to work, the result is the number of neutrons which are left to be absorbed by Th232 and U234. In other words this is the number of atoms of Pa233 and U235 formed per fissile absorption. Since each neutron absorbed in Pa233 results in an atom of Pa233 which is not allowed to decay to U233, the quantity (Pa233) must be subtracted a second time, as is done in equation (3A3). The result is the internal conversion ratio CR_o or the number of fissile atoms produced per absorption in a fissile atom. All of the values of the internal conversion ratio presented in this work were calculated with equation (3A3).

(3) The third definition of the internal conversion ratio is given by equation (3A4):

$$CR_o = \{[(Th232) + (U234)]\} - \{(Pa233)\} \qquad (3A4)$$

where

(Th232) = absorption in Th232 per fissile absorption.

(U234) = absorption in U234 per fissile absorption.

The first quantity in braces, i.e., $\{[(Th232)+(U234)]\}$, gives directly the number of absorptions in fertile material per fissile absorption or the number of atoms of Pa233 and U235 which are formed per fissile absorption. The quantity (Pa233) must be subtracted, as is done in equation

(3A4), to account for Pa233 atoms which, due to neutron absorptions, do not decay to U233. Once again, the result is the internal conversion ratio CR_o or the number of fissile atoms produced per absorption in a fissile atom.

In each of the three definitions of CR_o given above, it is seen that all Pa233 atoms which do not absorb neutrons are assumed to decay to U233 and are included in the production rate of fissile atoms. This condition is approached if the discharged fuel undergoes a long cooling period.

B. Primary Variables

1. Introduction

In section IIIB, the effects of the three primary variables on the conversion ratio are summarized. The primary variables are feed burnup (megawatt days/metric tonne of metal feed), volume of moderator/volume of fuel and fuel rod diameter. Throughout section IIIB, the secondary variables are held constant at the following values:

Volume zircaloy/volume fuel	0
Average specific power in core	1000 kw/kg fissile
Total thermal power in core	8333 MW(th)
Reprocessing loss	0

(It should be noted that a fixed average specific power and a fixed total thermal power dictate a fixed mass of fissile material in the reactor cores, viz. 8333 kg in this case.) The values of the feed burnup studied were 10,000, 20,000 and 30,000 mwd/t. The values of the volume of moderator/volume of fuel studied covered the ranges in which were found the

maximum conversion ratios for each fuel rod diameter at each feed burnup. The fuel rod diameters were decreased from a value of two inches in the anticipation that maximum conversion ratios would be found as a function of this parameter for each feed burnup. However, the maximum conversion ratio as a function of fuel rod diameter continued to increase as the rod diameter decreased, without a maximum conversion ratio for each feed burnup being found, as will be discussed.

The feed burnup affects the conversion ratio primarily through absorptions in nonsaturating fission products. The effect of the volume of moderator/volume of fuel is primarily through spectrum effects and moderator absorptions. By inspection of equation (3A3), it is therefore seen that the direct effect on the conversion ratio of these two primary variables is principally through their effect on $\bar{\eta}$ and absorptions in nuclides other than the fertile nuclides.

As the fuel rod diameter is decreased, the effective resonance integral of ThO_2 can increase on the order of 100%. This results in a large increase in the absorption of resonance neutrons by Th232. By inspection of equation (3A4), it is therefore seen that the direct effect on the conversion ratio of the fuel rod diameter is principally through its effect on the absorptions by a fertile nuclide itself, i.e., Th232.

All of the neutron balance results in the figures and tables of this chapter are normalized to one absorption (thermal plus resonance) in a fissile nuclide. As a result of this normalization, it is essential to keep in mind the relative fractions of resonance and thermal reactions when interpreting the results. The smaller the fuel rod diameter, the larger will be the effective resonance integral of any fuel nuclide, provided that its concentration change with decreasing fuel rod diameter is

small, as is usually the case. Therefore, the smaller the fuel rod diameter, the larger will be the fraction of resonance absorption in a fissile nucleus per total absorption in a fissile nucleus. As a result, those nuclides which are predominantly thermal absorbers, particularly the non-saturating fission products, are less effective poisons in small diameter rods with their increased fraction of resonance absorptions.

All of the conversion ratios presented in this work are calculated by equation (3A3). The internal conversion ratio is usually referred to in this work simply as the conversion ratio. The internal conversion ratios for the 32 combinations of the three primary variables studied in this work are listed in table 3.1.

2. Conversion ratio and its components for 20,000 mwd/t burnup

The conversion ratio and its components for a feed burnup of 20,000 mwd/t are shown in figure 3.1 as a function of volume of moderator/volume of fuel with fuel rod diameter as a parameter. A value of the conversion ratio is obtained by subtracting from a value of $(\bar{\eta}-1)$ the sum of parasitic absorptions plus leakage, D_2O absorption and 2 x Pa233 absorption, i.e., by use of equation (3A3).

The values of η, the number of fast neutrons produced by fission per absorption in a fissile nucleus, for the fissile nuclides vary approximately with neutron energy as follows:

Nuclide	2200 m/s	Resonance Region
U233	2.29	2.14
U235	2.06	1.59

The value of $(\bar{\eta}-1)$ in figure 3.1 increases with increasing volume of moderator/volume of fuel because the fraction of fissile absorptions

which occur in the resonance region, where the values of η are lower, is reduced. Also, as the conversion ratio increases with increasing volume of moderator/volume of fuel, the mass in the reactor of U233, with its higher values of η, increases and the mass of U235 decreases.

The D_2O absorptions increase with increasing volume of moderator/volume of fuel, of course, because of the added volume of D_2O. The values are higher and have steeper slopes for the larger rods because the greater depression of the thermal flux produces a higher relative thermal flux in the moderator region of the unit cells with the larger rods.

The Pa233 absorptions decrease with increasing volume of moderator/volume of fuel because of the decrease in resonance absorption by Pa233.

The curves of parasitic absorptions plus leakage do not vary greatly with increasing volume of moderator/volume of fuel. The curves for the smaller rods are lower primarily because of the decreased absorption in nonsaturating fission products. As mentioned previously, this is due in part to the increased reliance on resonance reactions of the smaller rods. In addition, the large increase in resonance absorption by Th232 with decreasing fuel rod diameter mentioned previously causes a decrease with decreasing fuel rod diameter of the number of neutrons slowed down to thermal energy per absorption in a fissile nucleus. This latter result causes the absorption by nonsaturating fission products to decrease with decreasing fuel rod diameter because the nonsaturating fission products are principally absorbers of thermal neutrons.

The conversion ratio curves initially increase with increasing volume of moderator/volume of fuel because of the increase in $(\bar{\eta}-1)$ and the decrease in Pa233 resonance absorptions. Eventually, however, these lat-

ter two items tend to level out while the D_2O absorptions continue to increase with increasing volume of moderator/volume of fuel. The conversion ratio curves thus reach maximum values. The curves for the larger rods reach peaks at lower values of volume of moderator/volume of fuel and the peaks are more pronounced because of the steeper slopes of their D_2O absorption curves.

The effect on the conversion ratio of decreasing the fuel rod diameter is interpreted with the use of equation (3A4). A decrease in the fuel rod diameter causes an increase in the effective resonance integral of ThO_2 of the order of 100%. This results in a large increase in the absorption of resonance neutrons by Th232. Therefore, the direct effect on the conversion ratio of decreasing the fuel rod diameter is to increase the absorptions by the fertile material Th232, a quantity which is included directly in equation (3A4). The indirect effect on the conversion ratio of decreasing the fuel rod diameter is reflected in equation (3A3) and, therefore, in figure 3.1. Because of the increased resonance absorption in Th232 with decreased fuel rod diameter, the number of neutrons slowed down to thermal energy per fissile absorption is reduced. Therefore, the number of thermal neutrons available for absorption in nonsaturating fission products is reduced. This is shown in figure 3.1 by the decrease in parasitic absorptions plus leakage with decreasing fuel rod diameter. The decrease in the number of neutrons slowed down to thermal energy per fissile absorption also causes the D_2O absorptions to decrease with decreasing fuel rod diameter. The D_2O absorptions also decrease with decreasing fuel rod diameter because of the decreasing thermal flux peak in the moderator of the unit cell.

Two other notes on the effect of decreasing the fuel rod diameter are as follows:

(1) The effective resonance integrals of the fuel nuclides other than Th232 are large in any case because these nuclides are very dilute. Therefore, decreasing the fuel rod diameter does not increase these effective resonance integrals by large percentages, as compared to the percentage increase in the effective resonance integral of Th232.

(2) Since a homogeneous system has higher Th232 effective resonance integrals than a heterogeneous system, the maximum conversion ratio which could appear in figure 3.1 would be for a homogeneous system.

3. Comparisons among burnups

In figure 3.2 are plotted the conversion ratios and absorptions by nonsaturating fission products versus volume of moderator/volume of fuel with feed burnup and fuel rod diameter as parameters. The conversion ratio curves tend to be more sharply peaked and the peaks are located at higher values of volume of moderator/volume of fuel for the higher burnups.

This is because the curves of ($\bar{\eta}$-1) have steeper slopes for the higher burnups. This latter effect is due to the higher concentrations of U235 in the reactors with the higher burnups and the resulting increased effectiveness of increasing values of volume of moderator/volume of fuel in increasing ($\bar{\eta}$-1). From 50% to 90% of the difference in conversion ratios for different burnups and a given volume of moderator/volume of fuel and fuel rod diameter is due to the difference in absorptions by nonsaturating fission products. The 50% figure applies at very low values of volume of moderator/volume of fuel and the 90% figure applies at very high values. Other causes for the difference are changes in ($\bar{\eta}$-1) and changes in absorptions by U236, Np237 and Pa233.

C. Secondary variables

1. Introduction

In Section IIIC the effects of the four secondary variables on the conversion ratio at the three feed burnups are summarized. The secondary variables are absorptions in zircaloy/absorption in a fissile nucleus (determined by the variable, volume of zircaloy/volume of fuel), average specific power in the core (kw/kg fissile), total thermal power in the core and fraction of the reactor discharge lost in reprocessing. Throughout section IIIC, the remaining two primary variables are held constant at the following values:

Volume moderator/volume fuel	30
Fuel rod diameter	1/4 inch

This combination of volume of moderator/volume of fuel and fuel rod diameter was selected because it gave very nearly the highest conversion ratio for each feed burnup.

The values of absorption in zircaloy/absorption in a fissile nucleus ranged from zero to 0.11. This upper limit is a bit high for zircaloy structural material but is a reasonable value for stainless steel. The values of the average specific power range from 1000 kw/kg fissile to 12,000 kw/kg fissile. This lower limit approximates the average specific power of today's H_2O reactors while the upper limit is about 50% above the values suggested by the Savannah River Laboratory for advanced D_2O reactors (B1, B2). The values of the total thermal power ranged from 8333 MW(th) to 500 MW(th). The values of the reprocessing loss ranged from zero to 4% of the reactor fuel discharge.

The absorption in zircaloy/absorption in a fissile nucleus affects the conversion ratio primarily by absorbing thermal neutrons which would otherwise be absorbed in Th232. The average specific power in the core affects the conversion ratio primarily through increased absorption of resonance and thermal neutrons by nuclei of Pa233 which would otherwise decay to U233. The primary effect of the change in total power is through changes in the size of the core, which change the net leakages out of the core and into the blanket. The increase in the reprocessing loss affects the conversion ratio primarily by increasing the loss rate of fissile nuclei.

When either the absorption in zircaloy/absorption in a fissile nucleus or the average specific power in the core is increased, the increased absorptions by zircaloy or Pa233 reduce the number of thermal neutrons which are available for absorption by the fissile nuclides. In order to maintain criticality, the number of resonance neutrons absorbed by the fissile nuclides must increase. In other words, an increase in either of these two secondary variables causes the neutron spectrum to become more epithermal.

The internal conversion ratios and conversion ratios with reprocessing loss for the 32 combinations of the secondary variables studied in this work are listed in table 3.2.

2. Absorption in zircaloy/absorption in a fissile nucleus

a. Conversion ratio and its components for 20,000 mwd/t burnup

The conversion ratio and its components are plotted in figure 3.3 as a function of the absorption in zircaloy/absorption in a fissile nucleus for a feed burnup of 20,000 mwd/t. The other secondary variables are held constant at the following values:

Average specific power	1000 kw/kg fissile
Total thermal power	8333 MW(th)
Reprocessing loss	0

A value of the conversion ratio for a given abscissa is obtained by subtracting from $(\bar{\eta}-1)$ the sum of D_2O absorption, 2 x Pa233 absorption, leakage and parasitic absorptions other than by zircaloy, and the abscissa itself.

The conversion ratio has a value of 1.0 at a value of absorption in zircaloy/absorption in a fissile nucleus of about 0.083. The conversion ratio curve and the curves of its components have discontinuous slopes at this point because when the conversion ratio falls below 1.0, fresh U235 is added to the reactor discharge fuel to make the new core feed. In other words, a change in the fuel cycle flow sheet occurs at this point.

The curve of $(\bar{\eta}-1)$ in figure 3.3 decreases with increasing absorption in zircaloy/absorption in a fissile nucleus because as the conversion ratio decreases, an increasing fraction of the core discharge is recycled into the core feed and, therefore, the concentration in the core of U235, with its lower value of η, increases. The curve of $(\bar{\eta}-1)$ decreases

more rapidly as the conversion ratio falls below 1.0 because U235 is added to the feed.

The shape of the curve of leakage and parasitic absorptions other than by zircaloy in figure 3.3 is due primarily to the shapes of the curves of absorptions by U236 and Np237. As the absorption in zircaloy/absorption in a fissile nucleus increases toward 0.083, an increasing fraction of the core discharge is recycled into the core feed. Therefore the concentration of U236 in the core increases rapidly. When the absorption in zircaloy/absorption in a fissile nucleus increases above 0.083 and the conversion ratio drops below 1.0, 100% of the core discharge is recycled into the feed. Further increases in the concentration of U236 in the core and, therefore, increases in absorptions in U236 are due primarily to captures in U235 whose concentration increases rapidly as the conversion ratio decreases below 1.0. Since Np237 is the product of neutron absorption in U236, the shapes of its absorption curves are similar to those of U236.

The curves of 2 x Pa233 absorption and D_2O absorption in figure 3.3 decrease with increasing absorption in zircaloy/absorption in a fissile nucleus. This is because the neutron spectrum becomes more epithermal as zircaloy is added to the system.

b. Comparisons among burnups.

In figure 3.4 are plotted the conversion ratios and in figure 3.5 are plotted $(\bar{\eta}-1)$ and the absorptions by nonsaturating fission products, U236 and Np237, with absorption in zircaloy/absorption in a fissile nucleus as abscissa and feed burnup as a parameter. The difference between the conversion ratio curves for different burnups at a given abscissa is due primarily to the differences in absorptions by nonsaturating fission products, U236 and Np237 and $(\bar{\eta}-1)$ shown in figure 3.5.

The curves of ($\bar{\eta}$ -1) are lower for the higher burnups because of the increased concentrations of U235 in the cores of these systems.

3. Average specific thermal power in the core

a. Conversion ratio and its components for 20,000 mwd/t burnup

The conversion ratio is plotted in figure 3.6 and its components are plotted in figure 3.7 as functions of the average specific power in the core for a feed burnup of 20,000 mwd/t. The other secondary variables are held constant at the following values:

Absorption in zircaloy/absorption in a fissile nucleus	0
Total thermal power	8333 MW(th)
Reprocessing loss	0

The conversion ratio has a value of 1.0 at an average specific power of about 6250 kw/kg fissile as shown in figure 3.6. As in the case of the results for absorption in zircaloy/absorption in a fissile nucleus, the conversion ratio curve and the curves of its components have discontinuous slopes at the point where the conversion ratio equals 1.0 because U235 makeup is started at this point.

The curve of ($\bar{\eta}$ -1) in figure 3.7 decreases rapidly with increasing average specific power because of the rapid increase of U235 concentration in the core.

The shape of the curve of parasitic absorptions plus leakage in figure 3.7 is determined primarily by the shapes of the U236 and Np237 absorption curves. The D_2O absorption curve decreases with increasing average specific power because of the increasing epithermal character of the neutron spectrum.

The curve of 2 x Pa233 absorption in figure 3.7 increases with increasing average specific power for two reasons. The first is that as

the fast and thermal fluxes increase, the Pa233 branching ratio shifts from β^- decay to neutron absorption. The second reason is that the Pa233 concentration in the core increases with increasing average specific power because of the increasing Th232 absorption rate. The second derivative of the curve of 2 x Pa233 absorption is negative because as the specific power increases, the conversion ratio decreases and the core becomes less dependent on U233 for power production and more dependent of U235.

b. Comparisons among burnups

In figure 3.8 are plotted the conversion ratios and in figure 3.9 are plotted $(\bar{\eta}-1)$, absorptions by nonsaturating fission products and 2 x Pa233 absorptions with average specific power as abscissa and feed burnup as a parameter.

In order to understand the effect on the conversion ratio of increasing the average specific power for different feed burnups, one compares the characteristics of a core with a feed burnup of 10,000 mwd/t to the characteristics of a core with a feed burnup of 20,000 mwd/t. For a burnup of 10,000 mwd/t, the fuel travels through the core at a relatively high axial velocity and depends to a large extent on the fissile material in the feed to supply the fissile material throughout the core. (If the axial velocity were infinite, then all of the fissile material in the core would be supplied by the feed.) For a burnup of 20,000 mwd/t, the fuel travels through the core at a relatively low axial velocity and depends less on the feed to supply the fissile material in the core and depends more on the fissile material produced in the core. Because of this, the Pa233 concentration is higher in the core with the higher burnup. Therefore, an increase in the average specific power is more effective in

decreasing the conversion ratio in a core with a high feed burnup and its relatively high Pa233 concentration.

The effect just mentioned is shown in the plots of conversion ratio for the three burnups in figure 3.8. The difference between any two curves for a given specific power is due primarily to the differences in the curves of $(\bar{\eta}-1)$, 2 x Pa233 absorption and absorptions by nonsaturating fission products shown in figure 3.9. The curve of 2 x Pa233 absorption for a burnup of 20,000 mwd/t has a larger value and its slope is greater than for the curve for a burnup of 10,000 mwd/t because of the higher Pa233 concentration in the core. The curve for a burnup of 30,000 mwd/t falls slightly below the curve for 20,000 mwd/t because of the increased competition for thermal neutrons in the 30,000 mwd/t core caused by the higher concentration of nonsaturating fission products. However, the concentration of Pa233 is higher in the 30,000 mwd/t core at all average specific powers and if the specific power were increased to higher values, the curve of 2 x Pa233 absorption for the 30,000 mwd/t core would rise above the curve of 20,000 mwd/t.

The curves of $(\bar{\eta}-1)$ in figure 3.9 are lower for the higher burnups because of the increased concentration of U235 in the cores of these systems.

4. Total thermal power or geometric buckling

The conversion ratio and its components are plotted in figure 3.10 as a function of B_g^2, the geometric buckling, for a feed burnup of 20,000 mwd/t. The corresponding thermal power in the core is also indicated on the abscissa of figure 3.10. The geometric buckling is defined as follows:

$$B_g^2 = \left[\left(\frac{\pi}{H_c}\right)^2 + \left(\frac{2.404}{R_c}\right)^2\right] \qquad (3B1)$$

where

H_c = physical height of core.

R_c = physical radius of core.

The conversion ratio is divided into the contribution from the core and from the blanket, and these conversion ratios are extrapolated to zero buckling or infinite core size. The other secondary variables are held constant at the following values:

Absorption in zircaloy/absorption in a fissile nucleus	0
Average specific power	1000 kw/kg fissile
Reprocessing loss	0

As the core size is decreased from infinity, the conversion ratio, core plus blanket, decreases because the overall fast and thermal leakages from the reactor increase. As the core size is decreased further, the conversion ratio, core plus blanket, increases because of the decrease in the calculated values of the overall fast leakage from the reactor in this range of decreasing core size. It is not known if this decrease in overall fast leakage from the reactor is real or due to inaccuracies in the approximation for ∇^2 used in calculating the leakages. However, it is evident that as long as there is a blanket two feet thick surrounding the core to catch most of the neutrons leaking out of the core, a decrease in the core size does not have a large effect on the conversion ratio, core plus blanket, at least until thermal power drops below 500 MW.

5. Reprocessing loss

The results of this section are plotted as a function of the fraction of the core and blanket discharge which is lost in reprocessing. The other secondary variables are held constant at the following values:

Absorption in zircaloy/absorption in a fissile nucleus	0
Average specific power	6000 kw/kg fissile
Total power	8333 MW(th)

The conversion ratio and its components are plotted in figure 3.11 as a function of the reprocessing loss. Two conversion ratios are shown. The internal conversion ratio is defined in section IIIA by equation (3A3) and is calculated by considering in its definition only the consumption rate of fissile material within the reactor. The conversion ratio with reprocessing loss is calculated with equation (3A1) by including the fissile material lost in reprocessing in the consumption rate of fissile material. The internal conversion ratio is found for a given abscissa by subtracting from $(\bar{\eta}-1)$ the sum of D_2O absorption, 2 x Pa233 absorption and parasitic absorptions plus leakage.

When the internal conversion ratio of a reactor is greater than 1.0, the reprocessing loss can range from zero to a value for which the conversion ratio with reprocessing loss equals 1.0 without affecting the reactor neutron balance itself. This is because not all of the discharged fuel is recycled back into the core feed when the internal conversion ratio is greater than 1.0, and reprocessing loss merely reduces the net amount of fissile material produced. When the conversion ratio with reprocessing loss is less than 1.0, the entire neutron balance must be recalculated because the feed composition is different for each value of the reprocessing loss.

The curve of $(\bar{\eta}-1)$ in figure 3.11 decreases with increasing reprocessing loss because of the feeding into the core of fresh U235 with its low value of η . The curve of parasitic absorptions plus leakage decreases with increasing reprocessing loss because of the removal of

U236 in the reprocessing loss stream. The curves of 2 x Pa233 absorption and D_2O absorption do not change significantly with increasing reprocessing loss. The internal conversion ratio curve first increases and then decreases with increasing reprocessing loss because of the behavior of the curves of $(\bar{\eta}-1)$ and parasitic absorptions plus leakage.

D. Application of results

1. Introduction

In order to expand the area of useful application of the results obtained for the 56 different combinations of reactor variables which were calculated in detail using the computer program, two methods of estimating the conversion ratio expected for thorium fueled, heavy water moderated reactors having other various combinations of values of the seven primary and secondary variables were developed. These methods each employ knowledge gained from the calculated cases concerning the effects of each of the seven variables on the conversion ratio to interpolate, and where necessary, to extrapolate, from the conditions for which detailed calculations were made to any new set of values of the variables. The two methods of estimating are referred to as the More Refined Approximate (MRA) procedure and the Less Refined Approximate (LRA) procedure to indicate the level of detail employed respectively in the two estimating procedures. The MRA and LRA procedures are described in detail in chapter VII and are illustrated there by some example problems. One of the example problems uses the same values of the primary and secondary variables as were used in a study by the Oak Ridge National Laboratory (R1). The results of the example problems are summarized beginning on the next page.

2. More Refined Approximate (MRA) procedure for estimating conversion ratios

In section IIIC, we have summarized the effect on the conversion ratio and its components of changing individual secondary variables with the primary variables set at the values in the first column of numbers below. In the present section IIID2, we summarize the results of an example problem, given in detail in chapter VII, in which the More Refined Approximate (MRA) procedure is used to estimate the effect on the conversion ratio and its components of changing all four secondary variables together, starting from values of the primary variables different from those employed in section IIIC. In the example problem summarized here, the primary variables have the values listed in the second column of numbers below:

	Values of primary variables	
	Section IIIC	This section
Burnup, mwd/t	10,000, 20,000 or 30,000	20,000
Vol. moderator/vol. fuel	30	20
Fuel rod diameter, inch	1/4	1

In the example problem summarized here, the secondary variables are changed from the values used in section IIIB which are repeated in the first column of numbers on the next page. These variables are changed one at a time in the order given to the values listed in the second column of numbers on the next page:

	Secondary variables changed	
	from section IIIB	to this section
Average specific power, kw/kg fissile	1000	3000
Absorption in zircaloy/absorption in a fissile nucleus	0	0.05
Reprocessing loss	0	0.02
Total power, MW(th)	8333	Anything over 500 MW(th)

These values of the primary and secondary variables are approximately those of the CANDU reactor, if fueled with ThO_2 (A2).

The steps in working out the example problem are illustrated in figure 3.12. In table 3.1 it is seen that the conversion ratio before any secondary variables are changed is 1.079. The change in average specific power from 1000 to 3000 kw/kg fissile is estimated to reduce the conversion ratio to 1.038. Next, the change in absorption in zircaloy/absorption in a fissile nucleus from 0 to 0.05 is estimated to reduce the conversion ratio further to 0.965. Then, the change in reprocessing loss fraction from 0 to 0.02 is estimated to reduce the conversion ratio further to 0.95. Change in total power from 8333 MW(th) to anything over 500 MW(th) is estimated to have no appreciable effect on conversion ratio. Therefore, the final estimated conversion ratio is 0.95.

3. Comparison of results from the MRA and LRA procedures with a conversion ratio calculated by the Oak Ridge National Laboratory

In a study of advanced converter reactors (R1), the Oak Ridge National Laboratory has calculated the conversion ratios for several designs of reactors fueled with thorium and U233 oxide and cooled and moderated by heavy water. Table 3.3 lists the values of the primary and secondary variables of one such reactor design, case G4, which are in the range

which lead to minimum power cost. It was necessary to substitute an assumed fuel rod equivalent diameter of one inch for the three concentric tube fuel element design of Oak Ridge case G4. In chapter VII detailed estimates are made of the conversion ratio of a reactor with the same values of the primary and secondary variables as Oak Ridge case G4. The More Refined Approximate (MRA) procedure mentioned above and the Less Refined Approximate (LRA) procedure are used for the estimates. The results are summarized below:

Oak Ridge calculation	More Refined Approximate procedure	Less Refined Approximate procedure
0.8255	0.87	0.88

In addition the present computer code was used to calculate directly the conversion ratio for this reactor, and a value of 0.8476 was obtained. The agreement between the MIT and Oak Ridge computer calculations is as good as might have been expected, in view of the uncertainty introduced in using a solid rod one inch in diameter as equivalent to the three concentric tubes of the Oak Ridge design. The agreement among the MRA and LRA procedures and the computer calculations is considered to be good enough to confirm the utility of these approximate procedures in estimating conversion ratios in heavy-water moderated thorium-fueled reactors with combinations of the principal design variables different from those studied in this report.

4. Extreme values of conversion ratio

The following table compares conversion ratios calculated in this work for three cases of major interest. The first case gives the maximum value of the conversion ratio found among all combinations of design variables studied. It is an impractical case because absorptions

in zircaloy have been taken as zero. The second case differs from the first in having as much zircaloy as the CANDU reactor, and hence may be considered to be practical. Addition of the zircaloy reduces conversion ratio from 1.1297 to 1.0813.

The second case is far from one leading to minimum power cost, however. The third case is in the range judged by the Oak Ridge National Laboratory to lead to minimum power cost. It has higher burnup, less moderator, larger fuel, more zircaloy and higher specific power than the second case. All of these changes reduce conversion ratio, from 1.0813 to 0.8662.

Case	1	2	3
Burnup, Mwd/t	10,000	10,000	28,800
Vol. ratio, moderator/fuel	30	30	16.6
Fuel diameter, inches	1/4	1/4	1
Vol. ratio, zircaloy/fuel	0.0	0.5	0.7
Avg. specific power, kw/kg	1000	1000	2700
Conversion ratio	1.1297	1.0813	0.8662

Power, 8333 MW(th)

Blanket thickness, 2 ft

Reprocessing losses, 0.00

It may be concluded that a practical heavy water reactor can be designed to breed on the ThO_2-$U^{233}O_2$ cycle, but that the changes in design conditions needed for minimum power cost reduce the conversion ratio to such an extent that breeding is not economically attractive.

Table 3.1: Effect of the Primary Variables on the Conversion Ratio

Values of the secondary variables

Volume zircaloy/volume fuel = 0
Average specific power in the core = 1000 kw/kg fissile
Total thermal power in the core = 8333 MW(th)
Reprocessing loss = 0

Feed burnup, mwd/t	Volume ratio, moderator/fuel	Fuel rod diameter, inches	Internal conversion ratio
10,000	10	2	1.0871
	20	2	1.1069
	30	2	1.1027
10,000	20	1	1.1176
	30	1	1.1213
	40	1	1.1187
10,000	30	1/4	1.1297
	40	1/4	1.1299
	50	1/4	1.1273
20,000	10	2	1.0424
	20	2	1.0682
	30	2	1.0664
20,000	10	1	1.0467
	20	1	1.0793
	30	1	1.0850
	40	1	1.0841
20,000	30	1/4	1.0947
	40	1/4	1.0953
	50	1/4	1.0935
20,000	30	1/10	1.0997
	40	1/10	1.0999
	50	1/10	1.0977
	60	1/10	1.0942
30,000	10	2	0.9942
	20	2	1.0331
	30	2	1.0340
30,000	20	1	1.0457
	30	1	1.0546
	40	1	1.0545
30,000	30	1/4	1.0650
	40	1/4	1.0670
	50	1/4	1.0659

Table 3.2: Effect of the Secondary Variables on the Conversion Ratio

Volume of moderator/ volume of fuel = 30
Fuel rod diameter = 1/4 inch

Feed burnup, mwd/t	Absorption ratio, zircaloy/fissile	Average specific power, kw/kg fissile	Total power, MW(th)	Fractional reprocessing loss	Internal conversion ratio	Conversion ratio with reprocessing loss
10,000	0	1000	8333	0	1.1297	-
	0.047573	1000	8333	0	1.0813	-
	0.107829	1000	8333	0	1.0132	-
20,000	0	1000	8333	0	1.0947	-
	0.046438	1000	8333	0	1.0467	-
	0.080404	1000	8333	0	1.0040	-
	0.088526	1000	8333	0	0.9916	-
	0.100535	1000	8333	0	0.9736	-
	0.112351	1000	8333	0	0.9552	-
30,000	0	1000	8333	0	1.0650	-
	0.036581	1000	8333	0	1.0248	-
	0.053616	1000	8333	0	0.9998	-
10,000	0	1000	8333	0	1.1297	-
	0	2000	8333	0	1.1092	-
	0	7000	8333	0	1.0542	-
	0	12000	8333	0	1.0344	-
20,000	0	1000	8333	0	1.0947	-
	0	2000	8333	0	1.0728	-
	0	5000	8333	0	1.0185	-
	0	6000	8333	0	1.0029	-
	0	7000	8333	0	0.9895	-
	0	8000	8333	0	0.9788	-
	0	10000	8333	0	0.9612	-
30,000	0	1000	8333	0	1.0650	-
	0	2000	8333	0	1.0407	-
	0	3000	8333	0	1.0188	-
20,000	0	1000	8333	0	1.0947	-
	0	1000	1000	0	1.0909	-
	0	1000	500	0	1.0923	-
20,000	0	6000	8333	0	1.0029	1.0029
	0	6000	8333	0.02	1.0035	0.9865
	0	6000	8333	0.04	1.0027	0.9696

Table 3.3: Primary and Secondary Variables for Oak Ridge Case G4

Primary variables	
Feed burnup, mwd/t	28,800
Volume moderator/volume fuel	16.6
Assumed fuel rod equivalent diameter, inch	1
Secondary variables	
Average specific power in core, kw/kg fissile	2700
Zircaloy absorption ratio	0.07
Overall fast and thermal leakages from reactor (Because of the absence of a blanket, this replaces total thermal power in the core or B_g^2 as the related secondary variable.)	0.025
Reprocessing loss	0.0

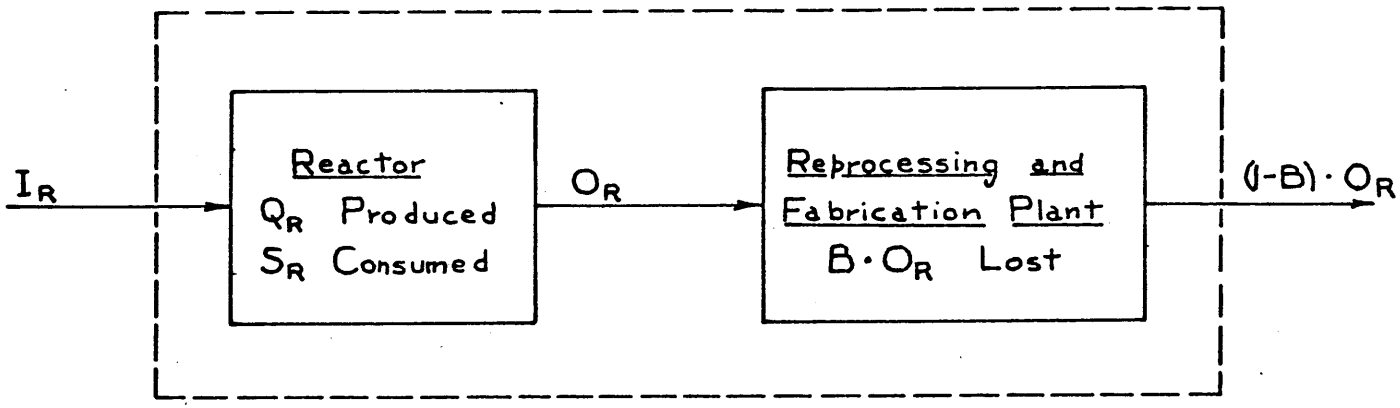

Figure 3.1A: Nomenclature for Defining Conversion Ratio

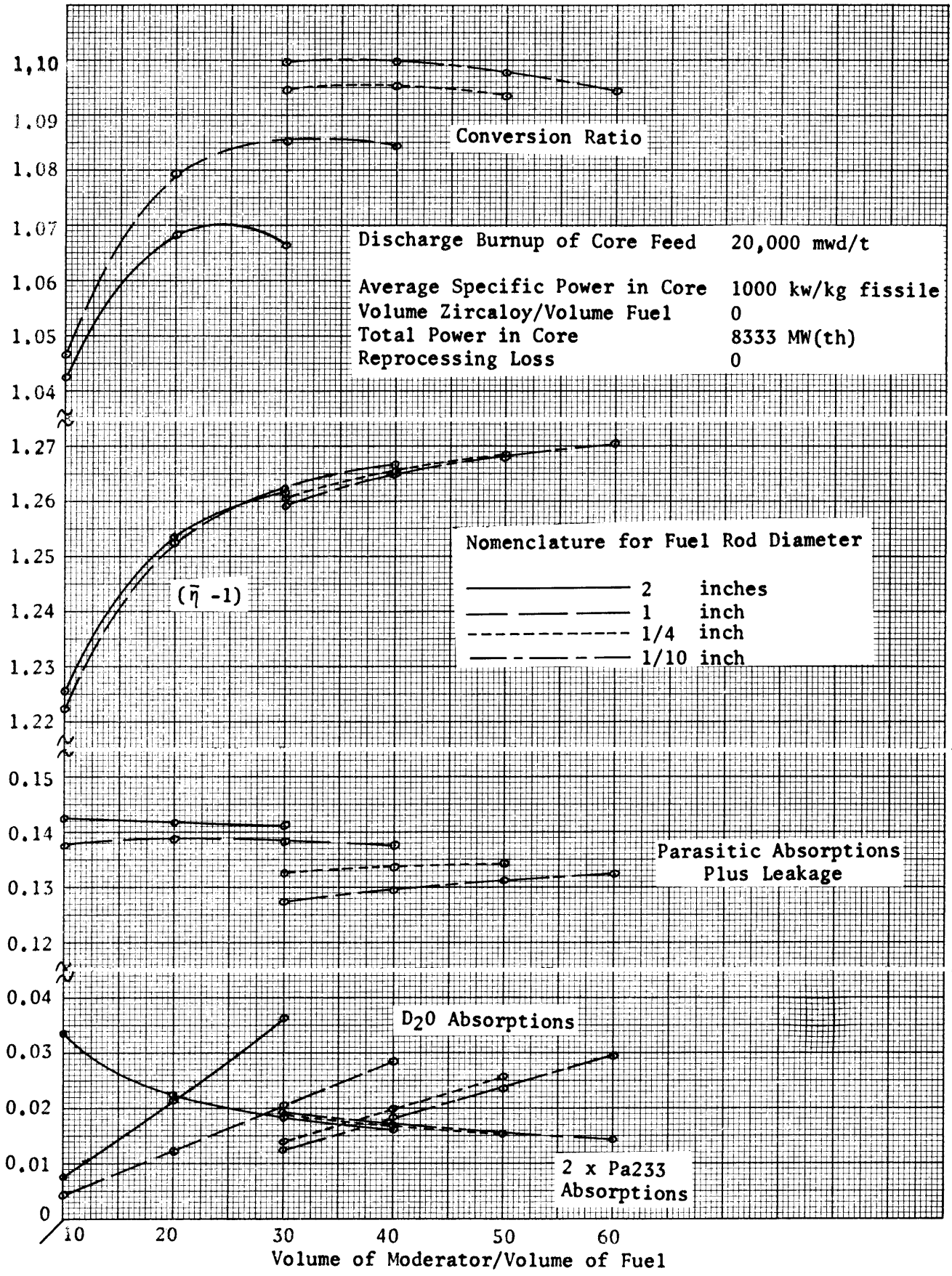

Figure 3.1: Conversion Ratio and its Components vs. Volume of Moderator/Volume of Fuel: 20,000 mwd/t Burnup

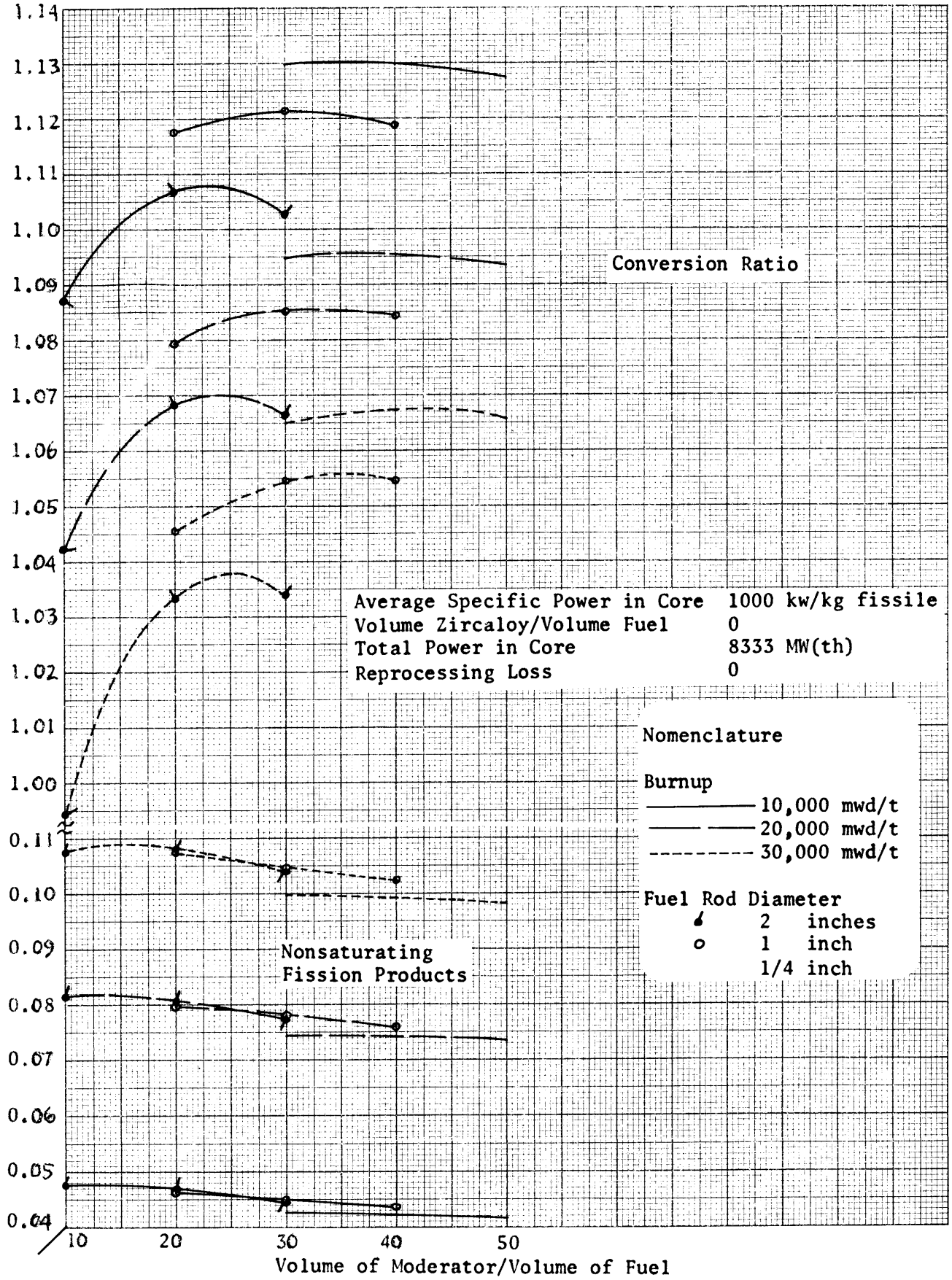

Figure 3.2: Conversion Ratio and Absorptions by Nonsaturating Fission Products vs. Volume of Moderator/Volume of Fuel: 10,000 mwd/t, 20,000 mwd/t, 30,000 mwd/t Burnups

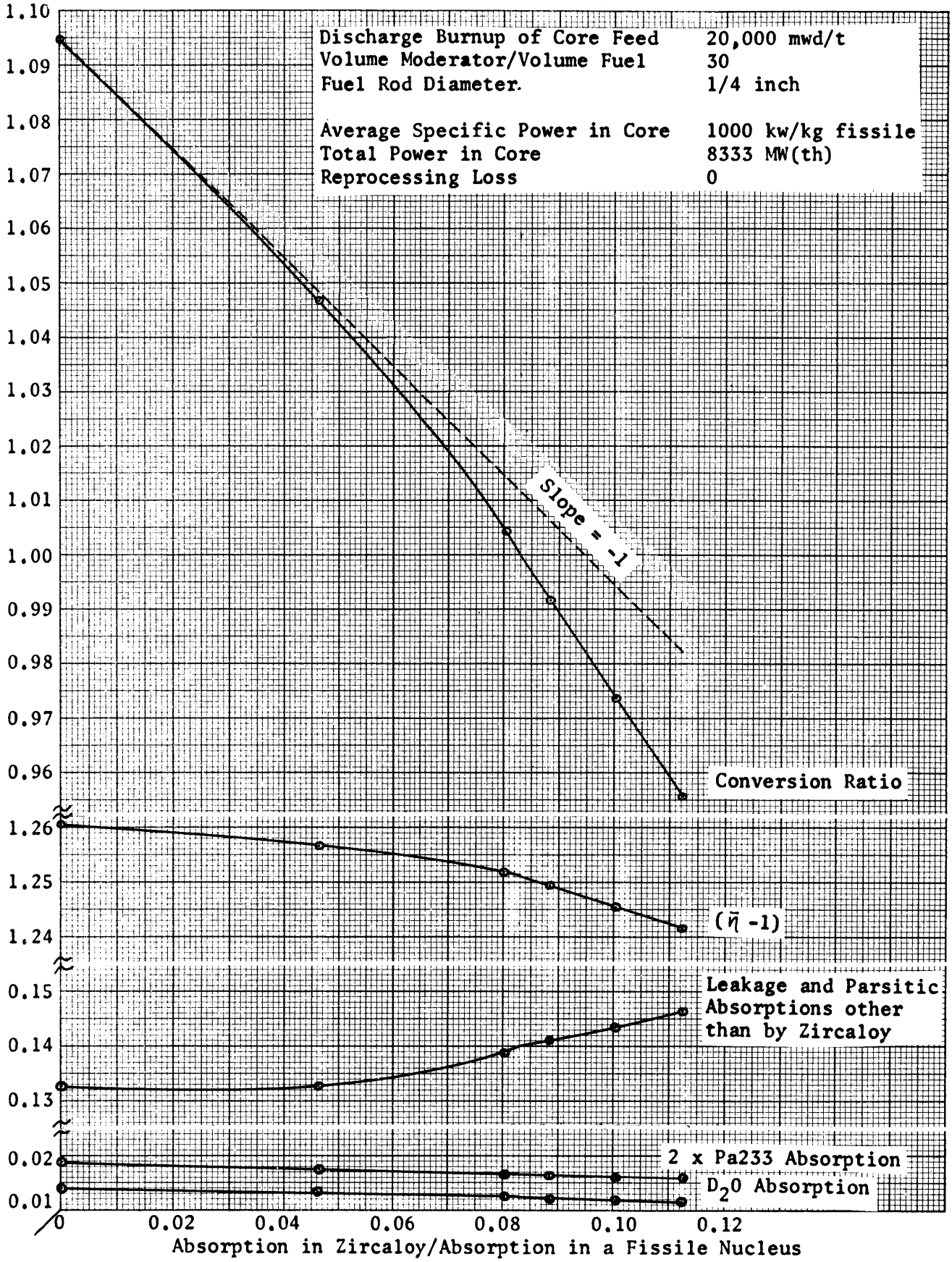

Figure 3.3: Conversion Ratio and its Components vs. Absorption in Zircaloy/Absorption in a Fissile Nucleus: 20,000 mwd/t Burnup

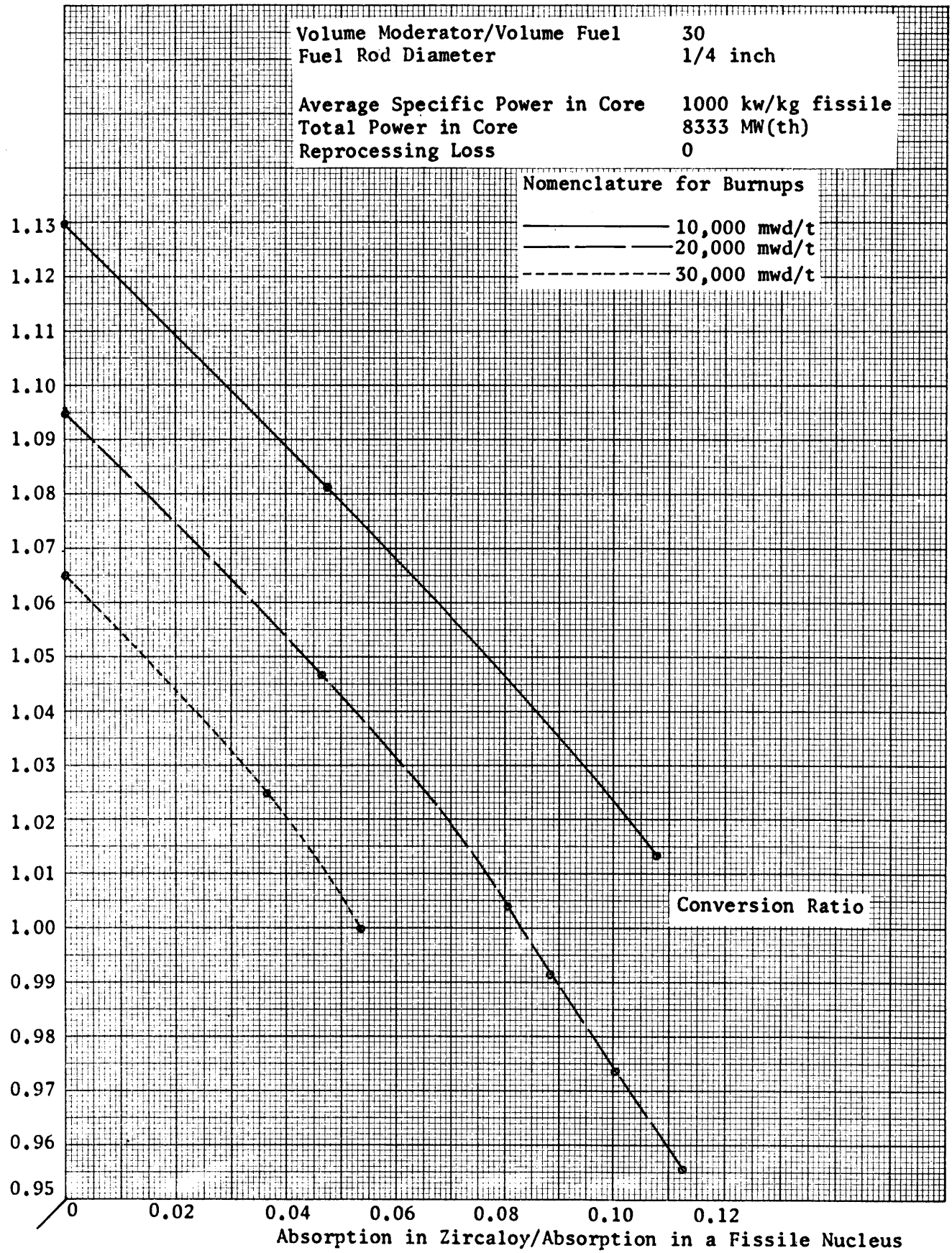

Figure 3.4: Conversion Ratio vs. Absorption in Zircaloy/Absorption in a Fissile Nucleus: 10,000 mwd/t, 20,000 mwd/t, 30,000 mwd/t Burnups

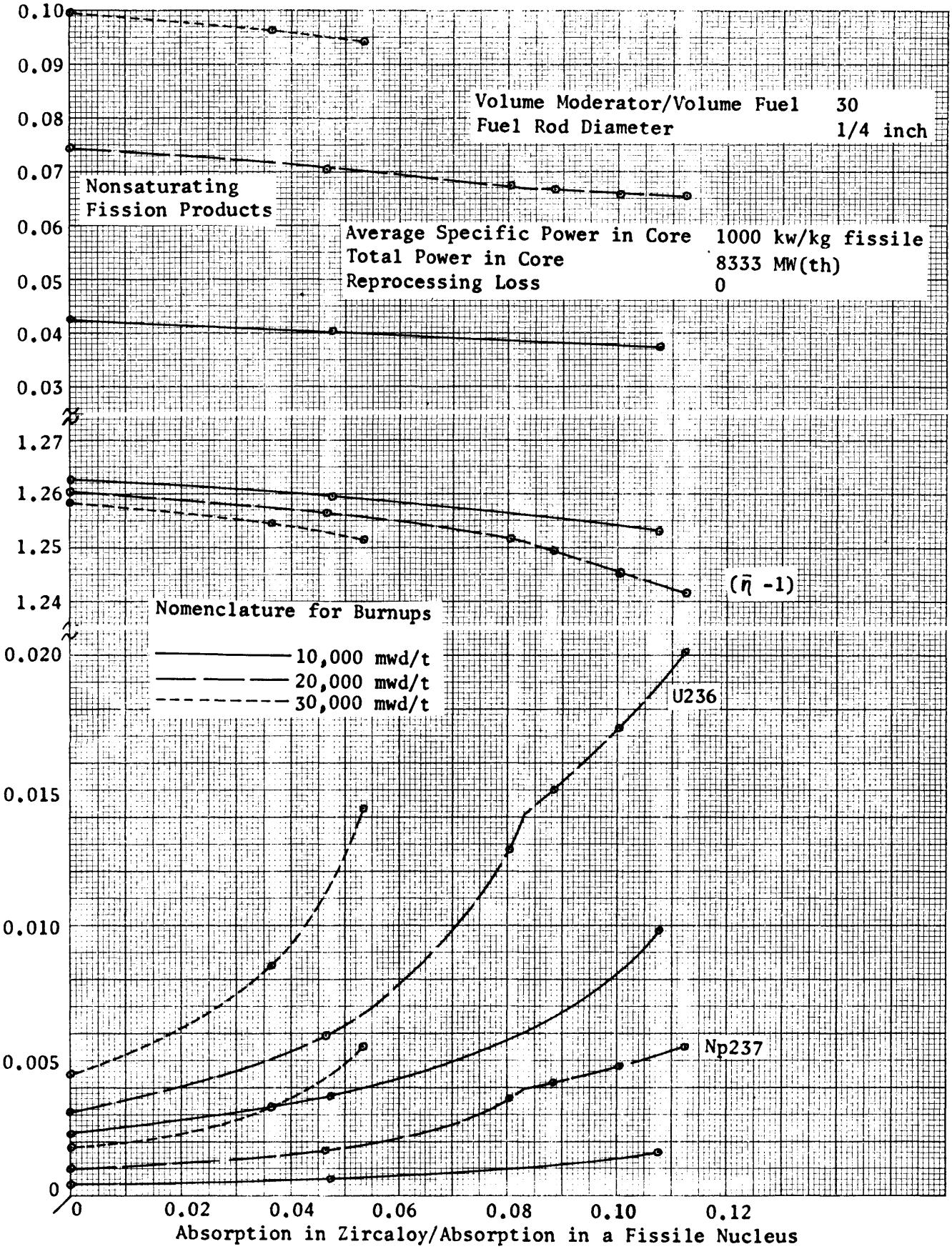

Figure 3.5: $(\bar{\eta} - 1)$ and Absorptions by U236, Np237 and Nonsaturating Fission Products vs. Absorption in Zircaloy/Absorption in a Fissile Nucleus: 10,000 mwd/t, 20,000 mwd/t, 30,000 mwd/t Burnups

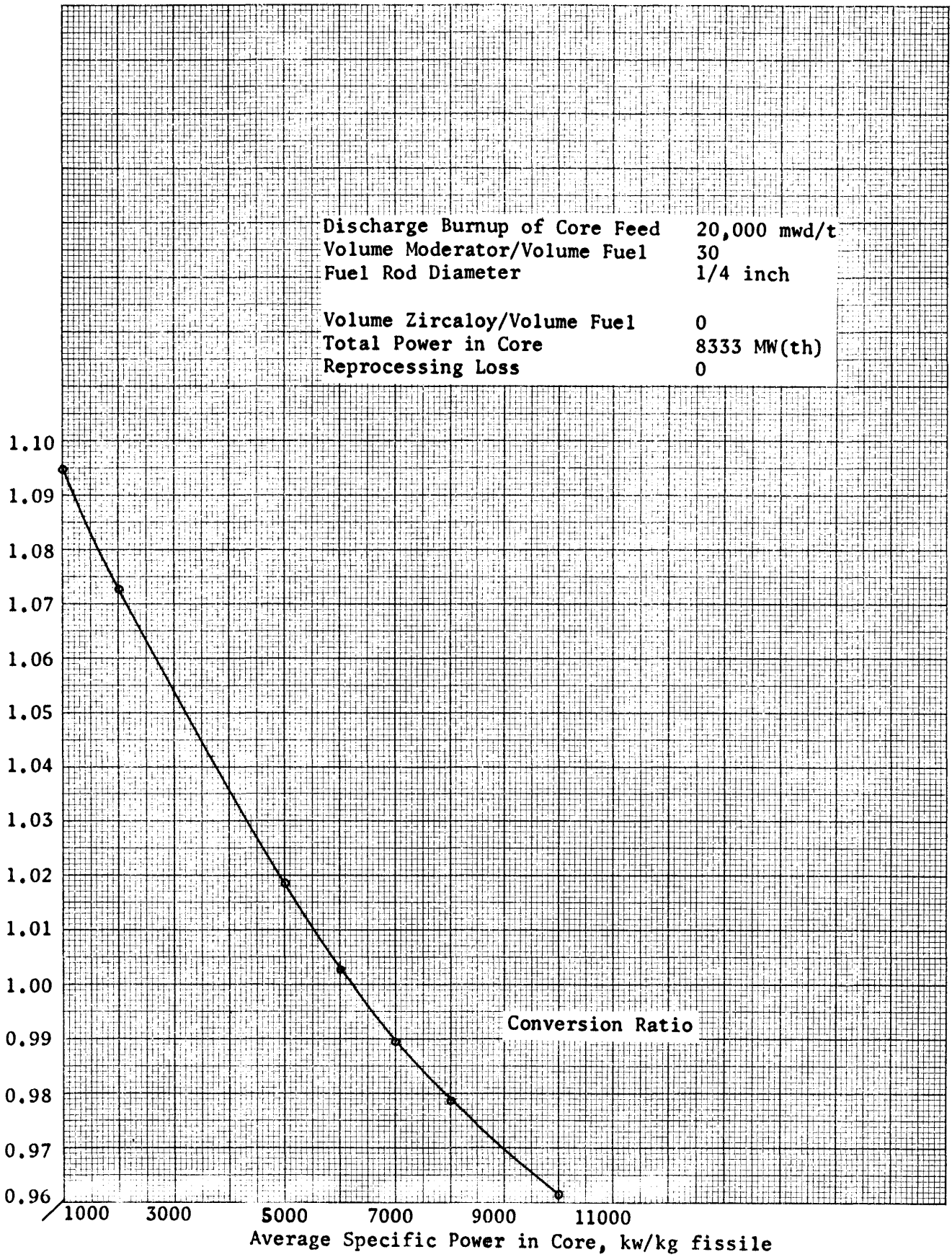

Figure 3.6: Conversion Ratio vs. Average Specific Power in Core: 20,000 mwd/t Burnup

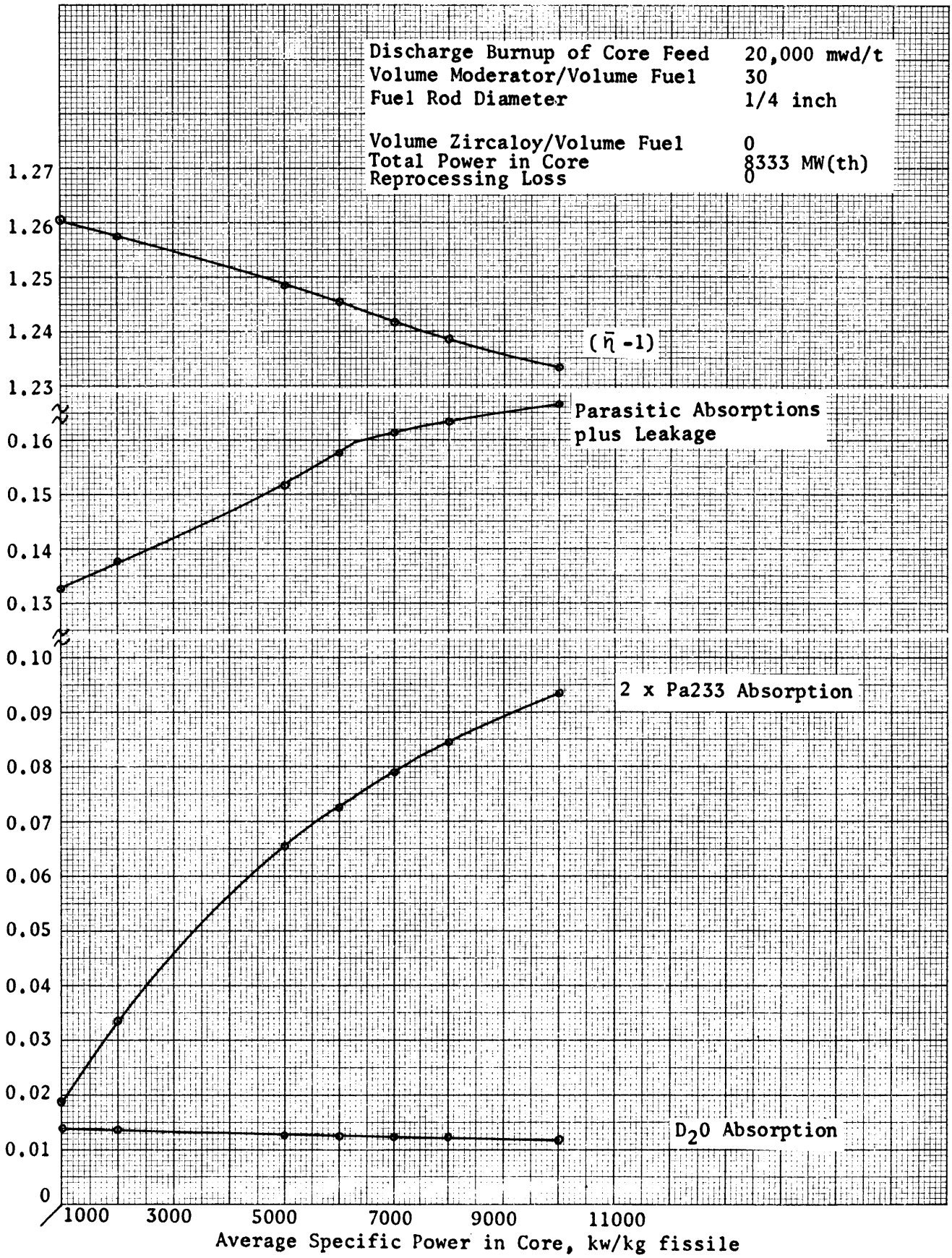

Figure 3.7: Components of the Conversion Ratio vs. Average Specific Power in Core: 20,000 mwd/t Burnup

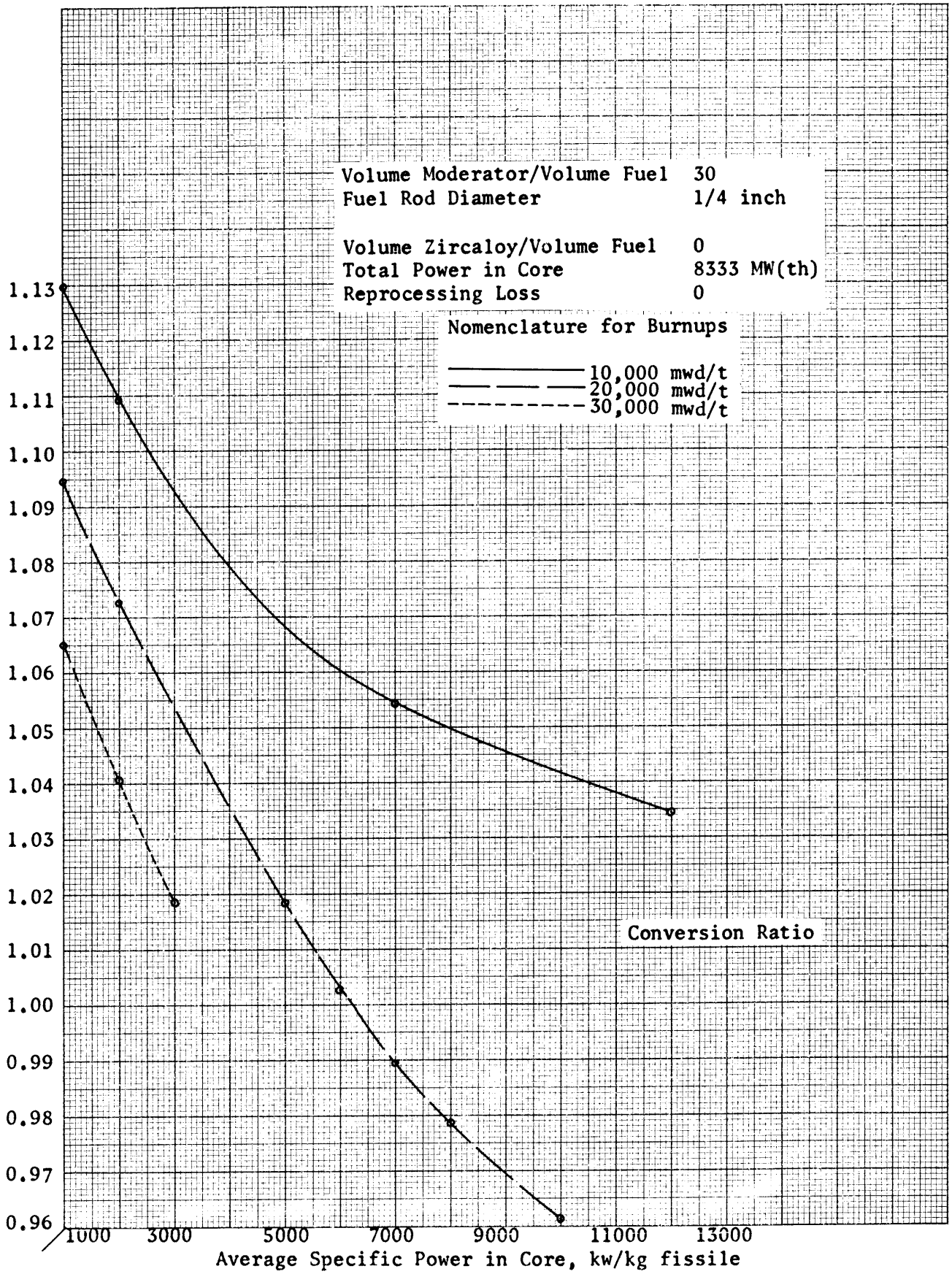

Figure 3.8: Conversion Ratio vs. Average Specific Power in Core: 10,000 mwd/t, 20,000 mwd/t, 30,000 mwd/t Burnups

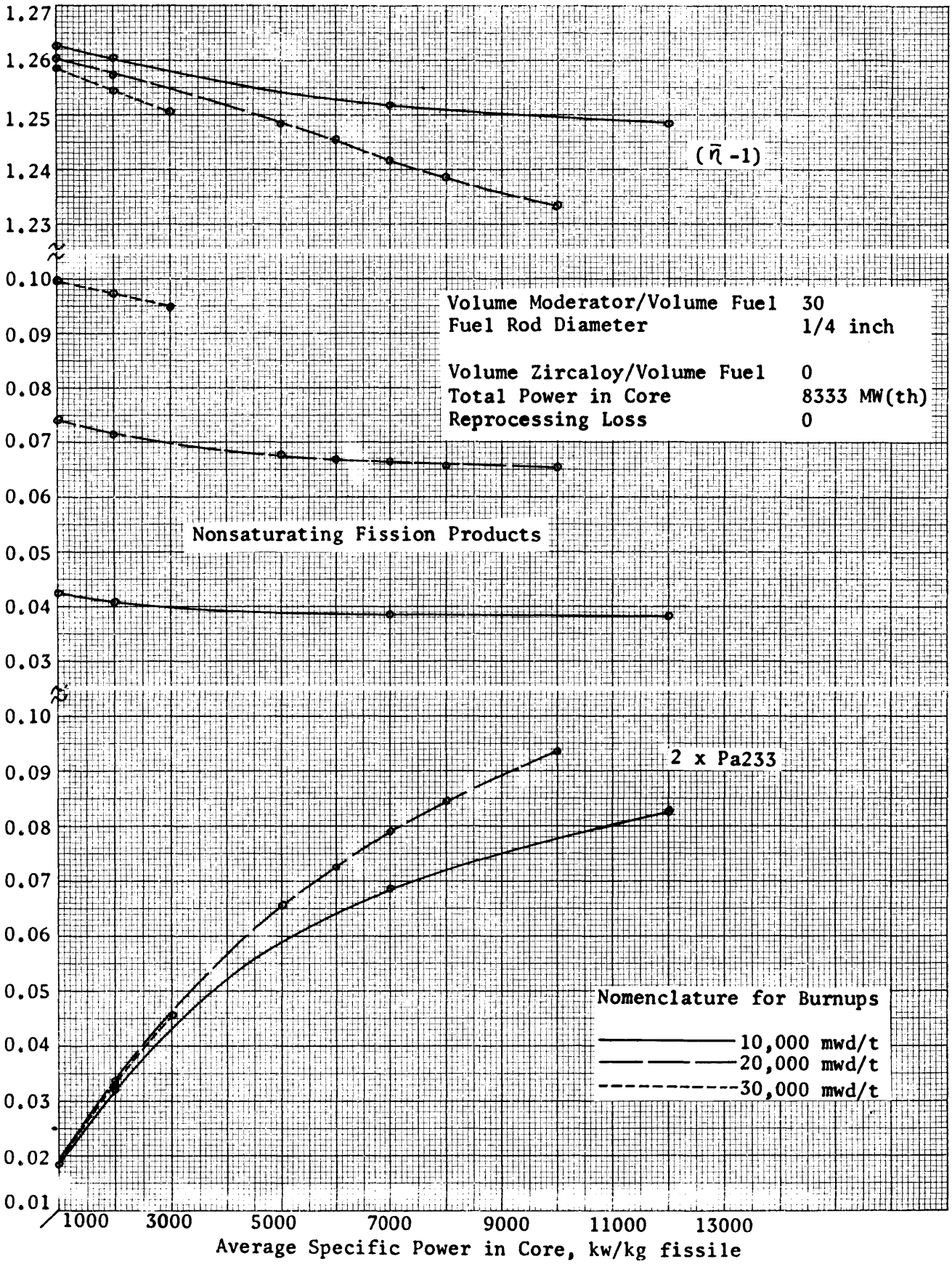

Figure 3.9: $(\bar{\eta} - 1)$, Nonsaturating Fission Product Absorptions, 2 x Pa233 Absorptions vs. Average Specific Power in Core: 10,000 mwd/t, 20,000 mwd/t, 30,000 mwd/t Burnups

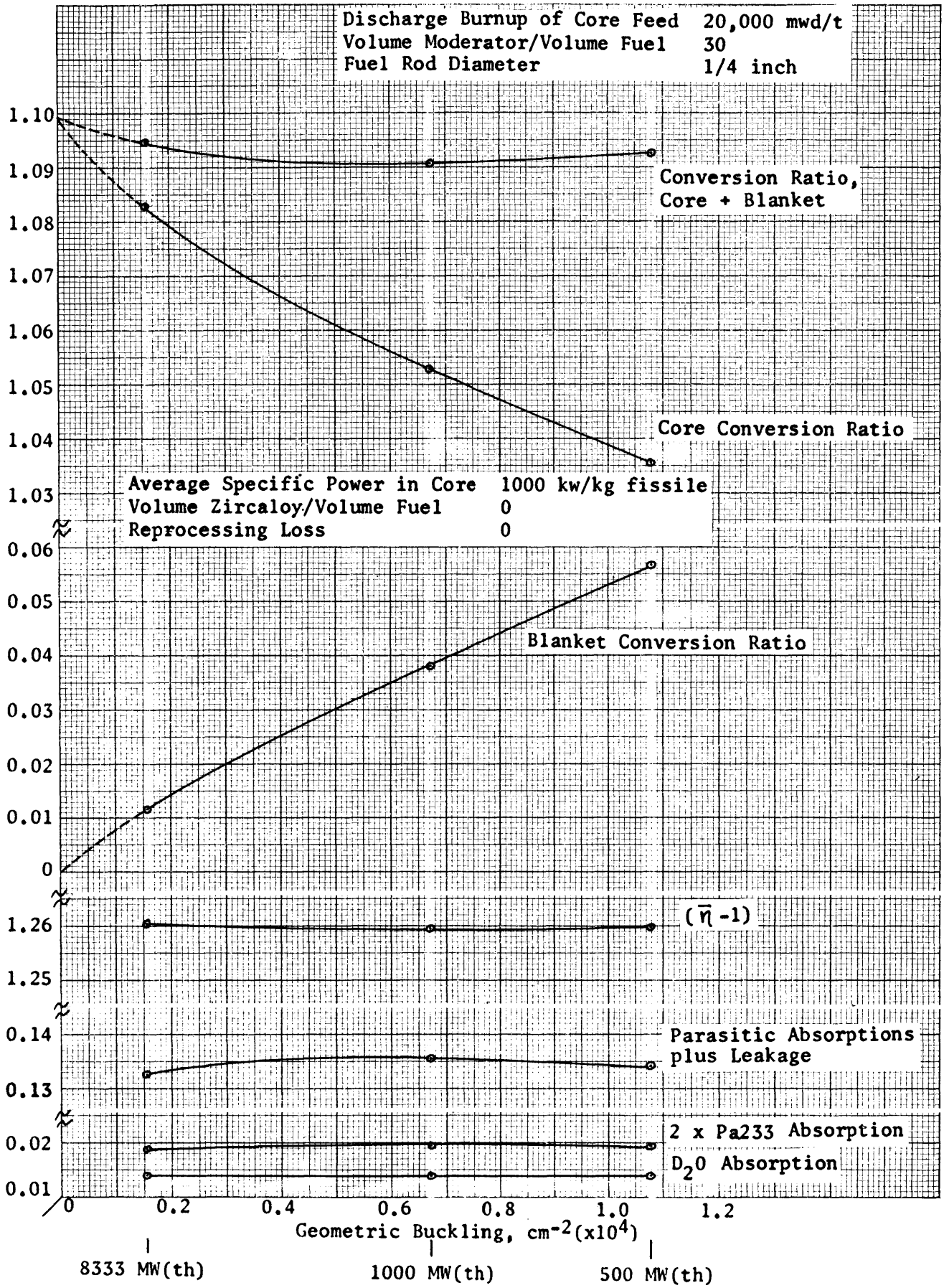

Figure 3.10: Conversion Ratio and its Components vs. Geometric Buckling: 20,000 mwd/t Burnup

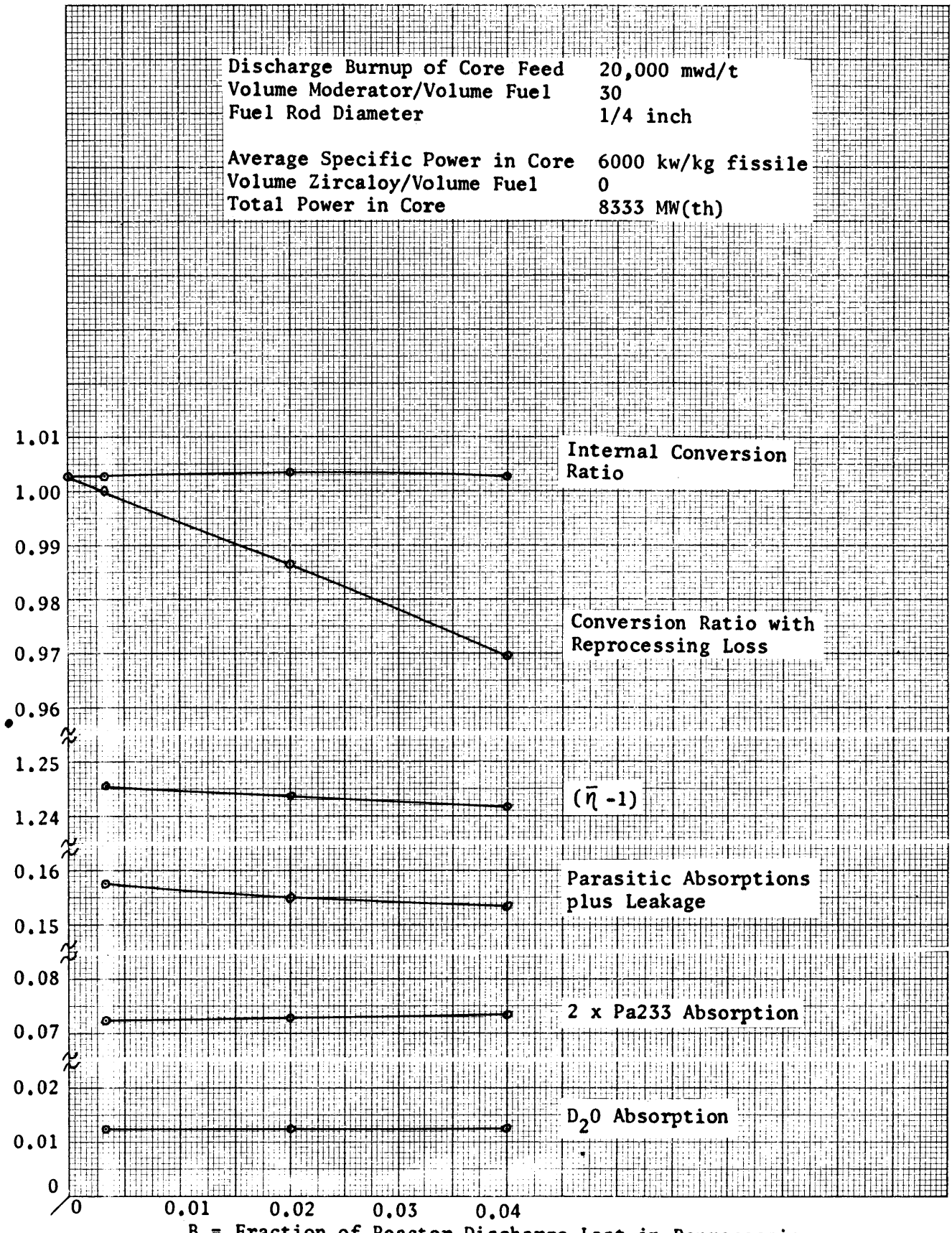

Figure 3.11: Conversion Ratio and its Components vs. Reprocessing Loss: 20,000 mwd/t Burnup

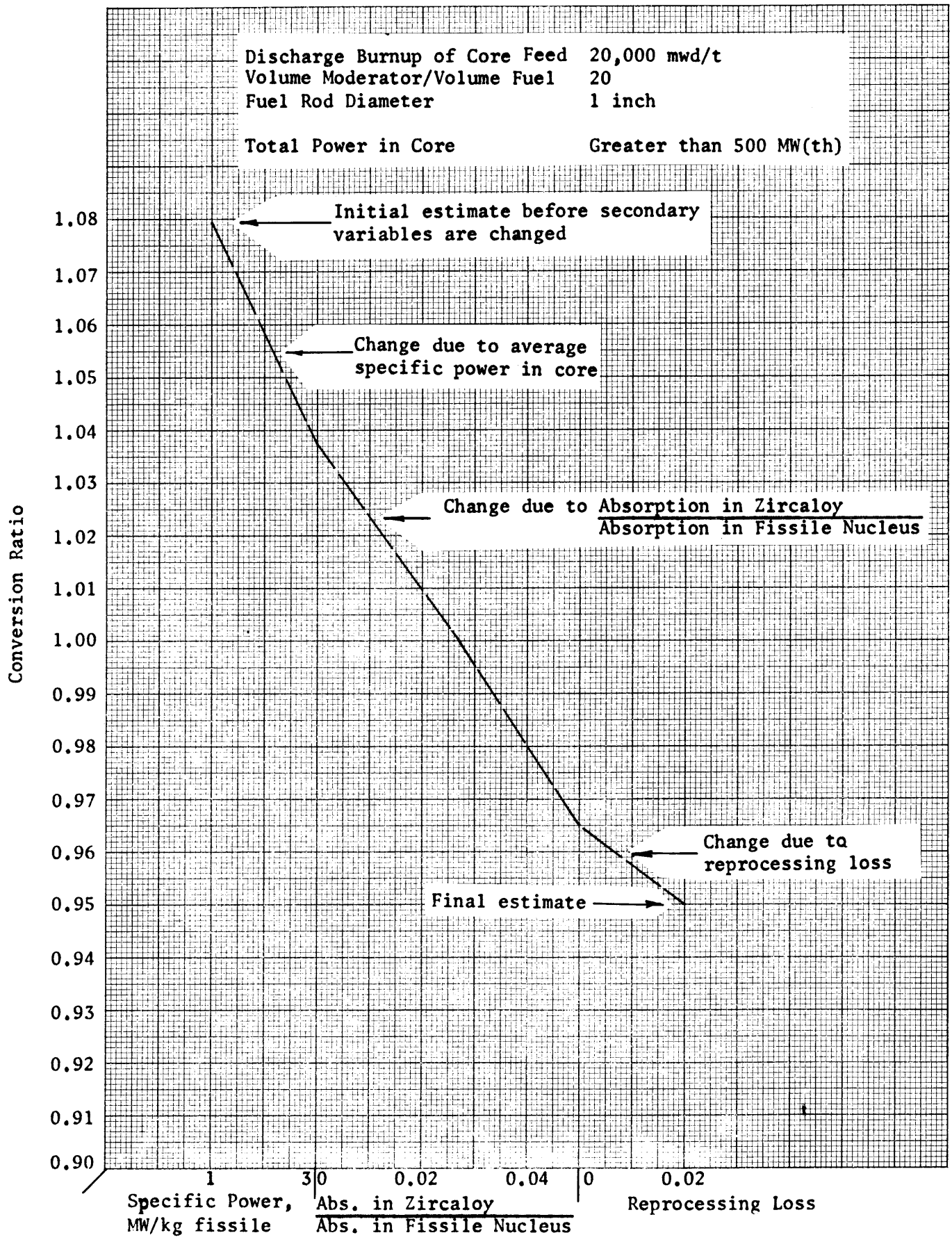

Figure 3.12: Steps in Example of Estimate of Effect of Changing All Secondary Variables on Conversion Ratio

CHAPTER IV

REACTOR PHYSICS MODELS AND CALCULATIONAL TECHNIQUES

A. Two group diffusion differential equations

The neutron behavior model used in this work is two-energy-group diffusion theory applied in the r-z directions of cylindrical coordinates in a maximum of three regions. The two energy groups considered are the fast or epi-resonance group and the thermal group. The two steady state diffusion equations are as follows:

Fast: $$D_1 \nabla^2 \phi_1 + q - \Sigma_1 \phi_1 = 0 \qquad (4A1)$$

Thermal: $$D \nabla^2 \phi + p \Sigma_1 \phi_1 - \Sigma_a \phi = 0 \qquad (4A2)$$

where

D_1, D = fast and thermal diffusion coefficients respectively, averaged over the unit cell, cm

ϕ_1, ϕ = fast and thermal fluxes respectively, volume averaged over the unit cell, $1/cm^2 sec$

q = fast source in the unit cell, $1/sec\ cm^3$ of cell

Σ_1 = fast removal cross section averaged over the unit cell, 1/cm

p = resonance escape probability

Σ_a = spectrum averaged thermal absorption cross section averaged over the unit cell, 1/cm

Two groups were selected because this was the minimum number of energy groups which would give a reasonable description of the neutron energy behavior and was the maximum number of energy groups which would permit

the consideration of the spatial variation of reactor properties in a reasonable length of computer time.

The neutron cycle is shown in figure 4.1. Fast fission in Th232 is not considered in this work because it adds at most a few tenths of a percent to the fast source* and the fast fission constants for Th232 are not well known. However fast fission is represented in figure 4.1 for completeness. The resonance region (from fission energy to 0.414 ev) is divided into three regions with one region occurring at about 5 ev, another region above 5 ev and the third region below 5 ev. This is because about 83% of the resonance absorption in U234 and about 72% of the resonance absorption in U236 occur at about 5 ev with the resonance absorption in the other nuclides more spread out above and below 5 ev. As can be seen from figure 4.1, the fast source q is

$$q = \frac{\epsilon}{1 - \epsilon \langle \bar{\bar{\eta}} (1-p) \rangle} \left[\nu \Sigma_f \phi + \langle \bar{\bar{\eta}} (1-p) \rangle D_1 \nabla^2 \phi_1 \right] \qquad (4A3)$$

where

$$\langle \bar{\bar{\eta}} (1-p) \rangle = \langle 1-p \rangle_3 \bar{\bar{\eta}}_1 + \langle 1-p \rangle_4 \bar{\bar{\eta}}_3 + p_{174} \left[\langle 1-p \rangle_9 \bar{\bar{\eta}}_2 + \langle 1-p \rangle_{10} \bar{\bar{\eta}}_4 \right]$$

$$\nu \Sigma_f = \nu_3 \Sigma_{f,3} + \nu_5 \Sigma_{f,5}$$

Substituting this value into equation (4A1), we then have for the two-group diffusion equations:

Fast: $$D_1 \nabla^2 \phi_1 + \{\epsilon \nu \Sigma_f\} \phi - \{[1 - \epsilon \langle \bar{\bar{\eta}} (1-p) \rangle] \Sigma_1\} \phi_1 = 0 \qquad (4A4)$$

Thermal: $$D \nabla^2 \phi + \{p \Sigma_1\} \phi_1 - \{\Sigma_a\} \phi = 0 \qquad (4A2)$$

*Hofmann (H2,S3) calculates a fast fission factor of 1.0023 for a 19 rod bundle of 0.566 inch diameter rods. The fast fission factor would be even nearer to unity in the single rods used in this study.

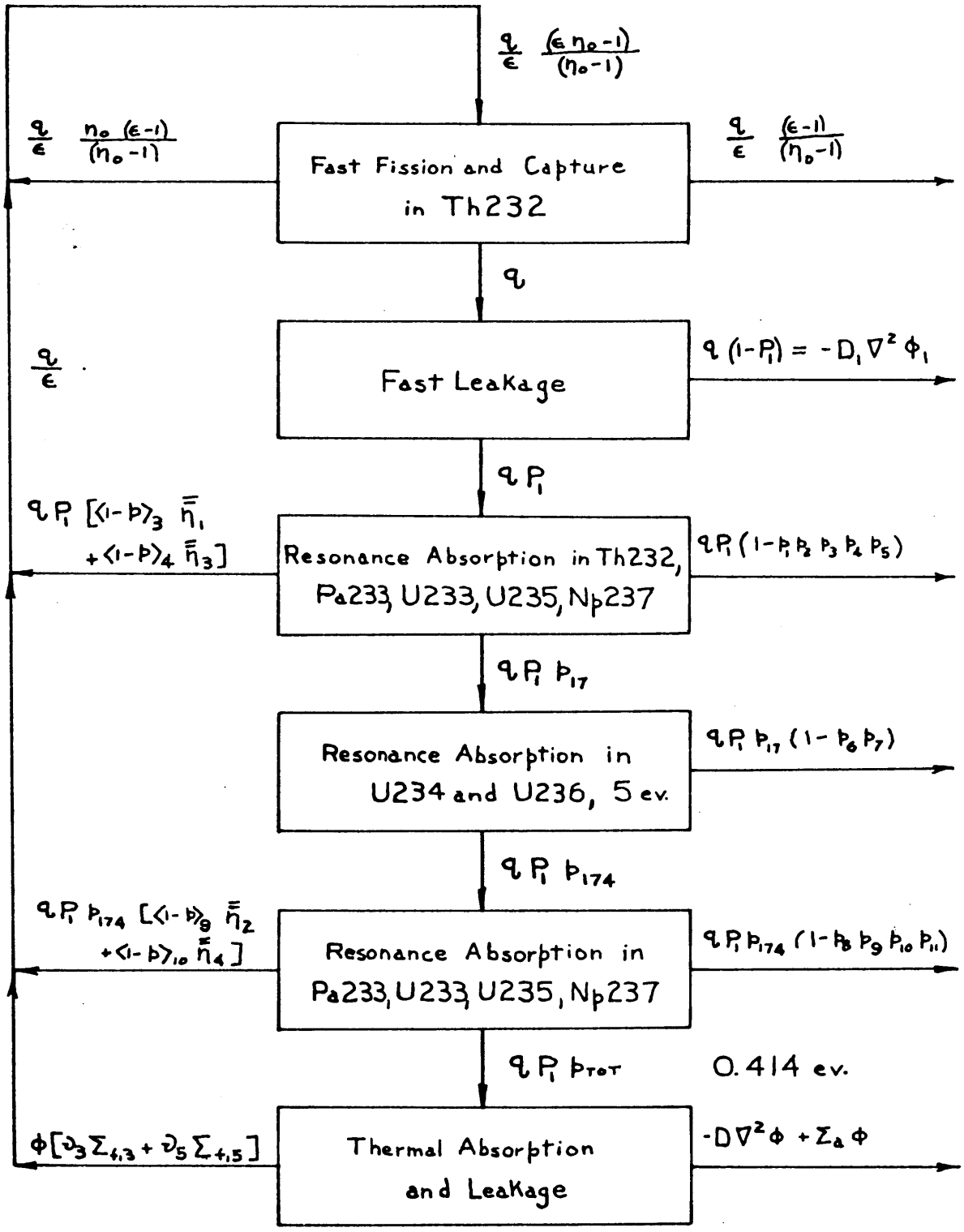

Figure 4.1: The Neutron Cycle

Figure 4.1 (continued)

Nomenclature for figure 4.1

Fast energy group

q = source of fast neutrons in the unit cell, 1/sec cm^3 of cell

ϵ = fast fission factor of Th232

η_o = number of fast neutrons produced per fast absorption in Th232

P_1 = Nonleakage probability for fast neutrons = $\frac{q + D_1 \nabla^2 \phi_1}{q}$

Φ_1 = fast flux, 1/sec cm^2

D_1 = fast diffusion coefficient averaged over the unit cell, cm

Resonance region

p_i = resonance escape probabilities with the following subscripts:

1 = Th232

2 = Pa233 above 5 ev

3 = U233 above 5 ev

4 = U235 above 5 ev

5 = Np237 above 5 ev

6 = U234

7 = U236

8 = Pa233 below 5 ev

9 = U233 below 5 ev

10 = U235 below 5 ev

11 = Np237 below 5 ev

$\langle 1-p \rangle_i$ = resonance absorption probability, with the same subscripts as for p_i.

Figure 4.1 (continued)

$\bar{\bar{\eta}}_j$ = number of fast neutrons produced per resonance absorption with the following subscripts

1 = U233 above 5 ev

2 = U233 below 5 ev

3 = U235 above 5 ev

4 = U235 below 5 ev

$P_{17} = P_1P_2P_3P_4P_5$

$P_{174} = P_{17}P_6P_7$

$P_{TOT} = P_{174}P_8P_9P_{10}P_{11}$ = p of equation (4A2)

Thermal energy group

ϕ = thermal flux volume averaged over the unit cell, 1/sec cm^2

D = thermal diffusion coefficient averaged over the unit cell, cm

$\Sigma_{f,3}$ = macroscopic spectrum averaged thermal fission cross section of U233 averaged over the unit cell, 1/cm

$\Sigma_{f,5}$ = macroscopic spectrum averaged thermal fission cross section of U235 averaged over the unit cell, 1/cm

Σ_a = total macroscopic spectrum averaged thermal absorption cross section averaged over the unit cell, 1/cm

ν_3 = number of fast neutrons produced per thermal fission in U233

ν_5 = number of fast neutrons produced per thermal fission in U235

The primary labor of any fuel cycle calculation is to solve simultaneously at each mesh point in the reactor the equations representing the neutron behavior, in this case equations (4A4) and (4A2). The problems involved in solving these equations can be divided into three broad areas as follows:

(1) Spatial approximations

(2) Nuclear properties

(3) Mathematical techniques

B. Spatial approximations

The two-group equations (4A4) and (4A2) can be represented as follows:

$$-\nabla^2\phi = Q - S\phi \qquad (4B1)$$

where

Table 4.1: Fast and Thermal Neutron Fluxes, Sources and Sinks

	Flux	Source(Q)	Sink(S)
Fast:	ϕ_1	$\frac{\epsilon \nu \Sigma_f}{D_1}\phi$	$\left[1-\epsilon\langle\bar{\eta}(1-p)\rangle\right]\frac{\Sigma_1}{D_1}$
Thermal:	ϕ	$\frac{p\Sigma_1}{D}\phi_1$	$\frac{\Sigma_a}{D}$

The usual method of numerically solving equation (4B1) is to make one volume integration and then use the divergence theorem to change the volume integral of the ∇^2-term into a surface integral, leaving it as a ∇ -term. The fluxes ultimately calculated are those at the corners of the finite volume elements and this procedure automatically takes care of the interface boundary conditions of continuous neutron fluxes and neutron currents. The ∇ -term equation is then approximated by a finite difference equation and, after the source and sink terms have been supplied,

is solved by standard procedures.

However, in this work, the finite difference approximation is made directly on the equation in ∇^2 , i.e. equation (4B1). The fluxes calculated are those at the centers of the finite volume elements and no attempt is made to equalize either interface fluxes or interface currents.

Figure 4.2 shows the mesh arrangement in a reactor quadrant with axial and radial blankets and reflectors and defines the terms in the upcoming equations. The radial mesh spacings in the core are all equal, the radial mesh spacings in the radial blanket are all equal and the radial mesh spacings in the radial reflector are all equal. The same holds true for the axial mesh spacings. The fuel properties at the center of each finite volume element are said to equal the fuel properties throughout that entire volume element.

The finite difference approximation for ∇^2 in cylindrical coordinates with no azimuthal dependence with unequal radial and axial mesh spacings is:

$$\nabla^2\phi = \frac{\partial^2\phi}{\partial r^2} + \frac{1}{r}\frac{\partial\phi}{\partial r} + \frac{\partial^2\phi}{\partial z^2} \cong$$

$$\frac{2}{\frac{1}{2}g_i + \frac{1}{4}(g_{i+1}+g_{i-1})}\left[\frac{\phi_{i+1,j}}{g_i+g_{i+1}} + \frac{\phi_{i-1,j}}{g_i+g_{i-1}} - \phi_{i,j}\left(\frac{1}{g_i+g_{i+1}} + \frac{1}{g_i+g_{i-1}}\right)\right]$$

$$+ \frac{1}{R_i - \frac{1}{2}g_i}\left[\frac{\phi_{i+1,j}}{g_i+g_{i+1}} - \frac{\phi_{i-1,j}}{g_i+g_{i-1}} + \frac{\phi_{i,j}}{g_i}\left(\frac{g_{i+1}}{g_i+g_{i+1}} - \frac{g_{i-1}}{g_i+g_{i-1}}\right)\right]$$

$$\frac{2}{\frac{1}{2}h_j + \frac{1}{4}(h_{j+1}+h_{j-1})}\left[\frac{\phi_{i,j+1}}{h_j+h_{j+1}} + \frac{\phi_{i,j-1}}{h_j+h_{j-1}} - \phi_{i,j}\left(\frac{1}{h_j+h_{j+1}} + \frac{1}{h_j+h_{j-1}}\right)\right]$$

(4B2)

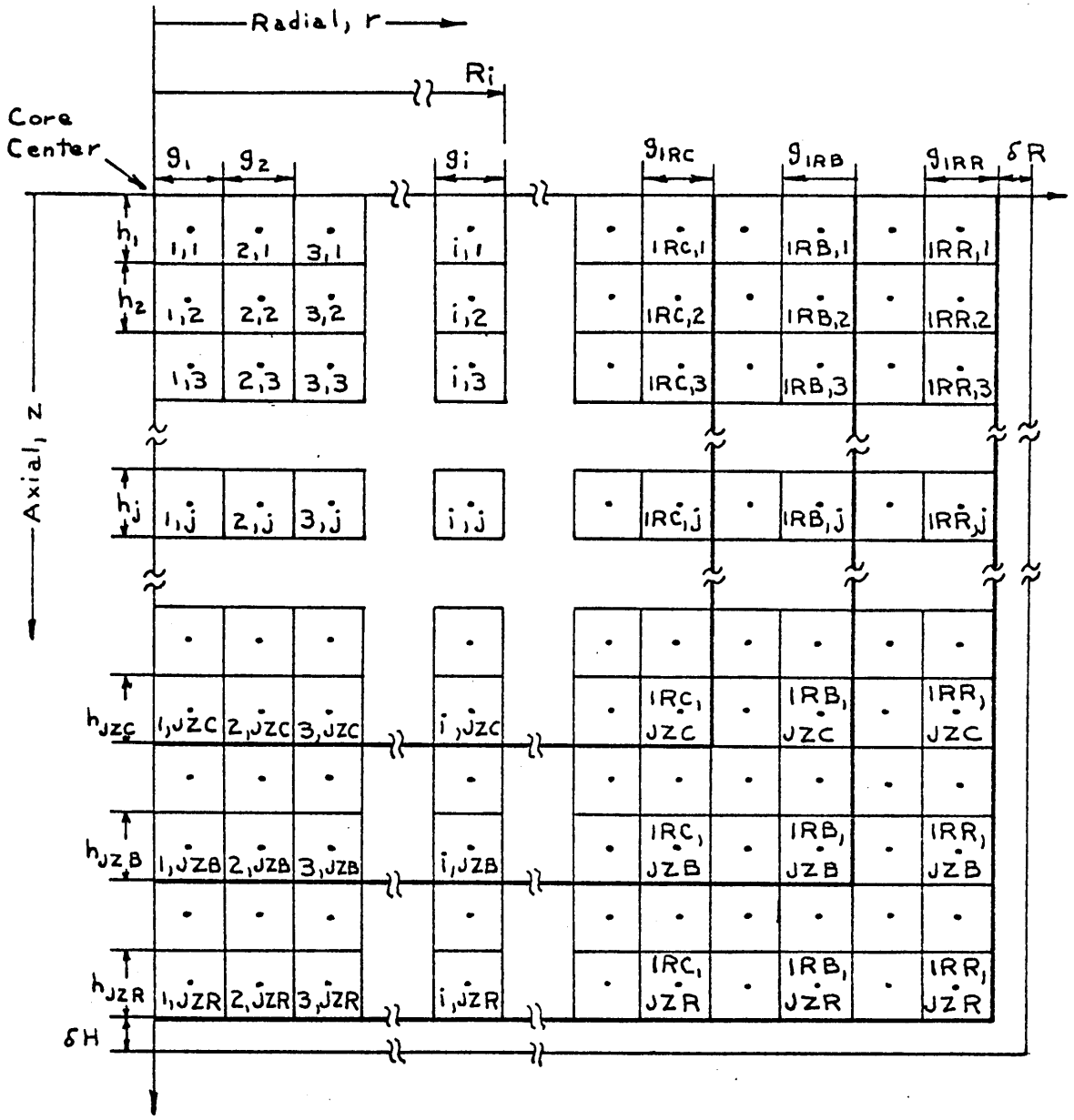

Figure 4.2: Mesh Representation of a Core Quadrant

The following purely geometric quantities are defined:

$$C152_i = \frac{-2}{g_i + g_{i+1}} \left[\frac{1}{\frac{1}{2} g_i + \frac{1}{4}(g_{i+1} + g_{i-1})} - \frac{1}{2R_i - g_i} \right] \qquad (4B3)$$

$$C153_i = \frac{-2}{g_i + g_{i+1}} \left[\frac{1}{\frac{1}{2} g_i + \frac{1}{4}(g_{i+1} + g_{i-1})} + \frac{1}{2R_i - g_i} \right] \qquad (4B4)$$

$$C15_j = \frac{-2}{[h_j + h_{j-1}]\left[\frac{1}{2} h_j + \frac{1}{4}(h_{j+1} + h_{j-1})\right]} \qquad (4B5)$$

$$C154_j = \frac{-2}{[h_j + h_{j+1}]\left[\frac{1}{2} h_j + \frac{1}{4}(h_{j+1} + h_{j-1})\right]} \qquad (4B6)$$

$$C151_{i,j} = \frac{2}{\frac{1}{2} g_i + \frac{1}{4}(g_{i+1} + g_{i-1})} \left[\frac{1}{g_i + g_{i+1}} + \frac{1}{g_i + g_{i-1}} \right]$$

$$- \frac{1}{R_i - \frac{1}{2} g_i} \left[\frac{g_{i+1} - g_{i-1}}{(g_i + g_{i+1})(g_i + g_{i-1})} \right]$$

$$+ \frac{2}{\frac{1}{2} h_j + \frac{1}{4}(h_{j+1} + h_{j-1})} \left[\frac{1}{h_j + h_{j+1}} + \frac{1}{h_j + h_{j-1}} \right]$$

$$- C_{7,i} - C_{8,j} \qquad (4B7)$$

where

$$C_{7,i} = 0 \,, \quad i \neq IRR$$

$$C_{7,i} = \frac{\delta R - \frac{1}{2} g_i}{\delta R + \frac{1}{2} g_i} \left[\frac{1}{g_i} \left(\frac{1}{\frac{1}{2} g_i + \frac{1}{4}(g_{i+1} + g_{i-1})} + \frac{0.5}{R_i - \frac{1}{2} g_i} \right) \right] , \quad i = IRR$$

δR = radial extrapolation length

$$C_{8,j} = \frac{1}{h_j \left[\frac{1}{2} h_j + \frac{1}{4}(h_{j+1} + h_{j-1}) \right]} , \quad j = 1$$

$$C_{8,j} = 0 , \quad 2 \leq j \leq JZR-1$$

$$C_{8,j} = \frac{\delta H - \frac{1}{2} h_j}{\delta H + \frac{1}{2} h_j} \left[\frac{1}{h_j} \left(\frac{1}{\frac{1}{2} h_j + \frac{1}{4}(h_{j+1} + h_{j-1})} \right) \right] , \quad j = JZR$$

δH = axial extrapolation length

(4B8)

represent the boundary conditions of flux symmetry across the reactor axis and midplane and zero fluxes at the extrapolated boundaries.

The differential equation (4B1) can now be written in finite difference form as follows:

$$\Phi_{i,j}\ [C151_{i,j}] + \Phi_{i-1,j}\ [C152_i] + \Phi_{i+1,j}\ [C153_i]$$

$$+ \Phi_{i,j-1}\ [C15_j] + \Phi_{i,j+1}\ [C154_j]$$

$$= Q_{i,j} - S_{i,j}\,\Phi_{i,j} \qquad (4B9)$$

C. Nuclear properties

As seen from table 4.1, the nuclear constants which are required are as follows:

Thermal region

$D,\ \bar{\sigma}_a,\ \bar{\sigma}_f,\ \nu$

Resonance region

$p,\ \bar{\bar{\eta}}$

Fast region

$D_1,\ \Sigma_1,\ \epsilon\,(=1)$

All regions

Fuel nuclide concentrations

1. Thermal region (0-0.414 ev)

a. Thermal diffusion coefficient, D

The thermal diffusion coefficient for the unit cell is calculated from the following equation:

$$D = \frac{1}{3\Sigma_{tr}}$$

$$= \frac{1}{3}\left[\frac{1}{\psi_o \bar{V}_o N_{ThO_2} \sigma_{tr,ThO_2} + \psi_2 \bar{V}_2 N_{Zr} \sigma_{tr,Zr} + \psi_1 \bar{V}_1 N_{D_2O} \sigma_{tr,D_2O}}\right] \qquad (4C1)$$

where

Σ_{tr} = macroscopic thermal transport cross section of the unit cell, 1/cm

σ_{tr} = microscopic thermal transport cross section

N_i = concentration of species i in its own region

$\bar{V}_i$ = volume fraction of a particular region in the unit cell (figure 4.3).

The thermal disadvantage factors ψ_o, ψ_2, ψ_1 are defined as follows:

$$\psi_o = \frac{\text{Average thermal flux in the fuel rod}}{\text{Average thermal flux in the unit cell}}$$

$$= \bar{\phi}_o \frac{V_o + V_2 + V_1}{\bar{\phi}_o V_o + \bar{\phi}_2 V_2 + \bar{\phi}_1 V_1} \qquad (4C1a)$$

$$\left.\begin{aligned}
\psi_z &= \frac{\text{Thermal flux at the surface of the fuel rod}}{\text{Average thermal flux in the unit cell}} \\
&= \phi_z \frac{V_o + V_z + V_1}{\bar{\phi}_o V_o + \phi_z V_z + \bar{\phi}_1 V_1} \\
\psi_1 &= \frac{\text{Average thermal flux in the moderator region}}{\text{Average thermal flux in the unit cell}} \\
&= \bar{\phi}_1 \frac{V_o + V_z + V_1}{\bar{\phi}_o V_o + \phi_z V_z + \bar{\phi}_1 V_1}
\end{aligned}\right\} \quad (4C1a)$$

It is assumed that the cladding causes a negligible depression of the thermal flux and therefore the thermal flux in the cladding is assumed to be that at the surface of the fuel rod.

Simple diffusion theory is used to derive the expressions for the thermal disadvantage factors.

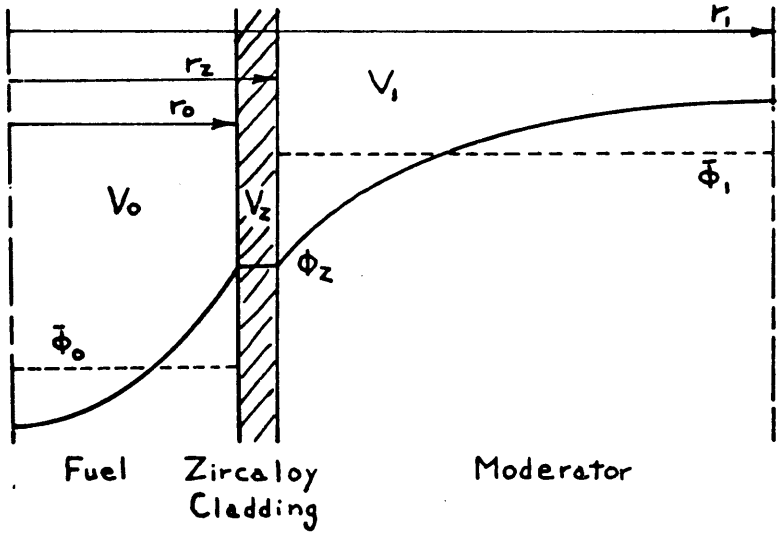

Figure 4.3: Unit Cell Parameters

The thermal utilization f is defined as follows:

$$\frac{1}{f} = \frac{\Sigma_{ao}\,\bar{\phi}_o V_o + \Sigma_{a1}\,\bar{\phi}_1 V_1 + \Sigma_{a,Zr}\,\phi_z V_z}{\Sigma_{ao}\,\bar{\phi}_o V_o}$$

$$= 1 + \left[\frac{\Sigma_{a1} V_1}{\Sigma_{ao} V_o} \cdot \frac{\bar{\phi}_1}{\bar{\phi}_o}\right] + \frac{\Sigma_{a,Zr} V_z}{\Sigma_{ao} V_o} F \qquad (4C2)$$

where

$$F \equiv \frac{\phi_z}{\bar{\phi}_o} \qquad (4C3)$$

Σ_{ao} = macroscopic 2200 m/s cross section of fuel region, 1/cm.

Σ_{a1} = macroscopic 2200 m/s cross section of moderator region, 1/cm.

$\Sigma_{a,Zr}$ = macroscopic 2200 m/s cross section of zircaloy, 1/cm.

ϕ's and V's are defined in figure 4.3.

Also from diffusion theory we have (K2)

$$\frac{1}{f} = 1 + \left[\frac{\Sigma_{a1} V_1}{\Sigma_{ao} V_o} F + (E-1)\right] + \frac{\Sigma_{a,Zr} V_z}{\Sigma_{ao} V_o} F \qquad (4C4)$$

where (E-1) is a fraction of the fuel absorptions and represents the extra absorptions in the moderator region due to the rise of the moderaor flux above the flux at the surface of the rod. By comparing equations

(4C2) and (4C4), it is seen that

$$\frac{\bar{\Phi}_1}{\bar{\Phi}_0} = F + (E-1)\frac{\Sigma_{a0} V_0}{\Sigma_{a1} V_1} \qquad (4C5)$$

By definition

$$\bar{\Phi}_{cell} = \frac{\bar{\Phi}_0 V_0 + \Phi_2 V_2 + \bar{\Phi}_1 V_1}{V_0 + V_2 + V_1} \qquad (4C6)$$

or

$$\frac{\bar{\Phi}_0}{\bar{\Phi}_{cell}} = \frac{1}{\frac{V_0}{V_{cell}} + \frac{\bar{\Phi}_1}{\bar{\Phi}_0}\frac{V_1}{V_{cell}} + \frac{\Phi_2}{\bar{\Phi}_0}\frac{V_2}{V_{cell}}} \qquad (4C7)$$

Finally

$$\psi_0 \equiv \frac{\bar{\Phi}_0}{\bar{\Phi}_{cell}} = \frac{1}{\bar{V}_0 + \left[F + (E-1)\frac{\Sigma_{a0} V_0}{\Sigma_{a1} V_1}\right]\bar{V}_1 + F\cdot\bar{V}_2} \qquad (4C8)$$

$$\psi_2 \equiv \frac{\Phi_2}{\bar{\Phi}_{cell}} = \frac{\Phi_2}{\bar{\Phi}_0}\frac{\bar{\Phi}_0}{\bar{\Phi}_{cell}} = F\cdot\psi_0 \qquad (4C9)$$

$$\psi_1 \equiv \frac{\bar{\Phi}_1}{\bar{\Phi}_{cell}} = \frac{\bar{\Phi}_1}{\bar{\Phi}_0}\frac{\bar{\Phi}_0}{\bar{\Phi}_{cell}} = \frac{\bar{\Phi}_1}{\bar{\Phi}_0}\psi_0 \qquad (4C10)$$

where $\frac{\bar{\Phi}_1}{\bar{\Phi}_0}$ is determined from equation (4C5)

Approximate expressions for F and (E-1) are as follows (A1,K1):

$$F \cong \frac{K_o r_o}{2} + \frac{16}{(K_o r_o + 4)^2} \qquad (4C11)$$

$$(E-1) \cong \frac{(K_1 r_1)^2}{2}\left[\frac{1}{1-\left(\frac{r_2}{r_1}\right)^2}\ln\left(\frac{r_1}{r_2}\right) - \frac{3}{4} + \frac{1}{4}\left(\frac{r_2}{r_1}\right)^2\right] \qquad (4C12)$$

where

K_o , K_1 = inverse thermal diffusion lengths of the fuel and moderator regions respectively, 1/cm.

r's are defined in figure 4.3.

b. Thermal cross sections, $\bar{\sigma}_a$, $\bar{\sigma}_f$

(I) Non-fuel

The hardened macroscopic thermal absorption cross sections for D_2O and zircaloy cladding are calculated as follows:

$$\bar{\Sigma}_{a,D_2O} = N_{D_2O}\,\sigma_{a,2200,D_2O}\,\psi_1\,\frac{\bar{\sigma}_{a,Th}}{\sigma_{a,2200,Th}} \qquad (4C13)$$

$$\bar{\Sigma}_{a,Zr} = N_{Zr}\,\sigma_{a,2200,Zr}\,\psi_2\,\frac{\bar{\sigma}_{a,Th}}{\sigma_{a,2200,Th}} \qquad (4C14)$$

where $\bar{\sigma}_{a,Th}$ is the absorption cross section for thorium averaged over the Wilkins spectrum. The thorium thermal absorption cross section is assumed to be a 1/v cross section only for the purpose of hardening the D_2O and zircaloy cross sections.

The resonance absorption in zircaloy is considered as a modification to its thermal absorption cross section. The resonance absorption probability is

$$\langle 1-p\rangle_{Zr} = 1 - \exp\left[\frac{-N_{Zr}\, I^{\infty}_{Zr}\, \bar{V}_Z}{\xi\, \Sigma_{s,nonfuel}\, (\bar{V}_Z + \bar{V}_1)}\right]$$

$$\cong \frac{N_{Zr}\, I^{\infty}_{Zr}\, \bar{V}_Z}{\xi\, \Sigma_{s,nonfuel}\, (\bar{V}_Z + \bar{V}_1)} \qquad (4C15)$$

where

I^{∞}_{Zr} = infinitely dilute resonance integral of zirconium

$$\xi\Sigma_{s,nonfuel} = \frac{(\xi\, \sigma_{s,epi}\, N\bar{V})_{D_2O} + (\xi\, \sigma_{s,epi}\, N\bar{V})_{Zr}}{(\bar{V}_1 + \bar{V}_Z)} \qquad (4C16)$$

Then

$$\bar{\Sigma}_{a,Zr,modified} = \bar{\Sigma}_{a,Zr}\, \bar{V}_Z + \frac{q}{\phi}\, P_1\, \langle 1-p\rangle_{Zr} \qquad (4C16a)$$

(II) Nonsaturating fission products

The nonsaturating fission products are defined as those whose microscopic thermal absorption cross sections are less than 10,000 barns. However, when the daughter of an irradiated nonsaturating fission product has a microscopic thermal cross section greater than 10,000 barns, that daughter remains with the nonsaturating fission products.

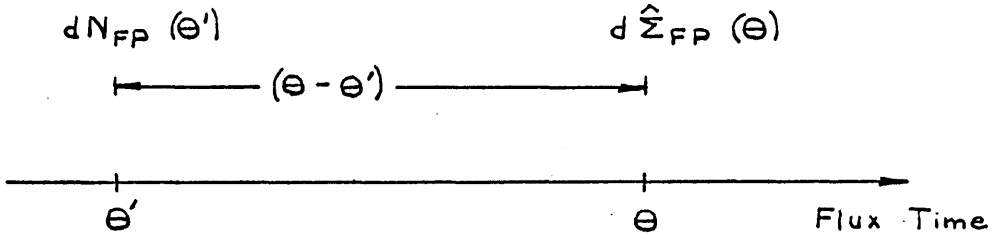

Figure 4.4: Nonsaturating Fission Products

Referring to figure 4.4, consider a group of nonsaturating fission products $dN_{FP}(\theta')$ produced at flux time θ'. The effective 2200 m/s macroscopic cross section $d\hat{\Sigma}_{FP}(\theta)$ of the fission products $dN_{FP}(\theta')$ at flux time θ, after they have been irradiated for a flux time $(\theta-\theta')$ is

$$d\hat{\Sigma}_{FP}(\theta) = \hat{\sigma}_{FP}(\theta-\theta')\, dN_{FP}(\theta') \qquad (4C17)$$

Integrating

$$\hat{\Sigma}_{FP}(\theta_o) = \int_0^{N_{FP}(\theta_o)} \hat{\sigma}_{FP}(\theta_o-\theta_o')\, dN_{FP}(\theta_o') \qquad (4C18)$$

where θ_o refers to the 2200 m/s flux time. Then, from Westcott (W6)

$$\bar{\Sigma}_{FP}(\theta_o) = \hat{\Sigma}_{FP}(\theta_o)\, \frac{\sqrt{\frac{\pi}{4}\frac{T_o}{T}}}{1-1.01\,r} \qquad (4C19)$$

where

T_o = 293 °K

T = moderator and neutron temperature, °K

r = Westcott r factor

Walker (W1,W2) has tabulated $\hat{\sigma}_{FP}(\theta_o)$ for the nonsaturating fission products of the fissile nuclides as a function of the Westcott $R(=r\sqrt{\frac{T}{T_o}})$ factor. The variation of $\hat{\sigma}_{FP}(\theta_o)$ with R is due to the resonance absorption in the nonsaturating fission products. The derivation of the Westcott r factor

is given in appendix A and the approximate evaluation of the integral (4C18) is given in section IVD.

(III) Saturating fission products

The saturating fission products are Xe135 and the "Sm" group, whose microscopic cross sections are greater than 10,000 barns. By definition, their production rate equals their destruction rate throughout the reactor. The "Sm" group includes Rh105, Cd113, Sm149, Sm151, Eu155 and Gd157.

The microscopic absorption cross sections of Xe and the"Sm" group are calculated as described in the next section for the fuel nuclides, although it is not necessary that a value for the "Sm" group be calculated at all. For Xe135, however, it is necessary that a value of the microscopic absorption cross section be calculated because its absorption rate has to be compared with its radioactive decay rate.

(IV) Other fuel nuclides

The nuclides whose microscopic absorption cross section remain to be calculated are Th232(abs), Pa233(abs), U233(abs and fiss), U234(abs), U235(abs and fiss), U236(abs) and Np237(abs). These cross sections must be averaged over the prevailing neutron energy spectrum in the thermal region which extends from 0 to 0.414 ev.

It is assumed that the neutron energy spectrum in the thermal region is that obtained from the solution of the Wilkins equation. Shanstrom (S1) discusses this assumption as well as the thermal cutoff energy of about 0.414 ev. The Wilkins equation is

$$x^2 \frac{d^2Y}{dx^2} + (2x^3 - 3x)\frac{dY}{dx} + (2x^2 - 4x^2 A(x) + 3)Y = 0 \qquad (4C20)$$

where

$x = \sqrt{\frac{E}{kT_{mod}}}$, the normalized velocity at energy E

kT_{mod} = neutron energy at moderator temperature T_{mod}. The neutron temperature and moderator temperature are assumed to be equal.

$Y = \frac{d\phi}{dx}$, the flux per unit velocity

$A(x) = \frac{\Sigma_a(x)}{\xi \Sigma_s}$, the hardening parameter at normalized velocity x

$$\Sigma_a(x) = \frac{\sum_{\text{Unit cell}}^{\text{All nuclides in unit cell}} N_i \sigma_{a_i}(x) \bar{V}_i \Psi_i}{\sum \bar{V}_i} \qquad (4C21)$$

= the total homogonized macroscopic cross section of the unit cell evaluated at the normalized velocity x

$\xi \Sigma_s$ = slowing down power of the unit cell

The solution of the Wilkins equation and the properties of the resulting spectrum are given by Shanstrom (S1).

After the Wilkins equation has been solved for $Y = \frac{d\phi}{dx}$, the hardened microscopic cross sections of the fuel nuclides mentioned above are then calculated by the following equation:

$$\bar{\sigma}_i = \frac{\int_0^{0.414\ ev} \frac{d\phi}{dx}\, \sigma_i(x)\, dx}{\int_0^{0.414\ ev} \frac{d\phi}{dx}\, dx} \qquad (4C22)$$

Values of the cross sections $\sigma_i(x)$ for the fuel nuclides for use in equations (4C21) and (4C22) were obtained from the Oak Ridge National Laboratory (G1,G2,G3) and are the same as were used in ORNL-3686.

Since the values of $\bar{\sigma}_i$ do not vary greatly from point to point in the reactor, they are calculated explicitly at only three mesh points in each of the core, radial blanket and axial blanket, i.e. at the numbered locations in figure 4.5. Linear interpolation is then used to obtain the values of $\bar{\sigma}_i$ at other mesh points in each of these three regions.

c. Fast neutrons produced per thermal fission, ν

The values of ν for U233 and U235 were also obtained from ORNL(G1). The value for U233 is 2.503 and the value for U235 is 2.430.

2. Resonance region

a. Resonance escape probability, p

The resonance escape probability for each fuel nuclide is calculated by the equation

$$p_i = \exp\left[\frac{-N_i\, I^i_{eff}\, \bar{V}_0}{\xi\, \Sigma_{s,nonfuel}\,(1-\bar{V}_0)}\right] \qquad (4C23)$$

where

I^i_{eff} = effective resonance absorption integral of nuclide, i.

The values of I^i_{eff} for the dilute fuel nuclides Pa233, U233, U234, U235, U236 and Np237 and the concentrated fuel nuclide ThO_2 are calculated as described below.

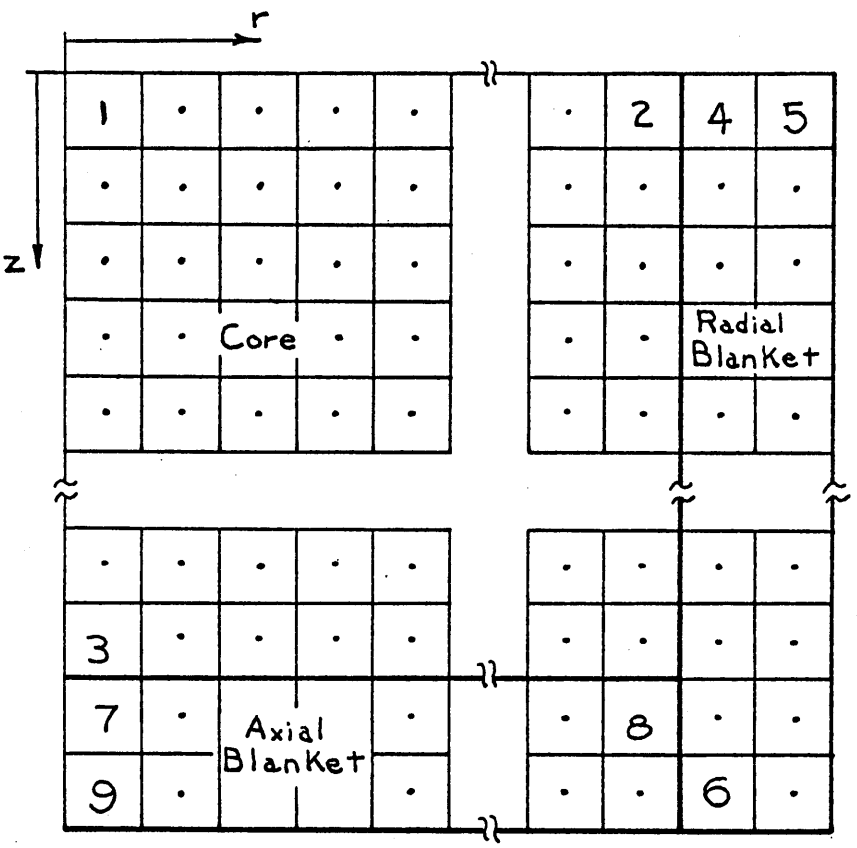

Figure 4.5: Reactor Quadrant Showing Locations of Mesh Points Where the Fuel Microscopic Cross Sections Are Averaged over the Wilkins Spectrum

(I) Dilute effective absorption resonance integrals, $I^i_{eff,\ dilute}$

(A) Derivation of second equivalence theorem

The heterogeneous effective resonance integrals of the dilute fuel nuclides are calculated by means of the second equivalence theorem as described by Dresner (D2).* This theorem states that the effective resonance integral of an absorber in a lump of fuel is the same as that for a homogeneous mixture of moderator and the same absorber in which the moderator potential scattering cross section per absorber nucleus (σ_M) of the homogeneous mixture equals $\left[\sigma_m + \frac{1}{N\bar{l}}\right]$ of the lump of fuel, where σ_m is the potential scattering cross section of any diluent of low atomic weight (oxide, carbide) in the lump per absorber nucleus, N is the concentration in the fuel of the absorber of interest and $\bar{l}$ is the average chord length in the lump. Dresner's derivation was for the case in which the absorber of interest was the only absorber of high atomic weight in the lump. The derivation given below considers the effect on the effective resonance integral of the absorber of interest of the other heavy absorbers in the lump. The derivation of the effective resonance integral given below is for a single resonance in the absorber of interest. The effective resonance integral of the absorber of interest over the entire resonance region is obtained by summing the effective resonance integrals of all of the resonances of the absorber of interest.

The assumptions made in the derivation are:

1. Each resonance is very wide compared to the energy loss per collision

---

*The equivalence theorem is also discussed in the following references, among others: C1,G7,G8,L1,L2,M4.

with a heavy absorber nucleus (Narrow Resonance Infinite Absorber or NRIA approximation). This means that scattering by the heavy absorbers produces a change in direction but not in energy.

2. Each resonance is very narrow compared to the energy loss per collision with the surrounding moderator or a lump diluent of low atomic weight (e.g. oxygen). Thus for the purpose of the calculation of resonance absorption, the potential scattering cross section of the lump diluent can be treated as an absorption cross section.

3. Because of 1 and 2, monoenergetic transport theory is applicable in the lump with scattering by the heavy absorber nuclei treated as scattering, and all other processes treated as absorption.

4. The resonance flux per unit lethargy $\phi(u)$ is constant throughout the lump and moderator both spatially (flat flux) and lethargywise (1/E flux).

5. Wigner's rational approximation for the escape probability from a lump holds.

6. There is no interaction among lumps (no Dancoff effect, H3).

Referring to figure 4.6, consider first those neutrons which appear in the lethargy interval du around the resonance lethargy u in the lump and whose last moderating collision was with a lump diluent nucleus. The source of these neutrons in du is independent of whether or not there is a resonance in du. If there were no resonance in du, the source would equal the sink which would equal $\Sigma_m \phi(u)$

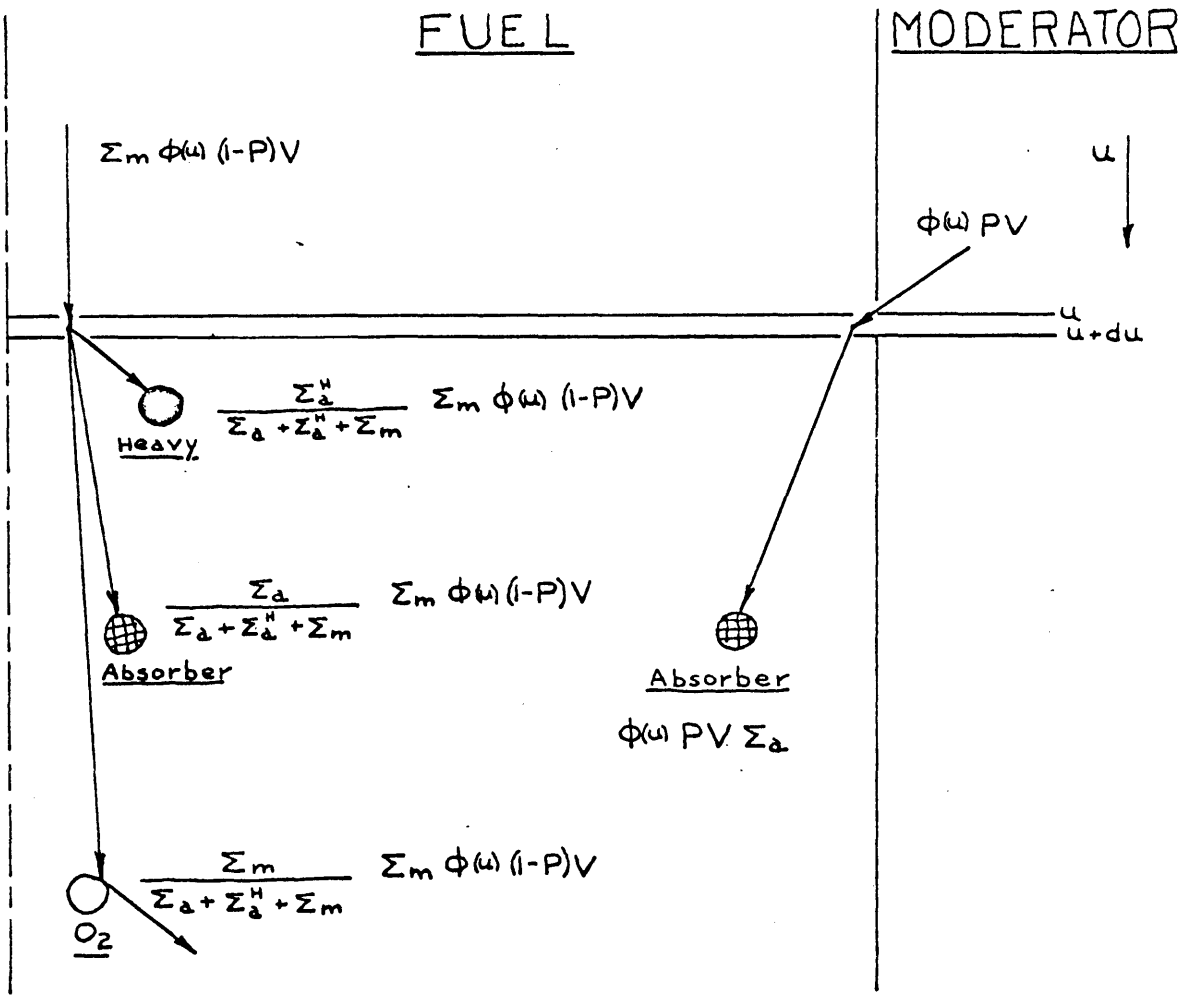

Figure 4.6: Fuel Lump and Moderator for the Derivation of the Second Equivalence Theorem of Resonance Absorption

where

Σ_m = the potential scattering cross section of the lump diluent

$\phi(u)$ = flux per unit lethargy

The number of these source neutrons in du which have their next collision in the lump is

$$\Sigma_m \phi(u) (1-P) V \qquad (4C24)$$

where

P = escape probability from a spatially uniform source in the lump

V = lump volume

The number of these source neutrons in du which are absorbed by the absorber of interest is

$$\frac{\Sigma_a}{\Sigma_a + \Sigma_a^H + \Sigma_m} \Sigma_m \phi(u) (1-P) V \qquad (4C25)$$

where

Σ_a^H = macroscopic absorption cross section of all heavy absorbers in the lump other than the absorber of interest

Σ_a = macroscopic absorption cross section of the absorber of interest in the lump

Consider now those neutrons which appear in du around u whose last moderating collision was with a moderator nucleus outside of the lump. According to monoenergetic transport theory (D2), the flux of neutrons in the lump which made their last collision in the moderator is

$$\phi(u) P \qquad (4C26)$$

The number of these neutrons which are absorbed by the absorber of interest is

$$\Sigma_a \phi(u) PV \tag{4C27}$$

The resonance integral is defined as that cross section which, when multiplied by the flux which would exist in the absence of the resonance, gives the true absorption rate. The effective resonance integral I_u for the resonance in du around u is thus given by

$$N I_u V \phi(u) = \int_0^\infty du \left[\frac{\Sigma_a}{\Sigma_a + \Sigma_a^H + \Sigma_m} \Sigma_m \phi(u) (1-P) V + \Sigma_a \phi(u) P V \right] \tag{4C28}$$

or

$$I_u = \int_0^\infty du \left[\frac{\sigma_a}{\sigma_a + \sigma_a^H + \sigma_m} \sigma_m (1-P) + \sigma_a P \right] \tag{4C29}$$

where

σ_a = microscopic absorption cross section of the absorber of interest

σ_a^H = macroscopic absorption cross section of the other heavy absorbers in the lump per atom of the absorber of interest

σ_m = macroscopic potential scattering cross section of the lump diluent per atom of the absorber of interest

Wigner's rational approximation gives for the escape probability from the lump

$$P = \frac{b-1}{b + \frac{\sigma_a^H}{\sigma_m} + \frac{\sigma_a}{\sigma_m}} \qquad (4C30)$$

where

$$b = 1 + \frac{1}{N\bar{l}\sigma_m}$$

where

N = concentration of the absorber of interest

$\bar{l}$ = average chord length in the lump = $\frac{4V}{S}$ for a cylindrical rod.

Substitution of equation (4C30) into equation (4C29) gives the final result:

$$I_u = \int_0^\infty du \left\{ \left[\frac{\sigma_a (b\sigma_m)}{\sigma_a + (b\sigma_m)} \right] \left[\frac{1}{1 + \frac{\Sigma_a^H}{N(b\sigma_m) + \Sigma_a}} \right] \right\} \qquad (4C32)$$

The first term in brackets in the integrand of equation (4C32) is the integrand of the homogeneous resonance integral in the NRIA approximation with $\left[b\sigma_m = \sigma_m + \frac{1}{N\bar{l}}\right]_{\text{Heterogeneous}}$ substituted for $[\sigma_M]_{\text{Homogeneous}}$. This is the basis for the second equivalence theorem, as previously stated. The second term in brackets in equation (4C32) corrects for the effect of the other heavy nuclides on the effective resonance integral of the absorber of interest.

An equation similar to equation (4C32) could be derived for the case

in which each resonance of the absorber of interest is very narrow compared to the energy loss per collision with an absorber nucleus (Narrow Resonance or NR approximation). However, when there are heavy absorbers in the lump other than the absorber of interest, as is the case in this work, the parameter for equivalence between the homogeneous and heterogeneous effective resonance integrals is not the same for the NR and NRIA approximations. By comparing the energy loss per collision with an absorber nucleus with the practical width (N2,W4,W5) of each resonance of each of the six dilute fuel nuclides, it was found that the following percentages of resonance absorptions took place in resonances in which the NR approximation held:

Pa233	0
U233	0
U234	3.2%
U235	1.7%
U236	2.6%
Np237	0

In addition, the equation for the calculation of the contribution of the 1/v portion of the resonance region to the effective resonance integral is identical to the equation for the NRIA approximation (K1). Therefore the NRIA approximation was used throughout the resonance region for each of the six dilute fuel nuclides.

Equation (4C32) applies to a single resonance in the absorber of interest. The effective resonance absorption integral of the absorber of interest, I^{i}_{eff}, over the entire resonance region is obtained by summing the effective resonance absorption integrals of all of the resonances of the absorber of interest as in equation (4C32a):

$$I^i_{eff} = \sum_{0.414\,ev}^{10^7\,ev} I_u$$

$$= \sum_{0.414\,ev}^{10^7\,ev} \left\{ \int_0^\infty du \left[\frac{\sigma_a (b\sigma_m)}{\sigma_a + (b\sigma_m)} \right] \left[\frac{1}{1 + \frac{\Sigma_a^H}{N(b\sigma_m) + \Sigma_a}} \right] \right\} \qquad (4C32a)$$

Since almost all of the contribution to the effective resonance integral of a single resonance comes from the immediate vicinity of the resonance, du can be replaced by Δu and the integration sign in equation (4C32a) deleted:

$$I^i_{eff} \cong \sum_{0.414\,ev} \left\{ \Delta u \left[\frac{\sigma_a (b\sigma_m)}{\sigma_a + (b\sigma_m)} \right] \left[\frac{1}{1 + \frac{\Sigma_a^H}{N(b\sigma_m) + \Sigma_a}} \right] \right\} \qquad (4C32b)$$

In this work, the effect of the other heavy absorbers in the lump on the effective resonance integral of the absorber of interest is neglected. That is, the second equivalence theorem is applied to each dilute absorber as if that absorber were the only one in the lump. This procedure is justified by the following considerations:

1. For a 16x15 mesh, which is used in most of this work, it is necessary that 8,640 effective resonance integrals be calculated for the dilute nuclides for each sweep through the reactor during a burnup calculation. By neglecting the effect of the other heavy absorbers, these effective resonance integrals can be calculated independently as a function of $[\sigma_M]_{Homogeneous}$. These results can then be fitted by polynomials

which can be used during a burnup calculation for the rapid determination of the 8,640 effective resonance integrals as a function of $\left[\sigma_m + \frac{1}{N\bar{l}}\right]_{\text{Heterogeneous}}$.

If equation (4C32b) were to be used directly for the determination of these 8,640 effective resonance integrals in a burnup calculation, an enormous amount of computer time would be required. About 30 minutes of IBM 7094 computer time are required for each case when the effect of the other heavy nuclides is neglected. The direct use of equation (4C32b) would probably double that computer time requirement.

2. With the nuclide concentrations encountered in this work, the neglect of the effect of the other heavy absorbers overestimates (relative to equation (4C32b)) the effective resonance integrals of the dilute nuclides by the following approximate amounts:

Pa233	20%
U233	10%
U234	10%
U235	25%
U236	35%
Np237	25%

However, reference (C1) states that the use of the equivalence theorem for a single absorber in a lump underestimates the heterogeneous effective resonance integral by about 10%. This is due primarily to the use of Wigner's rational approximation for the escape probability from a lump.

These errors thus approximately cancel one another in the cases of U233 and U234, which are major dilute resonance absorbers. Due to their

low concentrations, Pa233, U235, U236 and Np237 are only minor absorbers of resonance neutrons and the errors in their effective resonance integrals cause a negligible effect on the overall neutron balance and conversion ratio.

3. Experience has shown that considerable uncertainty exists in resonance data even from the most reliable sources. For example there exists in the literature a discrepancy of 10% in the infinitely dilute absorption resonance integral of U235 which is probably the most carefully and thoroughly studied of all the fuel nuclides. Since it is not the purpose of this work to develop a precise method for calculating effective resonance integrals but rather to calculate effective resonance integrals with the currently available data, it is felt that the method used is adequate.

4. No doppler correction is applied to the effective resonance integrals of the six dilute fuel nuclides. Since the calculational procedure probably overestimates the effective resonance integrals, the neglect of the doppler broadening decreases this error.

(B) Homogeneous effective resonance integrals

For the calculation of the homogeneous effective resonance integrals as a function of σ_M, equation (4C32b) is approximated by the following equation:

$$I^i_{eff} \cong \sum_{0.414\,ev}^{10^7\,ev} \Delta u \left[\frac{\sigma_a \sigma_M}{\sigma_a + \sigma_M}\right]_{Homogeneous} \qquad (4C33)$$

The values of σ_a vs. Δu for U233(absorption) are shown in figure 4.7 (G1). The cross sections are averaged over 68-0.25 lethargy intervals from 0.414 to 10^7 ev and include both the resonance and 1/v contributions. Resonance data in this form for all nuclides were obtained from Oak Ridge National Laboratory and are the same as were used in ORNL-3686 (G1).

Lethargy intervals 6 and 13 of U233(absorption) each contain more than one resonance. It is necessary to divide each of these lethargy intervals into smaller intervals which approximately cover each separate resonance before substituting the data into equation (4C33). The two data for each resonance which are needed for this division are the peak cross section and the practical width.

1. Peak cross section, σ_o – The peak cross section is defined by Hughes and Schwartz (H4). The data necessary for its calculation came from reference (G1).

2. Practical width - The practical width is due to Wigner (W4,W5) and is defined as the width of the Breit-Wigner resonance at the point where the absorption cross section equals the potential scattering cross section of the absorber (N2), as shown in figure 4.8.

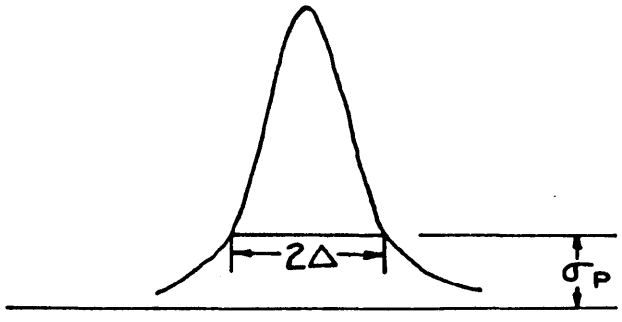

Figure 4.8: A Resonance Peak

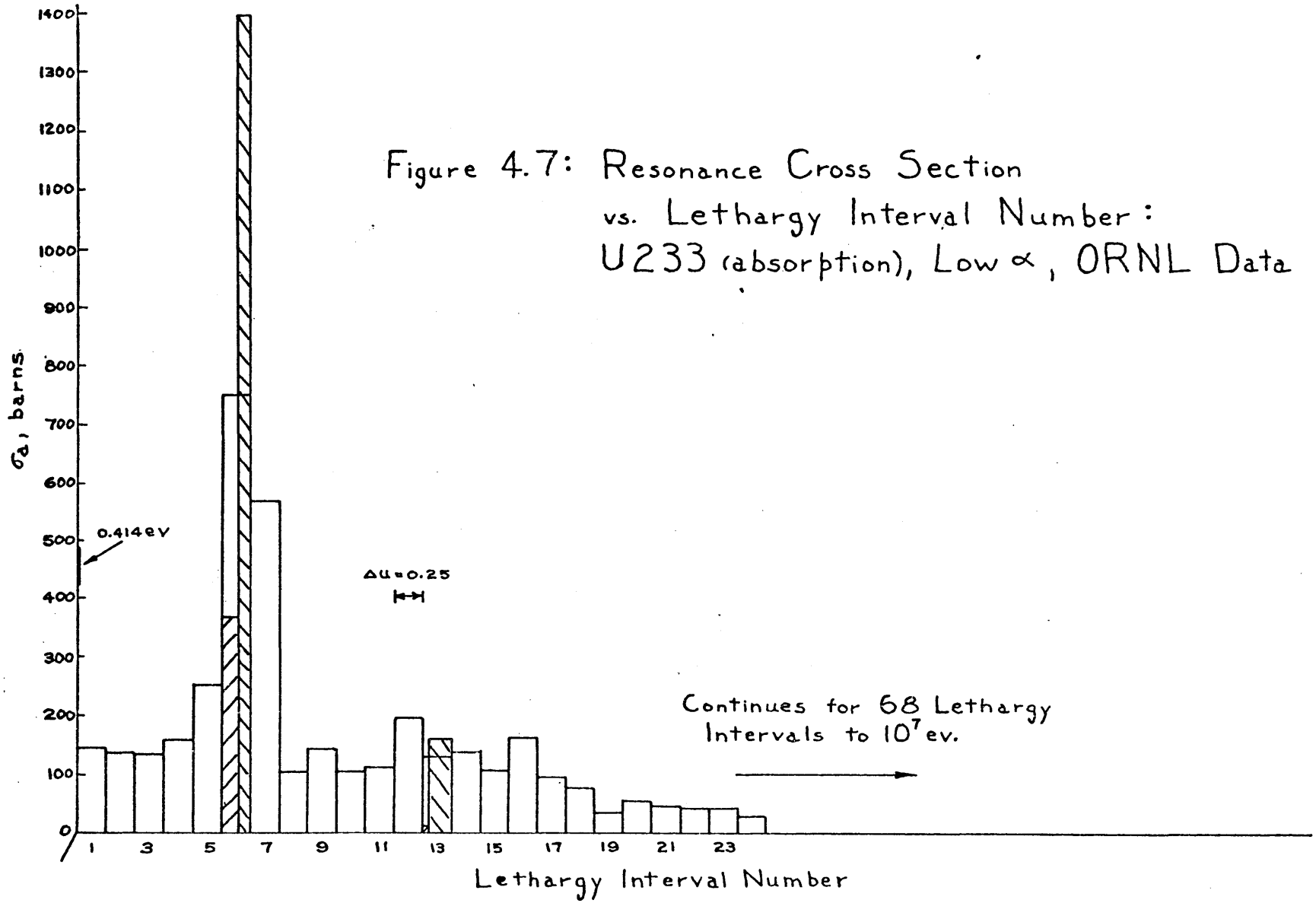

Figure 4.7: Resonance Cross Section vs. Lethargy Interval Number: U233 (absorption), Low α, ORNL Data

$$2\Delta = \Gamma \sqrt{\frac{\sigma_o}{\sigma_p} - 1} \qquad (4C34)$$

where

2Δ = practical width of resonance

Γ = total width of the resonance at half maximum

σ_o = peak cross section of the resonance

σ_p = potential scattering cross section of the resonance absorber

A lethargy interval which contains more than one resonance is then divided into lethargy intervals whose widths are proportional to the practical widths of the resonances, whose heights are proportional to the peak cross sections of the resonances and whose total lethargy integral in unchanged. This division for intervals 6 and 13 for U233 is shown on figure 4.7. Similar divisions were made for the other five dilute nuclides.

The homogeneous effective resonance integrals are then calculated as a function of σ_M for each of the six dilute nuclides by the use of equation (4C33). Cross sections used in this calculation are given in appendix B. The results for U233 are shown in figure 4.9 in the form of a plot of the effective resonance integral I^i_{eff} versus the potential scattering cross section per absorber atom σ_M . Fourth order polynomials are fitted to plots of effective resonance integrals versus $1/[\sigma_M]_{Homogeneous}$ and are used for the determination of the

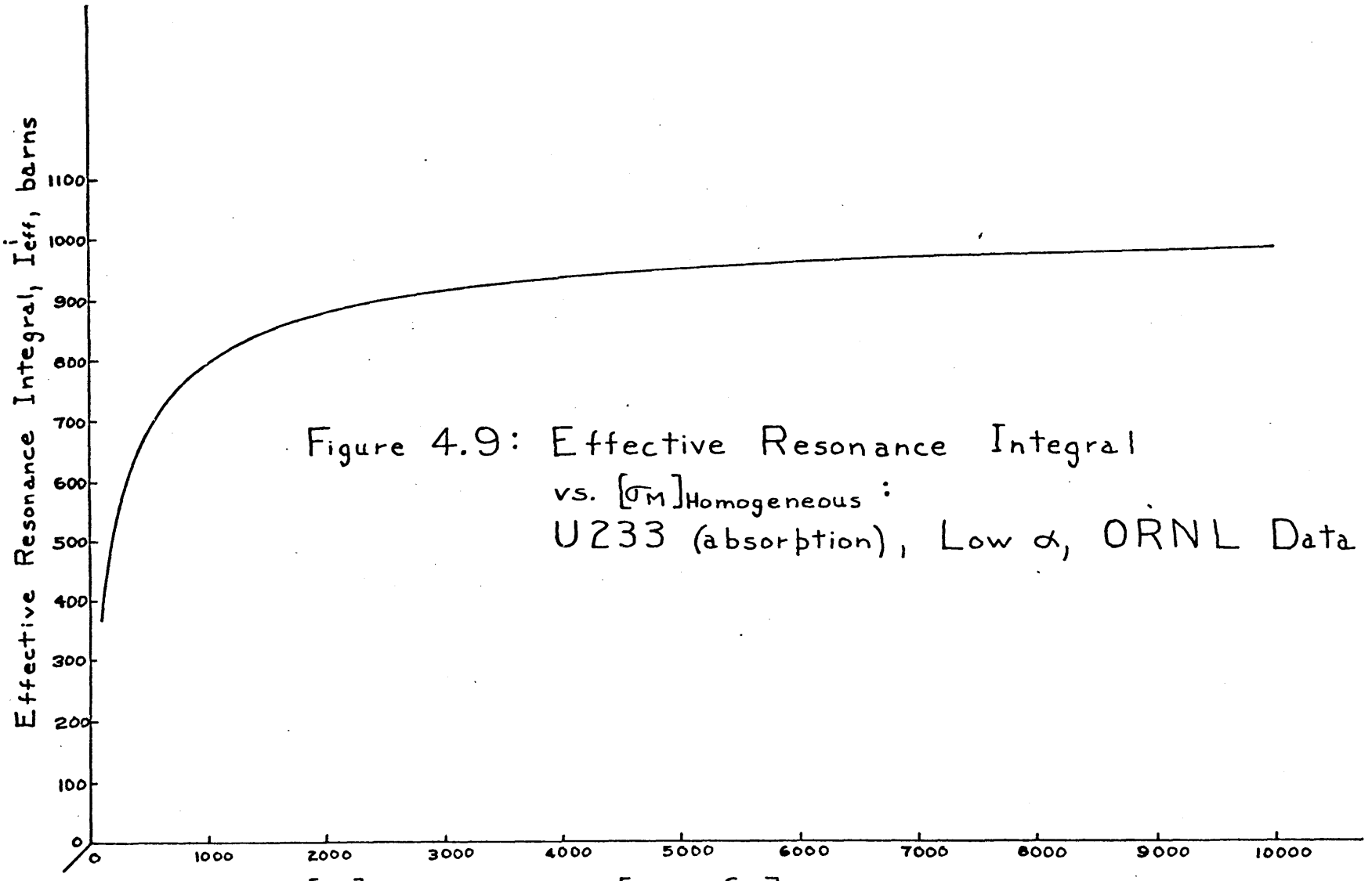

Figure 4.9: Effective Resonance Integral vs. $[\sigma_M]_{Homogeneous}$: U233 (absorption), Low α, ORNL Data

heterogeneous effective resonance integrals in the burnup calculations. The heterogeneous equivalence parameter can be reduced as follows:

$$\left[\sigma_m + \frac{1}{N\bar{l}}\right]_{Heterogeneous} = \left[\frac{\Sigma_{s,O_2} + \frac{1}{D_{rod}}}{N}\right]_{Heterogeneous} \quad (4C35)$$

where

Σ_{s,O_2} = macroscopic scattering cross section of the oxygen in the fuel rod

D_{rod} = fuel rod diameter

(II) Effective resonance integral of ThO_2

The effective resonance integral of ThO_2 is calculated from the Weitman experimental equation (W3):

$$I_{ThO_2}\,(\text{barns}) = 6.4 + 15.5\sqrt{\frac{S}{M_{ThO_2}}} \pm 5\%, \quad 0.15 \leq \frac{S}{M_{ThO_2}} \leq 0.65 \qquad (4C36)$$

where

S/M_{ThO_2} = surface area/mass of ThO_2, cm^2/gm

For $S/M_{ThO_2} < 0.15$, Weitman suggests

$$I_{ThO_2}\,(\text{barns}) = 20.4\sqrt{0.22 + \frac{S}{M_{ThO_2}}} + 0.1, \quad \frac{S}{M_{ThO_2}} < 0.15 \qquad (4C37)$$

Both of these equations include the 1/v contribution and were obtained at 20°C (T_o).

Corrections for the doppler broadening of ThO_2 were made with the Crowther calculated equation (C4):

$$\left(\frac{I}{I_o}\right)_{ThO_2} = 0.6427 + \left[0.4007 - 0.01809\sqrt{\frac{M_{ThO_2}}{S}}\right]\sqrt{\frac{T}{T_o}}$$

$$+ 0.01774\sqrt{\frac{T_o}{T}}\sqrt{\frac{M_{ThO_2}}{S}} - 0.04309\,\frac{T}{T_o},$$

$$0.2 \leq \frac{S}{M_{ThO_2}} \leq 2.0, \qquad 293\,°K \leq T \leq 1500\,K$$

(4C38)

where

$(I/I_o)_{ThO_2}$ = effective resonance integral of ThO_2 at temperature T divided by effective resonance integral of ThO_2 at temperature T_o (20 °C)

(III) Other resonance parameters

Some other resonance parameters are indicated in figure 4.10. The α values above and below 5 ev for U233 and U235 are calculated as follows:

$$\alpha_{upper,i} = \frac{\sum_{5ev}^{10^7 ev} \sigma_{a,i}\ \Delta u}{\sum_{5ev}^{10^7 ev} \sigma_{f,i}\ \Delta u} - 1 \qquad (4C39)$$

$$\alpha_{lower,i} = \frac{\sum_{0.414ev}^{5ev} \sigma_{a,i}\ \Delta u}{\sum_{0.414ev}^{5ev} \sigma_{f,i}\ \Delta u} - 1 \qquad (4C40)$$

where

$\sigma_{a,i}$ = microscopic resonance absorption cross section as a function of lethargy, u (G1)

$\sigma_{f,i}$ = microscopic resonance fission cross section as a function of lethargy, u (G1)

The fraction of the resonance absorption which occurs above 5 ev in Pa233, U233, U235 and Np237 is listed in figure 4.10. This quantity is calculated

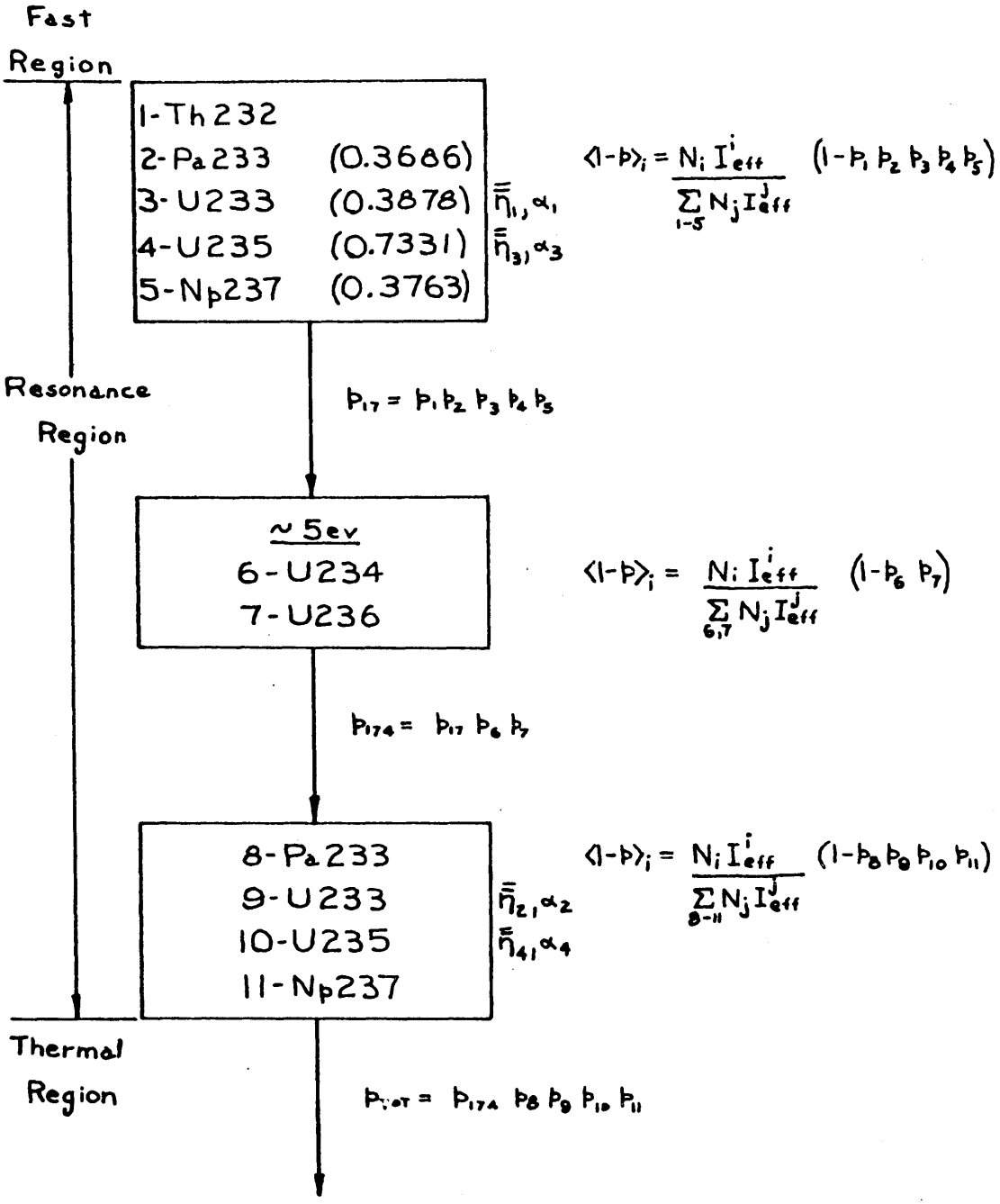

Figure 4.10: Miscellaneous Resonance Parameters

as follows:

$$f_i = \frac{\sum_{5ev}^{10^7 ev} \sigma_{a,i}\ \Delta u}{I_i^{\infty}} \qquad (4C41)$$

where

I_i^{∞} = infinitely dilute resonance integral of nuclide i (G1)

b. Number of fission neutrons produced per resonance absorption in a fissile atom, $\bar{\bar{\eta}}_j$

The quantities $\bar{\bar{\eta}}_j$ are indicated in figure 4.10. The $\bar{\bar{\eta}}_j$ values above and below 5 ev for U233 and U235 are calculated as follows:

$$\bar{\bar{\eta}}_j = \frac{\sum_{5ev}^{10^7 ev} \sigma_{f,i}\ \nu_i\ \Delta u}{\sum_{5ev}^{10^7 ev} \sigma_{a,i}\ \Delta u}, \quad \begin{cases} j = 1 \text{ for U233 above 5 ev} \\ j = 3 \text{ for U235 above 5 ev} \end{cases} \qquad (4C42)$$

$$\bar{\bar{\eta}}_j = \frac{\sum_{0.414\,ev}^{5 ev} \sigma_{f,i}\ \nu_i\ \Delta u}{\sum_{0.414ev}^{5ev} \sigma_{a,i}\ \Delta u}, \quad \begin{cases} j = 2 \text{ for U233 below 5 ev} \\ j = 4 \text{ for U235 below 5 ev} \end{cases} \qquad (4C43)$$

where

ν_i = number of fission neutrons produced per resonance fission by neutrons of various resonance energies (G1)

At thermal energies, the values of ν used are 2.430 for U235 and 2.503 for U233.

3. Fast region

a. Fast diffusion coefficient, D_1

The fast diffusion coefficient is calculated by adjusting of the value of D_1 for heavy water to allow for the volume fractions of ThO_2 and zircaloy (A1,K2):

$$(D_1)_{cell} = \frac{(\lambda_{tr,1})_{cell}}{3} = \frac{1}{3\,(\Sigma_{tr,1})_{cell}}$$

$$= \frac{(D_1)_{D_2O}}{\bar{V}_{D_2O}} \frac{1}{\left[\dfrac{(\bar{V}\,\Sigma_{tr,1})_{D_2O} + (\bar{V}\,\Sigma_{tr,1})_{ThO_2} + (\bar{V}\,\Sigma_{tr,1})_{Zr}}{(\bar{V}\,\Sigma_{tr,1})_{D_2O}}\right]}$$

$$= \frac{1}{3(\bar{V}\,\Sigma_{tr,1})_{D_2O}} \frac{(\bar{V}\,\Sigma_{tr,1})_{D_2O}}{(\bar{V}\,\Sigma_{tr,1})_{cell}} = \frac{1}{3\,(\Sigma_{tr,1})_{cell}} \qquad (4C44)$$

where

$\bar{V}_i$ = volume fraction of region i in unit cell

and subscript 1 refers to the fast group. The other symbols have their usual meanings.

b. Fast removal constant, Σ_1

The fast removal constant is calculated by the equation

$$(\Sigma_1)_{cell} = (D_1)_{cell} \Big/ \tau_{cell} \qquad (4C45)$$

The age τ_{cell} is calculated by adjusting of the value of τ for D_2O to allow for the volume fractions of ThO_2 and zircaloy (Al,K2):

$$\tau_{cell} = \frac{(D_1)_{cell}}{(\Sigma_1)_{cell}} = \frac{\frac{1}{3(\Sigma_{tr,1})_{cell}}}{(\Sigma_1)_{cell}}$$

$$= \frac{\tau_{D_2O}}{\bar{V}^2_{D_2O}} \frac{1}{\left[\frac{(\bar{V}\xi\Sigma_s)_{D_2O} + (\bar{V}\xi\Sigma_s)_{ThO_2} + (\bar{V}\xi\Sigma_s)_{Zr}}{(\bar{V}\xi\Sigma_s)_{D_2O}}\right]\left[\frac{(\bar{V}\Sigma_{tr,1})_{D_2O} + (\bar{V}\Sigma_{tr,1})_{ThO_2} + (\bar{V}\Sigma_{tr,1})_{Zr}}{(\bar{V}\Sigma_{tr,1})_{D_2O}}\right]}$$

$$= \frac{\frac{1}{(\bar{V}\Sigma_{tr,1})_{D_2O}}}{(\bar{V}\Sigma_1)_{D_2O}} \frac{\frac{(\bar{V}\Sigma_{tr,1})_{D_2O}}{(\bar{V}\Sigma_{tr,1})_{cell}}}{\frac{(\bar{V}\xi\Sigma_s)_{cell}}{(\bar{V}\xi\Sigma_s)_{D_2O}}} = \frac{\frac{1}{3(\Sigma_{tr,1})_{cell}}}{(\Sigma_1)_{cell}}$$

(4C46)

where

$\xi\Sigma_s$ = resonance slowing down power

c. Fast fission factor, ϵ

The fast fission factor is set equal to unity throughout this work. This is because Th232 fast fission adds at most a few tenths of a percent

to the fast source and its fast fission constants are not well known.

4. Fuel nuclide concentrations

The fuel nuclide reaction chain is shown in figure 4.11. Concentrations of Th233, Pa234 and U237 have been treated as negligibly small because of their short half-lives. The reaction rate equations for the fuel nuclides are as follows:

$$\text{Th232:}\quad \frac{dN_1}{dt} = -N_1 \bar{\sigma}_{a1} \phi - \frac{q}{V_{f1}} \left[P_1 \langle 1-p \rangle_1 \right] \qquad (4C47)$$

$$\text{Pa233:}\quad \frac{dN_2}{dt} = N_1 \bar{\sigma}_{a1} \phi - N_2 \left[\bar{\sigma}_{a2} + \frac{\lambda_{Pa}}{\phi} \right] \phi$$

$$+ \frac{q P_1}{V_{f1}} \left[\langle 1-p \rangle_1 - \langle 1-p \rangle_2 - p_{174} \langle 1-p \rangle_8 \right] \qquad (4C48)$$

$$\text{U233:}\quad \frac{dN_3}{dt} = \lambda_{Pa} N_2 - N_3 \bar{\sigma}_{a3} \phi$$

$$- \frac{q P_1}{V_{f1}} \left[\langle 1-p \rangle_3 + p_{174} \langle 1-p \rangle_9 \right] \qquad (4C49)$$

$$\text{U234:}\quad \frac{dN_4}{dt} = \left[N_3 (\bar{\sigma}_{a3} - \bar{\sigma}_{f3}) + N_2 \bar{\sigma}_{a2} - N_4 \bar{\sigma}_{a4} \right] \phi$$

$$+ \frac{q P_1}{V_{f1}} \left[\langle 1-p \rangle_3 \frac{\alpha_1}{1+\alpha_1} + p_{174} \langle 1-p \rangle_9 \frac{\alpha_2}{1+\alpha_2} + \langle 1-p \rangle_2 \right.$$

$$\left. + p_{174} \langle 1-p \rangle_8 - p_{17} \langle 1-p \rangle_6 \right] \qquad (4C50)$$

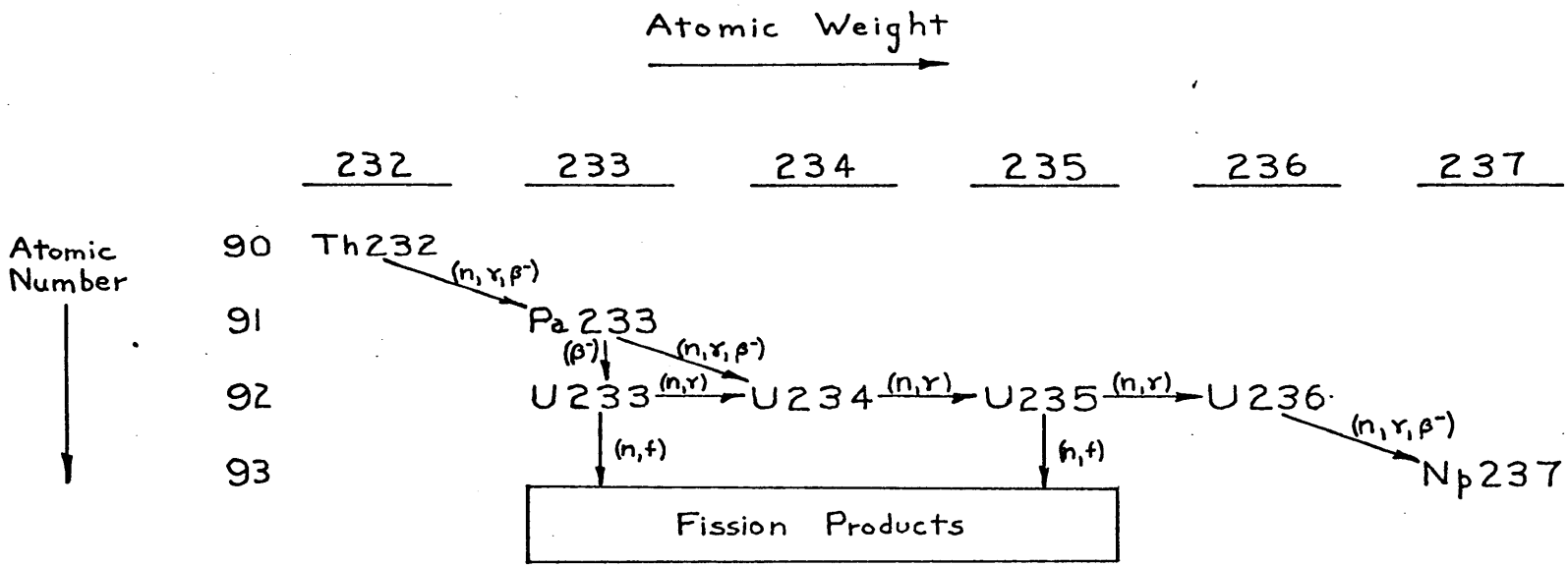

Figure 4.11: Fuel Reaction Chain

U235: $$\frac{dN_5}{dt} = \left[N_4 \bar{\sigma}_{a4} - N_5 \bar{\sigma}_{a5}\right]\phi$$

$$+ \frac{q P_1}{V_{f1}}\left[p_{17}\langle 1-p\rangle_6 - \langle 1-p\rangle_4 - p_{174}\langle 1-p\rangle_{10}\right]$$

(4C51)

U235: $$\frac{dN_6}{dt} = \left[N_5(\bar{\sigma}_{a5} - \bar{\sigma}_{f5}) - N_6 \bar{\sigma}_{a6}\right]\phi$$

$$+ \frac{q P_1}{V_{f1}}\left[\langle 1-p\rangle_4 \frac{\alpha_3}{1+\alpha_3} + p_{174}\langle 1-p\rangle_{10}\frac{\alpha_4}{1+\alpha_4}\right.$$

$$\left. - p_{17}\langle 1-p\rangle_7\right]$$

(4C52)

Np237: $$\frac{dN_7}{dt} = \left[N_6 \bar{\sigma}_{a6} - N_7 \bar{\sigma}_{a7}\right]\phi + \frac{q P_1}{V_{f1}}\left[p_{17}\langle 1-p\rangle_7\right.$$

$$\left. - \langle 1-p\rangle_5 - p_{174}\langle 1-p\rangle_{11}\right]$$

(4C53)

U233 fission products: $$\frac{dN_8}{dt} = N_3 \bar{\sigma}_{f3}\phi + \frac{q P_1}{V_{f1}}\left[\frac{\langle 1-p\rangle_3}{1+\alpha_1} + p_{174}\frac{\langle 1-p\rangle_9}{1+\alpha_2}\right]$$

(4C54)

U235 fission products: $$\frac{dN_9}{dt} = N_5 \bar{\sigma}_{f5}\phi + \frac{q P_1}{V_{f1}}\left[\frac{\langle 1-p\rangle_4}{1+\alpha_3} + p_{174}\frac{\langle 1-p\rangle_{10}}{1+\alpha_4}\right]$$

(4C55)

The saturation concentrations of the "Sm" group and Xe135 are given by:

"Sm" group:

$$N_{10}\bar{\sigma}_{10} = N_3\bar{\sigma}_{f3}y_{s2} + N_5\bar{\sigma}_{f5}y_{s3} + \frac{qP_1}{\phi V_{f1}}\left\{\left[\frac{\langle 1-p\rangle_3}{1+\alpha_1} + p_{174}\frac{\langle 1-p\rangle_9}{1+\alpha_2}\right]y_{s2} + \left[\frac{\langle 1-p\rangle_4}{1+\alpha_3} + p_{174}\frac{\langle 1-p\rangle_{10}}{1+\alpha_4}\right]y_{s3}\right\} \quad (4C56)$$

Xe135:

$$N_{11}\left[\bar{\sigma}_{11} + \frac{\lambda_{Xe}}{\phi}\right] = N_3\bar{\sigma}_{f3}y_{x2} + N_5\bar{\sigma}_{f5}y_{x3} + \frac{qP_1}{\phi V_{f1}}\left\{\left[\frac{\langle 1-p\rangle_3}{1+\alpha_1} + p_{174}\frac{\langle 1-p\rangle_9}{1+\alpha_2}\right]y_{x2} + \left[\frac{\langle 1-p\rangle_4}{1+\alpha_3} + p_{174}\frac{\langle 1-p\rangle_{10}}{1+\alpha_4}\right]y_{x3}\right\} \quad (4C57)$$

where the following notation has been used:

N = number of atoms per unit volume of fuel

ϕ = average thermal flux in the fuel

t = time

$\bar{\sigma}$ = microscopic cross section averaged over the Wilkins spectrum

q = fast source per unit volume of unit cell

V_{f1} = volume fraction of fuel in the unit cell

P_1 = fast nonleakage probability = $\dfrac{q + D_1\nabla^2\phi_1}{q}$

$D_1\nabla^2\phi_1$ = net fast leakage in per unit volume of unit cell

$p_{17} = p_1 p_2 p_3 p_4 p_5$

$p_{174} = p_{17} p_6 p_7$

λ = decay content

y = yield per fission

α = infinitely dilute capture resonance integral/infinitely dilute fission resonance integral

with the subscripts

1 = Th232
2 = Pa233
3 = U233
4 = U234
5 = U235
6 = U236
7 = Np237
8 = U233 fission product pairs
9 = U235 fission product pairs
10 = "Sm" group
11 = Xe135

} for $N, \bar{\sigma}$

1 = Th232
2 = Pa233 above 5 ev
3 = U233 above 5 ev
4 = U235 above 5 ev
5 = Np237 above 5 ev
6 = U234
7 = U236
8 = Pa233 below 5 ev
9 = U233 below 5 ev

} for $p, \langle 1-p \rangle$

10 = U235 below 5 ev
11 = Np237 below 5 ev
} for p, $\langle 1-p \rangle$

1 = U233 above 5 ev
2 = U233 below 5 ev
3 = U235 above 5 ev
4 = U235 below 5 ev
} for α

S2 = U233
S3 = U235
X2 = U233
X3 = U235
} for γ

D. Mathematical techniques

No new mathematical techniques are introduced in this work. The problems to which the more interesting techniques were applied are listed below:

1. Solution of the nuclide concentration equations (equations (4C47) - (4C55)).

The third order Runge-Kutta method is applied to the solution of these first order ordinary differential equations. The procedure is described by Hildebrand (H1).

2. Determination of the effective cross section of the nonsaturating fission products.

Equation (4C18) is approximated by

$$\hat{\Sigma}_{FP,K} \cong \sum_{N=1}^{K} \hat{\sigma}_{FP} \left(\theta_{0,K} - \theta_{0,N}\right) \Delta N_{FP,N} \qquad (4D1)$$

where

K refers to the axial mesh point of interest in a channel

N = index which ranges from the first axial mesh point in a channel to the mesh point, K, of interest

θ_0 = 2200 m/s flux time

$\Delta N_{FP,N}$ = nonsaturating fission products produced during time interval Δt_N

The approximations involved in solving equation (4D1) are discussed by Hofmann (H2,S3).

3. Determination of the flux shapes.

The finite difference equation (4B9) is rearranged as follows:

$$\Phi_{i,j} = F \left\{ \left[\Phi_{i-1,j}\, C152_i + \Phi_{i+1,j}\, C153_i + \Phi_{i,j-1}\, C15_j + \Phi_{i,j+1}\, C154_j - Q_{i,j} \right] / \left[-S_{i,j} - C151_{i,j} \right] \right\} + (1-F)\, \Phi_{i,j} \qquad (4D2)$$

where

F = Extrapolated Liebmann parameter which can range between 1 and 2. A value of 1.5 was used throughout this work.

The other terms are defined in section IVB.

Equation (4D2) defines the Extrapolated Liebmann mesh sweeping procedure as used in this work. A more detailed description is given by Clark and Hansen (C3), page 126.

4. Solution of the Wilkins equation

Equation (4C20) is solved by a fifth order Milne method as described by Shanstrom (S1).

E. Other concepts

1. Definitions of the conversion ratio

In this thesis, two conversion ratios are considered. These are the internal conversion ratio and the conversion ratio with reprocessing loss. The internal conversion ratio can be defined in three ways, all of which are equivalent. Each definition is discussed in detail below.

(1) The first definition of the conversion ratio is given by equation (4E1), with reference to figure 4.12:

$$CR_L = \frac{\text{Total fissile atom source}}{\text{Total fissile atom sink}} = \frac{Q_R}{S_R + B \cdot O_R} \qquad (4E1)$$

where

CR_L = conversion ratio with reprocessing loss

Q_R = source of fissile atoms in the reactor

S_R = sink of fissile atoms in the reactor

O_R = fissile atoms leaving the reactor

B = fraction of reactor discharge which is lost in reprocessing and fabrication

and in figure 4.12

I_R = fissile atoms entering the reactor

The internal conversion ratio is obtained by deleting from equation (4E1) the contribution to the total fissile atom sink of the reprocessing loss:

$$CR_o = \frac{Q_R}{S_R} \qquad (4E2)$$

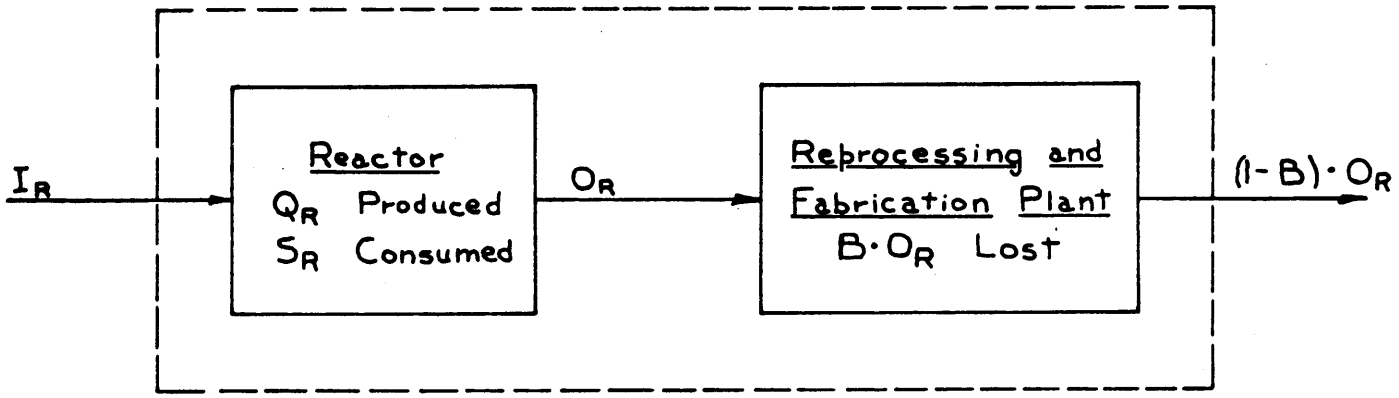

Figure 4.12: Nomenclature for Defining Conversion Ratio

where

CR_o = internal conversion ratio

The conversion ratio considered from the point of view described in this paragraph is used in this work only in calculating the conversion ratio with reprocessing loss with equation (4E1).

(2) The second definition of the internal conversion ratio is given by equation (4E2a):

$$CR_o = \left\{\left[(\bar{\eta})\right] - \left[(1) + (PAPL) + (D_2O) + (Zr) + (Pa233)\right]\right\} - \left\{(Pa\,233)\right\} \qquad (4E2a)$$

where

$(\bar{\eta})$ = number of fast neutrons produced by fission per absorption (resonance plus thermal) in a fissile nucleus (U233 plus U235).

(1) = absorption (resonance plus thermal) in a fissile nucleus (U233 plus U235) required to maintain the chain reaction.

(PAPL) = Parasitic Absorptions Plus Leakage per fissile absorption. The parasitic absorbers included in (PAPL) are U236, Np237, Xe135, the "Sm" group and nonsaturating fission products. The leakages are overall fast and thermal leakages from the reactor.

(D_2O) = absorption in heavy water per fissile absorption.

(Zr) = absorption in zircaloy (or other structural material) per fissile absorption.

(Pa233) = absorption in Pa233 per fissile absorption.

It is seen that the quantities in the second set of brackets, i.e., $[(1) + \cdots\cdots]$, include the overall leakages and absorptions in all nuclides in the reactor other than the fertile nuclides, Th232 and U234. Therefore, when this quantity is subtracted from $\bar{\eta}$, the total number of fast neutrons per fissile absorption with which one has to work, the result is the number of neutrons which are left to be absorbed by Th232 and U234. In other words this is the number of atoms of Pa233 and U235 formed per fissile absorption. Since each neutron absorbed in Pa233 results in an atom of Pa233 which is not allowed to decay to U233, the quantity (Pa233) must be subtracted a second time, as is done in equation (4E2a). The result is the internal conversion ratio CR_o or the number of fissile atoms produced per absorption in a fissile atom. All of the values of internal conversion ratio presented in this work were calculated with equation (4E2a).

(3) The third definition of the internal conversion ratio is given by equation (4E2b):

$$CR_o = \{[(Th232) + (U234)]\} - \{(Pa233)\} \qquad (4E2b)$$

where

(Th232) = absorption in Th232 per fissile absorption.

(U234) = absorption in U234 per fissile absorption.

The first quantity in braces, i.e., $\{[(Th232) + (U234)]\}$ gives directly the number of absorptions in fertile material per fissile absorption or the number of atoms of Pa233 and U235 which are formed per fissile absorption. The quantity (Pa233) must be subtracted, as is done in equation (4E2b), to account for Pa233 atoms which, due to neutron absorption, do not decay to U233. Once again, the result is the internal conversion ratio CR_o or the number of fissile atoms produced per absorption in a fissile atom.

In each of the three definitions of CR_o given above, it is seen that all Pa233 atoms which do not absorb neutrons are assumed to decay to U233 and are included in the production rate of fissile atoms. This condition is approached if the discharged fuel undergoes a long cooling period.

2. Absolute values of the thermal and fast fluxes

a. Introduction

As stated previously, the primary function of the fuel cycle calculation is to solve simultaneously at each mesh point in the reactor the two-energy-group diffusion equations which represent the neutron behavior. For a power producing reactor this includes the determination of the absolute values of the fast and thermal fluxes. The general diffusion equation and the two-group constants are repeated below from section IVB:

$$-\nabla^2 \Phi = Q - S\Phi \qquad (4B1)$$

where

Table 4.1: Fast and Thermal Neutron Fluxes, Sources and Sinks

	Flux	Source(Q)	Sink(S)
Fast:	Φ_1	$\frac{\epsilon \nu \Sigma_f}{D_1} \Phi$	$[1-\epsilon\langle \bar{\bar{\eta}} (1-p)\rangle] \frac{\Sigma_1}{D_1}$
Thermal:	Φ	$\frac{p\Sigma_1}{D} \Phi_1$	$\frac{\Sigma_a}{D}$

The absolute values of the fast and thermal fluxes are calculated in the subroutines SPFUN, SPACFX and SPFUN2. Only one or two passes are made through these three subroutines prior to a subsequent recalculation of the fuel properties since repeated passes performed when the source and sink terms are far from correct lead to unreasonable flux values.

b. Subroutine SPFUN

In this subroutine the source and sink terms listed in table 4.1 are calculated at each mesh point in the reactor. The values of ϕ and ϕ_1 in the source terms are from a previous estimate or iteration.

c. Subroutine SPACFX

In this subroutine the shapes of the fast and thermal flux distributions are calculated. In other words, $\phi_{(i,j)} / \phi_{(1,1)}$ and $\phi_{1(i,j)} / \phi_{1(1,1)}$ are determined at each mesh point, where the subscripts (1,1) refer to the mesh point nearest the core center as shown in figure 4.2.

The steps in the calculation of the flux shapes are as follows:

1. The fluxes and source terms of the energy group of interest are normalized so that the fluxes of the energy group of interest have an average value of 1. The following three equations apply:

$$C = \frac{\sum^{\frac{1}{4}\,\text{Reactor Volume}} \phi_{(i,j)}}{M} \qquad (4E2)$$

$$\bar{\phi}_{(i,j)} = \frac{\phi_{(i,j)}}{C} \qquad (4E3)$$

$$\bar{Q}(i,j) = \frac{Q(i,j)}{C} \qquad (4E4)$$

where

M = number of mesh points in 1/4 of the reactor

$\Phi(i,j)$, $Q(i,j)$ = flux and source terms respectively at point (i,j) for the energy group of interest

$\bar{\Phi}(i,j)$, $\bar{Q}(i,j)$ = normalized flux and source terms respectively

2. The diffusion equation (4B1) is again approximated by the finite difference equation:

$$\Phi^{\nu}_{(i,j)} = F\left\{\left[\Phi^{\nu}_{(i-1,j)}\, C152_i + \bar{\Phi}^{\nu-1}_{(i+1,j)}\, C153_i + \Phi^{\nu}_{(i,j-1)}\, C15_j + \bar{\Phi}^{\nu-1}_{(i,j+1)}\, C154_j - \bar{Q}(i,j)\right] \Big/ \left[-S(i,j) - C151_{i,j}\right]\right\} + (1-F)\,\bar{\Phi}^{\nu-1}_{(i,j)}$$

where

ν = iteration loop number

F = Extrapolated Liebmann parameter which can range between 1 and 2. A value of 1.5 is used throughout this work.

The other terms are defined in section IVB. A single sweep is made through the reactor mesh with equation (4E5).

3. The fluxes $\phi^{\nu}_{(i,j)}$ resulting from step 2 are again normalized as in step 1.

4. The following inequality is then tested at each mesh point in the reactor:

$$\left| \frac{\bar{\Phi}^{\nu}_{(i,j)} - \bar{\Phi}^{\nu-1}_{(i,j)}}{\bar{\Phi}^{\nu}_{(i,j)}} \right| < \epsilon \qquad (4E6)$$

If inequality (4E6) is not satisfied at each mesh point in the reactor, the steps 2, 3 and 4 are repeated until the inequality is satisfied.

5. The converged fluxes are normalized to $\bar{\Phi}^{\nu}_{(1,1)}$.

6. Steps 1-5 are repeated to obtain the flux shape of the second energy group.

d. Subroutine SPFUN2

In this subroutine, the absolute values of the fast and thermal fluxes are calculated as well as the specific power and power density at each mesh point in the reactor. The absolute value of the thermal flux is determined from the average specific power in the reactor. The steps are as follows:

1. The total homogenized spectrum averaged macroscopic fission cross section is calculated as follows:

$$\Sigma^{TOT}_{f(i,j)} = \Sigma_{f(i,j)} + \left[\left(\frac{q}{\phi} + \frac{D_1 \nabla^2 \phi_1}{\phi} \right) \left(\frac{1-\beta}{1+\alpha} \right) \right]_{(i,j)} \qquad (4E7)$$

where

Σ_f = total homogenized thermal fission cross section averaged over the Wilkins spectrum, 1/cm

$\left(\frac{1-p}{1+\alpha}\right)$ = resonance fission probability (figure 4.10)

$$= \frac{\langle 1-p\rangle_3}{1+\alpha_1} + \frac{\langle 1-p\rangle_4}{1+\alpha_3} + p_{174}\left\{\frac{\langle 1-p\rangle_9}{1+\alpha_2} + \frac{\langle 1-p\rangle_{10}}{1+\alpha_4}\right\}$$

2. Quantities proportional to the power density at each mesh point are calculated as follows:

$$(\text{Power density})_{(i,j)} = \left(\Sigma_{f(i,j)}^{TOT}\left[\frac{1}{cm}\right]\right)\frac{\phi_{(i,j)}\left[\frac{1}{cm^2\,sec}\right]}{\phi_{(1,1)}\left[\frac{1}{cm^2\,sec}\right]}\ 3.14\times10^{-11}\left[\frac{watts}{fiss/sec}\right]$$

$$= \frac{\left(3.14\times10^{-11}\right)\Sigma_{f(i,j)}^{TOT}\ \phi_{(i,j)}\ [watts/cm^3]}{\phi_{(1,1)}\left[\frac{1}{cm^2\,sec}\right]} \qquad (4E8)$$

3. The grams of fissile material $G_f(i,j)$ in the volume associated with each mesh point are transferred from subroutine CONCH.

4. The quantity $\phi_{(1,1)}$ is then obtained from equation (4E9):

$$\phi_{(1,1)} = \frac{\left(SPPTMX\left[\frac{watts}{gm\ fissile}\right]\right)\left(\sum^{\frac{1}{4}\ core\ volume} G_{f(i,j)}\left[\frac{gm\ fissile}{mesh\ point}\right]\right)}{\sum^{\frac{1}{4}\ core\ volume}\frac{(\text{Power density})_{(i,j)}\left[\frac{watts}{cm^3}\right]\ \Delta V\left[\frac{cm^3}{mesh\ point}\right]}{\phi_{(1,1)}\left[\frac{1}{cm^2\,sec}\right]}} \qquad (4E9)$$

where

SPPTMX = average specific power in the core, one of the parameters assigned a numerical value

The absolute values of the thermal flux can now be determined from and the thermal flux shape from subroutine SPACFX. The power density can be determined from equation (4E8). The specific power can be determined from equation (4E10):

$$(\text{Specific power})_{(i,j)} = \frac{(\text{Power density})_{(i,j)} \left[\frac{\text{watts}}{\text{cm}^3}\right] \quad \Delta V \left[\frac{\text{cm}^3}{\text{mesh point}}\right]}{G_{f(i,j)} \left[\frac{\text{gm fissile}}{\text{mesh point}}\right]} \tag{4E10}$$

Since the absolute value of the thermal flux if related to the fission rate in the reactor, it is also related to the source of fast neutrons. By analogy, one is led to determine the absolute value of the fast flux from the source of thermal neutrons in the reactor. This is done in the following manner:

1. If the thermal neutron balance equation is summed over the reactor volume, V_R, the following result is obtained:

$$\sum_{V_R} (p \Sigma_1 \phi_1) \Delta V = \sum_{V_R} (\Sigma_a \phi - D \nabla^2 \phi) \Delta V \tag{4E11}$$

2. Two quantities which can be calculated at this stage are the right hand side of equation (4E11) and

$$\sum_{V_R} \left(p \Sigma_1 \frac{\phi_1}{\phi_{1(1,1)}} \right) \Delta V$$

3. The final result is thus obtained:

$$\frac{\sum_{V_R} \left(\Sigma_a \phi - D \nabla^2 \phi \right) \Delta V}{\sum_{V_R} \left(p \Sigma_1 \frac{\phi_1}{\phi_{1(1,1)}} \right) \Delta V} = \frac{\sum_{V_R} \left(p \Sigma_1 \phi_1 \right) \Delta V}{\sum_{V_R} \frac{\left(p \Sigma_1 \phi_1 \right) \Delta V}{\phi_{1(1,1)}}} = \phi_{1(1,1)} \qquad (4E12)$$

With this value of $\phi_{1(1,1)}$ and the values of $\phi_{i(i,j)} / \phi_{1(1,1)}$ in hand, the absolute value of the fast flux at each mesh point in the reactor can be calculated.

Since by equation (4E12) the thermal neutron balance equation is forced to be satisfied on the average throughout the reactor, the normalization constant C from equation (4E2), used in determining the thermal flux shape, oscillates in a damped fashion around 1.0. The normalization constant C used in determining the shape of the fast flux is a free constant. The feed enrichment is adjusted to force this constant to equal 1.0, at which stage each of the two-group diffusion difference equations is satisfied at each mesh point in the reactor and the reactor is just critical.

CHAPTER V

EFFECT OF THE PRIMARY VARIABLES ON THE CONVERSION RATIO

A. Introduction

In this chapter the effects of the three primary variables on the conversion ratio are discussed. The primary variables are feed burnup (megawatt days/metric tonne of metal feed), volume of moderator/volume of fuel and fuel rod diameter. Throughout this chapter, the secondary variables are held constant at the following values:

Average specific power	1000 kw/kg fissile
Volume of zircaloy/volume of fuel	0
Reprocessing loss	0
Total power	8333 MW(th)

(It should be noted that a fixed average specific power and a fixed total thermal power dictate a fixed mass of fissile material in the reactor cores, viz. 8333 kg in this case.) The values of the feed burnup studied were 10,000, 20,000 and 30,000 mwd/t. The values of volume of moderator/volume of fuel studied covered the ranges in which were found the maximum conversion ratios for each fuel rod diameter at each feed burnup. The fuel rod diameters were decreased from a value of two inches in the anticipation that maximum conversion ratios would be found as a function of this parameter for each feed burnup. However the maximum conversion ratio continued to increase as the rod diameter decreased, without a maximum being found, as will be discussed.

The feed burnup affects the conversion ratio primarily through absorptions in nonsaturating fission products. The effect of the volume

of moderator/volume of fuel is primarily through spectrum effects and moderator absorptions. By inspection of equation (4E2a), it is therefore seen that the direct effect on the conversion ratio of these two primary variables is principally through their effect on $\bar{\eta}$ and absorptions in nuclides other than the fertile nuclides.

As the fuel rod diameter is decreased, the effective resonance integral of ThO_2 can increase on the order of 100%. This results in a large increase in the absorption of resonance neutrons by Th232. By inspection of equation (4E2b), it is therefore seen that the direct effect on the conversion ratio of the fuel rod diameter is principally through its effect on the absorptions by a fertile nuclide itself, i.e., Th232.

All of the neutron balance results in the figures and tables of this chapter are normalized to one absorption (thermal plus resonance) in a fissile nuclide. As a result of this normalization, it is essential to keep in mind the relative fractions of resonance and thermal reactions when interpreting the results. The smaller the fuel rod diameter, the larger will be the effective resonance integral of any fuel nuclide, provided that its concentration change with decreasing fuel rod diameter is small, as is usually the case. Therefore, the smaller the fuel rod diameter, the larger will be the fraction of resonance absorption in a fissile nucleus per total absorption in a fissile nucleus. As a result, those nuclides which are predominantly thermal absorbers, particularly the non-saturating fission products, are less effective poisons in small diameter rods with their increased fraction of resonance absorptions.

The fast or thermal neutron leakages referred to througout this work are defined from the following diagram:

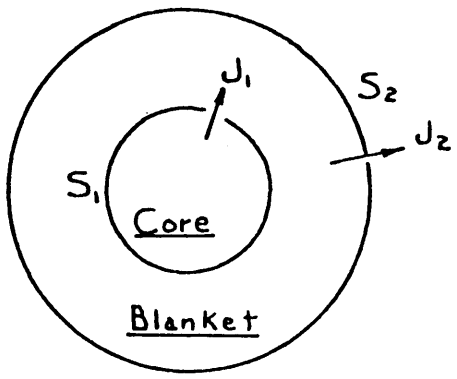

where

J_1 = net current out of core/fissile absorption per second

J_2 = net current out of reactor/fissile absorption per second

S_1 = surface area of core

S_2 = outer surface area of blanket

The leakages are defined as follows:

S_1J_1 = net leakage out of core

$S_2J_2 - S_1J_1$ = net leakage out of blanket

S_2J_2 = overall leakage from reactor

The variable "volume of moderator/volume of fuel" will hereafter be referred to simply as "moderator ratio." The results of this chapter are discussed in the burnup order of 20,000 mwd/t, 10,000 mwd/t and 30,000 mwd/t. This is because the 20,000 mwd/t case was studied most thoroughly with respect to the secondary variables, and the results of chapter VI are thus discussed in this order of burnup. The 20,000 mwd/t results in this chapter are discussed in great detail in order to establish the basic explanations for general trends for a given burnup. Only the

deviations, if any, from these general trends are discussed in detail for burnups of 10,000 mwd/t and 30,000 mwd/t.

B. Burnup of 20,000 mwd/tonne of metal feed

1. Conversion ratio and its components

Detailed neutron balances and conversion ratios for all combinations of values of primary variables studied are listed in table 5.1.

In figure 5.1 are shown the conversion ratio and its components for a burnup of 20,000 mwd/t plotted as a function of moderator ratio with fuel rod diameter as a parameter. The value of $\bar{\eta}$, the number of fast neutrons produced per fissile absorption, includes both thermal and resonance absorptions in both U233 and U235. A value of the conversion ratio is obtained by subtracting from a value of $(\bar{\eta}-1)$ the sum of parasitic absorptions* and leakage, D_2O absorption and 2 x Pa233 absorption, i.e., by use of equation (4E2a). Therefore, all Pa233 which is not destroyed by neutron absorption is assumed to decay to U233 and is included in the production rate of fissile material. The conversion ratios listed in table 5.1 were calculated in this manner. The conversion ratio also is equal to absorptions in Th232 and U234, minus absorptions in Pa233, as shown in equation (4E2b). Conversions ratios calculated by both equations (4E2a) and (4E2b), using the data from table 5.1, do not agree exactly due to the lack of complete convergence in the various iterative procedures used in the simultaneous solution of the two-energy-group diffusion difference equations.

---

*The parasitic absorbers are U236, Np237, Xe135, the "Sm" group, non-saturating fission products and zircaloy.

The values of η , the number of fast neutrons produced by fission per absorption in a fissile nucleus, for the fissile nuclides vary approximately with neutron energy as follows:

Nuclide	2200 m/s	Resonance Region
U233	2.29	2.14
U235	2.06	1.59

The value of $(\bar{\eta}-1)$ in figure 5.1 increases with increasing moderator ratio because the fraction of fissile absorptions which occurs in the resonance region is reduced. A higher fraction of the fissile absorptions thus occurs in the thermal region where the values of η are higher. Also, as the conversion ratio increases with increasing moderator ratio, the mass in the reactor of U233, with its higher values of η , increases and the mass of U235 decreases. At a moderator ratio of 10, $(\bar{\eta}-1)$ for the one inch rod is smaller than for the two inch rod. This is because the effective absorption resonance integrals of the fissile nuclides in the smaller rod are larger. At a moderator ratio of 30, however, $(\bar{\eta}-1)$ for the two inch rod is smaller than for the one inch rod because the reactor with the two inch rods has more absorptions in U235 with its smaller value of η . This latter result is shown in figure 5.6. The same line of reasoning is applicable when one compares the values of $(\bar{\eta}-1)$ for the other rod diameters.

The D_2O absorptions increase with increasing moderator ratio, of course, because of the added volume of D_2O. The values are higher and have steeper slopes for the larger rods because the greater depression of the thermal flux produces a higher relative thermal flux in the moderator region of the unit cells with the large rods.

The Pa233 absorptions decrease with increasing moderator ratio because of the decrease in resonance absorption. The smaller rods have the higher values of Pa233 absorption because the effective resonance integral of Pa233 in the smaller rods is larger and the Pa233 concentration is higher. The thermal absorption by Pa233 increases with increasing moderator ratio because of the increased thermal flux. These items are also shown in figure 5.2.

The individual components of the curves of parasitic absorptions and leakage will be discussed later. It is seen that these curves do not vary greatly with moderator ratio. The curves for the smaller rods are lower primarily because of the decreased absorption in nonsaturating fission products. As mentioned previously, this is due in part to the increased reliance on resonance reactions of the smaller rods. In addition, the large increase in resonance absorption by Th232 with decreasing fuel rod diameter mentioned previously causes a decrease with decreasing fuel rod diameter of the number of neutrons slowed down to thermal energy per absorption in a fissile nucleus. This is shown in figure 5.8 which is a plot of the number of neutrons slowed down to thermal energy per absorption in a fissile nucleus versus moderator ratio for 10,000 mwd/t, 20,000 mwd/t and 30,000 mwd/t burnups. This latter result causes the absorption by nonsaturating fission products to decrease with decreasing fuel rod diameter because the nonsaturating fission products are principally absorbers of thermal neutrons.

The conversion ratio curves increase initially with increasing moderator ratio because of the increase in $(\bar{\eta}-1)$ and the decrease in Pa233 resonance absorption. Eventually, however, these latter two items tend to level out while the D_2O absorptions continue to increase with

increasing moderator ratio. The conversion ratio curves thus reach maximum values. The curves for the large rods reach peaks at smaller values of moderator ratio and the peaks are more pronounced because of the steeper slopes of their D_2O absorption curves. The peaks in the flatter curves for the smaller rod sizes are difficult to locate precisely as a function of moderator ratio.

The effect on the conversion ratio of decreasing the fuel rod diameter is interpreted with the use of equation (4E2b). A decrease in the fuel rod diameter causes an increase in the effective resonance integral of ThO_2 of the order of 100%. This results in a large increase in the absorption of resonance neutrons by Th232. Therefore, the direct effect on the conversion ratio of decreasing the fuel rod diameter is to increase the absorptions by the fertile material Th232, a quantity which is included directly in equation (4E2b). The indirect effect on the conversion ratio of decreasing the fuel rod diameter is reflected in equation (4E2a) and, therefore, in figure 5.1. Because of the increased resonance absorption in Th232 with decreased fuel rod diameter, the number of neutrons slowed down to thermal energy per fissile absorption is reduced. Therefore, the number of thermal neutrons available for absorption in nonsaturating fission products is reduced. This is shown in figure 5.1 by the decrease in parasitic absorptions plus leakage with decreasing fuel rod diameter. The decrease in the number of neutrons slowed down to thermal energy per fissile absorption also causes D_2O absorptions to decrease with decreasing fuel rod diameter. The D_2O absorptions also decrease with decreasing fuel rod diameter because of the decreasing thermal flux peak in the moderator of the unit cell.

Two other notes on the effect of decreasing the fuel rod diameter are as follows:

(1) The effective resonance integrals of the fuel nuclides other than Th232 are large in any case because these nuclides are very dilute. Therefore, decreasing the fuel rod diameter does not increase these effective resonance integrals by large percentages, as compared to the increase in the effective resonance integral of Th232.

(2) Since a homogeneous system has higher Th232 effective resonance integrals than a heterogeneous system, the maximum conversion ratio which could appear in figure 5.1 would be for a homogeneous system.

2. Masses and mass fractions of fuel nuclides in the reactor cores

The seven fuel nuclides considered in this section are Th232, Pa233, U233, U234, U235, U236 and Np237. The masses and mass fractions of the fuel nuclides are listed in table 5.2. All but Np237 are plotted as a function of moderator ratio in figures 5.9 through 5.12.

The mass of Th232 in the core usually decreases as fuel rod diameter decreases. Because the smaller rods have higher effective resonance integrals and therefore lower resonance escape probabilities, higher enrichments are required in the cores with the smaller rod diameters in order to maintain criticality. Since all of the cores contain the same mass of fissile material, the only way of increasing the enrichment is to decrease the mass of Th232. The mass of Th232 increases as moderator ratio increases because the resonance escape probabilities rise and $\bar{\eta}$ rises so a lower core enrichment suffices to maintain critcality.

As the rod diameters decrease, the mass of Pa233 in the reactors

increases, because resonance absorption increases to a greater extent in Th232 than in Pa233. The mass of Pa233 for a given rod diameter increases with increasing moderator ratio and passes through a maximum, because the sum of resonance and thermal absorptions in Th232 passes through a maximum as shown in figure 5.7.

The mass of U233 in the core increases as moderator ratio increases because of the increasing conversion ratios. The mass of U233 in the core generally increases with decreasing fuel rod diameter also because of increasing conversion ratios.

The quantity of U235 in the core equals 8333 kg. minus the kg. of U233 in the core. Therefore the reasons which cause the quantity of U233 to increase also cause the U235 to decrease.

The curves of U234 and U236 mass resemble inverted conversion ratio curves. The reasons for this are as follows:

1. At a low moderator ratio, the conversion ratio is relatively low. A relatively large fraction of the core discharge is recycled into the feed which results in relatively large amounts of U234, U235 and U236 in the core.

2. As the moderator ratio is increased, the conversion ratio increases. Therefore, less discharged U234, U235 and U236 are recycled into the feed and the quantities of U234 and U236 in the core drop.

3. Shortly after a conversion ratio curve has passed its peak, the amount of discharged U234, U235 and U236 recycled into the reactor feed begins to increase again. Also at a high moderator ratio, the U234 and U236 resonance absorptions have been greatly reduced. Since resonance absorption is the primary sink for U236, the quantity of U236 in the reactor increases sharply. For U234, thermal absorption is still a large sink so the quantity of U234 in the reactor does not increase as sharply.

The quantities of U234 and U236 in the cores decrease with decreasing rod size because of increasing conversion ratios which require a smaller fraction of the core discharge be recycled into the feed.

The mass fraction curve of Th232 for the two inch rod is lower than the curve for the one inch rod although the mass of Th232 in the core is larger for the two inch rod than for the one inch rod at low moderator ratios. The larger quantities of U234 and U236 in the cores with the two inch rod cause the mass fraction of Th232 to drop. The same explanation applies when comparing the mass and mass fraction curves of Th232 for the other rod sizes.

The curves of mass fraction vs. moderator ratio for the other fuel nuclides follow directly from the curves of mass vs. moderator ratio. Some of these mass fraction curves will be referred to later.

3. Parasitic absorptions and leakage

The parasitic absorptions occur in the following nuclides: U236, Np237, Xe, the "Sm" group and the nonsaturating fission products. The leakages include both the overall fast and thermal leakages from the reactor.

When studying the curves of absorption by nonsaturating fission products, it is helpful to consider at the same time the curves for D_2O

absorption. These sets of curves are in figure 5.3 and 5.2 respectively. For a given burnup, the concentration of nonsaturating fission products throughout the fuel in the core is roughly fixed. Therefore as the moderator ratio increases, a fixed concentration of nonsaturating fission products competes with an increasing quantity of D_2O for the thermal neutrons. At large fuel rod diameters, D_2O in general is more effective as an absorber than as a moderator, when compared to the absorption by nonsaturating fission products, for two reasons:

1. The thermal flux has a severe dip in the large diameter fuel rod. Therefore an increase in D_2O volume occurs in a region of relatively high thermal flux. This effect is seen from the greater slopes and greater values of the D_2O absorption curves for the large diameter fuel rods in figure 5.2.

2. In a large diameter fuel rod with its smaller effective resonance integrals, the fraction of resonance reactions is smaller than in a smaller diameter rod for the same moderator ratio. Therefore any D_2O added to a unit cell with a large diameter fuel rod has a relatively small fraction of resonance neutrons to moderate. This is illustrated in figure 5.8. For a given range of moderator ratio, say from 30 to 40, the rate of increase of the neutrons slowed down to thermal energy per fissile absorption is smaller for the larger diameter rods.

Conversely, at small fuel rod diameters, D_2O is in general more effective as a moderator than as an absorber when compared to absorptions by nonsaturating fission products.

It is seen from figure 5.3 that in general the slopes of the curves of absorption by nonsaturating fission products increase as the fuel rod

diameter is decreased. This is explained by the reasons given above. That is, for the two inch diameter fuel rods, the added D_2O steals thermal neutrons away from the nonsaturating fission products while as the fuel rod diameter decreases, the added D_2O absorbs fewer thermal neutrons itself and moderates more resonance neutrons for the nonsaturating fission products to absorb. The unit cells with the one inch and two inch diameter rods at a moderator ratio of 10 are so epithermal, however, that the first addition of D_2O supplies more moderation than poison. It should also be noted that in general the curves of absorptions by nonsaturating fission products are lower for the smaller rods. This is because the smaller rods have a lower fraction of reactions in the thermal region where the nonsaturating fission products are most effective as absorbers. This is illustrated in figure 5.8 where it is seen that the smaller rods have a smaller number of neutrons slowed down to thermal energy per absorption by a fissile nucleus.

The absorptions by Xe and the "Sm" group are shown in figure 5.2. The absorptions by both of these thermal neutron absorbers increase as the moderator ratio increases because of the increased reliance of the reactor on thermal neutrons. In addition, absorptions by Xe increase because the increased thermal flux shifts the Xe branching ratio away from radioactive decay and toward thermal neutron absorptions.

The resonance absorption in U236 is shown in figure 5.2 and the thermal absorption in U236 in figure 5.4. It is interesting to note that U236 is primarily a resonance absorber in these reactors.

The U236 resonance absorption decreases with increasing moderator ratio. Although the U236 resonance integrals are larger for the smaller rods, the resonance absorption curves for the smaller rods fall below

those of the larger rods. This is because the smaller rods produce higher conversion ratios which require less U235 in the reactor, and thus a lower concentration of U236 is present in the reactor. The resonance absorption for the 1/10 inch rod is greater than for the 1/4 inch rod because the U236 concentration is sufficiently greater as shown in figure 5.12.

The U236 thermal absorption curves resemble in shape the U236 mass fraction curves in figure 5.12. For the two inch rod, the U236 concentration decreases by 28% in going from a moderator ratio of 10 to 20. The number of neutrons slowed down to thermal energy per absorption in fissile nucleus increases by 21% as shown in figure 5.8. Therefore the U236 thermal absorption decreases. In going from a moderator ratio of 20 to 30, both the U236 concentration and the number of neutrons slowed down to thermal energy increase so the U236 thermal absorption increases. The curve of U236 thermal absorptions for the 1/10 inch rod is below the curve for the 1/4 inch rod even though the concentration of U236 in the reactor with the 1/10 inch rods is greater than in the reactor with the 1/4 inch rods. This is because the curve of the neutrons slowed down to thermal energy per absorption in a fissile nucleus for the 1/10 inch rod is sufficiently below the curve for the 1/4 inch rod, as shown in figure 5.8. The U236 thermal absorption curves also tend to increase with increasing moderator ratio because of the increase in the number of neutrons slowed down to thermal energy.

The Np237 resonance absorption curves are shown in figure 5.2 and thermal absorption curves in figure 5.4. Since resonance absorption is the primary U236 sink, it is therefore the primary Np237 source. Therefore both the resonance and thermal absorption curves resemble the U236

resonance absorption curves.

The fast and thermal leakage curves are in figure 5.5. These curves are separated into net leakage out of the core and net leakage out of the blankets. The thermal leakage curves increase in absolute value with increasing moderator ratio because of the increased diffusion lengths for thermal neutrons. The thermal leakage for the larger rods is higher in absolute value than for the smaller rods because of the increased thermal flux dip in the larger rods. The fast leakage decreases in absolute value with increasing moderator ratio because of the increased slowing down power of the unit cell.

We are now in a position to discuss the shapes of the composite parasitic absorption and leakage curves in figure 5.1. The reactions of interest are

1. U236 resonance absorption
2. Np237 resonance absorption
3. Np237 thermal absorption
4. Nonsaturating fission products absorption
5. Xe thermal absorption
6. "Sm" group thermal absorption
7. Overall thermal leakage out of the reactor

The overall fast leakage out of the reactor and U236 thermal absorption have a negligible effect on the shapes of the curves.

In the cases considered in this work, items 1, 2 and 3 always decrease and items 5, 6 and 7 always increase with increasing moderator ratio. Item 4 sometimes increases and sometimes decreases with increasing moderator ratio, depending on the fuel rod diameter and moderator ratio.

It will be seen later that in the cases of burnups of 10,000 mwd/t

with their high conversion ratios and low concentrations of U236, the shapes of the absorption curves of Xe, the "Sm" group and nonsaturating fission products will play a major role in determining the shapes of the composite curves of parasitic absorption and leakage, while U236 resonance and Np237 absorption will play a minor role. At burnups of 30,000 mwd/t with their low conversion ratios and high concentrations of U236, the shapes of the curves of U236 resonance absorption and Np237 absorption will play the major role in determining the shapes of the composite curves at low moderator ratios where the U236 concentrations are highest. At a burnup of 20,000 mwd/t, the positive and negative absorption effects frequently cancel one another and the absorption by nonsaturating fission products is the key to understanding the behavior of the composite curves. It can be said of all the burnups that at high moderator ratios, the changes with moderator ratio of the U236 resonance absorption and its daughter Np237 absorption are almost negligible and therefore the shapes of the composite curves are determined almost entirely by the absorption by Xe, the "Sm" group and nonsaturating fission products.

Consider now the composite curves of parasitic absorption and leakage for 20,000 mwd/t in figure 5.1. For the two inch diameter rod, the absorption by nonsaturating fission products decreases with increasing moderator ratio. The decrease, along with the decrease in U236 resonance absorption and Np237 absorption, overcomes the positive changes in absorptions by Xe and the "Sm" group and the net thermal leakage and causes the composite curves to decrease with increasing moderator ratio. For the one inch diameter rod, the composite curve initially increases due to the initial increase in nonsaturating fission products absorption. The composite curve then decreases with increasing moderator ratio due largely to the

continued decrease in absorption by nonsaturating fission products. For the 1/4 inch diameter rod, the nonsaturating fission product absorption curve is almost flat and the change with moderator ratio of U236 resonance absorption and Np237 absorption are largely removed because of the high moderator ratio. The positive changes with increasing moderator ratio therefore prevail and the composite curve increases with increasing moderator ratio. For the 1/10 inch diameter rod, the trends just mentioned for the 1/4 inch rod continue and the composite curve increases more sharply with increasing moderator ratio. The composite curves decrease with decreasing rod diameter due to the decreased absorption by nonsaturating fission products.

4. Fissile absorptions

The absorptions by U233 and U235 are shown in figure 5.6. The thermal absorptions by U233 increase with increasing moderator ratio despite the decrease in concentration shown in figure 5.11 because of the more rapid increase in the number of neutrons slowed down to thermal energy as shown in figure 5.8. The thermal absorptions by U235 decrease with increasing moderator ratio because of the rapidly decreasing concentration of U235 in the reactors as shown in figure 5.12. The resonance absorptions by the two fissile nuclides decrease with increasing moderator ratio. The thermal and resonance absorptions in U235 decrease with decreasing rod diameter because of the decreased U235 concentrations in the reactors with higher conversion ratios.

5. Fertile absorptions

The absorptions by Th232 and U234 are shown in figure 5.7. The thermal absorption by Th232 decreases as the rod diameter decreases because of the decrease in the number of neutrons slowed down to thermal

energy per absorption in a fissile nucleus as shown in figure 5.8. The Th232 thermal absorption increases with increasing moderator ratio because of the increase with moderator ratio of the number of neutrons slowed down to thermal energy per absorption by a fissile nucleus. The resonance absorption by Th232 increases markedly with decreasing rod diameter. This is due to the increased effective resonance integrals of ThO_2 in the smaller rods and is the reason for the increasing conversion ratios with decreasing rod diameter as shown in figure 5.1. Increased moderation causes the resonance absorption to decrease with increasing moderator ratio.

The thermal absorptions by U234 increase with increasing moderator ratio despite the fact that the concentration of U234 in the reactor initially decreases as shown in figure 5.12. This is because the fractional decrease in concentration is much smaller than the fractional increase in the number of neutrons slowed down to thermal energy per absorption in fissile nucleus as shown in figure 5.8. The thermal absorptions in U234 decrease with decreasing rod size because again the number of neutrons slowed down to thermal energy per absorption in fissile nucleus decreases. The resonance absorption in U234 increases with decreasing rod diameter due to increasing resonance integrals and decreases with increasing moderator ratio due to increasing moderation.

C. Burnups of 10,000 mwd/tonne of metal feed and 30,000 mwd/tonne of metal feed

The conversion ratio and its components for a feed burnup of 10,000 mwd/t are plotted in figure 5.13 as a function of moderator ratio with fuel rod diameter as a parameter. Similar results for a feed burnup of

30,000 mwd/t are plotted in figure 5.14. The shapes of the composite curves of parasitic absorptions plus leakage shown in figures 5.13 and 5.14 were explained in the preceding section VB3. The complete neutron balance results are listed in table 5.1. The explanations for the general trends of the neutron balance results presented in section VB for a burnup of 20,000 mwd/t are valid for burnups of 10,000 and 30,000 mwd/t. The masses and mass fractions of the fuel nuclides in the core are listed in table 5.2. Figure 5.8 shows the number of neutrons slowed down to thermal energy per absorption in a fissile nucleus versus moderator ratio.

D. Comparisons among burnups

All of the results in this section are plotted with moderator ratio as abscissa and fuel rod diameter and feed burnup as parameters. The values of $(\bar{\eta}-1)$ are plotted in figure 5.16. It is seen that for a given rod diameter and moderator ratio, the slope of a curve of $(\bar{\eta}-1)$ is greater the greater the burnup. The reactors with high burnups have lower conversion ratios and therefore have higher U235 concentrations in the cores. As shown in section VB1, the difference between thermal and resonance values of η is much greater for U235 than for U233. Therefore in the reactors with high burnups and relatively high U235 concentrations, any added moderation is more effective in increasing $\bar{\eta}$. The increase in $\bar{\eta}$ due to additional moderation causes an increase in the Th232 absorption and thus the U233 concentration. As the U233 replaces the U235 in a system with a fixed mass of fissile material, $\bar{\eta}$ is increased by an additional amount. These reasons also explain why in figure 5.8 for a given rod diameter and moderator ratio the slope of the curve of neutrons slowed down to thermal energy per absorption in a fissile nucleus versus moderator ratio is greater the greater the burnup. Of course,

the curves of ($\bar{\eta}$ -1) are lower for the higher burnups because of the lower conversion ratios and the resulting higher concentrations of U235.

The conversion ratio and absorption by nonsaturating fission products are plotted in figure 5.15. The nonsaturating fission product curves are flatter the lower the burnup. As shown in figure 5.8, the number of neutrons slowed down to thermal energy per absorption in a fissile nucleus increases more rapidly with increasing moderator ratio for the higher burnups. However as shown in figure 5.19 and 5.21, the thermal absorptions in U233 and Th232 also increase more rapidly with increasing moderator ratio for the higher burnups. The latter effects prevail and the thermal neutrons available for absorption by nonsaturating fission products decrease more rapidly with increasing moderator ratio for the reactors with the higher burnups. Therefore the nonsaturating fission products absorption curves in figure 5.15 have a larger negative slope for the higher burnups.

The conversion ratio curves tend to be more sharply peaked and the peaks are located at higher moderator ratios for the higher burnups. This is because the curves of of ($\bar{\eta}$ -1) have steeper slopes for the higher burnups. From 50% to 90% of the difference in conversion ratios for different burnups and a given moderator ratio and fuel rod diameter is due to the difference in absorptions by nonsaturating fission products. The 50% value applies at very low moderator ratios and the 90% value applies at very high moderator ratios. Other causes for the difference are changes in ($\bar{\eta}$ -1) and changes in absorption by U236, Np237 and Pa233. The results for U236 and Np237 are shown in figure 5.17 and the results for Pa233 are shown in figure 5.18.

The absorptions by U236 decrease with decreasing rod diameter and

decreasing burnup because of the higher conversion ratios and lower U235 concentrations which accompany these changes. The absorptions by Np237, the daughter of U236, follow the same pattern.

The absorptions by U233 are shown in figure 5.19. The curves of U233(th,f) resemble the curves of $(\bar{\eta}-1)$ in figure 5.16. It is seen that once again for a given rod diameter and moderator ratio, the slopes are greater for the higher burnups. For the explanation of this, refer to the explanation for the $(\bar{\eta}-1)$ curves. The U233(th,f) absorptions are lower for the higher burnups. One reason for this is the increased reliance on U235 fissions for power production in the reactors with higher burnups and lower conversion ratios. Also because of the increased thermal absorption by nonsaturating fission products for the higher burnups, the fraction of reactions by the U233 in the thermal region is reduced and the fraction of reactions by U233 in the resonance region is increased. This is the reason for the increase in resonance reactions by U233 with increasing burnup for a given rod diameter and moderator ratio.

The absorptions by U235 are shown in figure 5.20. As the burnups decrease for a given rod diameter, the conversion ratios increase and the concentration of U235 in the reactor decreases. Therefore the U235 reactions decrease.

The absorptions by Th232 are shown in figure 5.21. The explanation for the increase in slope of the thermal absorption curves with increasing burnup for a given moderator ratio and rod diameter is the same as that previously given for the $(\bar{\eta}-1)$ curves of figure 5.16. The explanation for the decrease in the thermal absorption curves with increasing burnup is the same as the second reason previously given for the U233(th,f) curves. However, in contrast to the U233 resonance absorption curves,

the resonance absorption by Th decreases with increasing burnup. The fractional change in absorption probability, $\frac{d(1-p)}{(1-p)}$, for a nuclide is approximately equal to $\frac{dN}{N}$ where N is the concentration of the nuclide. Consider a given moderator ratio and fuel rod diameter and then increase the burnup. The fractional increase in U233 concentration, $\frac{dN}{N}$, is much greater than for Th232 because of the higher enrichment required for the higher burnup. Therefore the absorption probability for U233 increases much more than for Th232 in going to a higher burnup. Although the fraction of resonance reactions is higher for the higher burnups, the U233 steals resonance neutrons away from Th232 and the Th232 resonance absorptions decrease.

The curves for U234 absorption are given in figure 5.22. For a fixed moderator ratio and fuel rod diameter, the curves decrease with decreasing burnup because of the lower U234 concentrations at lower burnups, a result of the increased conversion ratios.

E. Other results of the calculations

In table 5.3 are listed the input and output flow rates of the fuel nuclides and the fissile nuclide consumption rates for the cases involving the primary variables. The ratios of the output flow rates of Pa233, U233 and U235 to the consumption rates of U233 and U235 are also presented. These latter figures are used in chapter VII when the effect on the conversion ratio of increasing the reprocessing loss is estimated.

When the conversion ratio is less than 1.0 and the reprocessing loss is zero, the steady state input and output flow rates of (U233 plus Pa233), U234 and U236 are equal. The figures in table 5.3 do not verify this fact exactly. This is, once again, due to the lack of complete convergence in the various iterative procedures used in the simultaneous solution of the two-energy-group diffusion difference equations.

Table 5.1: Neutron Balances for the Cases Involving the Primary Variables

Burnup, mwd/t	10,000	10,000	10,000	10,000	10,000	10,000	10,000	10,000	10,000	20,000	20,000
Volume moderator/volume fuel	10	20	30	20	30	40	30	40	50	10	20
Rod diameter, inches	2	2	2	1	1	1	1/4	1/4	1/4	2	2
Average specific power, kw/kg fissile	1000	1000	1000	1000	1000	1000	1000	1000	1000	1000	1000
Absorption ratio, zircaloy/fissile	0	0	0	0	0	0	0	0	0	0	0
Reprocessing loss, %	0	0	0	0	0	0	0	0	0	0	0
Total power, MW(th)	8333	8333	8333	8333	8333	8333	8333	8333	8333	8333	8333
Production of fast neutrons from											
Resonance fission of U233	0.490780	0.262292	0.180640	0.275122	0.188037	0.143327	0.208697	0.157440	0.126723	0.504750	0.268454
Resonance fission of U235	0.018624	0.007067	0.004462	0.006920	0.004176	0.003021	0.004305	0.003015	0.002344	0.023018	0.008449
Thermal fission of U233	1.585013	1.867383	1.962351	1.856886	1.961556	2.013660	1.940600	2.001710	2.037134	1.539644	1.839554
Thermal fission of U235	0.136764	0.119715	0.116784	0.116606	0.110447	0.108374	0.108984	0.105383	0.104180	0.158262	0.137087
Total ($\bar{\eta}$)	2.231181	2.256457	2.264237	2.255534	2.264216	2.268382	2.262586	2.267548	2.270381	2.225674	2.253544
Net fast leakage out of											
Core	0.018707	0.011398	0.008797	0.011915	0.009085	0.007596	0.009693	0.007913	0.006906	0.020389	0.011631
Blanket	-0.017238	-0.009693	-0.007120	-0.010127	-0.007339	-0.005896	-0.007880	-0.006187	-0.005218	-0.018836	-0.009913
Neutrons reaching resonance energy	2.229712	2.254752	2.262560	2.253746	2.262470	2.266682	2.260773	2.265822	2.268693	2.224121	2.251826
Resonance absorptions											
Th232, Core	0.320752	0.172141	0.117367	0.197632	0.135185	0.102676	0.205177	0.156692	0.126687	0.316718	0.170566
Th232, Blanket	0.002671	0.000786	0.000393	0.000941	0.000463	0.000283	0.000755	0.000451	0.000307	0.002983	0.000830
Pa233	0.013996	0.007724	0.005351	0.007686	0.005319	0.004065	0.005460	0.004152	0.003347	0.013977	0.007825
U233	0.229840	0.122631	0.084413	0.128649	0.087878	0.066965	0.097569	0.073578	0.059210	0.236418	0.125518
U234	0.044124	0.023010	0.016082	0.024285	0.016615	0.012784	0.018481	0.014019	0.011409	0.049711	0.025608
U235	0.011838	0.004469	0.002817	0.004378	0.002638	0.001906	0.002722	0.001904	0.001480	0.014638	0.005344
U236	0.006909	0.002990	0.002134	0.002734	0.001824	0.001408	0.001770	0.001263	0.001033	0.010736	0.004488
Np237	0.001267	0.000357	0.000197	0.000320	0.000166	0.000106	0.000154	0.000097	0.000067	0.003242	0.000908
Net production of thermal neutrons	1.598315	1.920644	2.033806	1.887121	2.012382	2.076489	1.928685	2.013666	2.065153	1.575698	1.910739
Overall thermal leakage from reactor	0.001048	0.002519	0.004017	0.001498	0.002256	0.003006	0.001639	0.002130	0.002619	0.001125	0.002540
Thermal absorptions											
Th232, Core	0.675510	0.859817	0.913371	0.848696	0.919740	0.951810	0.859051	0.911405	0.940293	0.622122	0.814597
Th232, Blanket	0.020565	0.017248	0.016220	0.014585	0.012924	0.012076	0.011682	0.010608	0.009957	0.022378	0.017598
Pa233	0.002899	0.003565	0.003777	0.003524	0.003780	0.003895	0.003718	0.003871	0.003949	0.002715	0.003457
U233 fission	0.633245	0.746058	0.784000	0.741864	0.783682	0.804499	0.775309	0.799724	0.813877	0.615119	0.734940
U233 capture	0.058943	0.069043	0.072412	0.068783	0.072485	0.074328	0.071776	0.073926	0.075158	0.057283	0.068008
U234	0.040292	0.045236	0.048419	0.042889	0.045290	0.047009	0.043203	0.044769	0.046068	0.045088	0.050380
U235 fission	0.056282	0.049265	0.048059	0.047986	0.045452	0.044598	0.044849	0.043368	0.042872	0.065128	0.056414
U235 capture	0.009853	0.008534	0.008299	0.008339	0.007867	0.007703	0.007774	0.007500	0.007403	0.011412	0.009776
U236	0.000613	0.000582	0.000634	0.000527	0.000543	0.000565	0.000506	0.000493	0.000510	0.000913	0.000849
Np237	0.000625	0.000392	0.000330	0.000351	0.000282	0.000246	0.000254	0.000209	0.000191	0.001505	0.000957
Xe135	0.030505	0.036057	0.038061	0.035754	0.037857	0.038944	0.037353	0.038592	0.039337	0.029989	0.035872
"Sm" group	0.012152	0.013739	0.014321	0.013667	0.014263	0.014576	0.014123	0.014474	0.014689	0.012075	0.013735
Nonsaturating fission products	0.047717	0.046668	0.044617	0.046219	0.044777	0.043637	0.042374	0.042065	0.041800	0.081200	0.080546
D_2O	0.007951	0.021948	0.037337	0.012631	0.021010	0.029565	0.014576	0.020603	0.026575	0.007569	0.021162
Zircaloy	0	0	0	0	0	0	0	0	0	0	0
Total consumption of thermal neutrons	1.598200	1.920671	2.033874	1.887313	2.012208	2.076457	1.928187	2.013737	2.065298	1.575621	1.910831
Conversion ratio	1.087118	1.106922	1.102656	1.117624	1.121295	1.118710	1.129668	1.129854	1.127281	1.042383	1.068205

Table 5.1: (continued)

Burnup, mwd/t	20,000	20,000	20,000	20,000	20,000	20,000	20,000	20,000	20,000	20,000	20,000
Volume moderator/volume fuel	30	10	20	30	40	30	40	50	30	40	50
Rod diameter, inches	2	1	1	1	1	1/4	1/4	1/4	1/10	1/10	1/10
Average specific power, kw/kg fissile	1000	1000	1000	1000	1000	1000	1000	1000	1000	1000	1000
Absorption ratio, zircaloy/fissile	0	0	0	0	0	0	0	0	0	0	0
Reprocessing loss, %	0	0	0	0	0	0	0	0	0	0	0
Total power, MW(th)	8333	8333	8333	8333	8333	8333	8333	8333	8333	8333	8333
Production of fast neutrons from											
Resonance fission of U233	0.184556	0.536601	0.281828	0.192209	0.146318	0.213692	0.161135	0.129574	0.229577	0.170898	0.136441
Resonance fission of U235	0.005292	0.023830	0.008201	0.004900	0.003523	0.005024	0.003521	0.002741	0.005305	0.003638	0.002802
Thermal fission of U233	1.938607	1.504969	1.830314	1.939985	1.994436	1.919169	1.982129	2.018415	1.902584	1.972764	2.012297
Thermal fission of U235	0.133367	0.156973	0.132404	0.124946	0.122212	0.122576	0.118853	0.117803	0.121645	0.117598	0.116540
Total ($\bar{\eta}$)	2.261822	2.222373	2.252747	2.262040	2.266489	2.260461	2.265638	2.268533	2.259111	2.264898	2.268080
Net fast leakage out of											
Core	0.008861	0.021325	0.011931	0.008645	0.007380	0.009089	0.007158	0.006309	0.009699	0.007604	0.006429
Blanket	-0.007184	-0.019792	-0.010169	-0.007024	-0.005754	-0.007434	-0.005642	-0.004800	-0.008012	-0.006018	-0.004925
Neutrons reaching resonance energy	2.260145	2.220840	2.250985	2.260419	2.264863	2.258806	2.264122	2.267024	2.257424	2.263312	2.266576
Resonance absorptions											
Th232, Core	0.116342	0.360145	0.195894	0.134093	0.101863	0.203587	0.155490	0.125719	0.279431	0.214677	0.174172
Th232, Blanket	0.000411	0.003565	0.000970	0.000458	0.000285	0.000713	0.000412	0.000284	0.001057	0.000607	0.000402
Pa233	0.005438	0.014155	0.007848	0.005506	0.004182	0.005705	0.004385	0.003518	0.005954	0.004522	0.003639
U233	0.086246	0.251441	0.131792	0.089831	0.068364	0.099908	0.075307	0.060543	0.107379	0.079893	0.063766
U234	0.017825	0.053879	0.027143	0.018499	0.014179	0.020697	0.015762	0.012818	0.021949	0.016534	0.013400
U235	0.003341	0.015173	0.005190	0.003095	0.002222	0.003177	0.002224	0.001729	0.003360	0.002300	0.001770
U236	0.003235	0.010624	0.004027	0.002601	0.002005	0.002449	0.001820	0.001508	0.002465	0.001813	0.001482
Np237	0.000512	0.003141	0.000800	0.000406	0.000263	0.000370	0.000234	0.000170	0.000362	0.000227	0.000165
Net production of thermal neutrons	2.026795	1.508717	1.877321	2.005930	2.071500	1.922200	2.008488	2.060735	1.835467	1.942739	2.007780
Overall thermal leakage from reactor	0.004004	0.000700	0.001472	0.002110	0.002879	0.001506	0.001886	0.002359	0.001419	0.001829	0.002213
Thermal absorptions											
Th232, Core	0.870778	0.584369	0.804965	0.878979	0.912801	0.821184	0.873196	0.902551	0.749803	0.818837	0.858785
Th232, Blanket	0.016306	0.020263	0.014607	0.012397	0.011762	0.010967	0.009618	0.009121	0.011000	0.009633	0.008878
Pa233	0.003692	0.002650	0.003447	0.003770	0.003871	0.003740	0.003943	0.004009	0.003690	0.003907	0.004020
U233 fission	0.774513	0.601266	0.731248	0.775064	0.796818	0.766748	0.791901	0.806398	0.760121	0.788160	0.803954
U233 capture	0.071537	0.056137	0.067811	0.071692	0.073615	0.070979	0.073198	0.074477	0.070397	0.072879	0.074267
U234	0.053895	0.041480	0.047201	0.049866	0.051668	0.047015	0.049012	0.050477	0.045752	0.047901	0.049547
U235 fission	0.054884	0.064598	0.054487	0.051418	0.050293	0.050443	0.048911	0.048479	0.050060	0.048394	0.047959
U235 capture	0.009479	0.011385	0.009472	0.008901	0.008688	0.008746	0.008459	0.008373	0.008683	0.008373	0.008284
U236	0.000940	0.000862	0.000750	0.000752	0.000783	0.000677	0.000688	0.000721	0.000647	0.000661	0.000689
Np237	0.000829	0.001413	0.000845	0.000667	0.000585	0.000588	0.000509	0.000471	0.000543	0.000477	0.000442
Xe135	0.037956	0.029412	0.035579	0.037804	0.038904	0.037300	0.038614	0.039368	0.036897	0.038356	0.039212
"Sm" group	0.014334	0.011940	0.013655	0.014271	0.014592	0.014122	0.014484	0.014706	0.014006	0.014410	0.014653
Nonsaturating fission products	0.077547	0.078210	0.079812	0.077980	0.076046	0.074165	0.074065	0.073483	0.069489	0.070575	0.070834
D_2O	0.036160	0.004358	0.012105	0.020237	0.028565	0.014019	0.019857	0.025666	0.012565	0.018238	0.023876
Zircaloy	0	0	0	0	0	0	0	0	0	0	0
Total consumption of thermal neutrons	2.026854	1.509043	1.877456	2.005908	2.071870	1.922199	2.008341	2.060659	1.835072	1.942630	2.007613
Conversion ratio	1.066368	1.046670	1.079349	1.085039	1.084135	1.094720	1.095308	1.093519	1.099743	1.099868	1.097692

Table 5.1: (continued)

Burnup, mwd/t	20,000	30,000	30,000	30,000	30,000	30,000	30,000	30,000	30,000	30,000
Volume moderator/volume fuel	60	10	20	30	20	30	40	30	40	50
Rod diameter, inches	1/10	2	2	2	1	1	1	1/4	1/4	1/4
Average specific power, kw/kg fissile	1000	1000	1000	1000	1000	1000	1000	1000	1000	1000
Absorption ratio, zircaloy/fissile	0	0	0	0	0	0	0	0	0	0
Reprocessing loss, %	0	0	0	0	0	0	0	0	0	0
Total power, MW(th)	8333	8333	8333	8333	8333	8333	8333	8333	8333	8333
Production of fast neutrons from										
Resonance fission of U233	0.113777	0.517454	0.274260	0.188277	0.287880	0.195780	0.148944	0.218174	0.164279	0.131995
Resonance fission of U235	0.002289	0.030332	0.010075	0.006251	0.009672	0.005671	0.004075	0.005805	0.004039	0.003143
Thermal fission of U233	2.037895	1.476428	1.809270	1.912813	1.802263	1.918365	1.974286	1.897366	1.963130	2.000280
Thermal fission of U235	0.116133	0.193162	0.156622	0.151782	0.149933	0.140012	0.137163	0.136881	0.132247	0.131294
Total ($\bar{\nu}$)	2.270094	2.217376	2.250227	2.259123	2.249748	2.259828	2.264468	2.258226	2.263695	2.266712
Net fast leakage out of										
Core	0.005708	0.025793	0.014144	0.010901	0.014133	0.010334	0.008493	0.010315	0.008302	0.007186
Blanket	-0.004259	-0.023304	-0.011732	-0.008594	-0.011751	-0.008161	-0.006441	-0.008207	-0.006348	-0.005329
Neutrons reaching resonance energy	2.268645	2.214887	2.247815	2.256816	2.247366	2.257655	2.262416	2.256118	2.261741	2.264855
Resonance absorptions										
Th232, Core	0.146486	0.311214	0.168748	0.115186	0.193945	0.132908	0.100990	0.201821	0.154204	0.124699
Th232, Blanket	0.000293	0.003600	0.000950	0.000473	0.001090	0.000515	0.000308	0.000787	0.000464	0.000314
Pa233	0.003029	0.013637	0.007669	0.005308	0.007764	0.005440	0.004191	0.005766	0.004412	0.003557
U233	0.053164	0.242426	0.128241	0.087988	0.134631	0.091502	0.069592	0.102008	0.076778	0.061676
U234	0.011345	0.056112	0.028353	0.019661	0.030135	0.020322	0.015606	0.022987	0.017444	0.014241
U235	0.001445	0.019304	0.006373	0.003947	0.006121	0.003583	0.002571	0.003671	0.002551	0.001984
U236	0.001279	0.019009	0.007113	0.005194	0.006068	0.003818	0.002956	0.003533	0.002632	0.002184
Np237	0.000129	0.007377	0.001889	0.001090	0.001584	0.000785	0.000515	0.000709	0.000448	0.000329
Net production of thermal neutrons	2.051475	1.542208	1.898479	2.017969	1.866028	1.998782	2.065687	1.914836	2.002808	2.055871
Overall thermal leakage from reactor	0.002596	0.001092	0.002510	0.004027	0.001325	0.001994	0.002655	0.001299	0.001715	0.002113
Thermal absorptions										
Th232, Core	0.883861	0.562761	0.770566	0.829321	0.764008	0.842557	0.877121	0.786244	0.839572	0.869387
Th232, Blanket	0.008466	0.026256	0.019759	0.018402	0.016117	0.013705	0.012533	0.011687	0.010438	0.009774
Pa233	0.004066	0.002462	0.003248	0.003472	0.003276	0.003605	0.003763	0.003655	0.003847	0.003938
U233 fission	0.814181	0.589863	0.722840	0.764208	0.720041	0.766426	0.788768	0.758037	0.784311	0.799153
U233 capture	0.075171	0.054965	0.066920	0.070604	0.066775	0.070895	0.072871	0.070187	0.072523	0.073825
U234	0.050912	0.050811	0.056141	0.060010	0.051840	0.054394	0.056595	0.050902	0.053038	0.054936
U235 fission	0.047791	0.079490	0.064453	0.062462	0.061701	0.057618	0.056446	0.056330	0.054423	0.054030
U235 capture	0.008247	0.013951	0.011172	0.010790	0.010730	0.009978	0.009752	0.009768	0.009414	0.009332
U236	0.000721	0.001579	0.001325	0.001497	0.001101	0.001082	0.001133	0.000947	0.000968	0.001018
Np237	0.000421	0.003202	0.001916	0.001705	0.001609	0.001252	0.001112	0.001087	0.000946	0.000880
Xe135	0.039761	0.029420	0.035663	0.037806	0.035401	0.037702	0.038881	0.037242	0.038582	0.039374
"Sm" group	0.014814	0.012016	0.013736	0.014353	0.013651	0.014283	0.014613	0.014126	0.014496	0.014725
Nonsaturating fission products	0.071039	0.107543	0.107995	0.104046	0.107193	0.104353	0.102346	0.099756	0.099148	0.098392
D_2O	0.029470	0.007278	0.020698	0.035521	0.011699	0.019683	0.027828	0.013539	0.019253	0.024925
Zircaloy	0	0	0	0	0	0	0	0	0	0
Total consumption of thermal neutrons	2.051517	1.542689	1.898942	2.018224	1.866467	1.999527	2.066417	1.914806	2.002674	2.055802
Conversion ratio	1.094226	0.994172	1.033136	1.034017	1.045654	1.054613	1.054450	1.065039	1.067035	1.065925

Table 5.2: Masses and Mass Fractions of Fuel Materials in Reactor Cores and Core Dimensions for the Cases Involving the Primary Variables

Average specific power 1000 kw/kg fissile
Volume zircaloy/volume fuel 0
Total power 8333 MW(th)
Reprocessing loss 0

Burnup, mwd/t	10,000	10,000	10,000	10,000	10,000	10,000	10,000	10,000	10,000	20,000	20,000	20,000	20,000	20,000	20,000	20,000
Volume moderator/volume fuel	10	20	30	20	30	40	30	40	50	10	20	30	10	20	30	40
Rod diameter, inches	2	2	2	1	1	1	1/4	1/4	1/4	2	2	2	1	1	1	1
Masses (kg)																
Th232 x 10^{-3}	575.55	631.97	640.49	629.48	648.68	654.97	613.33	632.24	641.37	538.12	603.38	614.50	518	602.25	624.51	632
Pa233	372	385	385	390	393	393	396	398	397	358	375	376	361	382	386	386
U233	7688	7847	7881	7854	7902	7922	7906	7930	7940	7574	7774	7817	7563	7789	7846	7868
U234	2525	2427	2474	2326	2329	2356	2252	2263	2288	2870	2721	2767	2715	2578	2576	2599
U235	645	485	451	477	429	410	429	402	391	758	559	517	772	545	487	464
U236	657	539	560	492	482	490	455	431	438	994	791	835	960	706	672	682
Np237	21.6	11.5	9.16	10.5	7.93	6.72	7.28	5.80	5.18	53.6	28.6	23.4	51.7	25.7	19.0	16.2
Mass fractions																
Th232	0.9797	0.9818	0.9820	0.9820	0.9825	0.9827	0.9817	0.9822	0.9825	0.9771	0.9801	0.9803	0.9775	0.9804	0.9812	0.9815
Pa233 x 10^{4}	6.33	5.98	5.90	6.08	5.95	5.90	6.34	6.18	6.08	6.50	6.10	6.00	6.81	6.22	6.06	5.99
U233 x 10^{2}	1.31	1.22	1.21	1.23	1.20	1.19	1.27	1.23	1.22	1.37	1.26	1.25	1.43	1.27	1.23	1.22
U234 x 10^{3}	4.30	3.77	3.79	3.63	3.53	3.53	3.60	3.52	3.50	5.21	4.42	4.41	5.12	4.20	4.04	4.04
U235 x 10^{4}	11.0	7.53	6.91	7.44	6.50	6.15	6.87	6.25	5.99	13.8	9.09	8.25	14.6	8.88	7.65	7.21
U236 x 10^{3}	1.12	0.837	0.859	0.768	0.730	0.735	0.728	0.670	0.671	1.80	1.29	1.33	1.81	1.15	1.06	1.06
Np237 x 10^{5}	3.68	1.79	1.40	1.64	1.20	1.01	1.17	0.901	0.793	9.740	4.651	3.736	9.751	4.176	2.984	2.519
Core radius, feet	16.97	21.70	24.82	21.67	24.92	27.45	24.47	27.13	29.31	16.64	21.42	24.54	16.43	21.41	24.66	27.18
Core height, feet	31.31	40.04	45.79	39.98	45.98	50.65	45.15	50.05	54.08	30.70	39.52	45.28	30.31	39.50	45.50	50.15

Burnup, mwd/t	20,000	20,000	20,000	20,000	20,000	20,000	20,000	30,000	30,000	30,000	30,000	30,000	30,000	30,000	30,000	30,000
Volume moderator/volume fuel	30	40	50	30	40	50	60	10	20	30	20	30	40	30	40	50
Rod diameter, inches	1/4	1/4	1/4	1/10	1/10	1/10	1/10	2	2	2	1	1	1	1/4	1/4	1/4
Masses (kg)																
Th232 x 10^{-3}	590	610	619	543.87	575.16	592.09	601.94	494.15	572.98	586.69	574.47	600.75	609.32	568.13	588.88	599.08
Pa233	390.1	392	391	391	393	393	392	336	360	361	367	373	374	378	380	380
U233	7848	7878	7888	7846	7879	7892	7899	7389	7689	7744	7714	7786	7812	7788	7823	7835
U234	2461	2486	2515	2417	2443	2477	2514	3292	3048	3094	2848	2823	2857	2677	2702	2748
U235	484.2	455	443	485	453	440	433	947	642	591	621	549	523	543	509	496
U236	611.2	603	622	589	582	596	617	1747	1242	1335	1041	970	990	860	853	882
Np237	16.99	14.2	12.9	15.9	13.3	12.1	11.4	117.0	58.0	48.9	49.4	36.2	31.2	31.8	26.7	24.4
Mass fractions																
Th232	0.9804	0.9809	0.9811	0.9789	0.9800	0.9804	0.9807	0.9728	0.9777	0.9781	0.9785	0.9795	0.9797	0.9788	0.9795	0.9798
Pa233 x 10^{4}	6.482	6.30	6.20	7.03	6.70	6.51	6.39	6.61	6.14	6.02	6.25	6.08	6.01	6.51	6.32	6.21
U233 x 10^{2}	1.304	1.27	1.25	1.41	1.34	1.31	1.29	1.45	1.31	1.29	1.31	1.27	1.26	1.34	1.30	1.28
U234 x 10^{3}	4.089	4.00	3.99	4.35	4.16	4.10	4.10	6.48	5.20	5.16	4.85	4.60	4.59	4.61	4.49	4.49
U235 x 10^{4}	8.046	7.32	7.02	8.73	7.72	7.29	7.05	18.6	11.0	9.85	10.6	8.95	8.41	9.36	8.47	8.11
U236 x 10^{3}	1.016	0.970	0.986	1.06	0.992	0.987	1.01	3.44	2.12	2.23	1.77	1.58	1.59	1.48	1.42	1.44
Np237 x 10^{5}	2.823	2.276	2.040	2.858	2.273	2.002	1.852	23.0	9.90	8.15	8.41	5.90	5.02	5.48	4.44	3.99
Core radius, feet	24.22	26.87	29.04	23.57	26.35	28.61	30.53	16.22	21.11	24.22	21.12	24.40	26.91	23.96	26.61	28.78
Core height, feet	44.69	49.58	53.58	43.49	48.62	52.79	56.33	29.93	38.95	44.69	38.97	45.02	49.65	44.21	49.10	53.10

Table 5.3: Fuel Flow Rates and Fissile Consumption Rates for the Cases Involving the Primary Variables

Burnup, mwd/t	10,000	10,000	10,000	10,000	10,000	10,000	10,000	10,000	10,000	20,000	20,000	20,000	20,000	20,000	20,000	20,000
Volume moderator/volume fuel	10	20	30	20	30	40	30	40	50	10	20	30	10	20	30	40
Rod diameter, inches	2	2	2	1	1	1	1/4	1/4	1/4	2	2	2	1	1	1	1
Average specific power, kw/kg fissile	1000	1000	1000	1000	1000	1000	1000	1000	1000	1000	1000	1000	1000	1000	1000	1000
Absorption ratio, zircaloy/fissile	0	0	0	0	0	0	0	0	0	0	0	0	0	0	0	0
Reprocessing loss, %	0	0	0	0	0	0	0	0	0	0	0	0	0	0	0	0
Total power, MW(th)	8333	8333	8333	8333	8333	8333	8333	8333	8333	8333	8333	8333	8333	8333	8333	8333
Fuel flow rates, kg/day																
Input																
Core																
Th232	817.09	818.93	819.01	819.12	819.60	819.69	818.97	819.43	819.63	407.47	408.92	409.01	407.30	409.16	409.50	409.57
U233	11.049	10.134	10.050	10.121	9.8417	9.7742	10.397	10.092	9.9619	5.8393	5.1614	5.0905	6.0235	5.1061	4.9017	4.8485
U234	3.4387	2.9802	3.0022	2.8547	2.7674	2.7744	2.8255	2.7512	2.7434	2.0766	1.7152	1.7140	2.0340	1.6119	1.5432	1.5380
U235	0.87819	0.59497	0.54672	0.58514	0.50942	0.48301	0.53805	0.48889	0.46857	0.54938	0.35212	0.32040	0.57861	0.34031	0.29136	0.27458
U236	0.89534	0.66188	0.68011	0.60395	0.57459	0.57783	0.57243	0.52351	0.52487	0.71956	0.49933	0.51774	0.71924	0.44203	0.40302	0.40420
Blanket																
Th232	12,679	10,488	9804.1	9104.6	8076.7	7532.6	7396.1	6713.9	6342.6	12,643	9294.8	8600.5	11,733	7889.6	6549.8	6223.3
Output																
Core																
Th232	807.27	808.87	809.00	808.92	809.36	809.47	808.62	809.07	809.30	398.19	399.30	399.41	397.95	399.38	399.65	399.72
Pa233	0.30771	0.26523	0.25343	0.28296	0.26721	0.26029	0.30145	0.28569	0.27812	0.11816	0.089180	0.083104	0.12901	0.093747	0.082258	0.080783
U233	11.310	10.682	10.585	10.777	10.568	10.495	11.174	10.906	10.768	5.8562	5.5191	5.4551	6.0847	5.5895	5.4768	5.4293
U234	3.6911	3.2754	3.2898	3.1660	3.0858	3.0898	3.1544	3.0828	3.0717	2.2170	1.9283	1.9250	2.1819	1.8488	1.7954	1.7903
U235	0.94253	0.65399	0.59913	0.64902	0.56793	0.53786	0.60047	0.54800	0.52469	0.58561	0.39618	0.35998	0.62076	0.39171	0.34016	0.32023
U236	0.96079	0.72664	0.74451	0.66957	0.63804	0.64091	0.63625	0.58675	0.58770	0.76936	0.56205	0.58181	0.77255	0.50680	0.46863	0.47012
Np237	0.056697	0.028111	0.022239	0.025793	0.019052	0.016051	0.018550	0.014402	0.012710	0.069659	0.034631	0.028160	0.070088	0.031254	0.022665	0.019241
Blanket																
Th232	12,679	10,488	9803.9	9104.5	8076.6	7532.5	7396.0	6713.7	6342.5	12,643	9294.7	8600.4	11,733	7889.5	6549.6	6223.1
Pa233	0.089699	0.068368	0.063656	0.057146	0.049113	0.045492	0.045271	0.040077	0.037323	0.080676	0.054737	0.050148	0.075227	0.044980	0.036118	0.034244
U233	0.13692	0.10525	0.095502	0.092407	0.079180	0.072638	0.074037	0.065659	0.060584	0.16548	0.12180	0.10925	0.15647	0.10435	0.086485	0.080322
S_R, Fissile material consumed in reactor, atoms/day (x 10^{-25})	2.5680	2.5394	2.5307	2.5403	2.5305	2.5265	2.5337	2.5275	2.5239	2.5737	2.5427	2.5338	2.5784	2.5441	2.5335	2.5282
O_R, Output from reactor of Pa233, U233 and U235, atoms/day (x 10^{-25})	3.3044	3.0433	2.9974	3.0650	2.9806	2.9496	3.1522	3.0618	3.0162	1.7587	1.5974	1.5656	1.8258	1.0686	1.5564	1.5365
O_R/S_R	1.2868	1.1984	1.1844	1.2065	1.1779	1.1675	1.2441	1.2114	1.1951	0.68333	0.62824	0.61788	0.70813	0.63231	0.61434	0.60777

Table 5.3: (continued)

Burnup, mwd/t	20,000	20,000	20,000	20,000	20,000	20,000	20,000	30,000	30,000	30,000	30,000	30,000	30,000	30,000	30,000	30,000
Volume moderator/volume fuel	30	40	50	30	40	50	60	10	20	30	20	30	40	30	40	50
Rod diameter, inches	1/4	1/4	1/4	1/10	1/10	1/10	1/10	2	2	2	1	1	1	1/4	1/4	1/4
Average specific power, kw/kg fissile	1000	1000	1000	1000	1000	1000	1000	1000	1000	1000	1000	1000	1000	1000	1000	1000
Absorption ratio, zircaloy/fissile	0	0	0	0	0	0	0	0	0	0	0	0	0	0	0	0
Reprocessing loss, %	0	0	0	0	0	0	0	0	0	0	0	0	0	0	0	0
Total power, MW(th)	8333	8333	8333	8333	8333	8333	8333	8333	8333	8333	8333	8333	8333	8333	8333	8333
Fuel flow rates, kg/day																
Input																
Core																
Th232	409.26	409.53	409.60	408.66	409.12	409.30	409.36	270.20	271.90	272.00	272.22	272.61	272.67	272.49	272.71	272.77
U233	5.1467	4.9742	4.9002	5.6038	5.2840	5.1326	5.0604	4.3248	3.6605	3.5830	3.5697	3.3640	3.3167	3.5060	3.3667	3.3089
U234	1.5507	1.5129	1.5078	1.6566	1.5777	1.5543	1.5541	1.7671	1.3593	1.3455	1.2471	1.1653	1.1625	1.1582	1.1224	1.1246
U235	0.30563	0.27664	0.26701	0.33297	0.29229	0.27708	0.26816	0.54848	0.28699	0.25685	0.27217	0.22728	0.21317	0.23618	0.21160	0.20344
U236	0.38580	0.36745	0.37335	0.40484	0.37693	0.37459	0.38175	0.93676	0.55488	0.58167	0.45705	0.40173	0.40352	0.37327	0.35570	0.36152
Blanket																
Th232	6049.6	5310.8	4997.8	6159.6	5380.9	4917.4	4660.4	15,643	10,437	9492.5	8282.9	6649.2	5939.2	5493.1	4747.2	4312.2
Output																
Core																
Th232	399.28	399.54	399.63	398.63	399.08	399.28	399.37	261.52	262.71	262.79	262.84	263.10	263.15	262.86	263.04	263.11
Pa233	0.092724	0.084181	0.081438	0.10868	0.095050	0.087935	0.084619	0.075750	0.050634	0.046516	0.050272	0.042222	0.038982	0.043852	0.038861	0.036733
U233	5.8132	5.6695	5.5908	6.2939	6.0097	5.8559	5.7611	3.9575	3.7125	3.6634	3.7701	3.6899	3.6580	3.9365	3.8351	3.7789
U234	1.8190	1.7846	1.7771	1.9324	1.8574	1.8311	1.8254	1.7672	1.4787	1.4688	1.4007	1.3479	1.3466	1.3612	1.3334	1.3317
U235	0.35836	0.32760	0.31332	0.38819	0.34511	0.32556	0.31503	0.48997	0.31172	0.28126	0.30611	0.26224	0.24699	0.27690	0.25196	0.24114
U236	0.45248	0.43394	0.43993	0.47173	0.44320	0.44103	0.44832	0.93896	0.60437	0.63604	0.51396	0.46451	0.46847	0.43851	0.42211	0.42898
Np237	0.021558	0.017507	0.015723	0.021952	0.017556	0.015499	0.014359	0.10142	0.046295	0.038793	0.039762	0.028503	0.024463	0.026757	0.021934	0.019795
Blanket																
Th232	6049.5	5310.6	4997.7	5159.5	5380.9	4917.3	4660.3	15,643	10,436	9492.2	8282.7	6649.0	5939.1	5493.0	4747.1	4312.1
Pa233	0.037364	0.031403	0.029330	0.039797	0.032800	0.029213	0.027429	0.13778	0.081982	0.073916	0.062263	0.047630	0.041783	0.038766	0.032135	0.028930
U233	0.074924	0.064735	0.060628	0.076097	0.065337	0.059559	0.056248	0.15727	0.11967	0.10917	0.10545	0.090311	0.082504	0.082265	0.073374	0.068544
S_R, Fissile material consumed in reactor, atoms/day (x 10^{-25})	2.5349	2.5292	2.5257	2.5360	2.5299	2.5263	2.5243	2.5824	2.5448	2.5362	2.5469	2.5357	2.5307	2.5368	2.5305	2.5272
O_R, Output from reactor of Pa233, U233 and U235, atoms/day (x 10^{-25})	1.6481	1.5967	1.5703	1.7851	1.6924	1.6434	1.6140	1.2448	1.1051	1.0788	1.1097	1.0680	1.0514	1.1315	1.0936	1.0737
O_R/S_R	0.65016	0.63129	0.62174	0.70389	0.66898	0.65051	0.63939	0.48206	0.43427	0.42535	0.43572	0.42118	0.41548	0.44606	0.43218	0.42486

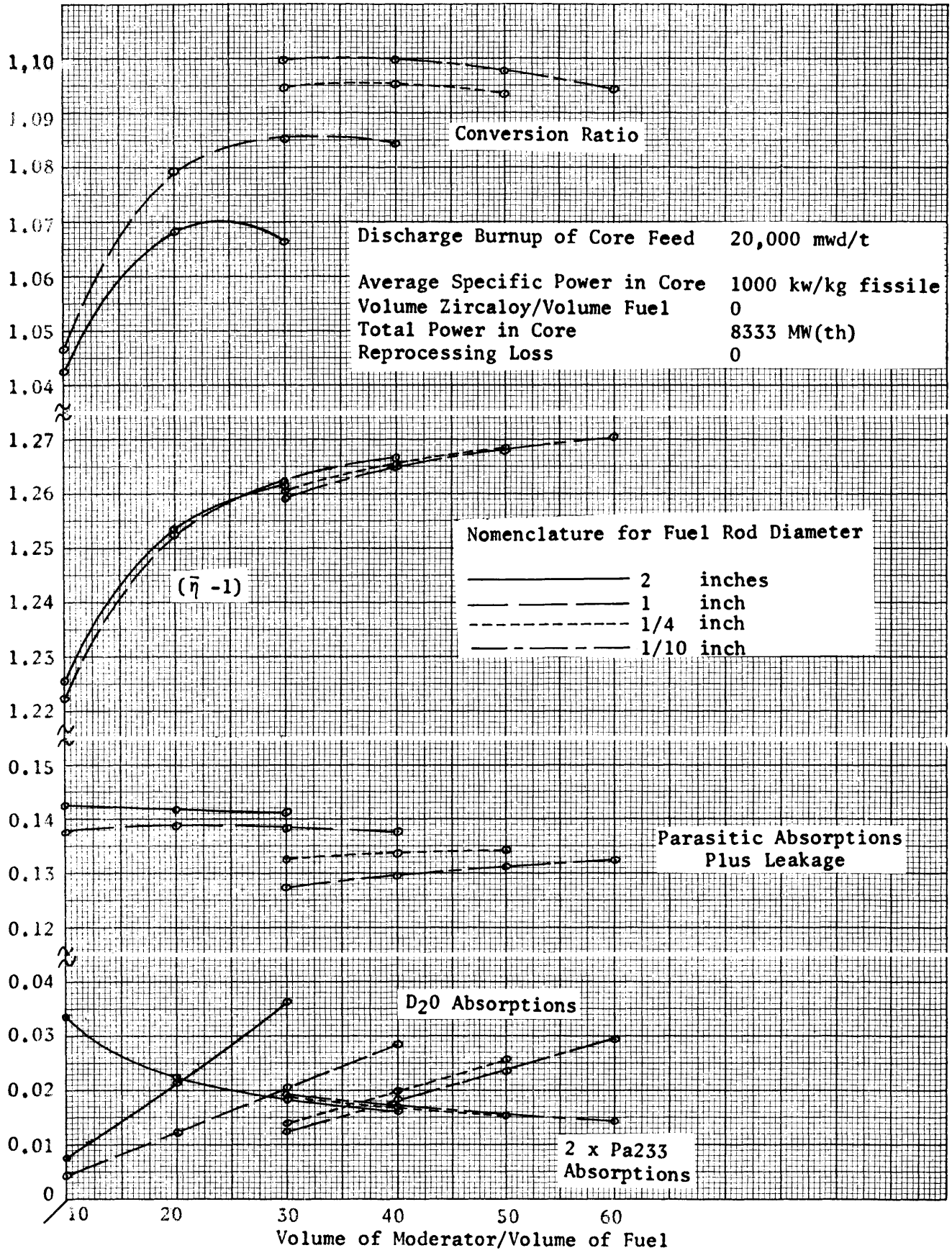

Figure 5.1 : Conversion Ratio and its Components vs. Volume of Moderator/ Volume of Fuel: 20,000 mwd/t Burnup

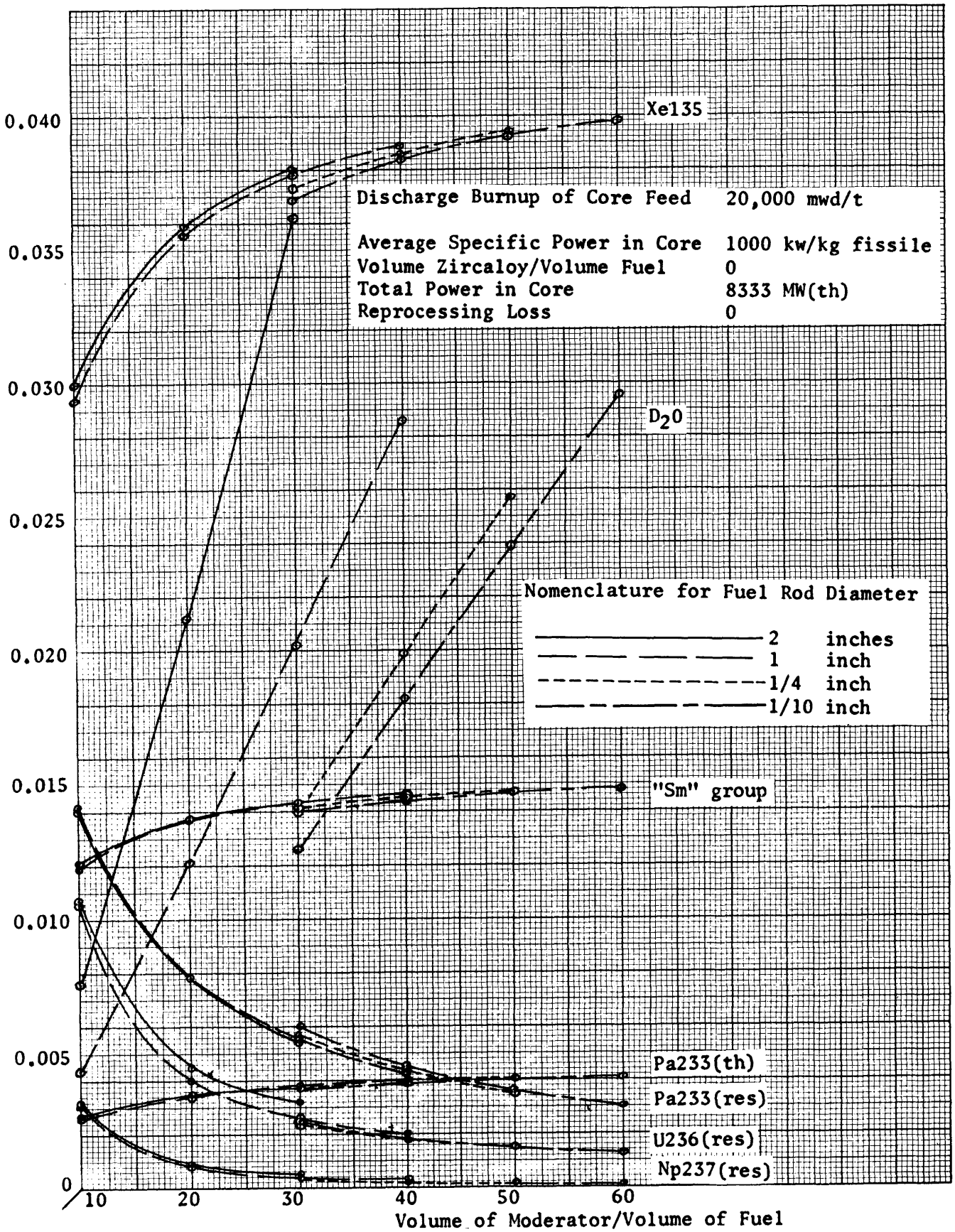

Figure 5.2: Absorptions by Pa233(th,res), U236(res), Np237(res), Xe135, "Sm" group, D_2O vs. Volume of Moderator/Volume of Fuel: 20,000 mwd/t Burnup

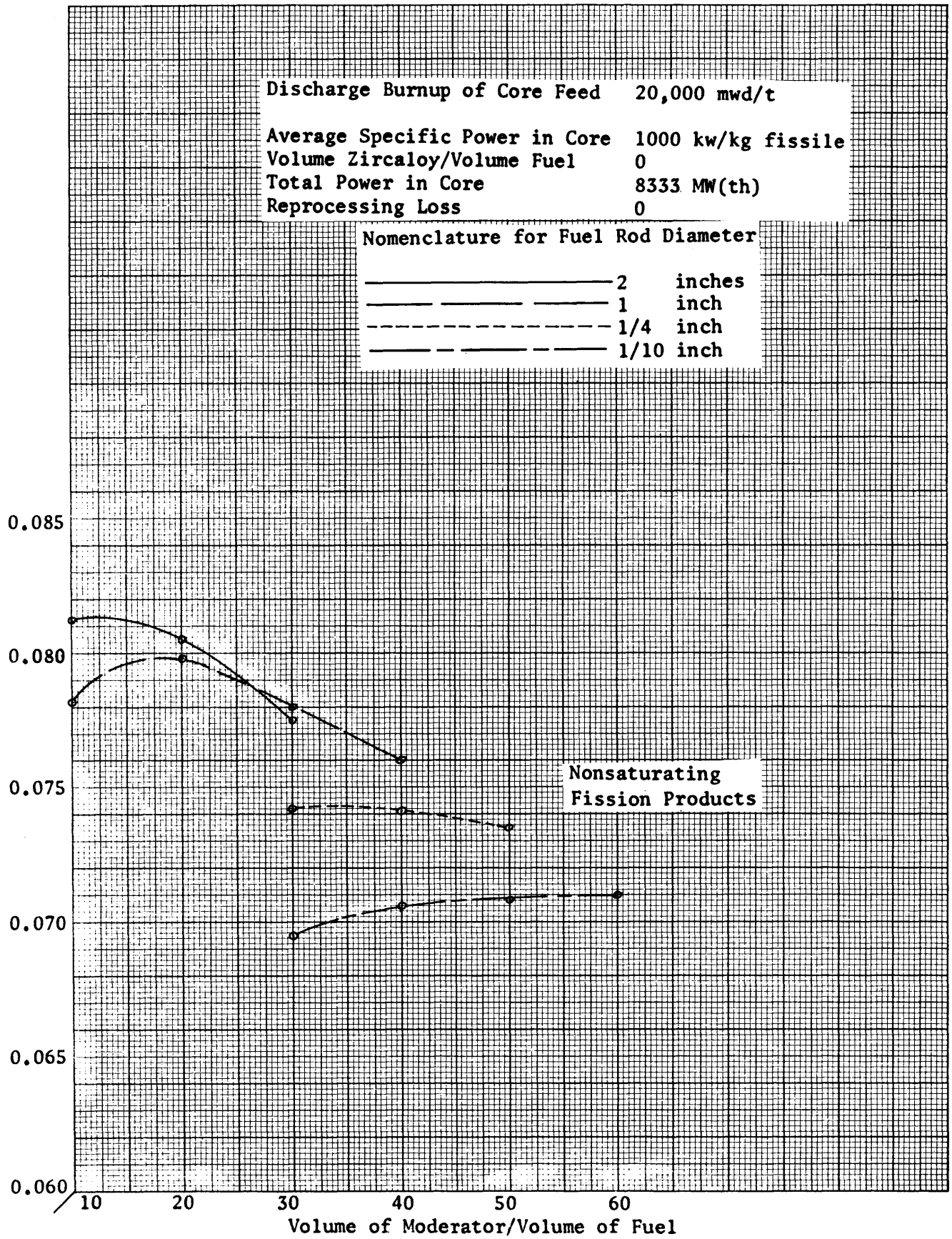

Figure 5.3: Absorptions by Nonsaturating Fission Products vs. Volume of Moderator/Volume of Fuel: 20,000 mwd/t Burnup

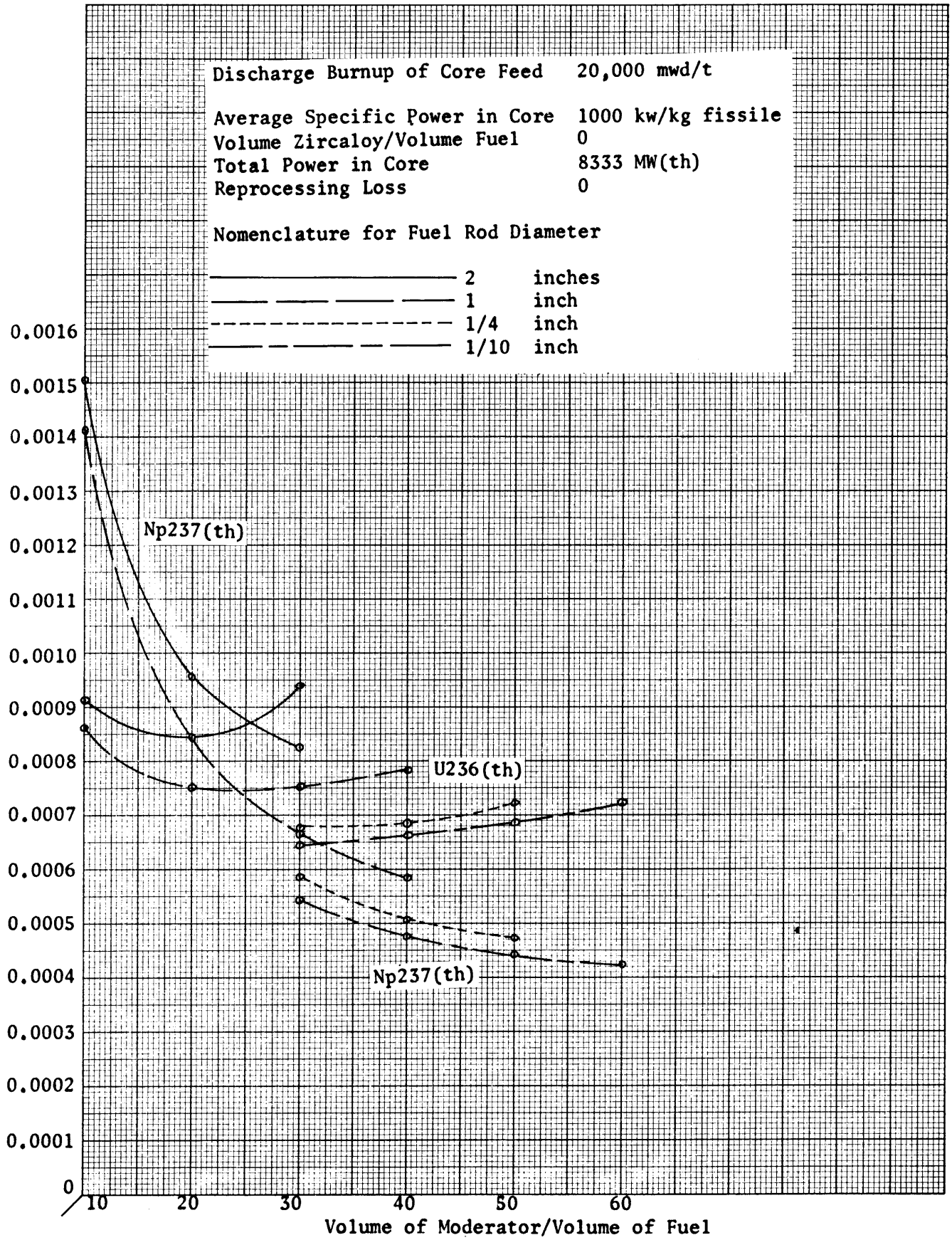

Figure 5.4: Absorptions by U236(th), Np237(th) vs. Volume of Moderator/ Volume of Fuel: 20,000 mwd/t Burnup

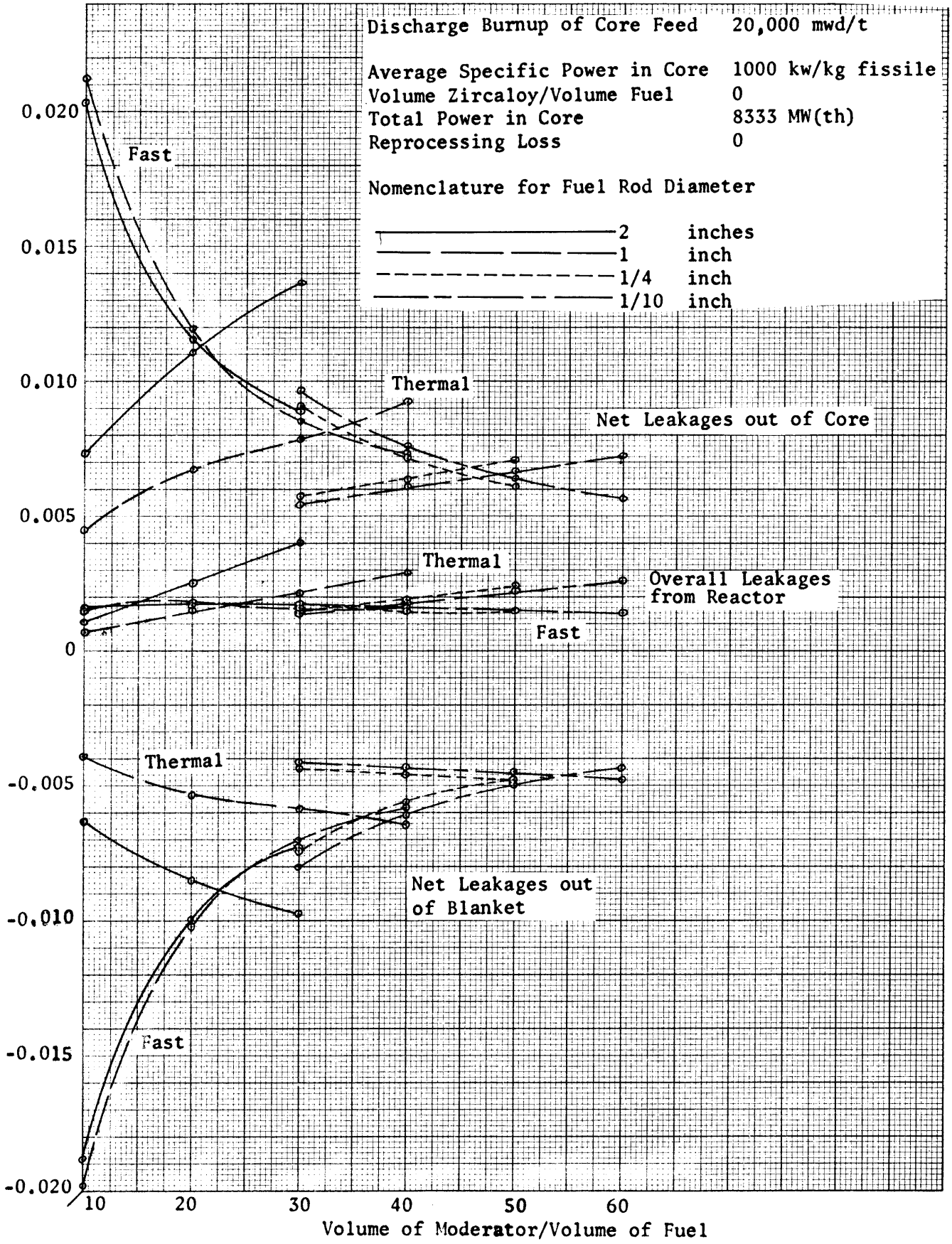

Figure 5.5: Fast and Thermal Leakages vs. Volume of Moderator/Volume of Fuel: 20,000 mwd/t Burnup

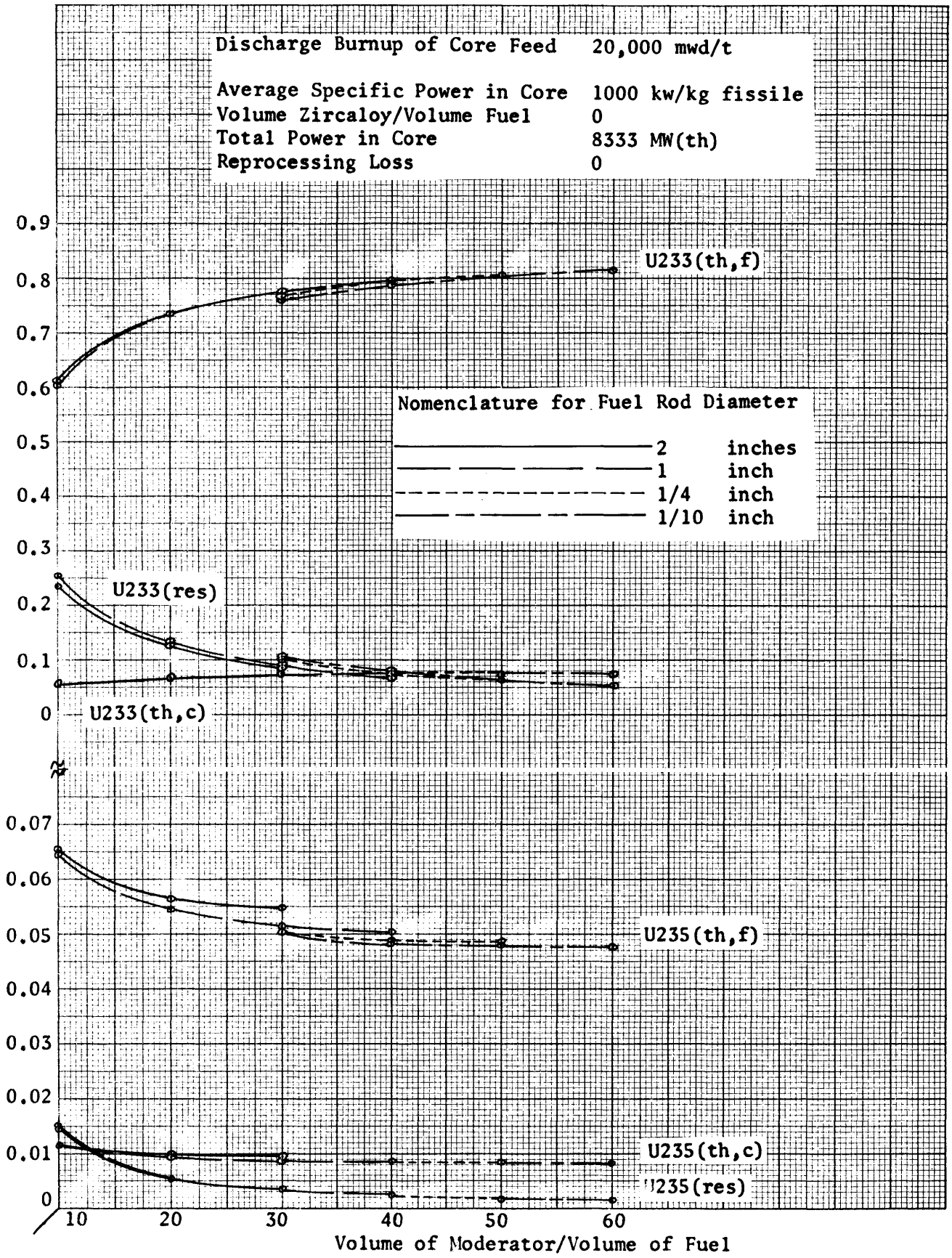

Figure 5.6: Absorptions by Fissile Nuclides vs. Volume of Moderator/Volume of Fuel: 20,000 mwd/t Burnup

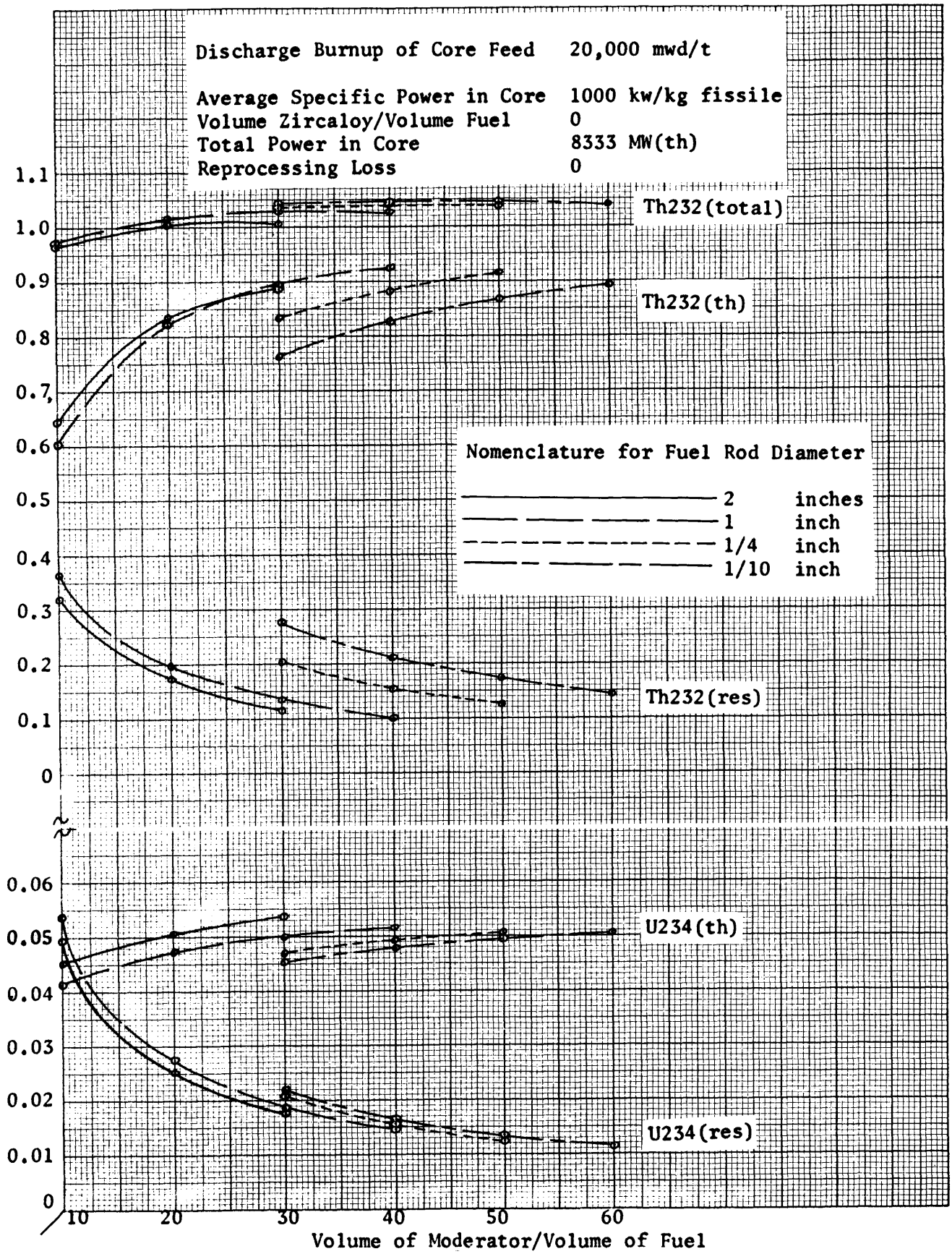

Figure 5.7: Absorptions by Fertile Nuclides vs. Volume of Moderator/Volume of Fuel: 20,000 mwd/t Burnup

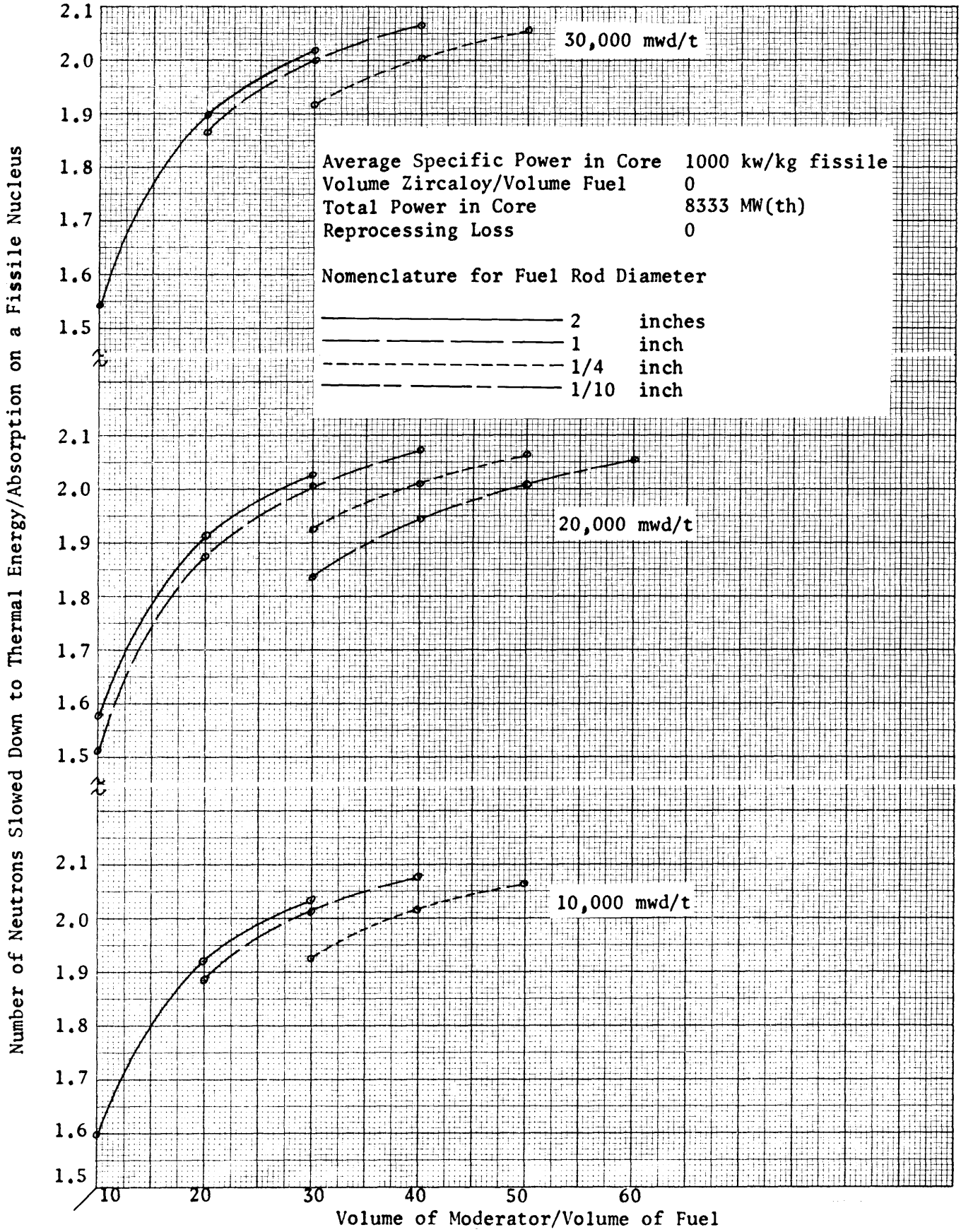

Figure 5.8: Number of Neutrons Slowed Down to Thermal Energy/Absorption in a Fissile Nucleus vs. Volume of Moderator/Volume of Fuel: 10,000 mwd/t, 20,000 mwd/t, 30,000 mwd/t Burnups

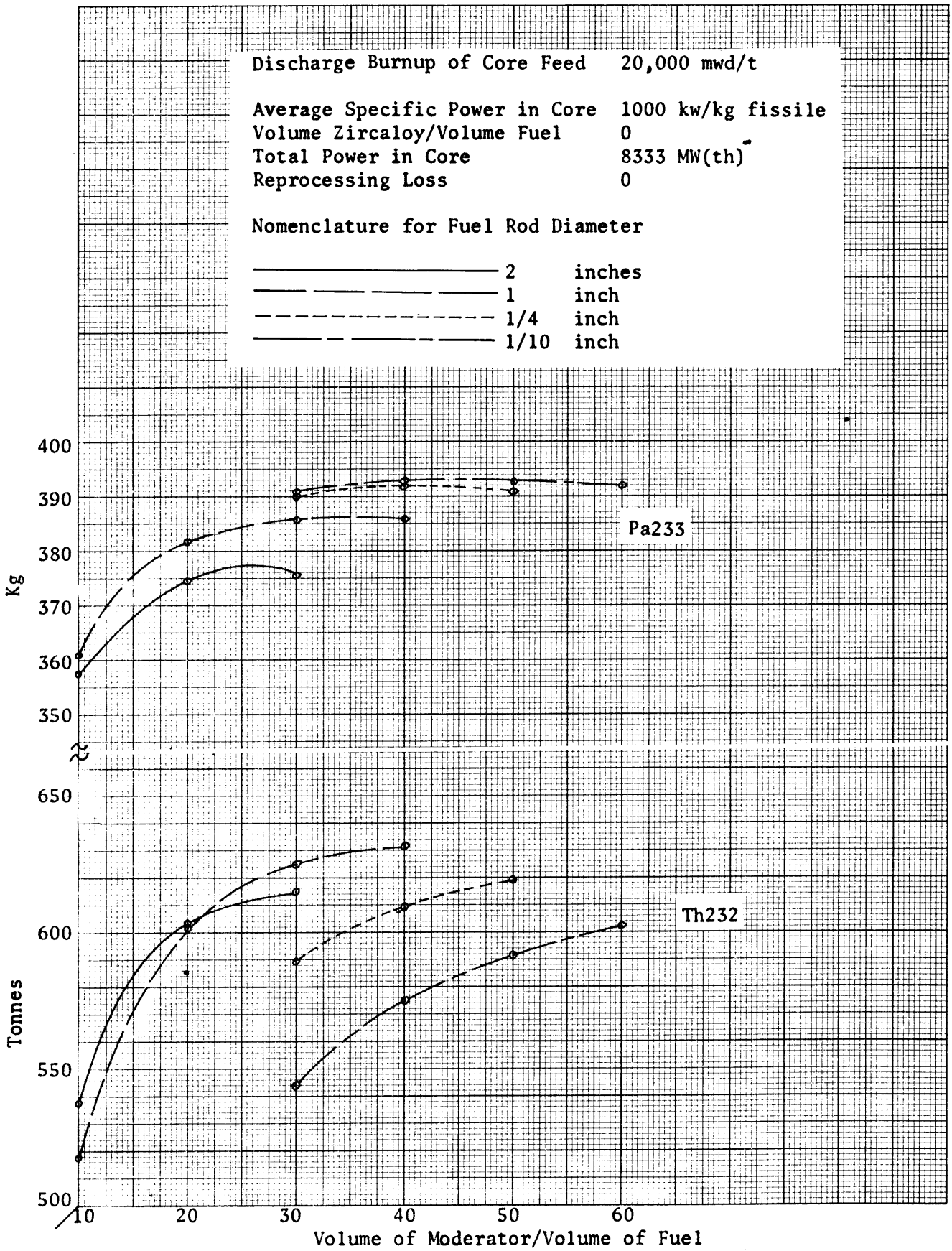

Figure 5.9: Masses of Th232 and Pa233 in Reactor Cores vs. Volume of Moderator/ Volume of Fuel: 20,000 mwd/t Burnup

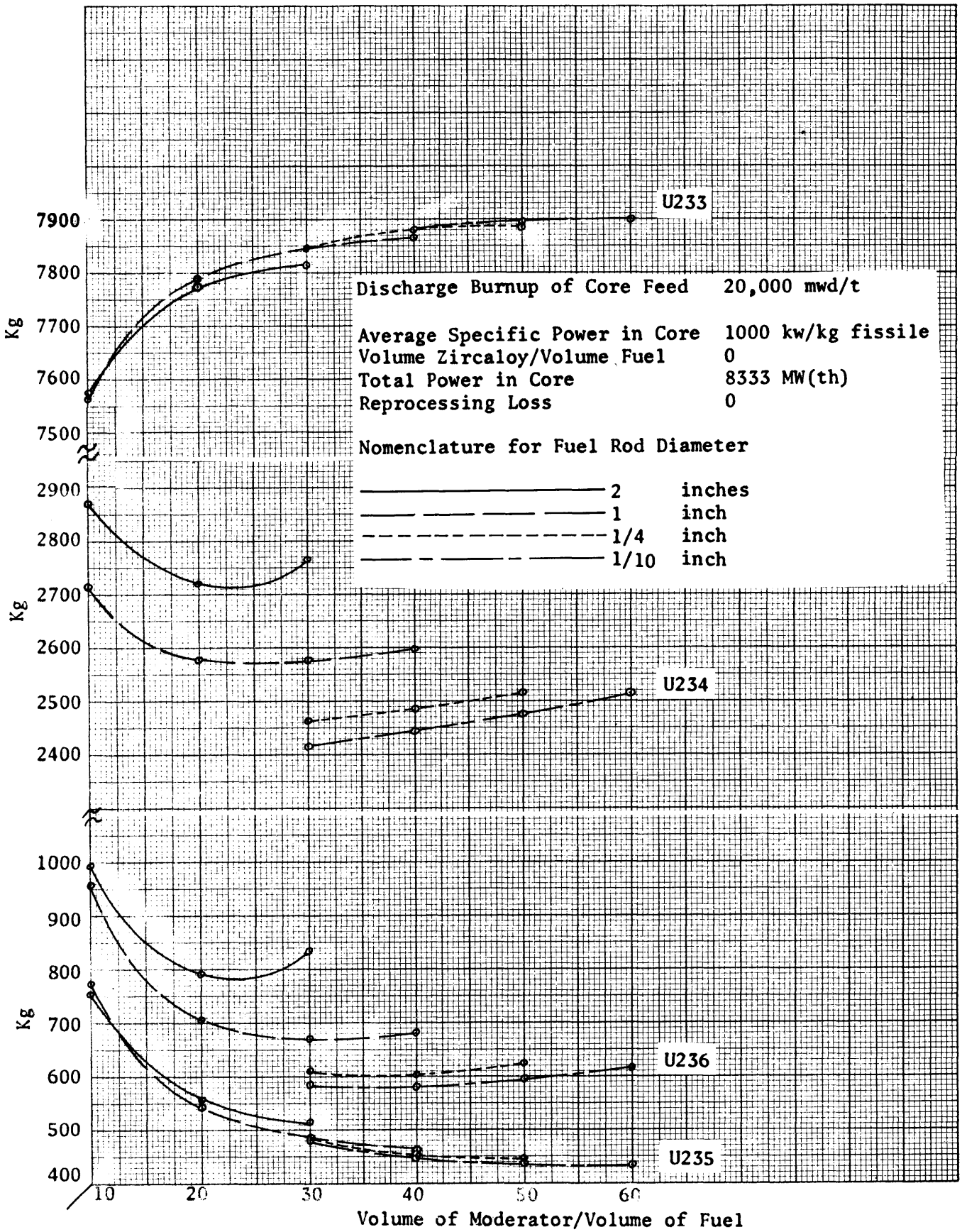

Figure 5.10: Masses of U233, U234, U235 and U236 in Reactor Cores vs. Volume of Moderator/Volume of Fuel: 20,000 mwd/t Burnup

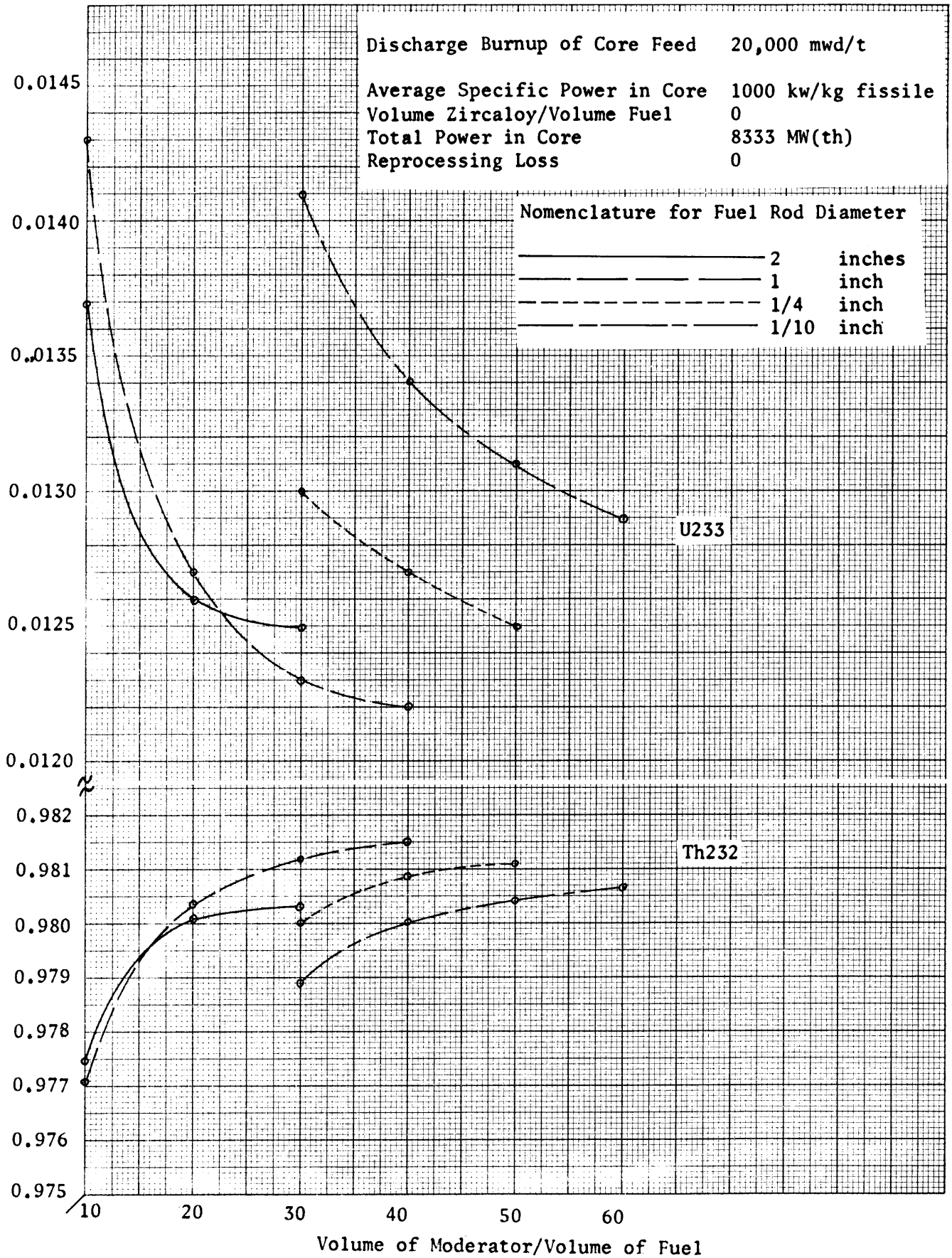

Figure 5.11: Mass Fractions of Th232 and U233 in Reactor Cores vs. Volume of Moderator/Volume of Fuel: 20,000 mwd/t Burnup

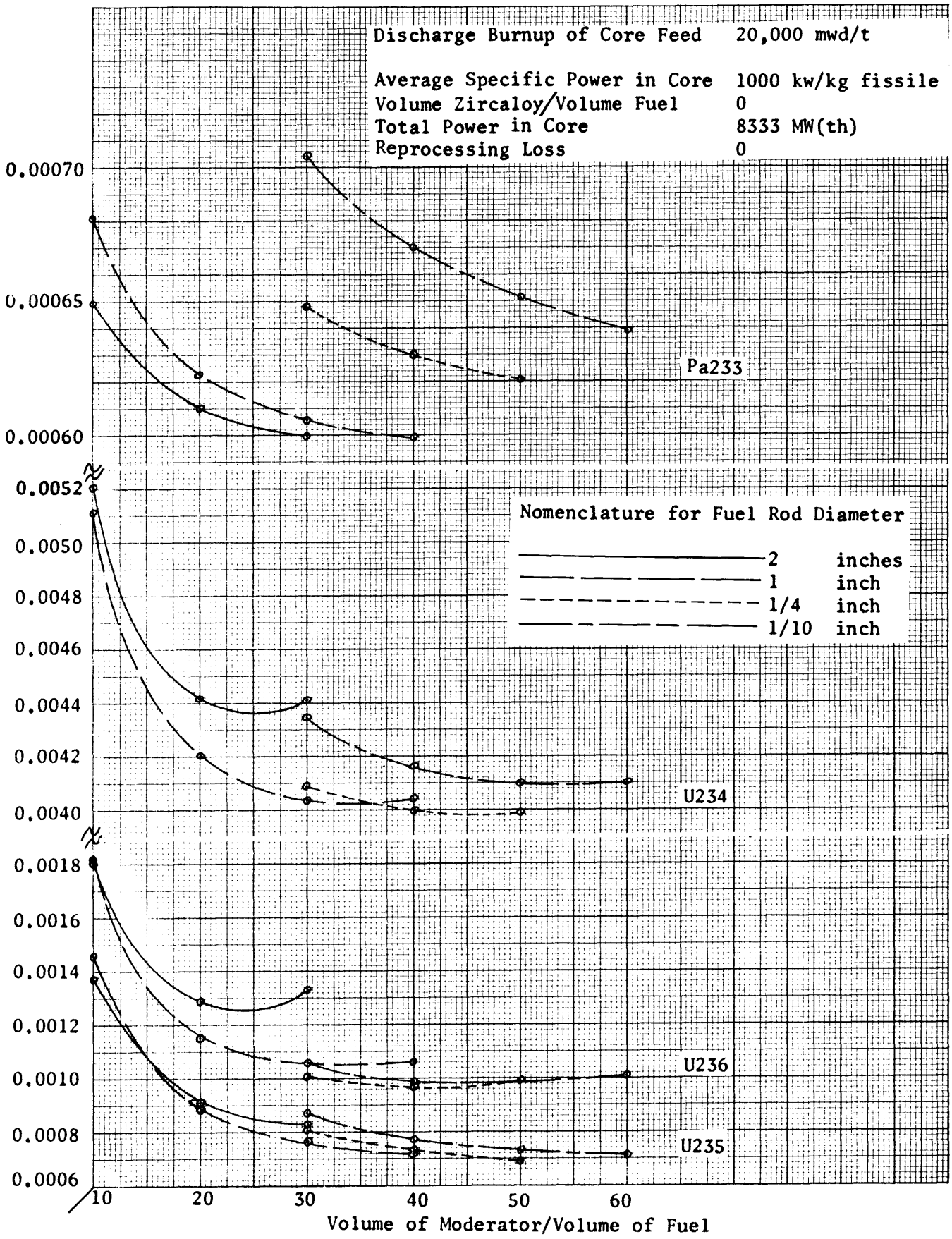

Figure 5.12: Mass Fractions of Pa233, U234, U235, and U236 in Reactor Cores vs. Volume of Moderator/Volume of Fuel: 20,000 mwd/t Burnup

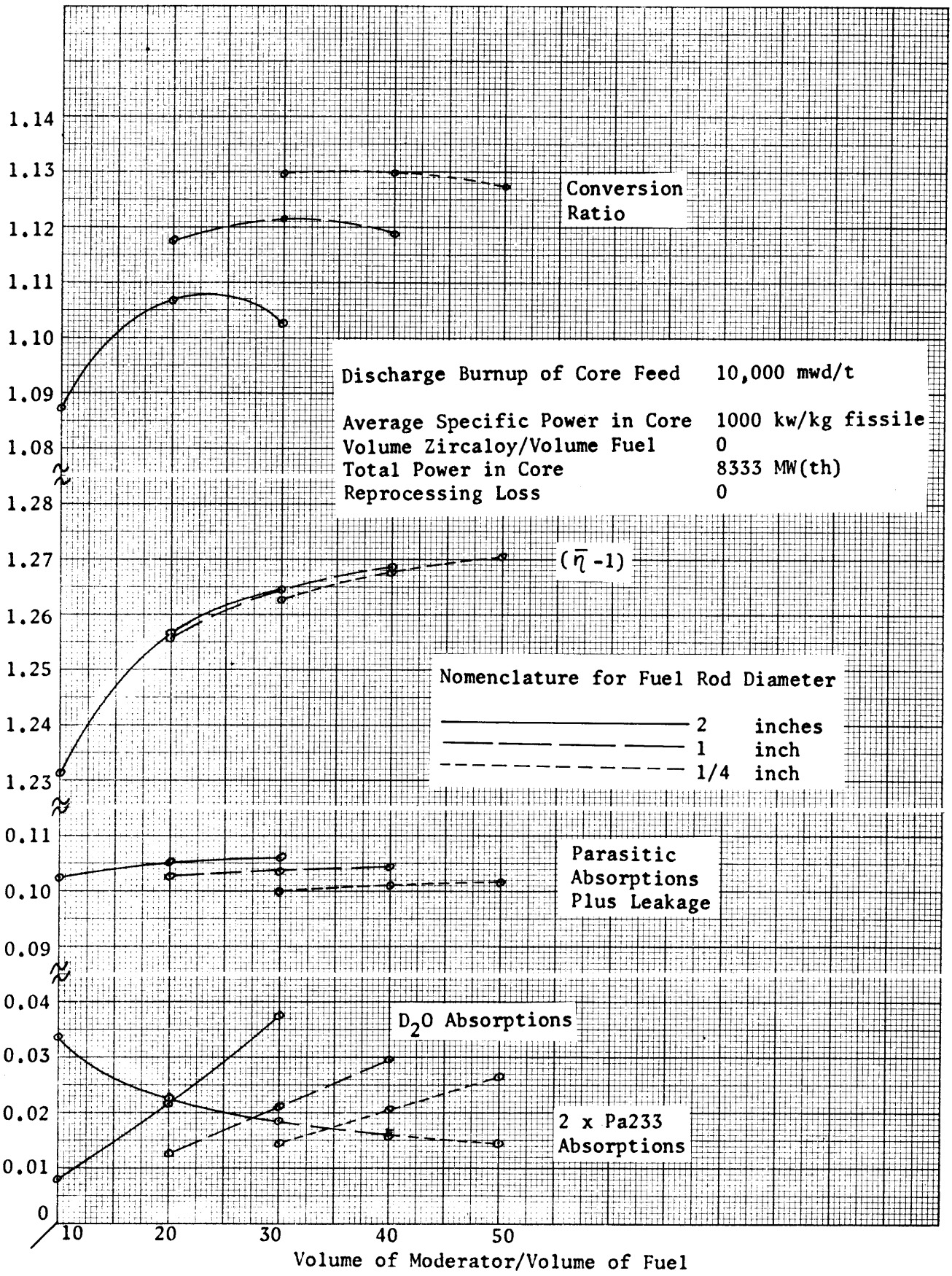

Figure 5.13: Conversion Ratio and its Components vs. Volume of Moderator/ Volume of Fuel: 10,000 mwd/t Burnup

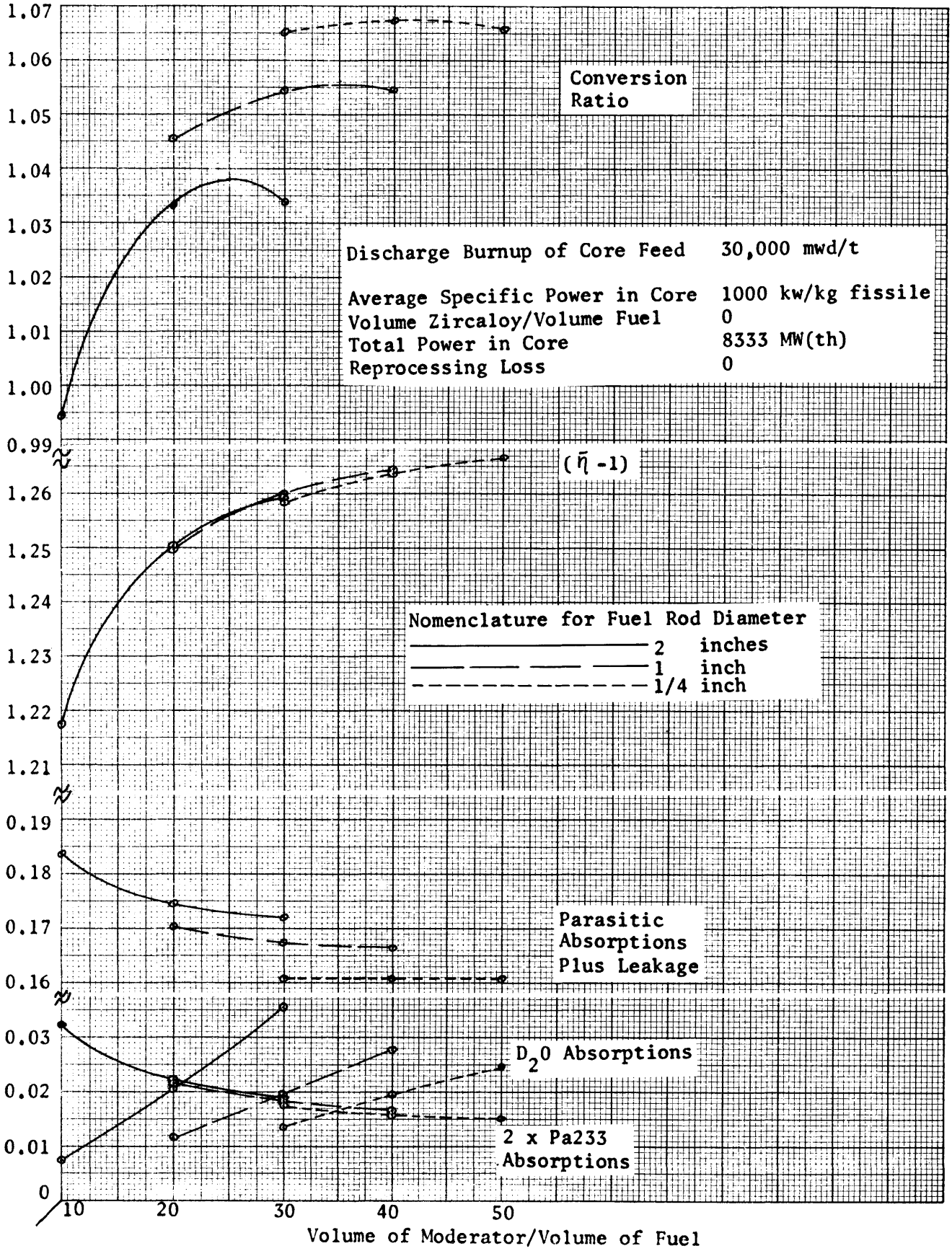

Figure 5.14: Conversion Ratio and its Components vs. Volume of Moderator/ Volume of Fuel: 30,000 mwd/t Burnup

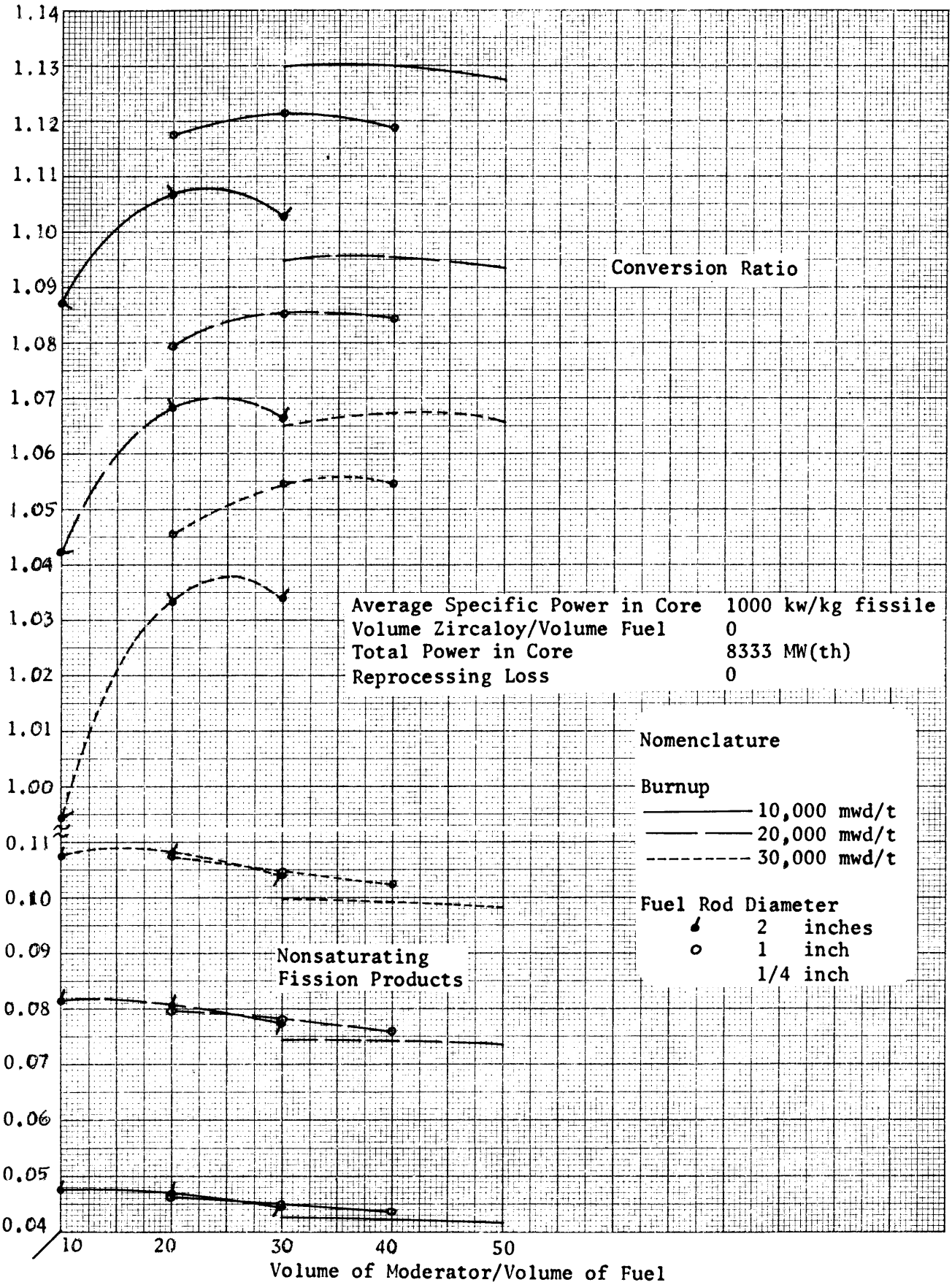

Figure 5.15 : Conversion Ratio and Absorptions by Nonsaturating Fission Products vs. Volume of Moderator/Volume of Fuel: 10,000 mwd/t, 20,000 mwd/t, 30,000 mwd/t Burnups

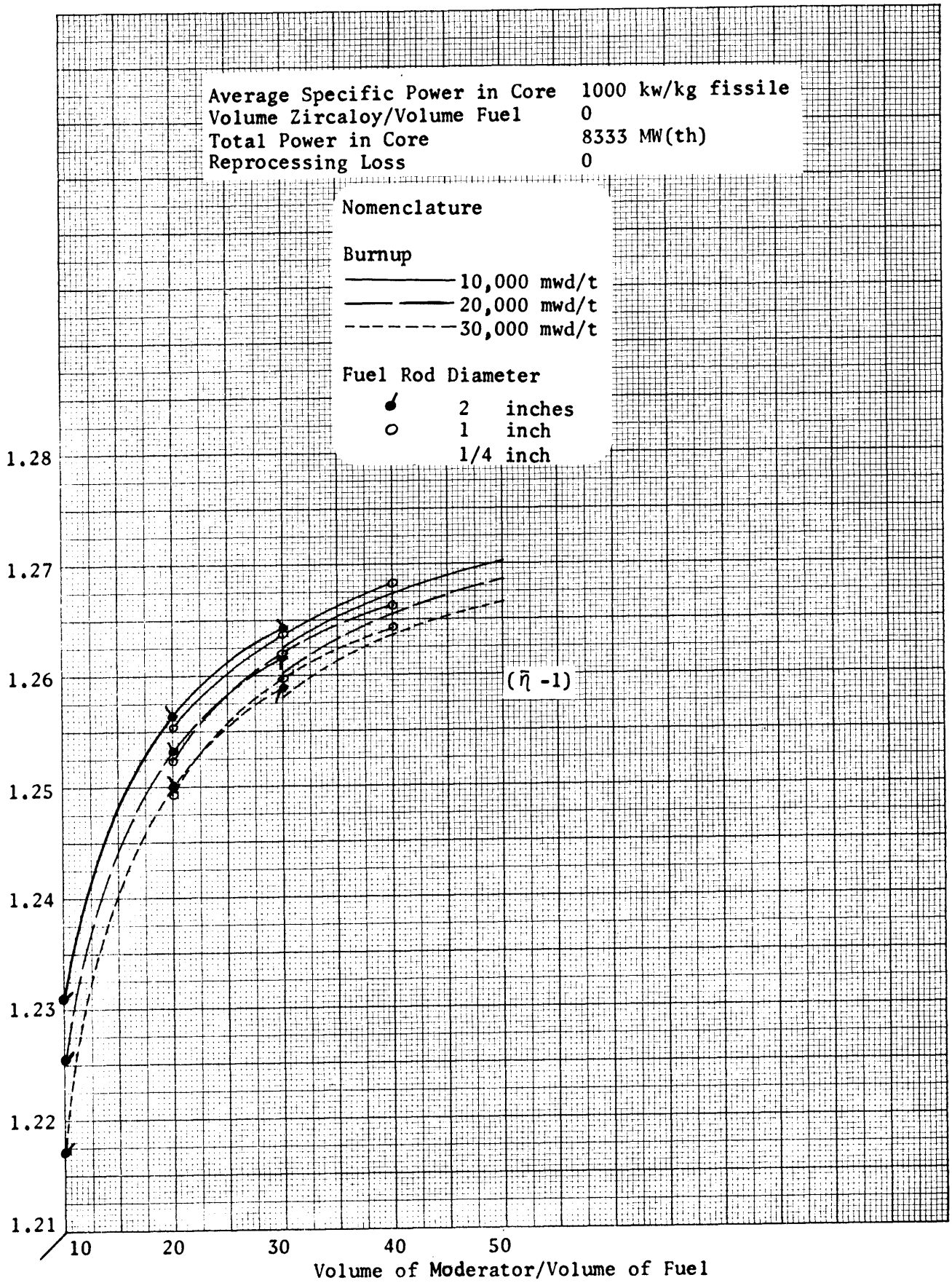

Figure 5.16: $(\bar{\eta} - 1)$ vs. Volume of Moderator/Volume of Fuel: 10,000 mwd/t, 20,000 mwd/t, 30,000 mwd/t Burnups

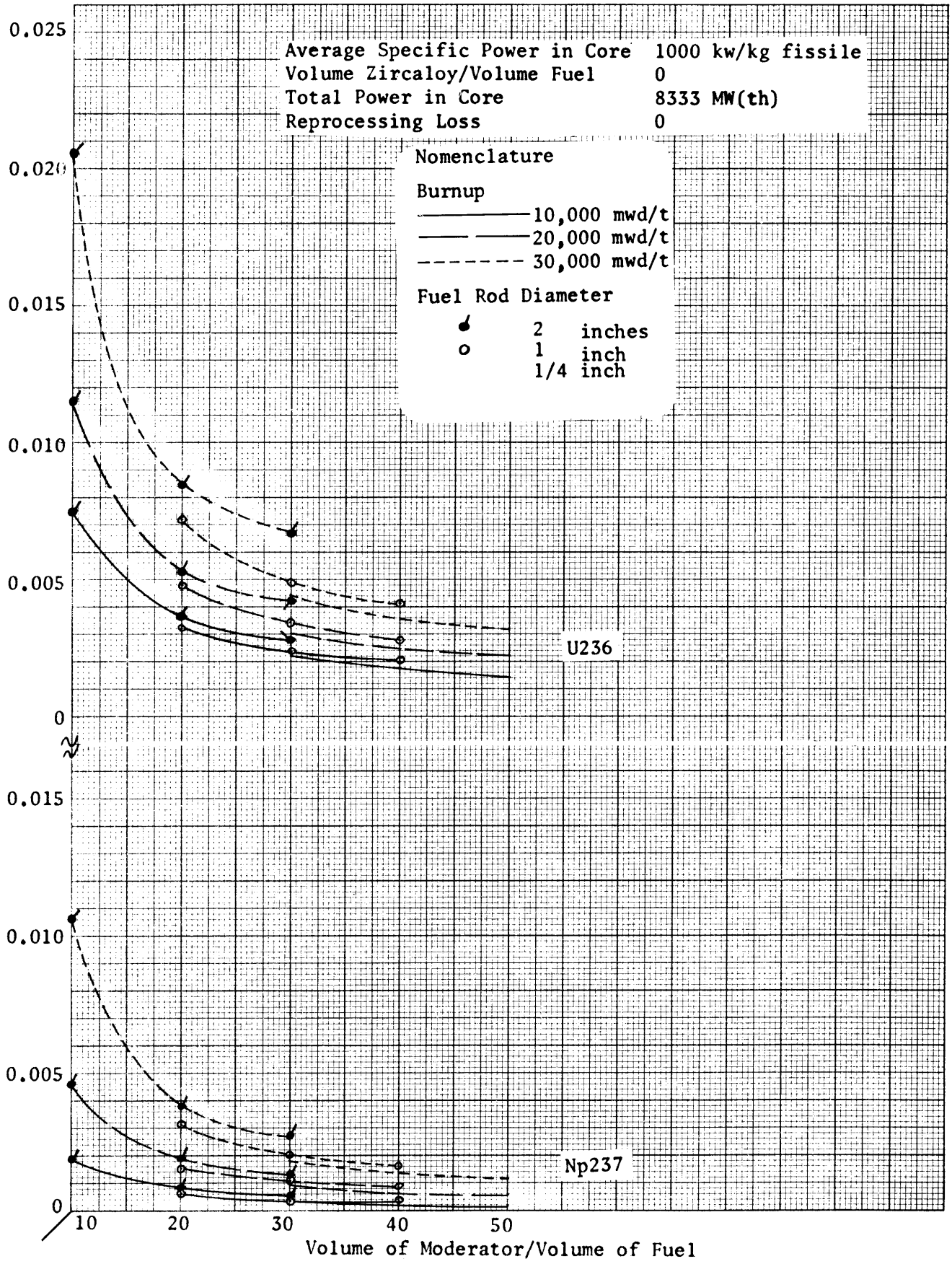

Figure 5.17: Absorptions by U236 and Np237 vs. Volume of Moderator/Volume of Fuel: 10,000 mwd/t, 20,000 mwd/t, 30,000 mwd/t Burnups

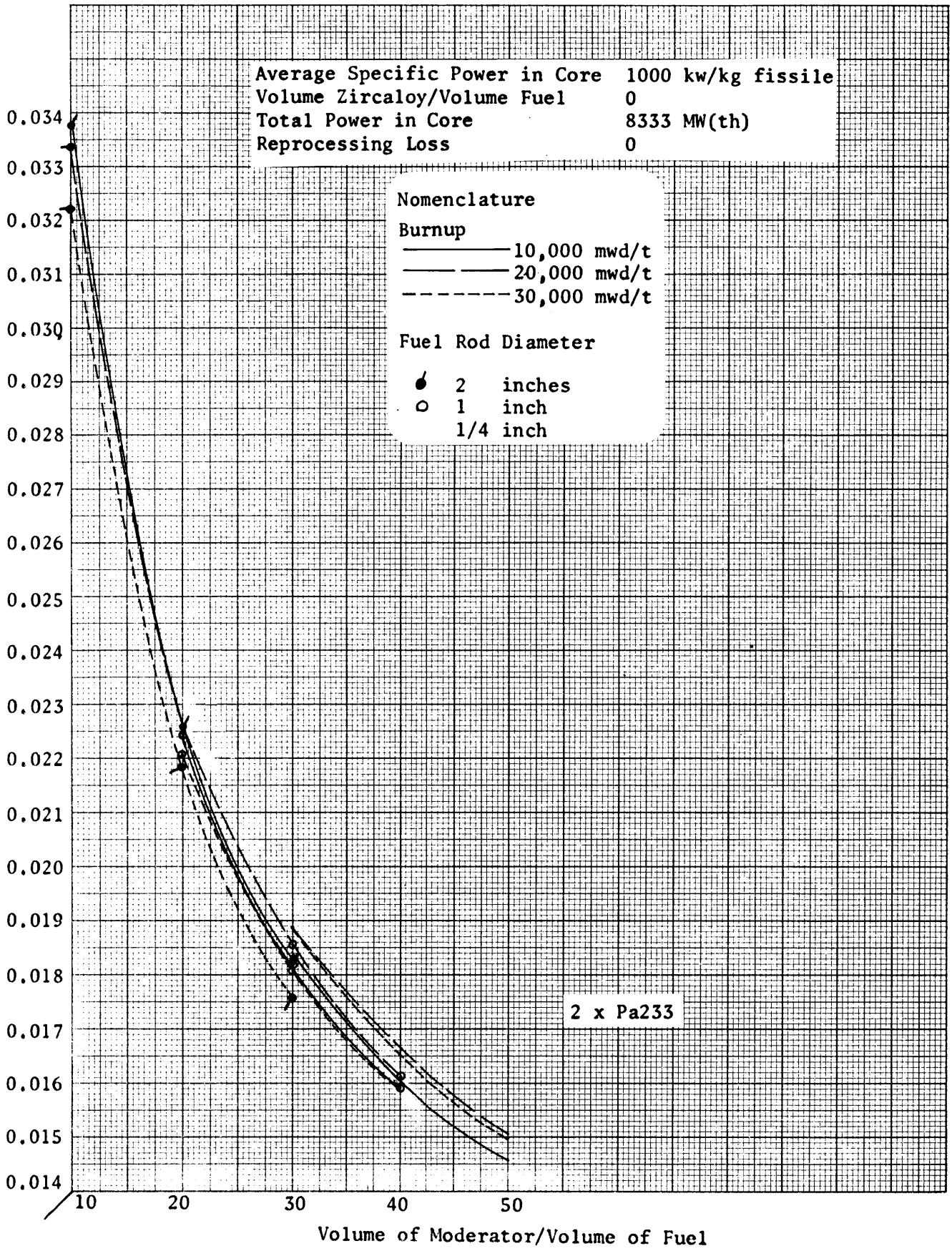

Figure 5.18: 2 x Pa233 Absorptions vs. Volume of Moderator/Volume of Fuel: 10,000 mwd/t, 20,000 mwd/t, 30,000 mwd/t Burnups

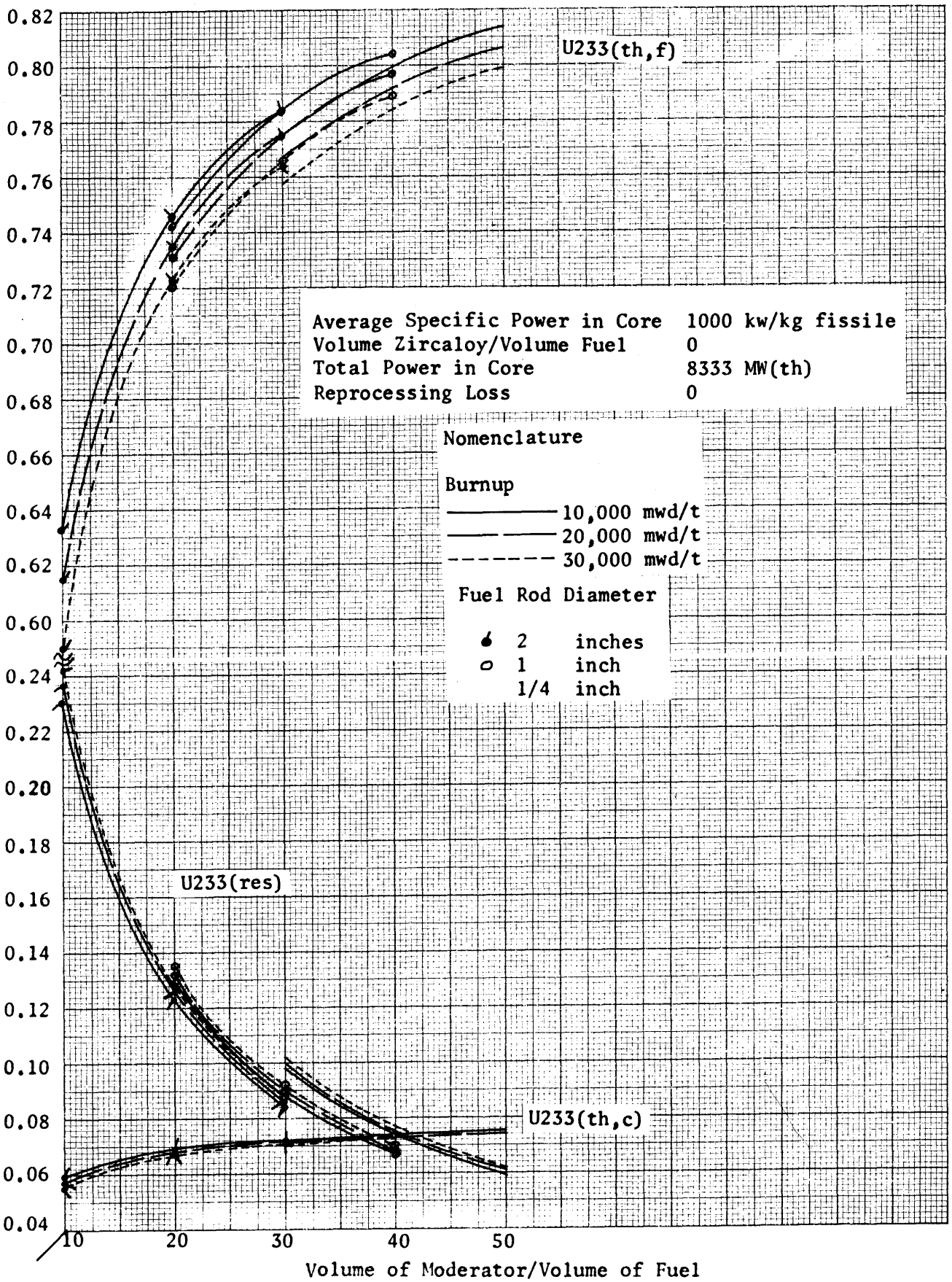

Figure 5.19: Absorptions by U233 vs. Volume of Moderator/Volume of Fuel: 10,000 mwd/t, 20,000 mwd/t, 30,000 mwd/t Burnups

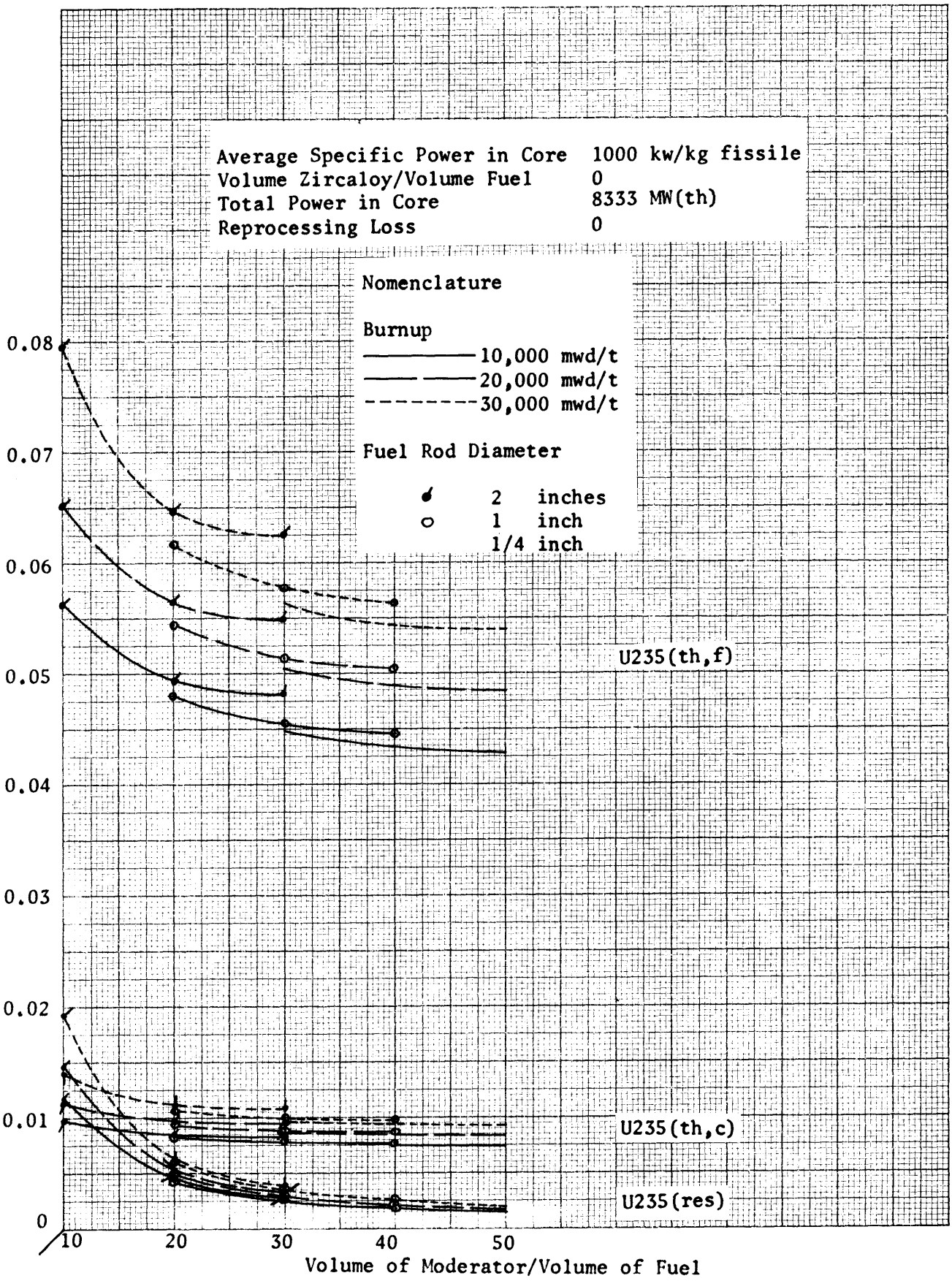

Figure 5.20: Absorptions by U235 vs. Volume of Moderator/Volume of Fuel: 10,000 mwd/t, 20,000 mwd/t, 30,000 mwd/t Burnups

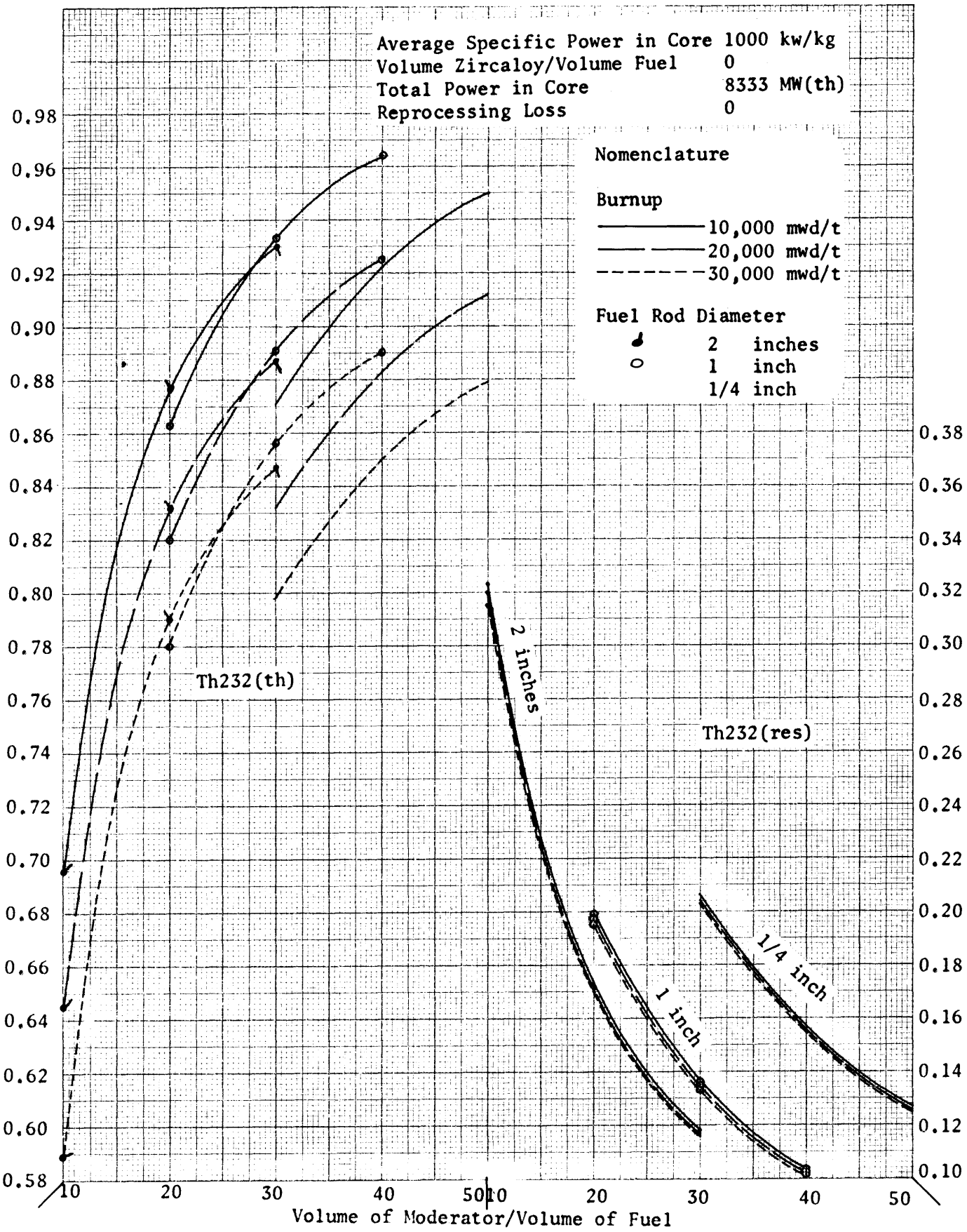

Figure 5.21: Absorptions by Th232 vs. Volume of Moderator/Volume of Fuel: 10,000 mwd/t, 20,000 mwd/t, 30,000 mwd/t Burnups

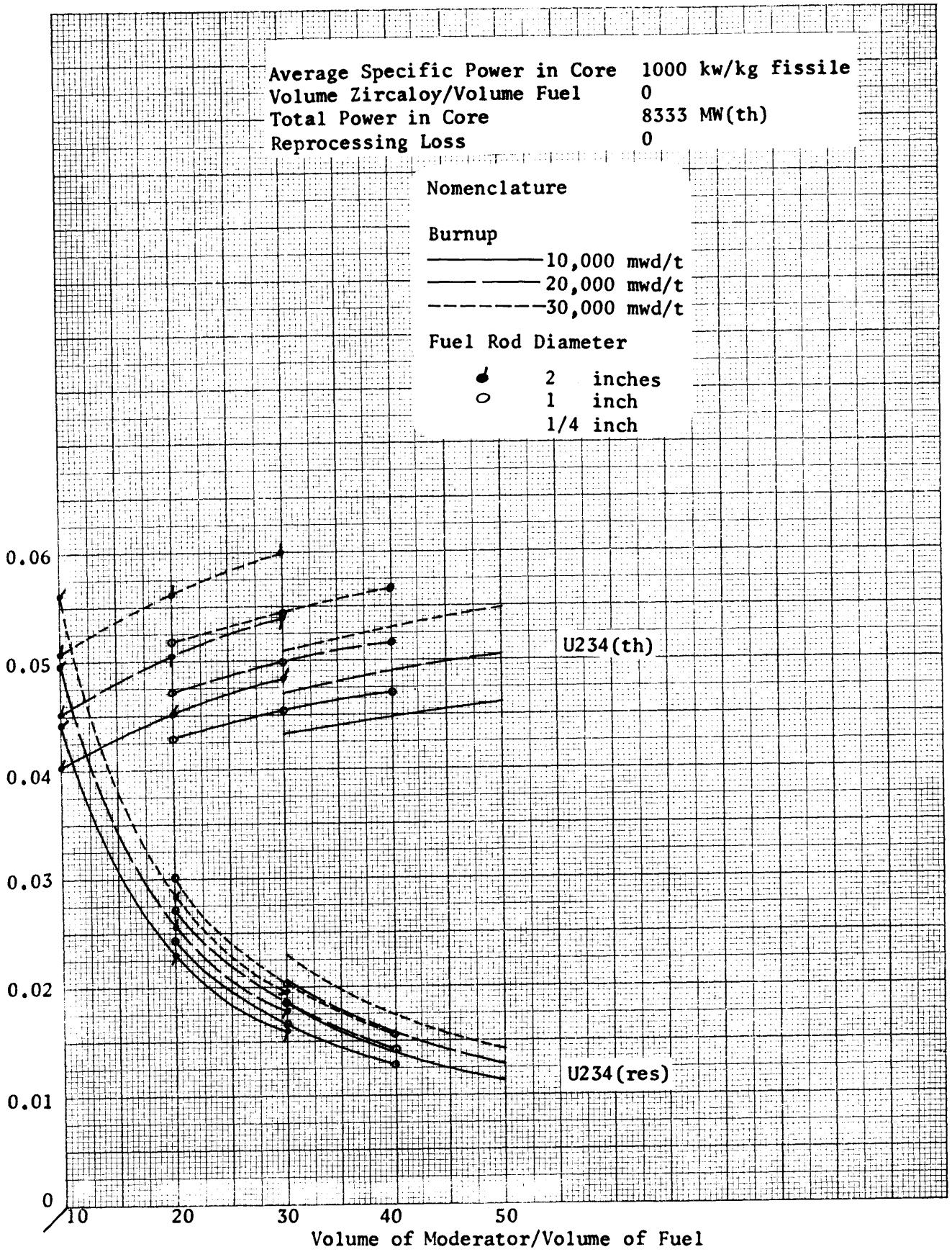

Figure 5.22: Absorptions by U234 vs. Volume of Moderator/Volume of Fuel: 10,000 mwd/t, 20,000 mwd/t, 30,000 mwd/t Burnups.

CHAPTER VI

EFFECT OF THE SECONDARY VARIABLES ON THE CONVERSION RATIO

A. Introduction

In this chapter the effects of the four secondary variables on the conversion ratio at the three feed burnups are discussed. The secondary variables are absorption in zircaloy/absorption in a fissile nucleus (determined by the variable, volume of zircaloy/volume of fuel), average specific power in the core (kw/kg fissile), reprocessing loss and total power in the core. Throughout this chapter, the remaining two primary variables are held constant at the following values:

Volume of moderator/volume of fuel	30
Fuel rod diameter	1/4 inch

This combination of volume of moderator/volume of fuel and fuel rod diameter was selected because it gave very nearly the highest conversion ratio for each feed burnup as is shown in figures 5.1, 5.13 and 5.14. The values of absorption in zircaloy/absorption in a fissile nucleus ranged from zero to about 0.11. This upper limit is a bit high for zircaloy cladding but is a reasonable value for the ratio of absorptions in cladding to absorptions in fissile material when stainless steel is used for cladding. The values of the average specific power ranged from 1000 kw/kg fissile to 12,000 kw/kg fissile. This lower limit approximates the average specific power of today's light water reactors while the upper limit is about 50% above the values suggested by the Savannah River Laboratory for advanced heavy water reactors (B1,B2). The values of reprocessing loss ranged from zero to 4% of the reactor fuel discharge.

The values of the total thermal power ranged from 8333 MW to 500 MW.

The absorption in zircaloy/absorption in a fissile nucleus affects the conversion ratio primarily by absorbing thermal neutrons which would otherwise have been absorbed in thorium. The average specific power in the core affects the conversion ratio primarily through increased absorptions of resonance and thermal neutrons by nuclei of Pa233 which would otherwise decay to U233. The increase in the reprocessing loss affects the conversion ratio primarily by increasing the fissile sink as shown in equation (4E1). The primary effect of the change in total power is through changes in the size of the core, which changes the net leakages out of the core and into the blanket.

There is a basic difference between the interpretations of the results for the secondary variables and the results for the primary variables. When the effects of the primary variables were studied, a feed burnup and fuel rod diameter were selected, the moderator ratio was increased and, as a result, the conversion ratio changed. That is, the change in the conversion ratio was looked upon, for the most part, as the <u>effect</u> of changing the primary variables. However, when one increases the absorption in zircaloy/absorption in a fissile nucleus or the average specific power of the core, one deliberately decreases the conversion ratio. Therefore, this deliberate decrease in the conversion ratio can be looked upon as a <u>cause</u> of other changes in the system.

When either the absorption in zircaloy/absorption in a fissile nucleus or the average specific power in the core is increased, the increased absorptions by zircaloy or Pa233 reduce the number of thermal neutrons which are available for absorption by the fissile nuclides. In order to maintain criticality, the number of resonance neutrons absorbed

by the fissile nuclides must increase. In other words, an increase of these two secondary variables causes the neutron spectrum to become more epithermal.

All of the neutron balance results are contained in table 6.1. The internal conversion ratios were calculated with equation (4E2a). The conversion ratios with reprocessing loss were calculated with equation (4E1). The masses and compositions of reactor inventories are given in table 6.2. The input and output flow rates of the fuel nuclides and the fissile nuclide consumption rates are listed in table 6.3. Selected results from these tables are plotted with the secondary variables as abscissa and feed burnup as a parameter.

B. Absorption in zircaloy per absorption in a fissile nucleus

1. Burnup of 20,000 mwd/tonne of metal feed

a. Conversion ratio and its components

The variable "absorption in zircaloy/absorption in a fissile nucleus" will hereafter be referred to as "zircaloy absorption ratio." The conversion ratio and its components are plotted in figure 6.1 as a function of the zircaloy absorption ratio for a feed burnup of 20,000 mwd/t. The other secondary variables are held constant at the following values:

Average specific power	1000 kw/kg fissile
Reprocessing loss	0
Total power	8333 MW(th)

A value of the conversion ratio for a given abscissa is obtained by subtracting from ($\bar{\eta}$-1) the sum of D_2O absorption, 2 x Pa233 absorption, leakage and parasitic absorptions other than by zircaloy, and the abscissa itself.

The conversion ratio has a value of 1.0 at a zircaloy absorption ratio of about 0.083. The conversion ratio curve and the curves of its

components have discontinuous slopes at this point because when the conversion ratio falls below 1.0, fresh U235 is added to the reactor discharge fuel to make the new core feed. In other words, a change in the fuel cycle flow sheet occurs at this point.

The curve of $(\bar{\eta}-1)$ in figure 6.1 decreases with increasing zircaloy absorption ratio because as the conversion ratio decreases, an increasing fraction of the core discharge is recycled into the core feed and, therefore, the concentration in the feed of U235, with its lower value of η, increases. Also as the zircaloy absorption ratio increases, the neutron spectrum becomes more epithermal and this causes $\bar{\eta}$ to decrease further. The curve of $(\eta-1)$ decreases more rapidly as the conversion ratio falls below 1.0 because fresh U235 is added to the feed.

The $(\bar{\eta}-1)$ curves are related to the curves of the neutrons slowed down to thermal energy per absorption in a fissile nucleus. These curves are shown in figure 6.6 for the three burnups. They decrease with increasing zircaloy absorption ratio just as the curves of $(\bar{\eta}-1)$ do. However, after dropping below a conversion ratio of 1.0, the curve of neutrons slowed down to thermal energy per absorption in a fissile nucleus decreases at a slower rate with increasing zircaloy absorption ratio for 20,000 mwd/t although the curves of $(\bar{\eta}-1)$ decrease at a faster rate. This is because of the decrease in the rate of increase in resonance absorption with increasing zircaloy absorption ratio of U236 and Np237 as shown in figure 6.2 and U234 as shown in figure 6.5.

The behavior of the curve of leakage and parasitic absorptions other than by zircaloy in figure 6.1 is due primarily to the behavior of the curves of absorptions by U236 and Np237 shown in figure 6.2. As the zircaloy absorption ratio increases toward 0.083, an increasing fraction

of the core discharge is recycled into the core feed. Therefore the concentration of U236 in the core increases rapidly. When the zircaloy absorption ratio increases above 0.083 and the conversion ratio drops below 1.0, 100% of the core discharge is recycled into the feed. Further increases in the concentration of U236 in the core and, therefore, increases in absorption by U236 are due primarily to captures by U235 whose concentration in the core increases rapidly as the conversion ratio decreases below 1.0. Since Np237 is the (n, β^-, γ) daughter of U236, the shapes of its absorption curves are similar to those of U236.

The curve of 2 x Pa233 absorption of figure 6.1 decreases with increasing zircaloy absorption ratio for reasons made clearer in figure 6.2. The Pa233 thermal absorption decreases because of the decrease in the number of neutrons slowed down to thermal energy per absorption in a fissile nucleus as shown in figure 6.6 and the increased competition for the thermal neutrons caused by the added zircaloy. The resonance absorption decreases because Pa233 loses out in the competition for resonance neutrons with the other resonance absorbers.

The absorption by D_2O shown in figure 6.1 decreases with increasing zircaloy absorption ratio because of the decrease in the number of neutrons slowed down to thermal energy per absorption in a fissile nucleus and the increased competition for the thermal neutrons caused by the added zircaloy.

As previously stated, the conversion ratio is given by the following equation:

Conversion ratio = [($\bar{\eta}$ -1) - (D_2O absorptions) - (2 x Pa233 absorption) - (leakage and parasitic absorptions other than by zircaloy)] - [zircaloy absorption ratio]

(6B1)

If the only effect of the addition of zircaloy to the reactor system was to absorb thermal neutrons which would have otherwise have been absorbed in thorium, all of the curves in figure 6.1 other than the conversion ratio curve would be horizontal lines and the conversion ratio curve would have a slope of -1. The deviation of the conversion ratio curve from a 45° line at any value of zircaloy absorption ratio is therefore a measure of the deviation of the other curves from horizontal lines.

b. Parasitic absorptions plus leakage

In general the fast and thermal leakages in table 6.1 increase with increasing zircaloy absorption ratio because of increased fast and thermal flux gradients. This is true for the thermal leakage despite the fact that the thermal diffusion length decreases.

The absorption by the "Sm" group is shown in figure 6.2. It increases with increasing zircaloy absorption ratio despite the decrease in the number of neutrons slowed down to thermal energy per absorption in a fissile nucleus as shown in figure 6.6. This is because the fission yield of the "Sm" group is about 50% higher for U235 than for U233. The absorption by Xe135 shown in figure 6.2 decreases with increasing zircaloy absorption ratio because of the decrease in the number of neutrons slowed down to thermal energy per absorption in a fissile nucleus. The absorption by nonsaturating fission products shown in figure 6.3 decreases with increasing absorption ratio for the same reason as that given for Xe135 plus the fact that the nonsaturating fission products lose out to the added zircaloy in the competition for thermal neutrons.

c. Fissile absorptions

The absorptions by U233 and U235 are shown in figure 6.4. The thermal

absorptions by U233 decrease with increasing zircaloy absorption ratio because of the decrease in the number of neutrons slowed down to thermal energy per absorption in a fissile nucleus and the increased competition for thermal neutrons by other absorbers, notably U234, U235 and zircaloy. The decrease in U233 thermal absorption is more rapid after the conversion ratio drops below 1.0 because of the feeding of fresh U235 into the core.

The U233 resonance absorption initially increases with increasing zircaloy absorption ratio because of the increasing epithermal character of the spectrum. After the conversion ratio drops below 1.0 and fresh U235 is added to the feed, the U233 concentration increases less rapidly with increasing zircaloy absorption ratio and the U233 resonance absorption decreases.

All of the U235 absorptions increase with increasing zircaloy absorption ratio because the U235 concentration in the core rapidly increases with decreasing conversion ratio.

d. Fertile absorptions

The absorption by Th232 and U234 are shown in figure 6.5. The Th232 resonance absorption decreases with increasing zircaloy absorption ratio because of the rapidly increasing concentration of other resonance absorbers. The Th232 thermal absorption decreases because of the decrease in the number of neutrons slowed down to thermal energy per absorption in a fissile nucleus and the increased competition for thermal neutrons by U234, U235 and the added zircaloy.

The U234 absorptions increase with increasing zircaloy absorption ratio for conversion ratio greater than 1.0 because as the conversion ratio decreases an increasing fraction of the core discharge is recycled into the core feed. For conversion ratio less than 1.0, when 100% of the

core discharge is recycled into the core feed, the U234 absorptions drop because the U233 thermal captures and resonance absorptions drop as shown more clearly in figure 6.11.

2. Burnups of 10,000 mwd/t and 30,000 mwd/t.

The conversion ratio and its components for 10,000 mwd/t and 30,000 mwd/t are shown in figures 6.7 and 6.8 respectively with zircaloy absorption ratio as abscissa. The other secondary variables are held constant at the same values as for 20,000 mwd/t. The complete neutron balance results are listed in table 6.1. The components of the neutron balance other than those plotted in figures 6.7 and 6.8 behave in a similar fashion to the same components for a burnup of 20,000 mwd/t.

3. Comparisons among burnups

The results of this section are plotted with zircaloy absorption ratio as abscissa and feed burnup as a parameter. The conversion ratios are shown in figure 6.9. The difference between conversion ratios for different burnups and a given zircaloy absorption ratio is due primarily to the differences in the quantities shown in figure 6.10. These quantities are $(\bar{\eta}-1)$ and absorptions by nonsaturating fission products, U236 and Np237. The principal effect on conversion ratio, naturally, is from the nonsaturating fission products, which have the greatest effect at the highest burnup.

The absorptions by U233 are shown in figure 6.11. The thermal absorptions decrease with increasing burnup because of the decrease in the number of neutrons slowed down to thermal energy per absorption in a fissile nucleus as shown in figure 6.6 and because of the increasing reliance on U235 fissions for power production. The resonance absorptions

by U233 increase with increasing burnup because of the increasing epithermal character of the spectrum.

The absorptions by U235 are shown in figure 6.2. All of these absorptions increase with increasing burnup because of the rapidly increasing U235 concentrations in the cores with the lower conversion ratios.

The absorptions by Th232 are shown in figure 6.13. The thermal absorptions decrease with increasing burnup because, once again, of the decrease in the number of neutrons slowed down to thermal energy per absorption in a fissile nucleus. The resonance absorptions decrease with increasing burnup because of the rapid increase with increasing burnup of the concentrations of other resonance absorbers.

The absorptions by U234 are shown in figure 6.14. At higher burnups and lower conversion ratios, a larger fraction of the core discharge is recycled into the feed. This causes the U234 concentrations and absorptions to increase.

4. Structural materials other than zircaloy

If neutron absorbing structural materials other than zircaloy were present in the core, their effect on the conversion ratio could be estimated approximately by finding the volume ratio of zircaloy which would have the name thermal neutron absorption as the other sturctural material, from equation (6B2)

$$V_{Zr} = \frac{\psi_i \Sigma_i^{2200} V_i}{\Sigma_{Zr}^{2200}} \qquad (6B2)$$

where

V_{Zr} = volume ratio, zircaloy to fuel, equivalent to other material

V_i = volume ratio, other material to fuel

ψ_i = ratio of average thermal flux to which other material is exposed to thermal flux at surface of fuel

Σ_{Zr}^{2200} = macroscopic absorption cross section of zircaloy for 2200 m/sec neutrons, 0.00910 cm^{-1} (appendix B)

Σ_i^{2200} = macroscopic absorption cross section for 2200 m/sec neutrons of other material, e.g. 0.267 cm^{-1} for stainless steel (T1).

Using the equivalent value of volume of zircaloy/volume of fuel calculated with equation (6B2) in table 6.1, one can arrive at the corresponding values of the conversion ratio and the components of the neutron balance.

C. Average specific power in the core

1. Burnup of 20,000 mwd/tonne of metal feed

a. Conversion ratio and its components

The results of section VIC are plotted as a function of the average specific power in the core. The conversion ratio and its components are plotted in figures 6.15 and 6.16 for a feed burnup of 20,000 mwd/t. The other secondary variables are held constant at the following values:

Zircaloy absorption ratio	0
Reprocessing loss	0
Total power	8333 MW(th)

A value of the conversion ratio for a given abscissa is obtained by sub-

tracting from ($\bar{\eta}$-1) the sum of D_2O absorption, 2 x Pa233 absorption and parasitic absorptions plus leakage.

The principal effect on conversion ratio of increasing the specific power is to increase neutron absorption by Pa233. This increased absorption is a consequence of the higher flux which accompanies higher specific power, which increases the fraction of Pa233 which absorbs neutrons and decreases the fraction which decays to U233.

A comparison of the effects on the conversion ratio of the absorption of a neutron by zircaloy and by Pa233 is instructive. When a neutron is absorbed by zircaloy, the primary effect is to remove a neutron which would otherwise have been absorbed by Th232. When a neutron is absorbed by Pa233, that neutron is prevented from being absorbed by Th232 and the Pa233 nucleus is prevented from decaying to U233. Thus, absorption of a neutron by Pa233 in itself has twice the effect on conversion ratio of absorption of a neutron by zircaloy. But that is not all. In addition, the neutron absorbed by Pa233 produces a U234 nucleus which competes with the Th232 nuclei for the neutrons available for absorption in fertile material. Since η of the U235 produced by neutron absorption in U234 is less than η of the U233 eventually produced by the neutron absorption in Th232, an incremental increase in 2 x Pa233 absorption is more effective in lowering the conversion ratio than an incremental increase in the zircaloy absorption ratio. This effect is seen in figure 6.16A which shows a plot of the conversion ratio versus the zircaloy absorption ratio from section VIB and a plot of the conversion ratio versus (2 x Pa233 absorption - 0.019)* from this section.

---

*0.019 is 2 x Pa233 absorptions at the standard specific power of 1000 kw/kg.

The conversion ratio has a value of 1.0 at an average specific power of about 6250 kw/kg fissile as shown in figure 6.15. As in the case of the results for the zircaloy absorption ratio, the conversion ratio curve and the curves of its components have discontinuous slopes at the point where the conversion ratio equals 1.0 because U235 makeup feed is started at this point.

The curve of $(\bar{\eta}-1)$ shown in figure 6.16 decreases rapidly with increasing specific power because of the rapid buildup of U235, as indicated previously. The curves of neutrons slowed down to thermal energy per absorption in a fissile nucleus are shown in figure 6.22 for all three feed burnups. The curve for 20,000 mwd/t decreases less rapidly with increasing specific power after the conversion ratio drops below 1.0. This is because of the less rapid increase with increasing specific power in the resonance neutrons absorbed by several of the nuclides, notably U236 and Np237 as shown in figure 6.17 and U234 as shown in figure 6.21.

The shape of the curve of parasitic absorptions plus leakage shown in figure 6.16 is determined by the U236 and Np237 absorption curves shown in figure 6.17.

The D_2O absorption curve shown in figure 6.16 decreases with increasing specific power because of the decrease in the number of neutrons slowed down to thermal energy per absorption in a fissile nucleus and the increased competition for thermal neutrons by other nuclides.

The absorptions by Pa233 shown in figure 6.16 increase with increasing specific power for two reasons. The first is that as the fast and thermal fluxes increase, the Pa233 branching ratio shifts from β^- decay to neutron absorption. The second reason is that the Pa233 concentration in

the core increases with increasing specific power because of the increasing Th232 absorption rate. The Pa233 resonance and thermal absorptions are shown in figure 6.17. The second derivatives of the Pa233 absorption curves are negative because as the specific power increases, the conversion ratio decreases and the core becomes less dependent on U233 for power production and more dependent on U235. Because the second derivative of the 2 x Pa233 absorption curve is negative, the second derivative of the curve of the conversion ratio is positive.

b. Parasitic absorptions plus leakage

The net fast and thermal leakages out of the core and into the blanket are shown in figure 6.19. The absolute values of the net leakages increase as specific power increases due to the increasing flux gradients. The overall thermal leakage from the reactor also increases with increasing specific power because of the increasing thermal flux gradient. However, the overall fast leakage from the reactor, after an initial increase, decreases with increasing specific power. As the specific power increases and the core volume decreases, the two-foot thick blanket represents an increasing fraction of the total reactor volume and slows down an increasing fraction of the fast neutrons leaking out of the core. This, presumably, causes the overall fast leakage from the reactor to decrease at high specific power. It is not clear, however, that this decrease in overall fast leakage from the reactor with increasing average specific power actually occurs. It is seen in figure 6.19 that the overall leakage from the reactor is the difference between the two numbers whose absolute values are large: the net leakage out of the core and the net leakage into the blanket. The errors in calculating these net leakages, $[(\Sigma D_{fast} \nabla^2 \phi_{fast} \triangle \text{Volume})/(\text{fissile absorptions})]$, using the difference

approximation for ∇^2, are probably as large as the calculated overall fast leakage from the reactor. In any event, the overall fast leakage from the reactor, whatever its value, is inconsequential in this study of the effects of the average specific power.

The absorption by the "Sm" group is shown in figure 6.17. The "Sm" group absorption increases with increasing specific power because of its 50% larger fission yield from U235 fissions than from U233 fissions. The absorption by the nonsaturating fission products is shown in figure 6.18. These absorptions decrease with increasing specific power because of the decrease in the number of neutrons slowed down to thermal energy per absorption in a fissile nucleus and the increase in thermal absorptions by Pa233, U234, U235 and Xe135. The Xe135 absorption curve, shown in figure 6.18, increases with increasing specific power because the increasing thermal flux causes the Xe branching ratio to shift from radioactive decay toward thermal neutron absorption.

c. Fissile absorptions

The absorptions by U233 and U235 are shown in figure 6.20. The thermal absorptions by U233 decrease with increasing specific power because of the decrease in the number of neutrons slowed down to thermal energy per absorption in a fissile nucleus and the increased competition for thermal neutrons by other absorbers, notably Pa233, U234, U235 and Xe135.

The U233 resonance absorption initially increases with increasing specific power because of the increased epithermal character of the spectrum. After the conversion ratio drops below 1.0 and fresh U235 is added to the feed, the U233 concentration increases less rapidly with increasing specific power and the U233 resonance absorptions decrease.

The U235 absorptions increase with increasing specific power. This is because of the rapid increase of U235 concentration with decreasing conversion ratio.

d. Fertile absorptions

The absorptions by Th232 and U234 are shown in figure 6.21. The Th232 thermal absorption decreases with increasing specific power because of the decrease in the number of neutrons slowed down to thermal energy per absorption by a fissile nucleus and because of the increased competition from other nuclides, notably Pa233, U234 and Xe135, for the thermal neutrons. The resonance absorption in Th232 decreases with increasing specific power because the Th232 concentration decreases while the concentrations of the other fuel nuclides increase.

The U234 absorptions increase with increasing specific power because of the increasing concentration of U234 in the core. The U234 concentration in the core increases because of increasing Pa233 absorptions and increasing recycle of core discharge into the feed as the conversion ratio decreases. After the conversion ratio drops below 1.0 and 100% of the core discharge is recycled, the U234 concentration and absorptions continue to increase because of increasing Pa233 absorptions.

2. Burnups of 10,000 mwd/t and 30,000 mwd/t

The conversion ratio and its components for 10,000 mwd/t are shown in figure 6.23 and 6.24 and for 30,000 mwd/t in figure 6.25 with average specific power in the core as abscissa. The other secondary variables are held constant at the same values as for 20,000 mwd/t. The complete neutron balances are listed in table 6.1. The components of the neutron balance other than those plotted in figures 6.24 and 6.25 behave in a similar fashion to the same components for a burnup of 20,000 mwd/t.

3. Comparison among burnups

The results of this section are plotted with average specific power in the core as abscissa and feed burnup as a parameter. In order to understand the effect on the conversion ratio of increasing the average specific power for different feed burnups, one compares the characteristics of a core with a feed burnup of 10,000 mwd/t to the characteristics of a core with a feed burnup of 20,000 mwd/t. For a burnup of 10,000 mwd/t, the fuel travels through the core at a relatively high axial velocity and depends to a large extent on the fissile material in the feed to supply the fissile material throughout the core. (If the axial velocity were infinite, then all of the fissile material in the core would be supplied by the feed.) For a burnup of 20,000 mwd/t, the fuel travels through the core at a relatively low axial velocity and depends less on the feed to supply the fissile material in the core and depends more on the fissile material produced in the core. Because of this, the Pa233 concentration is higher in the core with the higher burnup. Therefore, an increase in the average specific power is more effective in decreasing the conversion ratio in a core with a high feed burnup and its relatively high Pa233 concentration.

The effect just mentioned is shown in the plots of conversion ratio for the three burnups in figure 6.26. The difference between any two curves for a given specific power is due primarily to the differences in the curves of $(\bar{\eta}-1)$, 2 x Pa233 absorption and absorptions by nonsaturating fission products shown in figure 6.27 and the differences in the curves of U236 and Np237 absorptions shown in figure 6.28. The curve of 2 x Pa233 absorption for a burnup of 20,000 mwd/t has a larger value and its slope is greater than for the curve for a burnup of 10,000 mwd/t because of the higher Pa233 concentration in the core. The curve for a

a burnup of 30,000 mwd/t falls slightly below the curve for 20,000 mwd/t because of the increased competition for thermal neutrons in the 30,000 mwd/t core caused by the higher concentration of nonsaturating fission products. However, the concentration of Pa233 is higher in the 30,000 mwd/t core at all average specific powers and if the specific power were increased to higher values, the curve of 2 x Pa233 absorption for the 30,000 mwd/t core would rise above the curve for 20,000 mwd/t.

The curves of $(\bar{\eta}-1)$ in figure 6.27 for the higher burnups decrease more rapidly with increasing specific power than for the lower burnups. As the average specific power increases, the neutron spectrum becomes more epithermal. A core with a higher burnup has a higher concentration of U235. Therefore an increase in the epithermal component of the spectrum is more effective in lowering $\bar{\eta}$ in a core with a hugh burnup. This also explains the differences in the shapes of the curves of neutrons slowed down to thermal energy per fissile absorption in figure 6.22.

The curves of U236 and Np237 absorptions are shown in figure 6.28. The curves for the higher burnups have steeper slopes because of the more rapid decrease of conversion ratio with increasing specific power and the resulting more rapid increase of U235, U236 and Np237 concentrations in the core.

The U233 absorptions are shown in figure 6.29. The shapes and relative positions of the U233 thermal absorption curves for different burnups are clearly determined by the shapes and relative positions of the curves of neutrons slowed down to thermal energy per fissile absorptions shown in figure 6.22. The U233 thermal absorption curves also decrease with increasing burnup because of the increasing reliance of the core on U235 fissions. The U233 resonance absorptions increase with

increasing burnup because of the increasing epithermal character of the spectrum.

The U235 absorptions are shown in figure 6.30. These curves are almost mirror images of the U233 thermal absorption curves. The resonance absorption curves increase with increasing feed burnup because of the rapidly increasing concentration of U235 in the core.

The Th232 absorption curves are shown in figure 6.31. The thermal absorption curves resemble the curves of neutrons slowed down to thermal energy per fissile absorption shown in figure 6.22. The resonance absorption curves decrease with increasing feed burnup because of the rapid increase in concentration of other resonance absorbers.

The U234 absorptions are shown in figure 6.32. As the burnup increases, the concentrations of U234 and absorptions by U234 increase because of the increased fraction of the core discharge which is recycled into the feed as the conversion ratio decreases.

D. Total thermal power or geometric buckling

This section is concerned with the effect on the conversion ratio of changes in the size and power level of the reactor, keeping the average specific power in the core constant at 1000 kw/kg fissile, keeping the ratio of core height to core radius constant at 1.845 and keeping the blanket thickness constant at two feet (60.96 cm). Calculations have been made for the three following cases:

Thermal Power, MW	Core Dimensions, cm Height, H_c	Radius, R_c	Geometric Buckling, B_g^2, cm^{-2}
8333	1362	738.2	0.1594×10^{-4}
1000	663.8	359.8	0.6705×10^{-4}
500	523.2	283.6	1.079×10^{-4}

The geometric buckling is defined as

$$B_g^2 = \left[\left(\frac{\pi}{H_c}\right)^2 + \left(\frac{2.404\theta}{R_c}\right)^2\right] \qquad (6D1)$$

The results of this section have been plotted against a scale linear in the geometric buckling because of the expectation, confirmed in figure 6.35, that the net leakage from the core into the blanket would be nearly linear in this variable. The power corresponding to the buckling has been indicated in each figure.

Other variables held constant in this study were

Burnup	20,000 mwd/t
Zircaloy absorption ratio	0
Average specific power	1000 kw/kg fissile
Reprocessing loss	0

The slowing down length in the blanket is 11.3 cm and the thermal diffusion length in the blanket is 15.5 cm.

The conversion ratio and its components are plotted in figure 6.33. The conversion ratio is divided into the contributions from the core and from the blanket. The conversion ratios are extrapolated to a core of infinite size or zero buckling. In this condition the contribution of the blanket to the conversion ratio is zero. As the core volume decreases from infinity, the fractional leakage of neutrons from the core increases from zero. Some of these neutrons pass through the blanket without being absorbed, so that the conversion ratio decreases as the core size is reduced. However, as the core size becomes smaller, the ratio of blanket volume to core volume increases, so that the blanket absorbs a larger fraction of the neutrons leaking from the core, as the core becomes smaller.

The calculations of this section suggest that for relatively small cores, in going from 1000 to 500 MW(th), the overall fast leakage from the reactor decreases, as shown in figure 6.35. This causes the conversion ratio to increase and is due, presumably, to the increased effectiveness of the blanket in the small systems in slowing down the fast neutrons leaking out of the core. This situation is similar to that encountered in section VIC during the study of the effects of increasing the average specific power in the core. It is not clear that this decrease in overall fast leakage from the reactor with decreasing core size actually occurs. It is seen in figure 6.35 that the overall leakage from the reactor is the difference between two numbers whose absolute values are large: the net fast leakage out of the core and the net fast leakage into the blanket. The errors in calculating these net leakages, $[(\Sigma_{\text{fast}}^{\prime} D_{\text{fast}} \nabla^2\phi_{\text{fast}} \Delta\text{volume})/(\text{fissile absorptions})]$, using the difference approximation for ∇^2, are probably as large as the calculated overall fast leakage from the reactor. In any case, as long as there is a blanket of fixed thickness surrounding the core to stop fast and thermal neutrons leaking out of the core, a decrease in core size does not have a large effect on the conversion ratio, at least down to a thermal power of 500 MW.

When interpreting some of the other results of the effect of the buckling on reactor, the following reasoning applies. When the core size is decreased from a large volume, a principal effect of the increase in the net leakage out of the core is to decrease the reactivity of the system. To compensate for this, the concentrations of the fissile and other nuclides in the core must be increased. This increase in concentration causes an increase in the rate of absorption of thermal neutrons by some of these nuclides. When the core size is decreased from a small

value, when the net leakage of neutrons out of the core is already relatively large, a principal effect is to cause thermal neutrons in the core to leak away from the thermal poisons in the core and the rate of absorption of thermal neutrons by these nuclides decreases. In the cases of both large and small cores, the increase in the leakage of thermal neutrons out of the core necessitates an increase in the epithermal component of the spectrum in order to maintain sufficient absorptions in fissile nuclides for criticality.

The remaining neutron balance results for this study are plotted in figure 6.34 through 6.37. These results can all be interpreted in the light of the information in the preceeding two paragraphs.

E. Reprocessing loss

1. Conversion ratio and its components

The results of section VIE are plotted as a function of the fraction of the core and blanket discharge which is lost in reprocessing. The other secondary variables are held constant at the following values:

Zircaloy absorption ratio	0
Average specific power	6000 kw/kg fissile
Total power	8333 MW(th)

The conversion ratio and its components are plotted in figure 6.38. Two conversion ratios are shown. The one with the higher value (internal conversion ratio) is calculated by considering only the sink of fissile material within the reactor, i.e., by use of equation (4E2a). This is the same conversion ratio which has been used in this work up to this point. The conversion ratio with the lower value (conversion ratio with reprocessing loss) is calculated by including the

reprocessing loss in the fissile sink. The internal conversion ratio is calculated for a given abscissa by subtracting from ($\bar{\eta}$-1) the sum of D_2O absorption, 2 x Pa233 absorption and parasitic absorptions plus leakage.

When the internal conversion ratio of a reactor is greater than 1.0, the reprocessing loss can range from zero to a value for which the conversion ratio with reprocessing loss equals 1.0 without affecting the reactor neutron balance itself. This is because not all of the discharged fuel is recycled back into the core feed when the internal conversion ratio is greater than 1.0, and reprocessing losses merely reduce the net amount of fissile material produced. When the conversion ratio with reprocessing loss is greater than 1.0, it can be calculated with the fissile material input-output-sink data in tables 5.3 and 6.3 and equation (4E1). When the conversion ratio with reprocessing loss is less than 1.0, the entire neutron balance must be recalculated because the feed composition is different for each value of the reprocessing loss.

The curve of ($\bar{\eta}$-1) in figure 6.38 decreases with increasing reprocessing loss because of the feeding into the core of fresh U235 with its lower value of η . The curve of parasitic absorptions plus leakage decreases with increasing reprocessing loss because of the removal of U236 in the reprocessing loss stream. The second derivative of this curve is positive because as the reprocessing loss increases, the decrease in U236 concentration in the core caused by the increase in the U236 lost in the reprocessing loss stream tends to be offset by neutron captures in the increasing U235 concentration caused by the increased feeding of U235 into the core. The curves of 2 x Pa233 absorption and D_2O absorption increase with increasing reprocessing loss because as U234 and U236 are

removed in the reprocessing loss stream, more neutrons are made available for absorption by Pa233, D_2O and other nuclides.

The internal conversion ratio curve first increases and then decreases with increasing reprocessing loss because of the behavior of the curves of $(\bar{\eta} - 1)$ and parasitic absorptions plus leakage. The conversion ratio with reprocessing loss curve continually decreases with increasing reprocessing loss because of the inclusion of the reprocessing loss in the fissile sink.

2. Parasitic absorptions plus leakage

The curves of the parasitic absorptions are in figure 6.39. The changes of the fast and thermal leakages with reprocessing loss are extremely small and are not plotted. The U236 absorption curves decrease because of the removal of U236 in the reprocessing loss stream. The Np237 curves also decrease because Np237 is the (n, β^-, γ) daughter of U236. The absorption curves of the other nuclides increase with increasing reprocessing loss because as U234 and U236 are removed in the reprocessing loss stream, more neutrons become available for absorption in these nuclides.

3. Fissile absorptions

The absorption by U233 and U235 are shown in figure 6.40. The U233 absorption curves decrease with increasing reprocessing loss because of the removal of U233 in the reprocessing loss stream. The U235 absorption curves increase because of the feeding of fresh U235 into the core as the reprocessing loss increases.

4. Fertile absorptions

The absorptions by Th232 and U234 are shown in figure 6.41. The

U234 absorptions decrease with increasing reprocessing loss because of U234 removal in the reprocessing loss stream. The absorptions by Th232 increase with increasing reprocessing loss because as U234 and U236 are removed in the reprocessing loss stream, more neutrons become available for absorption by Th232.

F. Other results of the calculations

In table 6.3 are listed the input and output flow rates of the fuel nuclides and the fissile nuclide consumption rates for the cases involving the secondary variables. The comments of section VE also apply to these results.

Table 6.1: Neutron Balances for the Cases Involving the Secondary Variables

Secondary variable changed	← Zircaloy absorption ratio →									← Average specific power →		
Burnup, mwd/t	10,000	10,000	20,000	20,000	20,000	20,000	20,000	30,000	30,000	10,000	10,000	10,000
Volume moderator/volume fuel	30	30	30	30	30	30	30	30	30	30	30	30
Rod diameter, inches	1/4	1/4	1/4	1/4	1/4	1/4	1/4	1/4	1/4	1/4	1/4	1/4
Average specific power, kw/kg fissile	1000	1000	1000	1000	1000	1000	1000	1000	1000	2000	7000	12,000
Absorption ratio, zircaloy/fissile	0.047573	0.107829	0.046438	0.080404	0.088526	0.100535	0.112351	0.036581	0.053616	0	0	0
Volume zircaloy/volume fuel	0.5	1.2	0.5	0.9	1.0	1.15	1.3	0.4	0.6	0	0	0
Reprocessing loss, %	0	0	0	0	0	0	0	0	0	0	0	0
Total power, MW(th)	8333	8333	8333	8333	8333	8333	8333	8333	8333	8333	8333	8333
Production of fast neutrons from												
Resonance fission of U233	0.217675	0.230825	0.223088	0.231543	0.232048	0.231682	0.231068	0.226305	0.231072	0.211647	0.220138	0.224051
Resonance fission of U235	0.005408	0.007783	0.006437	0.008248	0.009218	0.011002	0.012754	0.007237	0.008386	0.005137	0.008170	0.009671
Thermal fission of U233	1.907670	1.846527	1.880134	1.835874	1.814161	1.775547	1.738992	1.860136	1.832837	1.916899	1.839255	1.804817
Thermal fission of U235	0.128563	0.167871	0.146812	0.176183	0.194022	0.226909	0.258226	0.160687	0.179164	0.126424	0.184276	0.209583
Total ($\bar{\eta}$)	2.259316	2.253006	2.256471	2.251848	2.249449	2.245140	2.241040	2.254365	2.251459	2.260107	2.251839	2.248122
Net fast leakage out of												
Core	0.011001	0.012564	0.011529	0.013253	0.013724	0.014341	0.014585	0.013358	0.015067	0.017241	0.042938	0.055283
Blanket	-0.008948	-0.010287	-0.009407	-0.010840	-0.011216	-0.011724	-0.011941	-0.010612	-0.011974	-0.015209	-0.038942	-0.053321
Neutrons reaching resonance energy	2.257263	2.250629	2.254349	2.249435	2.246941	2.242523	2.238396	2.251619	2.248366	2.258075	2.247843	2.246160
Resonance absorptions												
Th232, Core	0.204180	0.202241	0.202308	0.200698	0.200172	0.199440	0.198773	0.200452	0.199281	0.203822	0.199057	0.196745
Th232, Blanket	0.000856	0.000982	0.000900	0.001035	0.001071	0.001118	0.001139	0.001014	0.001142	0.001447	0.003675	0.005023
Pa233	0.005309	0.005169	0.005389	0.005225	0.005179	0.005139	0.005122	0.005361	0.005214	0.009596	0.021243	0.025856
U233	0.101773	0.107936	0.104310	0.108275	0.108515	0.108346	0.108061	0.105818	0.108057	0.098955	0.102946	0.104787
U234	0.021818	0.028390	0.024764	0.029633	0.030052	0.029980	0.029783	0.026968	0.029985	0.021312	0.030780	0.035042
U235	0.003420	0.004924	0.004071	0.005219	0.005833	0.006963	0.008072	0.004578	0.005307	0.003249	0.005170	0.006122
U236	0.002922	0.007830	0.004682	0.010259	0.012061	0.013937	0.016177	0.006743	0.011472	0.002355	0.005901	0.008466
Np237	0.000249	0.000653	0.000698	0.001516	0.001777	0.002043	0.002366	0.001349	0.002295	0.000199	0.000480	0.000682
Net production of thermal neutrons	1.916736	1.892504	1.907227	1.887575	1.882281	1.875557	1.868903	1.899336	1.885613	1.917140	1.878591	1.863437
Overall thermal leakage from reactor	0.001756	0.001789	0.001766	0.001889	0.001944	0.001978	0.001971	0.001534	0.001649	0.002326	0.003814	0.004596
Thermal absorptions												
Th232, Core	0.801917	0.718742	0.761465	0.705859	0.693337	0.676512	0.661493	0.733924	0.700864	0.828556	0.738766	0.700223
Th232, Blanket	0.012460	0.012996	0.012789	0.013865	0.014193	0.014463	0.014479	0.014031	0.015303	0.021459	0.048892	0.063758
Pa233	0.003403	0.003015	0.003314	0.003020	0.002951	0.002871	0.002811	0.003213	0.003013	0.006397	0.013220	0.015583
U233 fission	0.762153	0.737726	0.751152	0.733469	0.724795	0.709368	0.694763	0.743162	0.732256	0.765841	0.734820	0.721061
U233 capture	0.070572	0.068342	0.069570	0.067949	0.067153	0.065731	0.064382	0.068842	0.067853	0.070907	0.068067	0.66808
U234	0.048502	0.058758	0.053403	0.061038	0.061116	0.059748	0.058245	0.057108	0.061860	0.048956	0.067372	0.075112
U235 fission	0.052907	0.069083	0.060417	0.072503	0.079844	0.093378	0.106266	0.066127	0.073730	0.052026	0.075834	0.086248
U235 capture	0.009175	0.011990	0.010480	0.012584	0.013860	0.016214	0.018455	0.011473	0.012798	0.009022	0.013163	0.014975
U236	0.000788	0.001949	0.001219	0.002549	0.002970	0.003385	0.003886	0.001721	0.002862	0.000657	0.001528	0.002126
Np237	0.000386	0.000921	0.001037	0.002120	0.002450	0.002763	0.003145	0.001956	0.003211	0.000319	0.000712	0.000972
Xe135	0.037033	0.036600	0.036866	0.036536	0.036473	0.036413	0.036373	0.036777	0.036552	0.041852	0.045894	0.046589
"Sm" group	0.014108	0.014110	0.014115	0.014126	0.014166	0.014250	0.014331	0.014126	0.014137	0.014147	0.014231	0.014265
Nonsaturating fission products	0.040083	0.037184	0.070393	0.067327	0.066682	0.065886	0.065262	0.096196	0.094098	0.040750	0.038835	0.038191
D_2O	0.013638	0.012301	0.013066	0.012198	0.012006	0.011740	0.011500	0.012727	0.012230	0.014273	0.013362	0.013017
Zircaloy	0.047573	0.107829	0.046438	0.080404	0.088526	0.100535	0.112351	0.036581	0.053616	0	0	0
Total consumption of thermal neutrons	1.916454	1.893335	1.907490	1.887436	1.882466	1.875235	1.869713	1.899498	1.886032	1.917488	1.878510	1.863524
Conversion ratio	1.081313	1.013195	1.046663	1.004022	0.991626	0.973573	0.955167	1.024761	0.999791	1.109211	1.054160	1.034378

Table 6.1: (Continued)

Secondary variable changed	Average specific power								Total power		Reprocessing loss	
Burnup, mwd/t	20,000	20,000	20,000	20,000	20,000	20,000	30,000	30,000	20,000	20,000	20,000	20,000
Volume moderator/volume fuel	30	30	30	30	30	30	30	30	30	30	30	30
Rod diameter, inches	1/4	1/4	1/4	1/4	1/4	1/4	1/4	1/4	1/4	1/4	1/4	1/4
Average specific power, kw/kg fissile	2000	5000	6000	7000	8000	10,000	2000	3000	1000	1000	6000	6000
Absorption ratio, zircaloy/fissile	0	0	0	0	0	0	0	0	0	0	0	0
Volume zircaloy/volume fuel	0	0	0	0	0	0	0	0	0	0	0	0
Reprocessing loss, %	0	0	0	0	0	0	0	0	0	0	2	4
Total power, MW(th)	8333	8333	8333	8333	8333	8333	8333	8333	1000	500	8333	8333
Production of fast neutrons from												
Resonance fission of U233	0.217030	0.225230	0.227783	0.227807	0.227482	0.226888	0.222257	0.225692	0.217703	0.220242	0.224802	0.221140
Resonance fission of U235	0.006099	0.009576	0.010807	0.012336	0.013691	0.016063	0.007214	0.008695	0.005222	0.005257	0.011361	0.012178
Thermal fission of U233	1.890269	1.806758	1.780060	1.747856	1.720173	1.673506	1.861557	1.826536	1.912532	1.910720	1.767647	1.749197
Thermal fission of U235	0.143964	0.206801	0.226792	0.253812	0.277359	0.316925	0.163352	0.189663	0.124381	0.123508	0.240178	0.259336
Total ($\bar{\eta}$)	2.257362	2.248365	2.245442	2.241811	2.238705	2.233382	2.254380	2.250586	2.259838	2.259727	2.243988	2.241851
Net fast leakage out of												
Core	0.017327	0.039821	0.045561	0.050564	0.055040	0.062674	0.020054	0.028882	0.028908	0.041994	0.045413	0.045342
Blanket	-0.015340	-0.034855	-0.040830	-0.046205	-0.051115	-0.059834	-0.017291	-0.026088	-0.026697	-0.041412	-0.040683	-0.040577
Neutrons reaching resonance energy	2.255375	2.243399	2.240711	2.237452	2.234780	2.230542	2.251617	2.247792	2.257627	2.259145	2.239258	2.237086
Resonance absorptions												
Th232, Core	0.202017	0.197245	0.195679	0.194382	0.193320	0.191494	0.199861	0.197883	0.201400	0.200112	0.195850	0.195922
Th232, Blanket	0.001460	0.003292	0.003853	0.004358	0.004819	0.005637	0.001643	0.002470	0.002549	0.003948	0.003839	0.003829
Pa233	0.010188	0.020535	0.022972	0.025117	0.027010	0.030134	0.010281	0.014369	0.005933	0.005921	0.023033	0.023078
U233	0.101477	0.105335	0.106539	0.106556	0.106409	0.106138	0.103927	0.105544	0.101785	0.102973	0.105140	0.103424
U234	0.024207	0.034403	0.037654	0.039013	0.039860	0.041291	0.027348	0.031612	0.021296	0.021390	0.035766	0.033652
U235	0.003857	0.006061	0.006843	0.007812	0.008671	0.010176	0.004564	0.005503	0.003303	0.003325	0.007192	0.007709
U236	0.003525	0.009969	0.014076	0.016614	0.018233	0.021025	0.005625	0.008984	0.002583	0.002555	0.012171	0.010668
Np237	0.000522	0.001443	0.002028	0.002382	0.002602	0.002976	0.001118	0.001774	0.000397	0.000390	0.001751	0.001531
Net production of thermal neutrons	1.908122	1.865116	1.851067	1.841218	1.833856	1.821671	1.897250	1.879653	1.918381	1.918531	1.854516	1.857273
Overall thermal leakage from reactor	0.002273	0.003601	0.003904	0.004188	0.004478	0.004989	0.001953	0.002512	0.002686	0.003691	0.003906	0.003931
Thermal absorptions												
Th232, Core	0.787091	0.699799	0.673445	0.655341	0.641368	0.618035	0.746040	0.710112	0.792706	0.776713	0.679703	0.685563
Th232, Blanket	0.021280	0.043539	0.049719	0.055230	0.060202	0.068785	0.022728	0.032652	0.035461	0.052832	0.049747	0.049793
Pa233	0.006518	0.012222	0.013348	0.014364	0.015259	0.016670	0.006313	0.008560	0.003804	0.003750	0.013478	0.013598
U233 fission	0.755201	0.721837	0.711171	0.698305	0.687244	0.668600	0.743730	0.729739	0.764096	0.763372	0.706211	0.698840
U233 capture	0.069945	0.066887	0.065907	0.064732	0.063704	0.061995	0.068893	0.067615	0.070754	0.070689	0.065451	0.064768
U234	0.053929	0.073187	0.079002	0.080828	0.081702	0.083102	0.059159	0.067063	0.047362	0.046960	0.075009	0.070485
U235 fission	0.059245	0.085103	0.093330	0.104450	0.114139	0.130422	0.067223	0.078051	0.051185	0.050826	0.098839	0.106723
U235 capture	0.010275	0.014776	0.016210	0.018146	0.019833	0.022670	0.011664	0.013549	0.008876	0.008814	0.017167	0.018536
U236	0.000947	0.002505	0.003487	0.004073	0.004428	0.005027	0.001459	0.002271	0.000697	0.000680	0.003018	0.002652
Np237	0.000803	0.002050	0.002806	0.003237	0.003486	0.003893	0.001653	0.002538	0.000615	0.000597	0.002439	0.002147
Xe135	0.041700	0.044964	0.045312	0.045596	0.045816	0.046120	0.041555	0.043302	0.037313	0.037231	0.045373	0.045444
"Sm" group	0.014152	0.014249	0.014279	0.014345	0.014405	0.014505	0.014163	0.014203	0.014098	0.014077	0.014335	0.014410
Nonsaturating fission products	0.071524	0.067914	0.066889	0.066323	0.065912	0.065264	0.097114	0.094839	0.074873	0.074276	0.067248	0.067618
D_2O	0.013674	0.012727	0.012437	0.012257	0.012128	0.011917	0.013116	0.012742	0.013966	0.013991	0.012527	0.012613
Zircaloy	0	0	0	0	0	0	0	0	0	0	0	0
Total consumption of thermal neutrons	1.908557	1.865360	1.851246	1.841415	1.834104	1.821994	1.896763	1.879748	1.918492	1.918499	1.854451	1.857121
Conversion ratio	1.072843	1.018463	1.002853	0.989476	0.978754	0.961218	1.040672	1.018769	1.090925	1.092315	{1.003467* {0.986515**	{1.002720* {0.969593**

* Internal conversion ratio

** Conversion ratio with reprocessing loss

Table 6.2: Masses and Mass Fractions of Fuel Materials in Reactor Cores and Core Dimensions for the Cases Involving the Secondary Variables

Secondary variable changed	Zircaloy absorption ratio									Average specific power		
Burnup, mwd/t	10,000	10,000	20,000	20,000	20,000	20,000	20,000	30,000	30,000	10,000	10,000	10,000
Volume moderator/volume fuel	30	30	30	30	30	30	30	30	30	30	30	30
Rod diameter, inches	1/4	1/4	1/4	1/4	1/4	1/4	1/4	1/4	1/4	1/4	1/4	1/4
Average specific power, kw/kg fissile	1000	1000	1000	1000	1000	1000	1000	1000	1000	2000	7000	12,000
Absorption ratio, zircaloy/fissile	0.047573	0.107829	0.046438	0.080404	0.088526	0.100535	0.112351	0.036581	0.053616	0	0	0
Reprocessing loss, %	0	0	0	0	0	0	0	0	0	0	0	0
Total power, MW(th)	8333	8333	8333	8333	8333	8333	8333	8333	8333	8333	8333	8333
Masses (kg)												
Th232 x 10^{-3}	575.23	520.65	549.42	512.13	504.18	493.04	483.37	531.25	508.79	295.37	75.487	41.769
Pa233	373.2	340.2	366.3	344.1	339.2	332.6	326.9	357.5	344.3	358	219	151
U233	7824	7659	7748	7623	7549	7402	7268	7691	7614	3910	1086	625.2
U234	2549	3128	2822	3254	3267	3201	3129	3028	3298	1278	506	329
U235	510	674	585	709	786	928	1065	643	721	249	104	69.3
U236	714	1787	1110	2340	2733	3121	3592	1573	2628	295	197	160
Np237	11.3	27.7	30.9	64.5	75.0	85.0	97.1	58.7	97.8	4.71	3.06	2.44
Mass fractions												
Th232	0.9796	0.9745	0.9775	0.9727	0.9716	0.9704	0.9690	0.9755	0.9719	0.9798	0.9727	0.9690
Pa233 x 10^{4}	6.355	6.368	6.517	6.536	6.537	6.546	6.553	6.564	6.577	11.9	28.2	35.0
U233 x 10^{2}	1.332	1.434	1.378	1.448	1.455	1.457	1.457	1.412	1.455	1.300	1.399	1.450
U234 x 10^{3}	4.34	5.85	5.02	6.18	6.30	6.30	6.27	5.55	6.30	4.24	6.52	7.63
U235 x 10^{4}	8.69	12.62	10.41	13.47	15.15	18.26	21.35	11.81	13.77	8.26	13.4	16.1
U236 x 10^{3}	1.22	3.34	1.97	4.44	5.27	6.14	7.20	2.89	5.02	0.979	2.54	3.71
Np237 x 10^{5}	1.92	5.18	5.50	12.25	14.45	16.73	19.46	10.78	18.68	1.56	3.94	5.66
Core radius, feet	24.10	23.52	23.79	23.37	23.28	23.15	23.05	23.55	23.29	19.19	12.21	10.03
Core height, feet	44.46	43.39	43.89	43.12	42.95	42.71	42.53	43.45	42.97	35.41	22.53	18.51

Secondary variable changed	Average specific power								Total power		Reprocessing loss	
Burnup, mwd/t	20,000	20,000	20,000	20,000	20,000	20,000	30,000	30,000	20,000	20,000	20,000	20,000
Volume moderator/volume fuel	30	30	30	30	30	30	30	30	30	30	30	30
Rod diameter, inches	1/4	1/4	1/4	1/4	1/4	1/4	1/4	1/4	1/4	1/4	1/4	1/4
Average specific power, kw/kg fissile	2000	5000	6000	7000	8000	10,000	2000	3000	1000	1000	6000	6000
Absorption ratio, zircaloy/fissile	0	0	0	0	0	0	0	0	0	0	0	0
Reprocessing loss, %	0	0	0	0	0	0	0	0	0	0	2	4
Total power, MW(th)	8333	8333	8333	8333	8333	8333	8333	8333	1000	500	8333	8333
Masses (kg)												
Th232 x 10^{-3}	282.28	100.82	81.072	67.822	58.207	45.028	268.59	170.64	68.398	33.478	81.827	82.497
Pa233	363	286	263.2	245	229	201	353	329	45.41	22.30	265.8	268.1
U233	3883	1502	1237	1044	901.4	704.3	3841	2525	941.3	470.9	1228	1214
U234	1414	774	699.0	615	545	445	1557	1182	296.3	146.7	663.4	622.7
U235	285	165	151.5	146	140	129	325	252	58.74	29.13	161.1	174.6
U236	428	456	531.1	533	509	463	662	689	75.29	36.68	459.6	403.4
Np237	11.9	12.5	14.38	14.3	13.5	12.2	24.7	25.7	2.06	1.00	12.50	11.00
Mass fractions												
Th232	0.9779	0.9692	0.9655	0.9631	0.9614	0.9584	0.9754	0.9715	0.9797	0.9793	0.9670	0.9683
Pa233 x 10^{4}	12.6	27.5	31.34	34.8	37.8	42.8	12.8	18.7	6.504	6.523	31.41	31.47
U233 x 10^{2}	1.345	1.444	1.473	1.483	1.489	1.499	1.395	1.438	1.348	1.378	1.451	1.425
U234 x 10^{3}	4.90	7.44	8.324	8.73	9.00	9.47	5.65	6.73	4.244	4.291	7.840	7.309
U235 x 10^{4}	9.87	15.9	18.04	20.7	23.1	27.5	11.8	14.3	8.413	8.521	19.04	20.49
U236 x 10^{3}	1.48	4.38	6.325	7.57	8.41	9.85	2.40	3.92	1.078	1.073	5.432	4.735
Np237 x 10^{5}	4.12	12.0	17.13	20.3	22.3	26.0	8.97	14.6	2.955	2.924	14.77	12.91
Core radius, feet	18.95	13.48	12.55	11.84	11.25	10.34	18.68	16.08	11.81	9.305	12.58	12.61
Core height, feet	34.96	24.87	23.15	21.84	20.76	19.08	34.46	29.67	21.79	17.17	23.21	23.27

Table 6.3: Fuel Flow Rates and Fissile Consumption Rates for the Cases Involving the Secondary Variables

Secondary variable changed	← Zircaloy absorption ratio →									← Average specific power →		
Burnup, mwd/t	10,000	10,000	20,000	20,000	20,000	20,000	20,000	30,000	30,000	10,000	10,000	10,000
Volume moderator/volume fuel	30	30	30	30	30	30	30	30	30	30	30	30
Rod diameter, inches	1/4	1/4	1/4	1/4	1/4	1/4	1/4	1/4	1/4	1/4	1/4	1/4
Average specific power, kw/kg fissile	1000	1000	1000	1000	1000	1000	1000	1000	1000	2000	7000	12,000
Absorption ratio, zircaloy/fissile	0.047573	0.107829	0.046438	0.080404	0.088526	0.100535	0.112351	0.036581	0.053616	0	0	0
Reprocessing loss, %	0	0	0	0	0	0	0	0	0	0	0	0
Total power, MW(th)	8333	8333	8333	8333	8333	8333	8333	8333	8333	8333	8333	8333
Fuel flow rates, kg/day												
Input												
Core												
Th232	816.91	812.28	407.71	405.45	404.86	404.28	403.62	271.25	270.06	817.20	810.72	807.32
U233	11.221	12.416	5.7541	6.2931	6.3432	6.3558	6.3531	3.9635	4.2383	11.329	14.105	15.333
U234	3.4823	4.8282	1.9939	2.5403	2.5938	2.5966	2.5840	1.4743	1.7197	3.3642	5.3182	6.2860
U235	0.69604	1.0404	0.41374	0.55312	0.67591	0.91738	1.1534	0.31335	0.37639	0.65583	1.0951	1.3193
U236	0.97512	2.7523	0.78488	1.8242	2.1651	2.5201	2.9538	0.76667	1.3704	0.77720	2.0705	3.0507
Blanket												
Th232	7548.1	7575.7	7110.0	7755.5	7997.5	8188.0	8086.7	7469.9	8534.8	13,975	30,577	36,653
Output												
Core												
Th232	807.12	803.30	398.32	396.61	396.13	395.71	395.20	262.12	261.26	807.16	801.57	798.54
Pa233	0.32205	0.34567	0.11398	0.12927	0.13420	0.13906	0.14115	0.062285	0.072668	0.88032	3.3126	4.5966
U233	11.515	12.060	5.9341	6.0527	6.0615	6.0650	6.0662	3.9797	4.0065	11.238	10.770	10.373
U234	3.7164	4.8791	2.1449	2.5538	2.5937	2.5953	2.5851	1.5612	1.7202	3.6695	5.5095	6.4183
U235	0.74354	1.0517	0.44532	0.55672	0.59318	0.65192	0.70972	0.33213	0.37649	0.71466	1.1344	1.3471
U236	1.0411	2.7914	0.84444	1.8401	2.1738	2.5334	2.9660	0.81254	1.3736	0.84797	2.1455	3.1158
Np237	0.030572	0.081747	0.041476	0.091399	0.10777	0.12495	0.14551	0.051461	0.088125	0.024781	0.062181	0.089322
Blanket												
Th232	7548.0	7575.5	7109.8	7755.3	7997.3	8187.9	8086.5	7469.7	8534.7	13,975	30,577	36,653
Pa233	0.048613	0.051732	0.047885	0.055169	0.057658	0.059898	0.060053	0.056511	0.066574	0.12069	0.42619	0.60055
U233	0.079324	0.082923	0.083898	0.088470	0.089660	0.090632	0.091056	0.089652	0.093357	0.099589	0.086251	0.071762
S_R, Fissile material consumed in reactor, atoms/day (x 10^{-25})	2.5363	2.5417	2.5392	2.5427	2.5455	2.5480	2.5527	2.5409	2.5437	2.5360	2.5428	2.5463
O_R, Output from reactor of Pa233, U233 and U235, atoms/day (x 10^{-25})	3.2846	3.5124	1.7122	1.7773	1.7920	1.8101	1.8260	1.1681	1.1927	3.3738	4.0649	4.3901
O_R/S_R	1.2950	1.3819	0.67430	0.69895	0.70398	0.71039	0.71534	0.45974	0.46887	1.3303	1.5986	1.7241

Table 6.3: (continued)

Secondary variable changed	Average specific power								Total power		Reprocessing loss	
Burnup, mwd/t	20,000	20,000	20,000	20,000	20,000	20,000	30,000	30,000	20,000	20,000	20,000	20,000
Volume moderator/volume fuel	30	30	30	30	30	30	30	30	30	30	30	30
Rod diameter, inches	1/4	1/4	1/4	1/4	1/4	1/4	1/4	1/4	1/4	1/4	1/4	1/4
Average specific power, kw/kg fissile	2000	5000	6000	7000	8000	10,000	2000	3000	1000	1000	6000	6000
Absorption ratio, zircaloy/fissile	0	0	0	0	0	0	0	0	0	0	0	0
Reprocessing loss, %	0	0	0	0	0	0	0	0	0	0	2	4
Total power, MW(th)	8333	8333	8333	8333	8333	8333	8333	8333	1000	500	8333	8333
Fuel flow rates, kg/day												
Input												
Core												
Th232	408.00	403.92	402.12	400.99	400.19	398.76	271.29	269.96	49.057	24.514	402.83	403.36
U233	5.7772	7.3210	7.7477	8.0014	8.2047	8.5471	4.0582	4.5478	0.66221	0.34482	7.5822	7.3820
U234	1.9047	3.0365	3.4323	3.6084	3.7225	3.9209	1.4735	1.8000	0.19399	0.097966	3.2058	2.9577
U235	0.38380	0.64682	0.74275	0.92170	1.0868	1.3730	0.30719	0.38506	0.038551	0.019510	0.86414	1.0282
U236	0.57615	1.7863	2.6008	3.1172	3.4548	4.0539	0.62699	1.0518	0.049438	0.024589	2.2129	1.9051
Blanket												
Th232	12,970	28,936	33,390	37,373	40,910	46,706	13,413	20,644	2372.4	1760.8	33,489	33,602
Output												
Core												
Th232	398.37	395.15	393.62	392.67	392.01	390.80	262.06	261.08	47.894	23.942	394.26	394.73
Pa233	0.33460	1.2409	1.5223	1.7811	2.0183	2.4318	0.18972	0.38392	0.011429	0.0060749	1.5245	1.5260
U233	5.8914	5.7901	5.7288	5.6390	5.5494	5.3875	3.9942	3.9900	0.70698	0.35655	5.6889	5.6397
U234	2.1342	3.1101	3.4439	3.6082	3.7224	3.9203	1.6132	1.8721	0.22549	0.11392	3.2707	3.0806
U235	0.43076	0.66311	0.74540	0.81687	0.87744	0.98615	0.33742	0.40062	0.044822	0.022700	0.74106	0.74249
U236	0.64708	1.8304	2.6113	3.1193	3.4570	4.0559	0.68840	1.0939	0.057478	0.028605	2.2578	1.9840
Np237	0.031323	0.089616	0.12710	0.15071	0.16597	0.19246	0.042996	0.069313	0.0027111	0.0013434	0.10992	0.096385
Blanket												
Th232	12,970	28,936	33,389	37,372	40,909	46,704	13,413	20,643	2372.3	1760.8	33,488	33,601
Pa233	0.11819	0.36372	0.43413	0.49785	0.55549	0.65558	0.13492	0.23859	0.017688	0.013850	0.43451	0.43486
U233	0.10088	0.092965	0.088725	0.084746	0.081057	0.074545	0.10206	0.10364	0.026563	0.019226	0.088889	0.089114
S_R, Fissile material consumed in reactor, atoms/day (x 10^{-25})	2.5385	2.5462	2.5476	2.5516	2.5545	2.5589	2.5398	2.5438	0.30430	0.15220	2.5496	2.5508
O_R, Output from reactor of Pa233, U233 and U235, atoms/day (x 10^{-25})	1.7770	2.1062	2.2013	2.2788	2.3464	2.4636	1.2297	1.3222	0.20870	0.10814	2.1906	2.1788
O_R/S_R	0.70003	0.82720	0.86408	0.89308	0.91856	0.96237	0.48416	0.51979	0.68584	0.71052	0.85918	0.85416

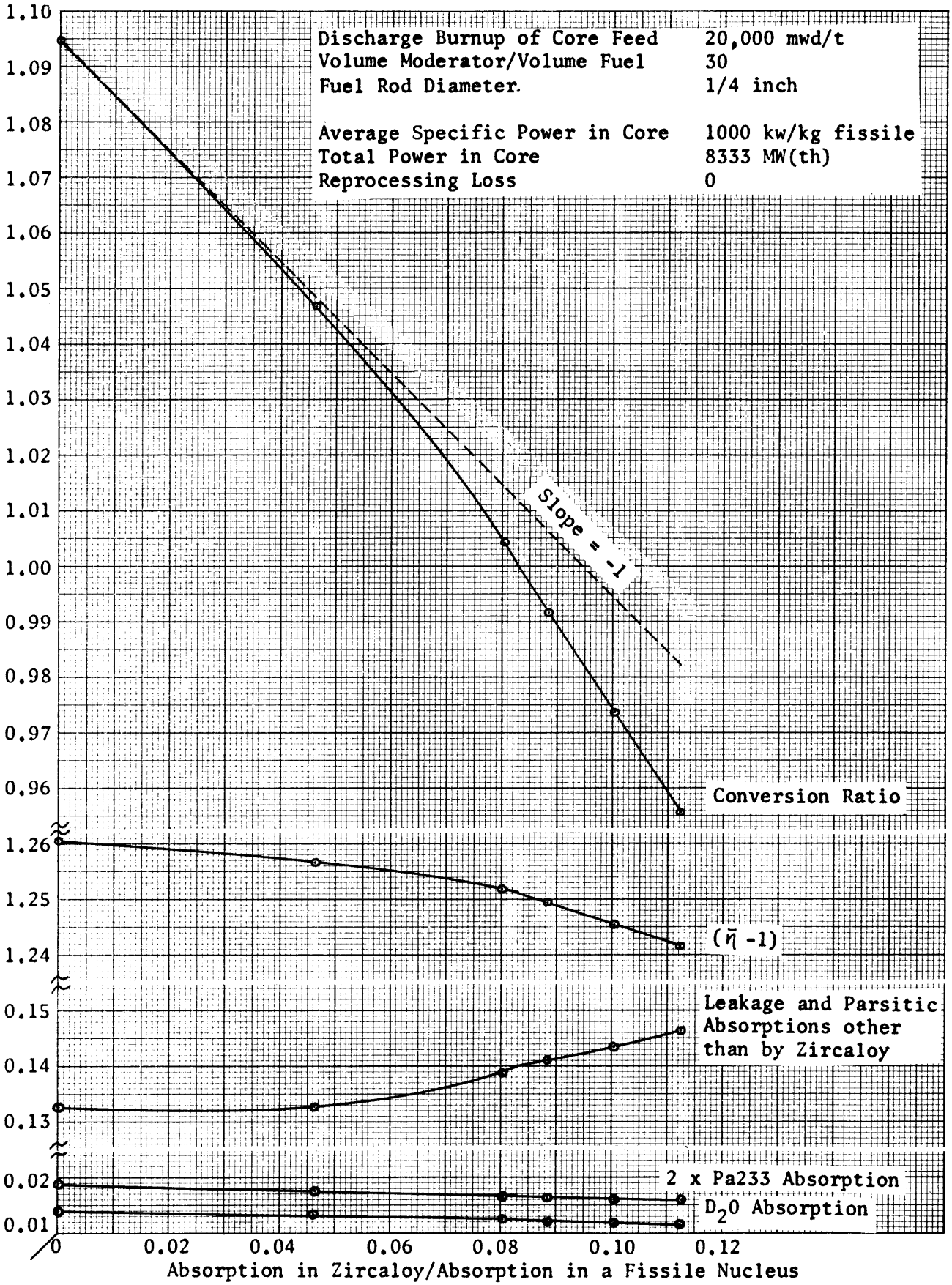

Figure 6.1: Conversion Ratio and its Components vs. Absorption in Zircaloy/Absorption in a Fissile Nucleus: 20,000 mwd/t Burnup

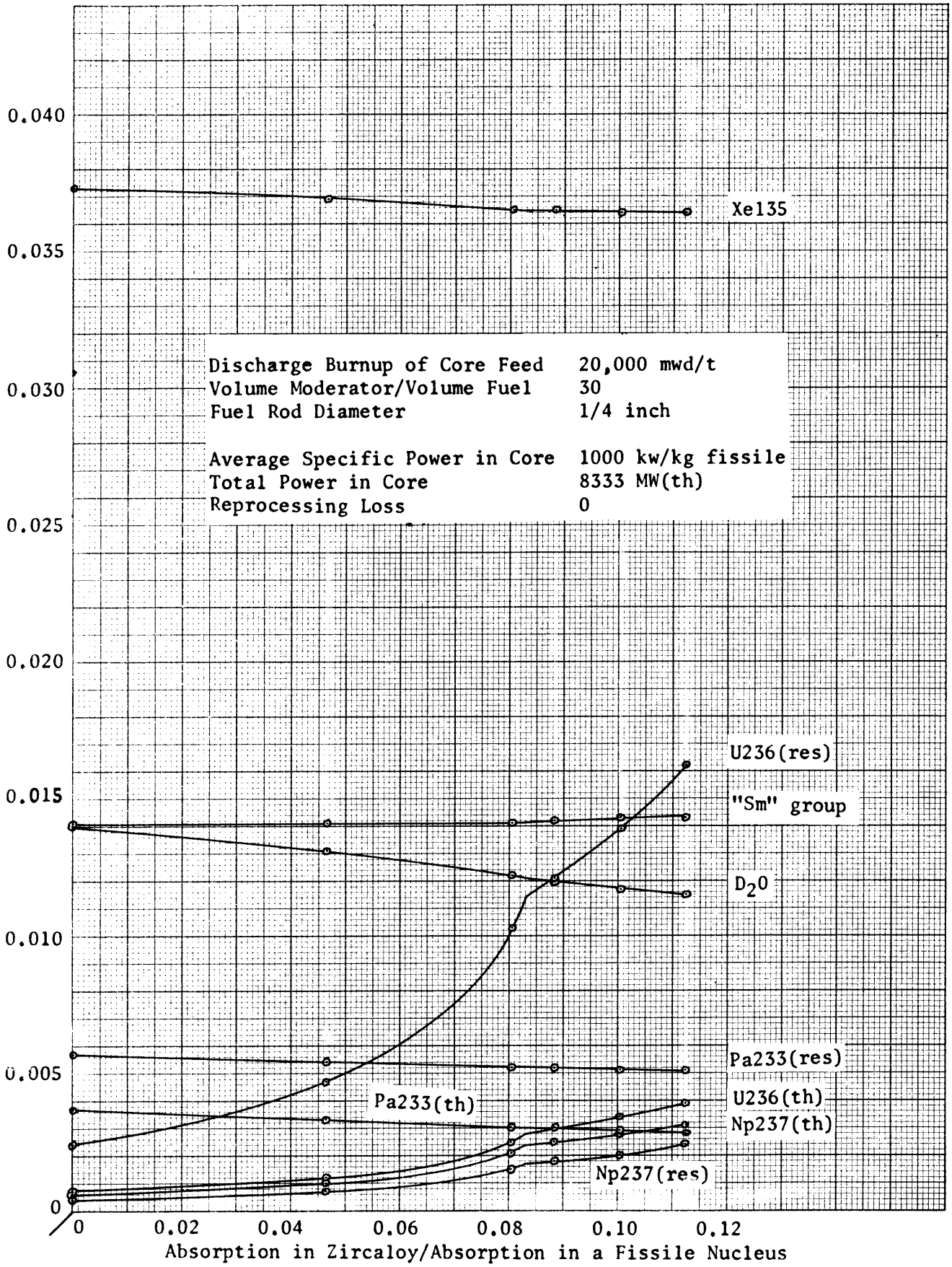

Figure 6.2: Absorptions by Pa233(th,res), U236(th,res), Np237(th,res), Xe135, "Sm" group, D_2O vs. Absorption in Zircaloy/Absorption in a Fissile Nucleus: 20,000 mwd/t Burnup

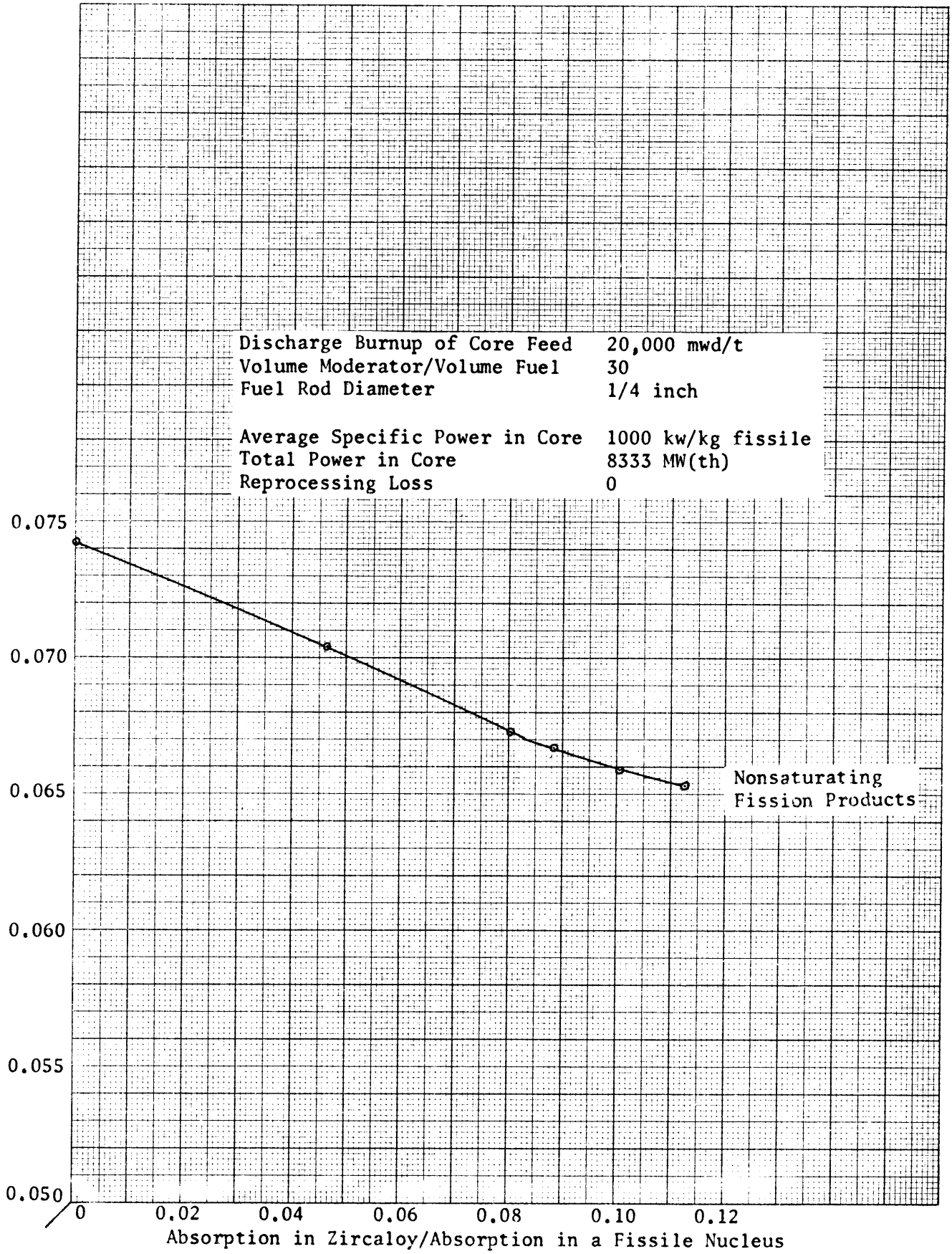

Figure 6.3: Absorption by Nonsaturating Fission Products vs. Absorption in Zircaloy/Absorption in a Fissile Nucleus: 20,000 mwd/t Burnup

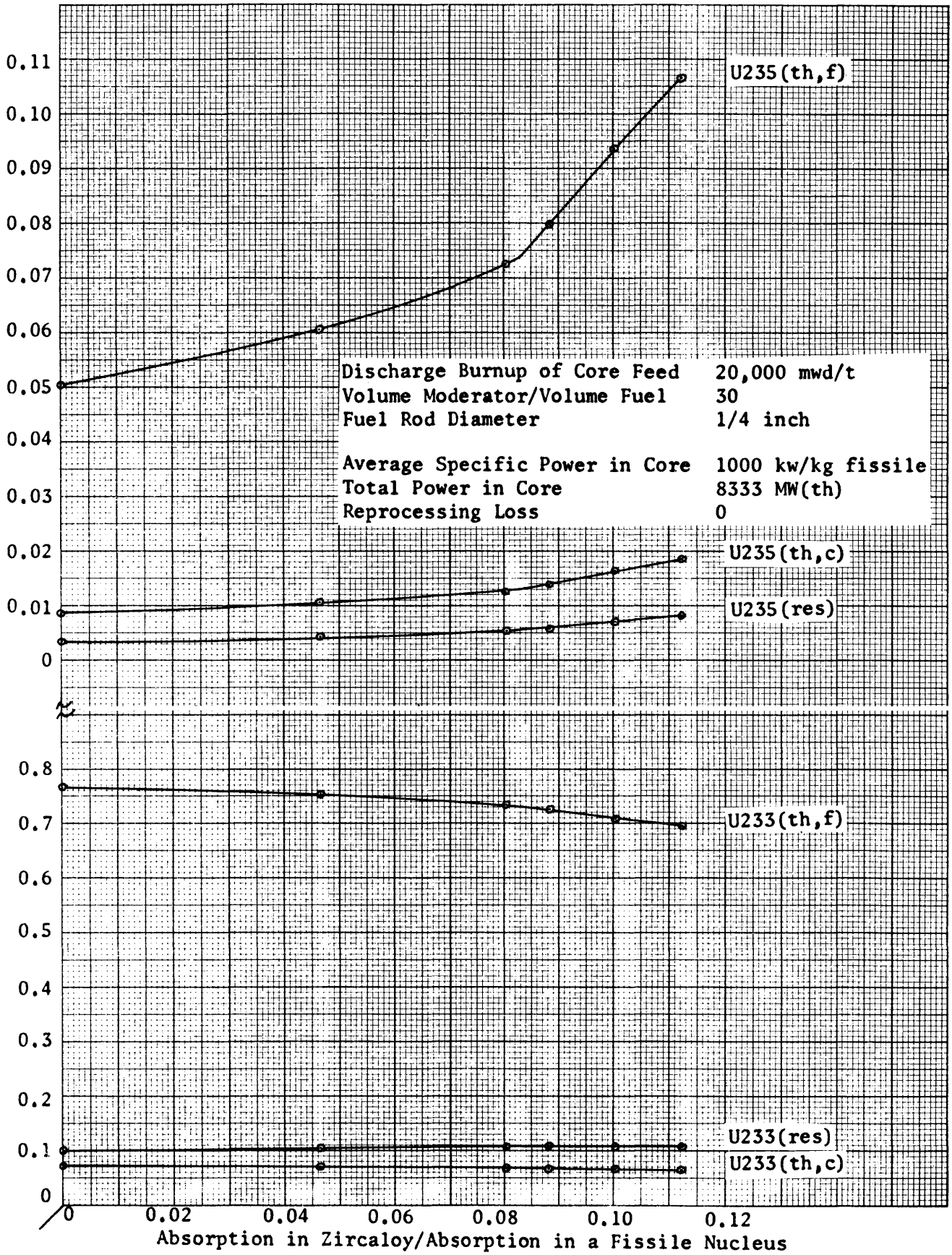

Figure 6.4: Absorptions by Fissile Nuclides vs. Absorption in Zircaloy/ Absorption in a Fissile Nucleus: 20,000 mwd/t Burnup

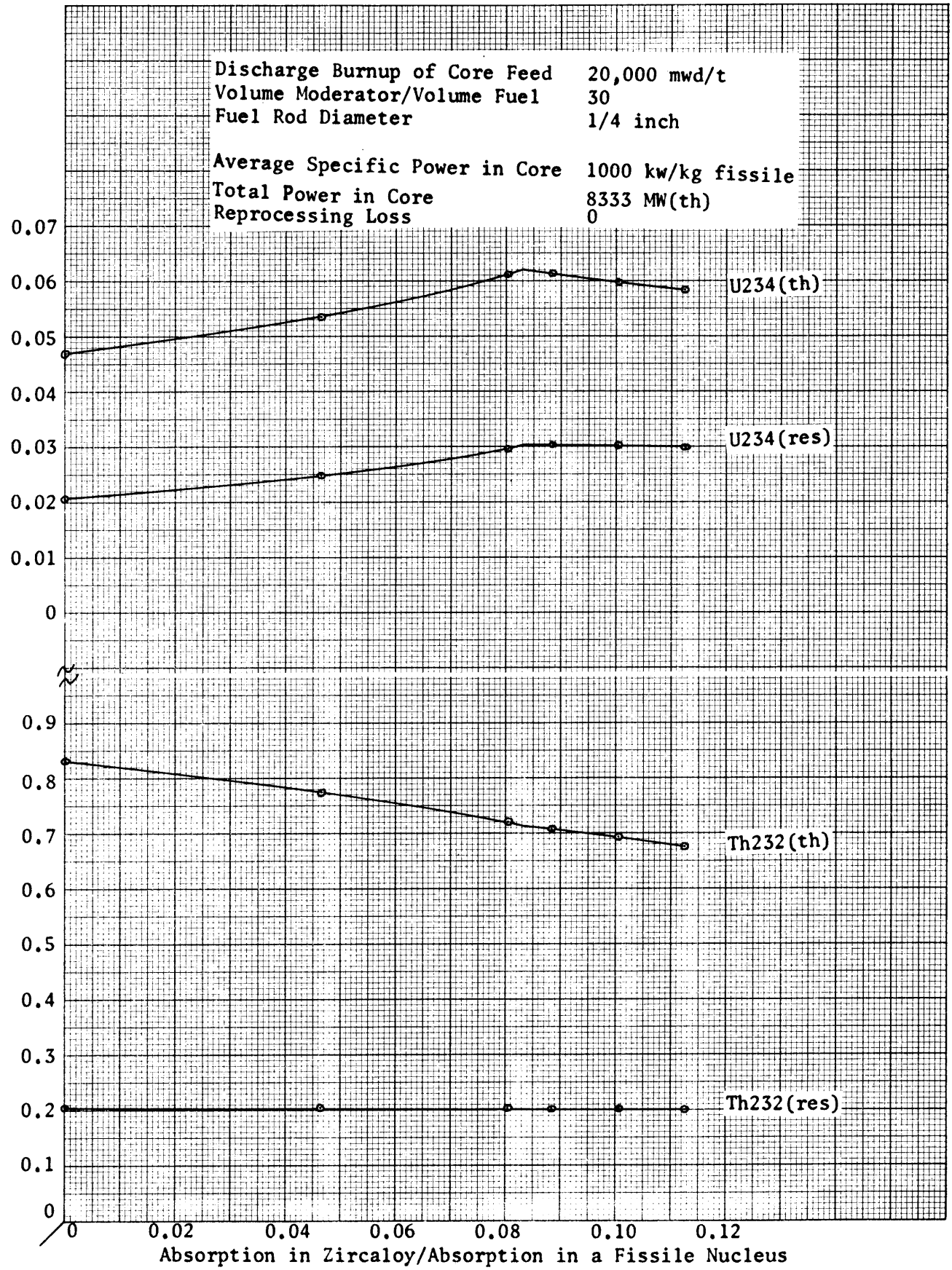

Figure 6.5: Absorptions by Fertile Nuclides vs. Absorption in Zircaloy/ Absorption in a Fissile Nucleus: 20,000 mwd/t Burnup

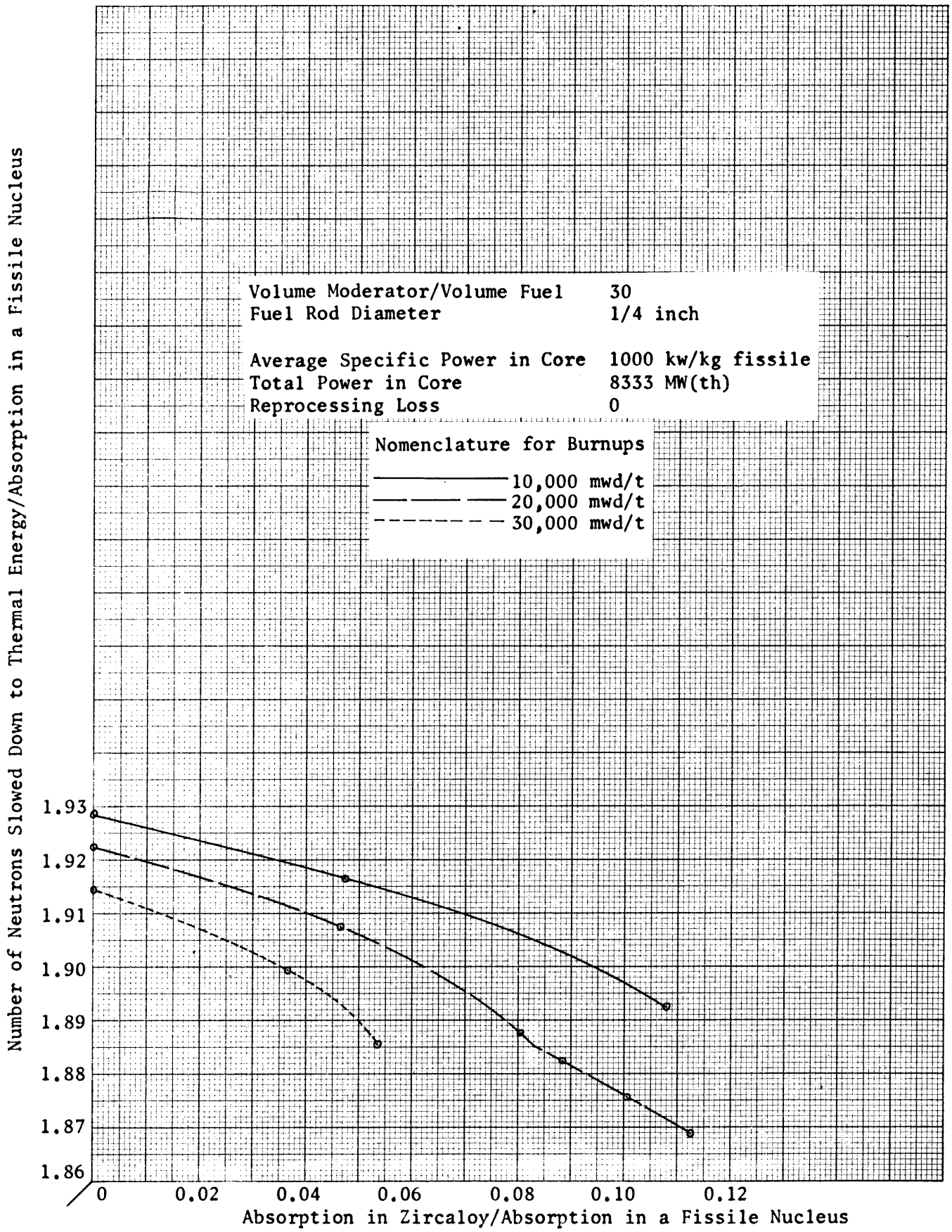

Figure 6.6: Number of Neutrons Slowed Down to Thermal Energy/Absorption in a Fissile Nucleus vs. Absorption in Zircaloy/Absorption in a Fissile Nucleus: 10,000 mwd/t, 20,000 mwd/t, 30,000 mwd/t Burnups

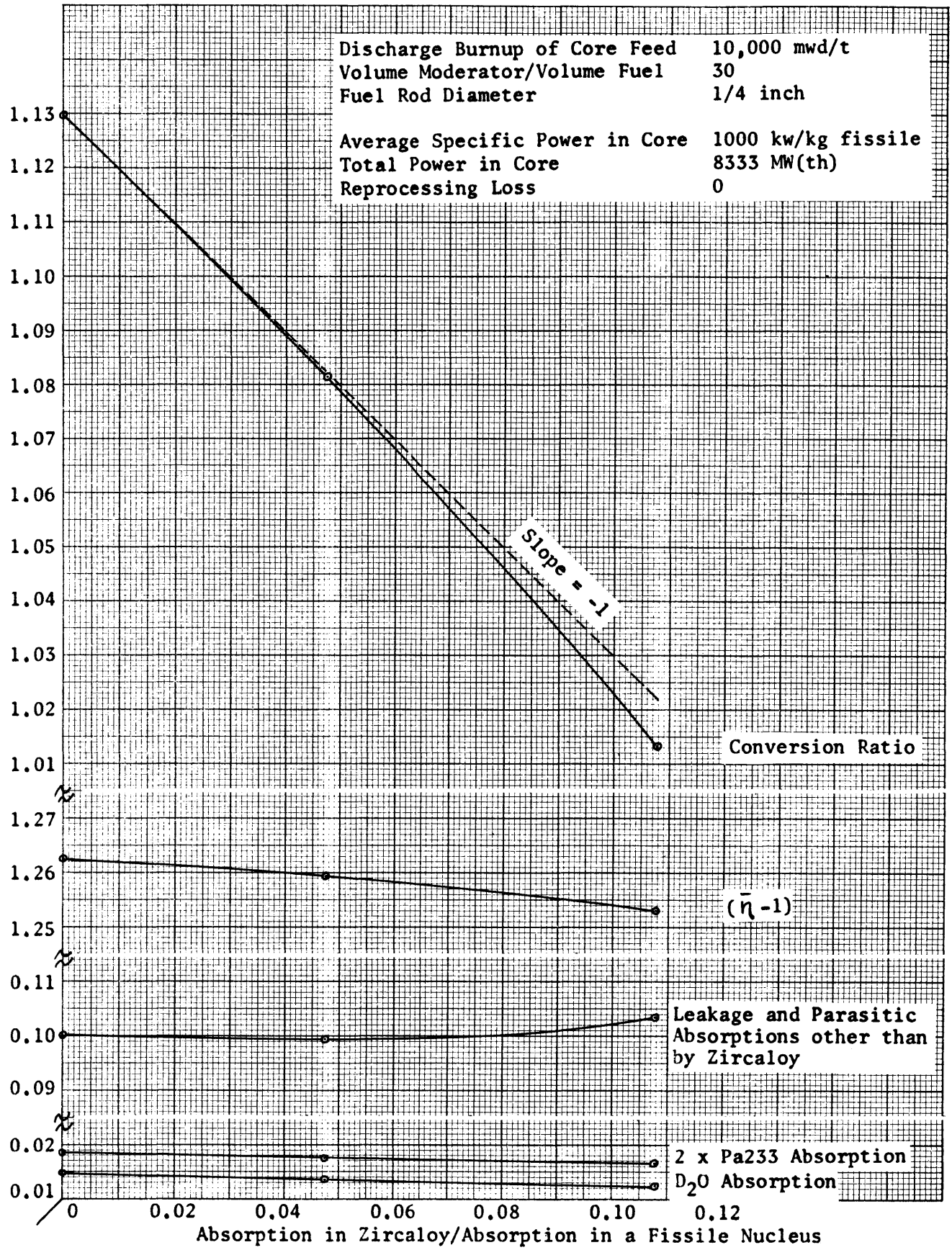

Figure 6.7: Conversion Ratio and its Components vs. Absorption in Zircaloy/Absorption in a Fissile Nucleus: 10,000 mwd/t Burnup

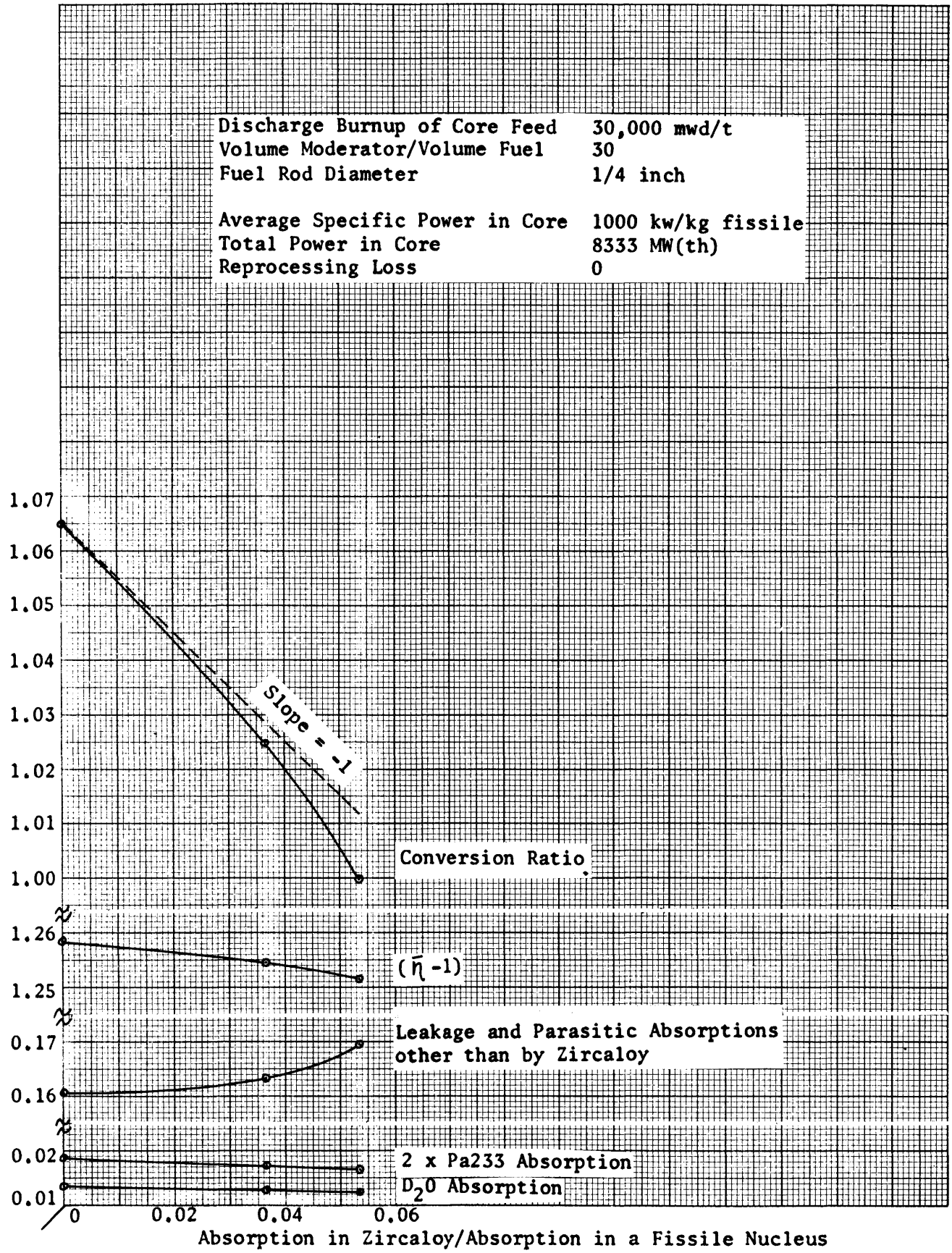

Figure 6.8: Conversion Ratio and its Components vs. Absorption in Zircaloy/ Absorption in a Fissile Nucleus: 30,000 mwd/t Burnup

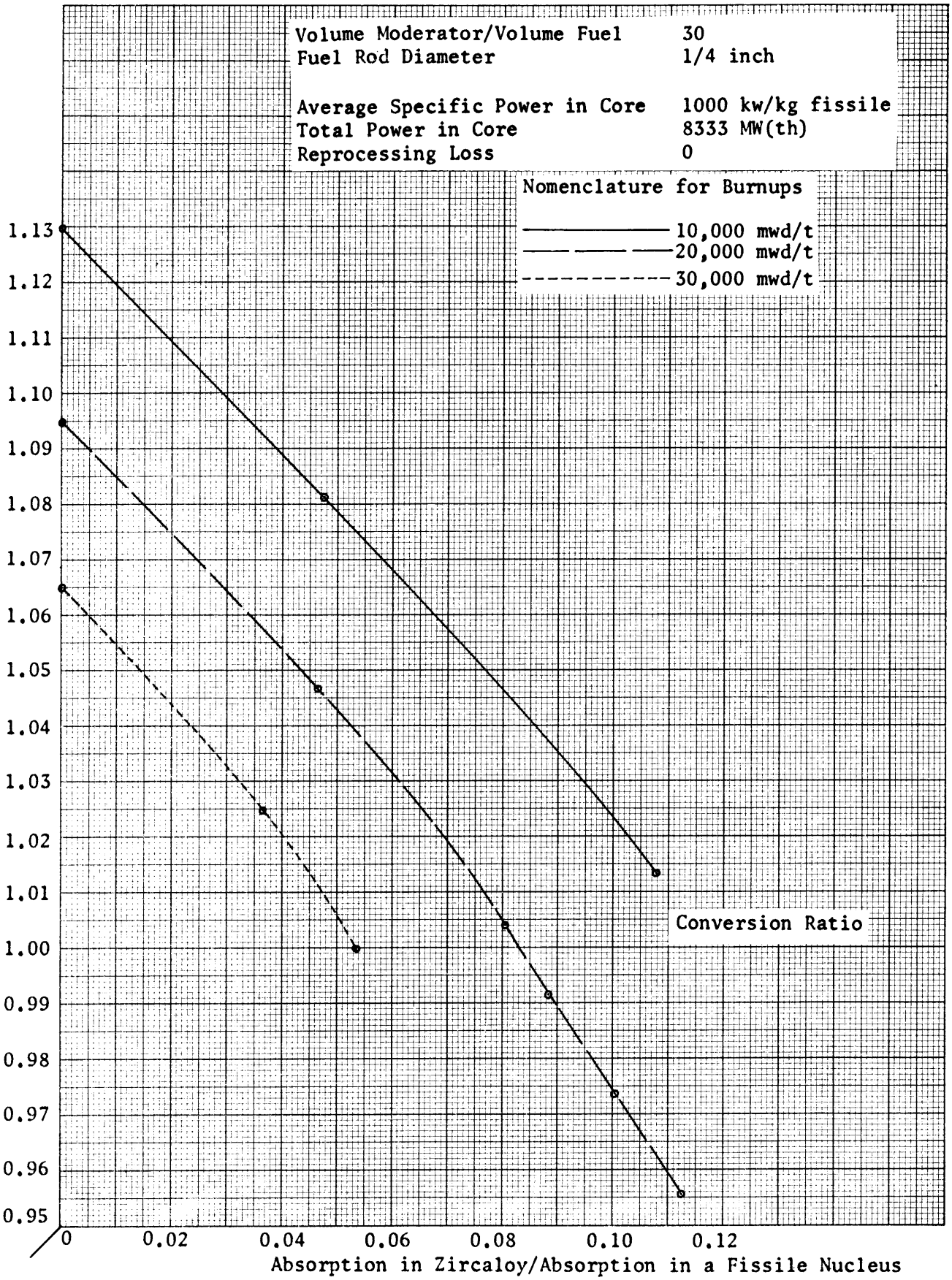

Figure 6.9 : Conversion Ratio vs. Absorption in Zircaloy/Absorption in a Fissile Nucleus: 10,000 mwd/t, 20,000 mwd/t, 30,000 mwd/t Burnups

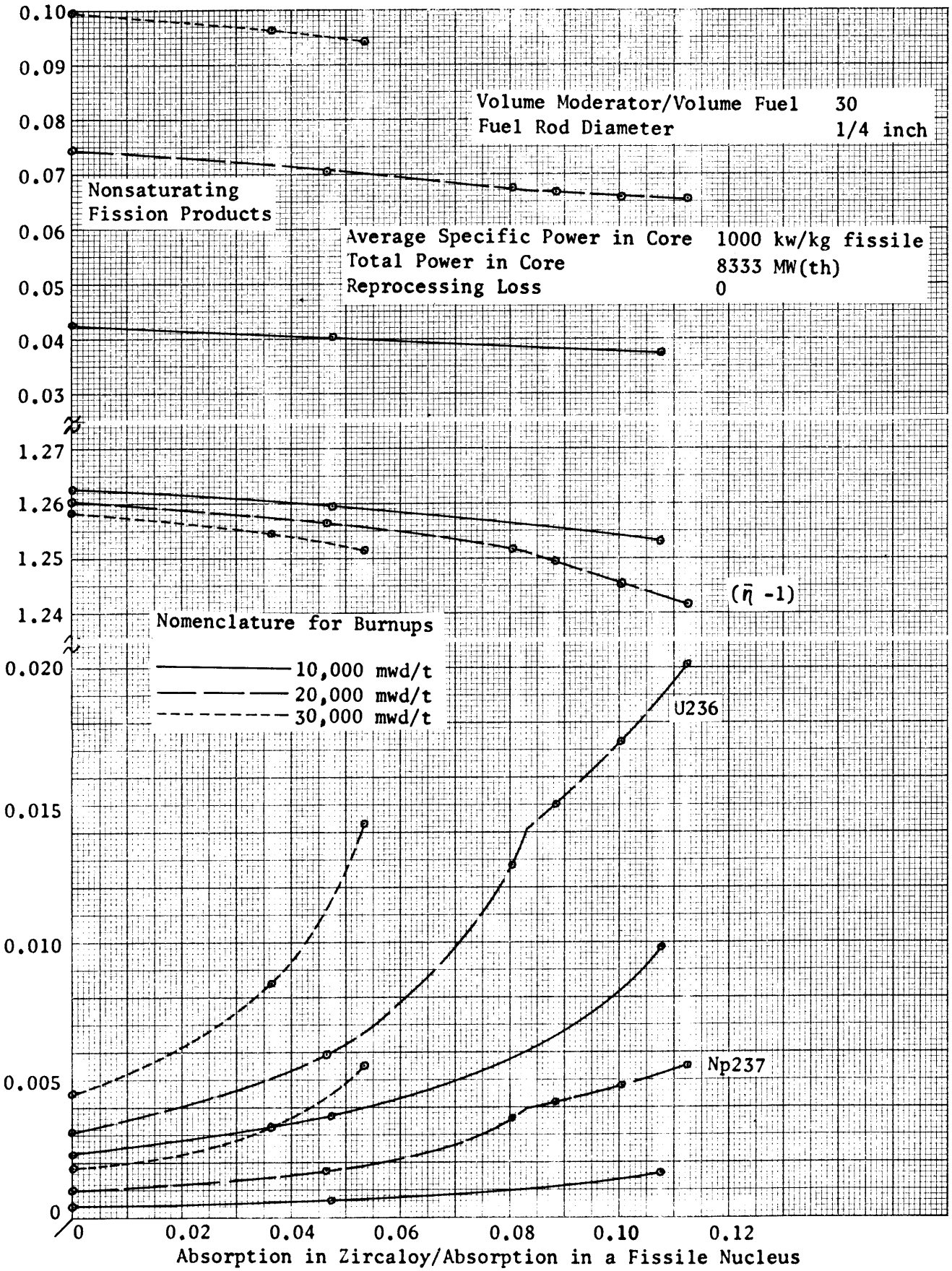

Figure 6.10 : $(\bar{\eta} - 1)$ and Absorptions by U236, Np237 and Nonsaturating Fission Products vs. Absorption in Zircaloy/Absorption in a Fissile Nucleus: 10,000 mwd/t, 20,000 mwd/t, 30,000 mwd/t Burnups

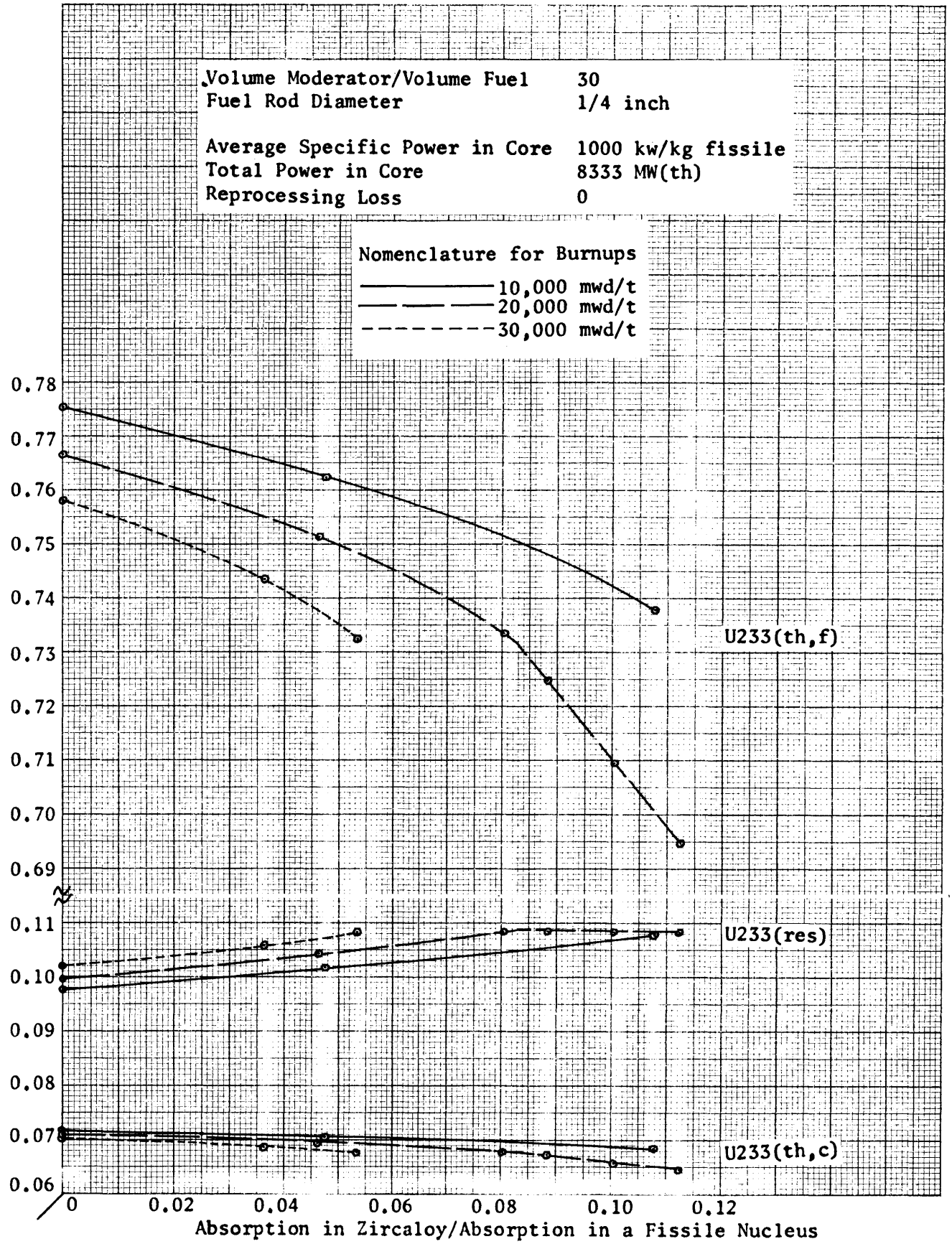

Figure 6.11: Absorptions by U233 vs. Absorption in Zircaloy/Absorption in a Fissile Nucleus: 10,000 mwd/t, 20,000 mwd/t, 30,000 mwd/t Burnups

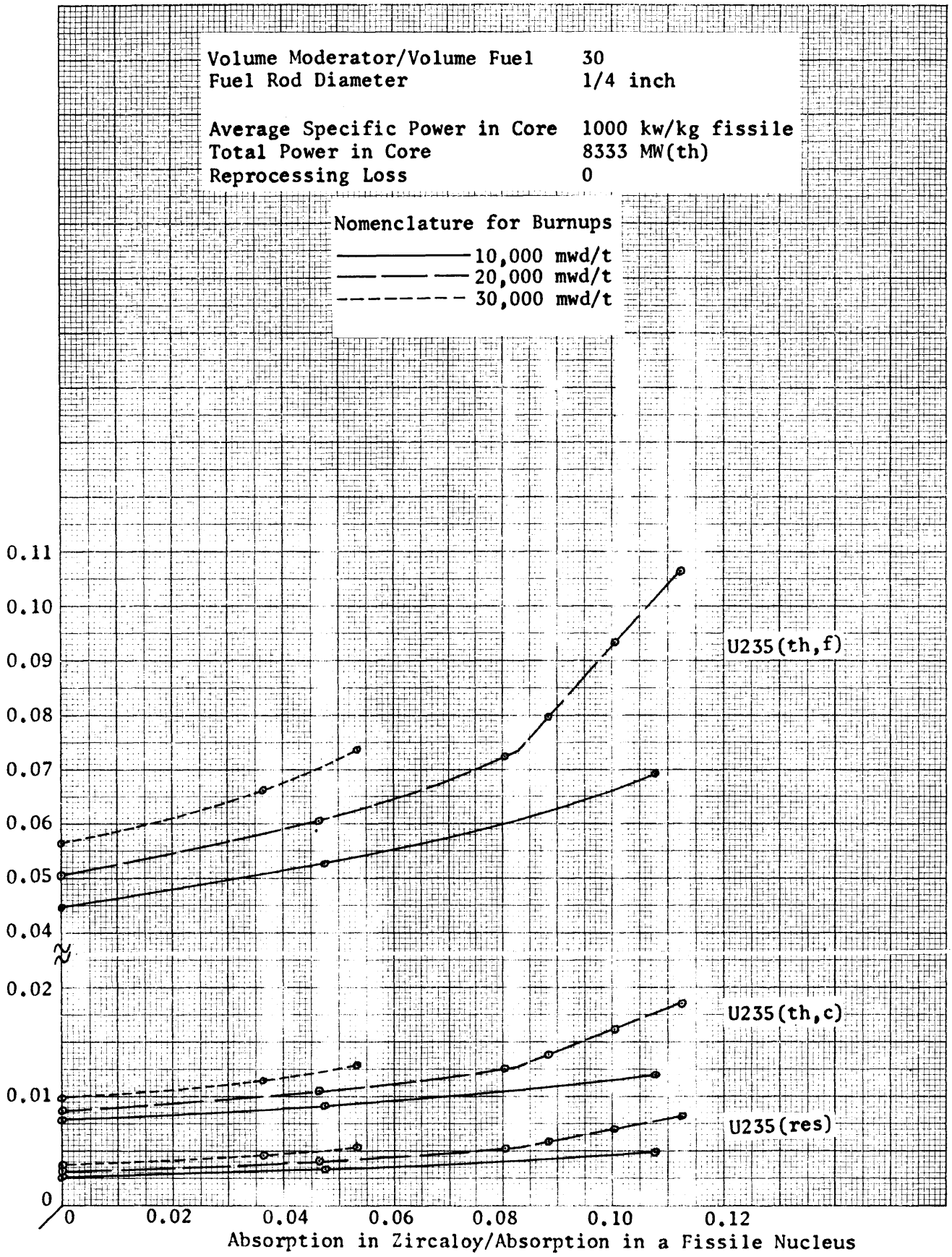

Figure 6.12: Absorptions by U235 vs. Absorption in Zircaloy/Absorption in a Fissile Nucleus: 10,000 mwd/t, 20,000 mwd/t, 30,000 mwd/t Burnups

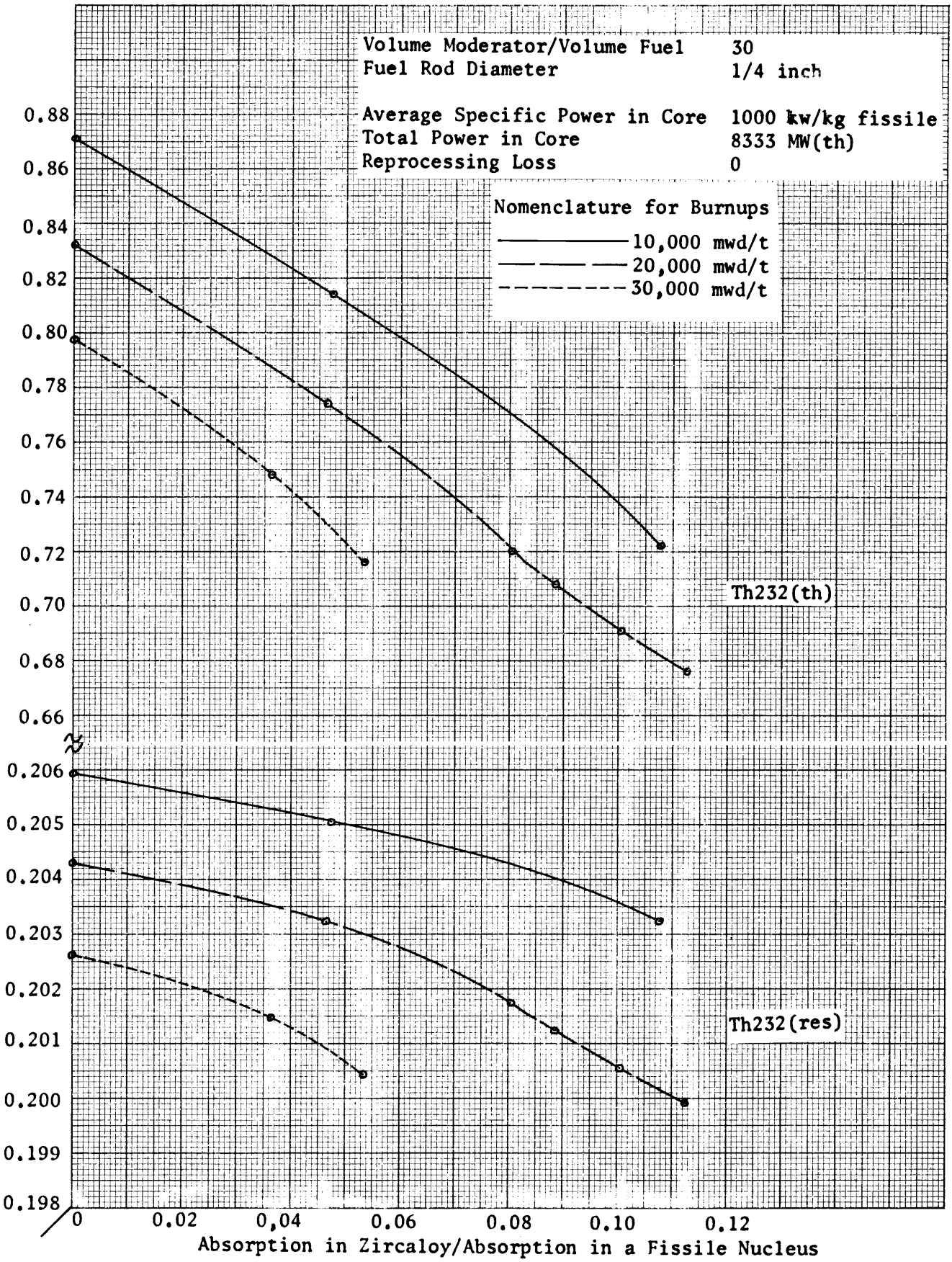

Figure 6.13: Absorptions by Th232 vs. Absorption in Zircaloy/Absorption in a Fissile Nucleus: 10,000 mwd/t, 20,000 mwd/t, 30,000 mwd/t Burnups

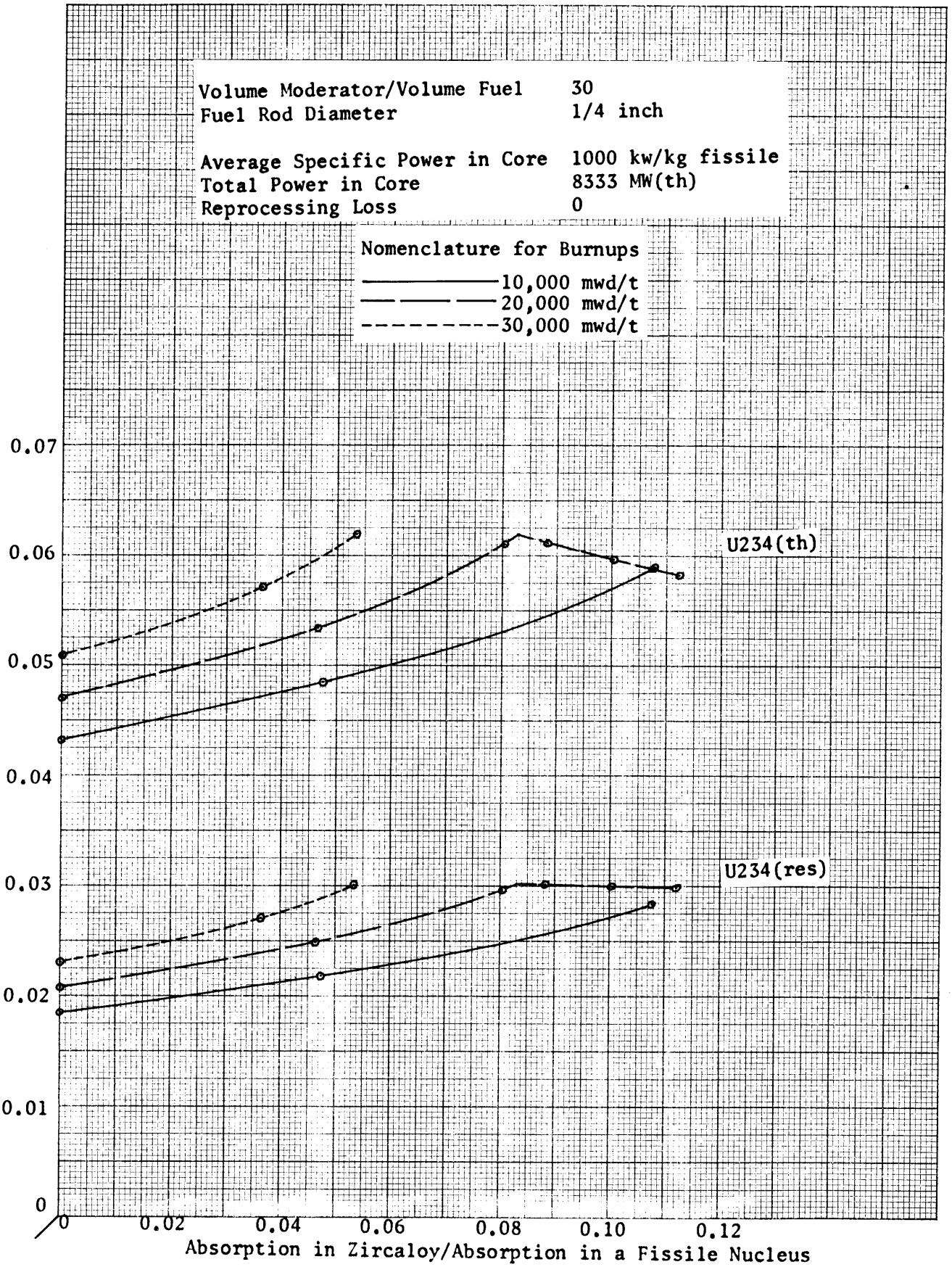

Figure 6.14: Absorptions by U234 vs. Absorption in Zircaloy/Absorption in a Fissile Nucleus: 10,000 mwd/t, 20,000 mwd/t, 30,000 mwd/t Burnups

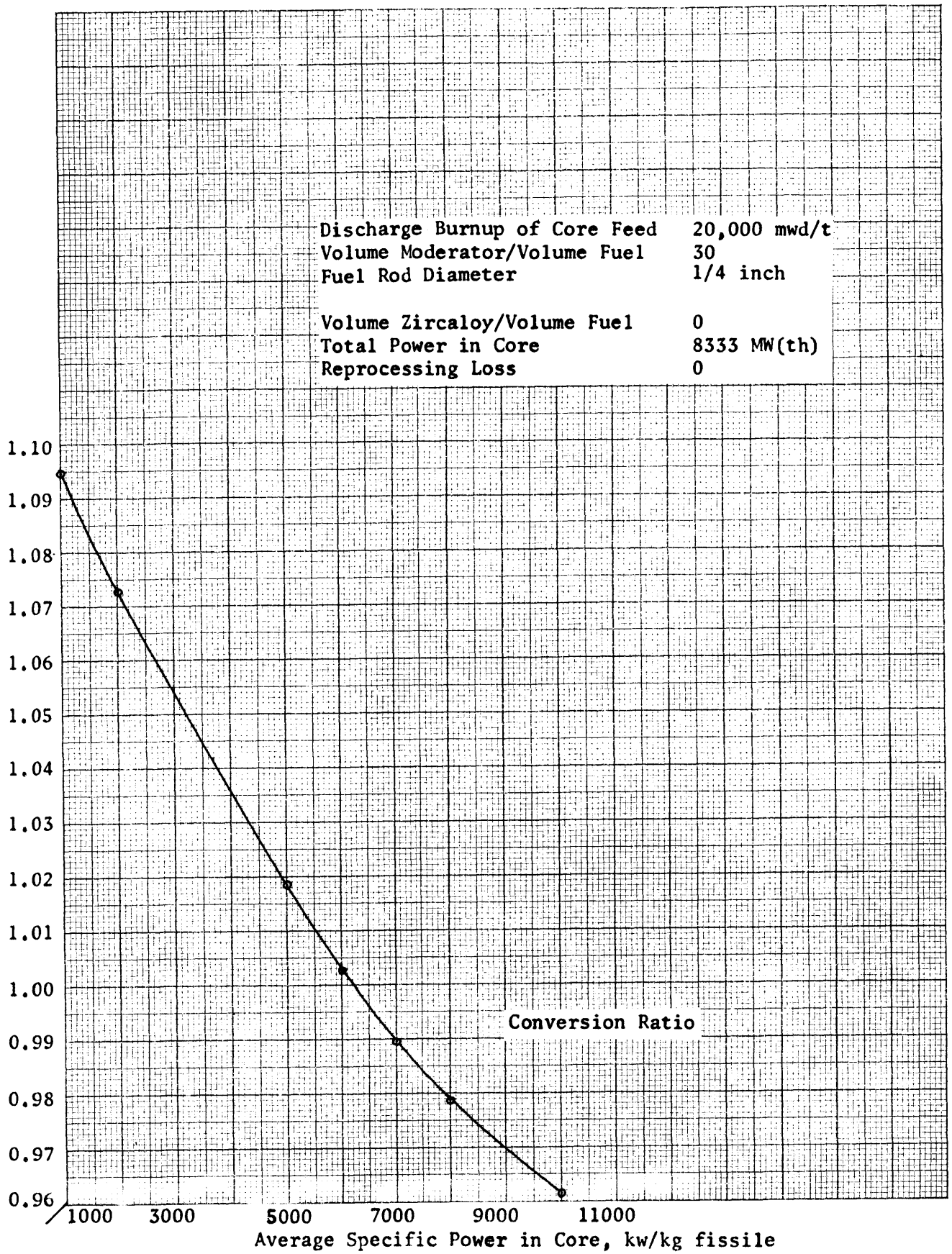

Figure 6.15 : Conversion Ratio vs. Average Specific Power in Core: 20,000 mwd/t Burnup

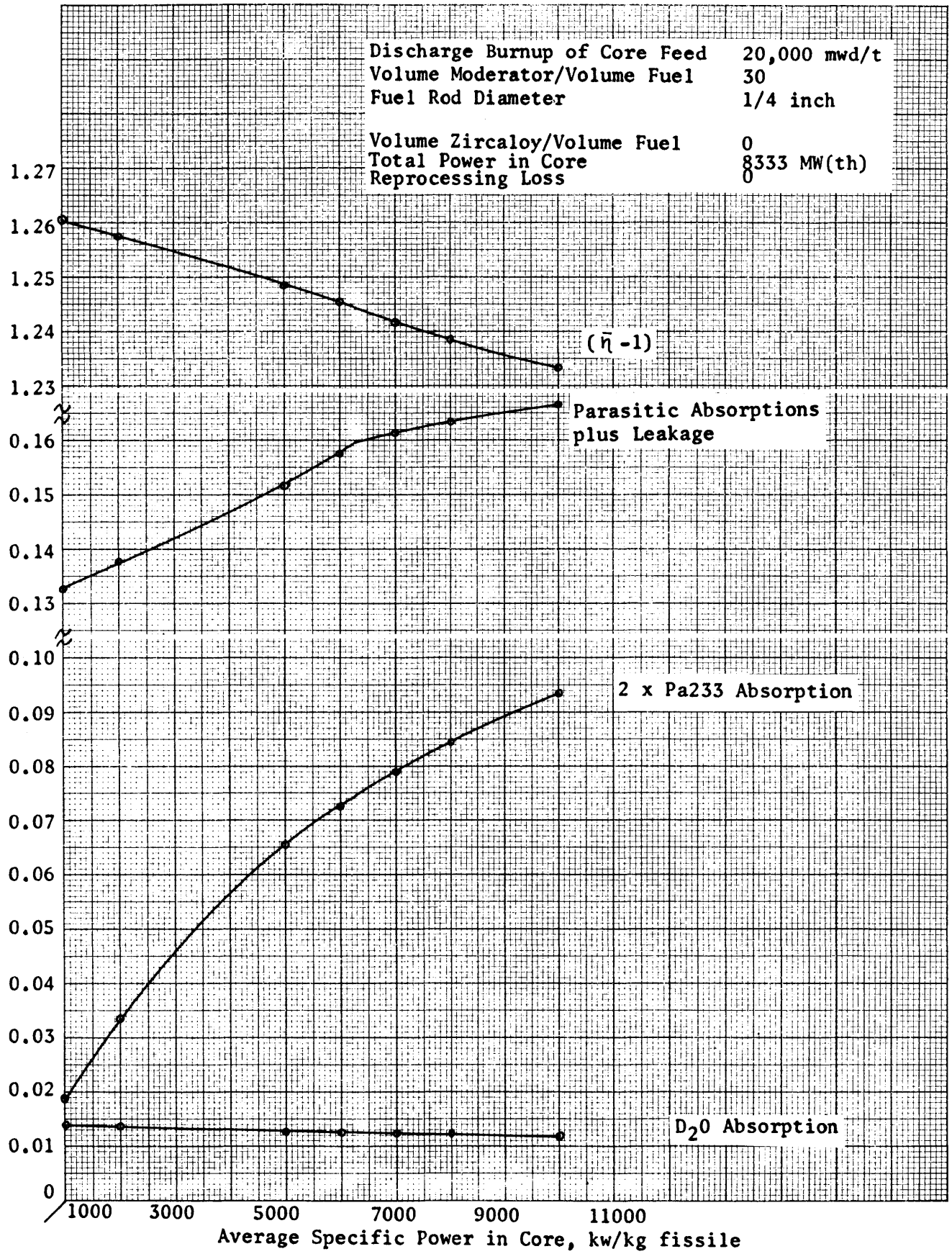

Figure 6:16 : Components of the Conversion Ratio vs. Average Specific Power in Core: 20,000 mwd/t Burnup

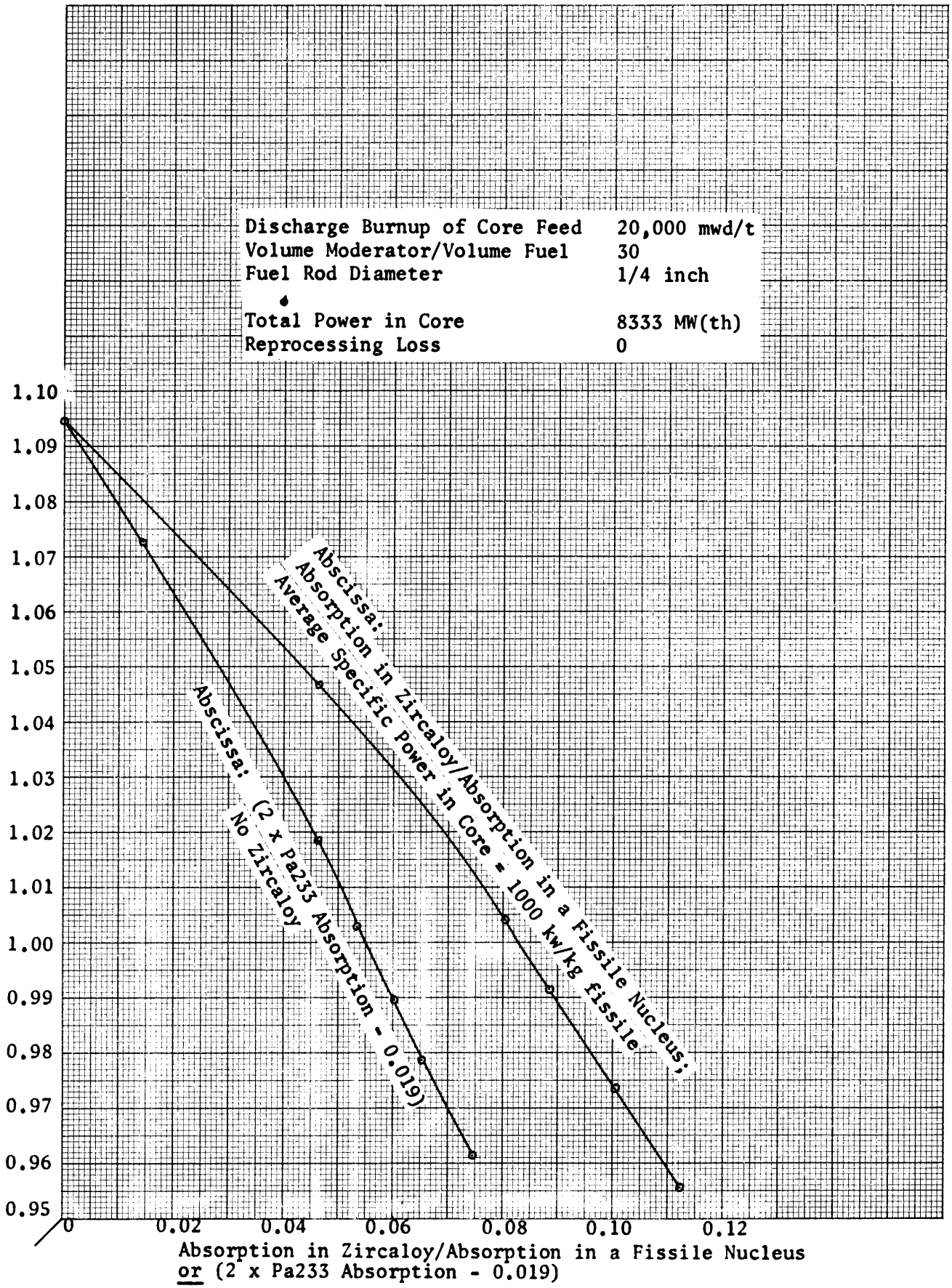

Figure 6.16A: Comparison of the Effect on the Conversion Ratio of Absorption in Zircaloy/Absorption in a Fissile Nucleus and 2 x Pa233 Absorption

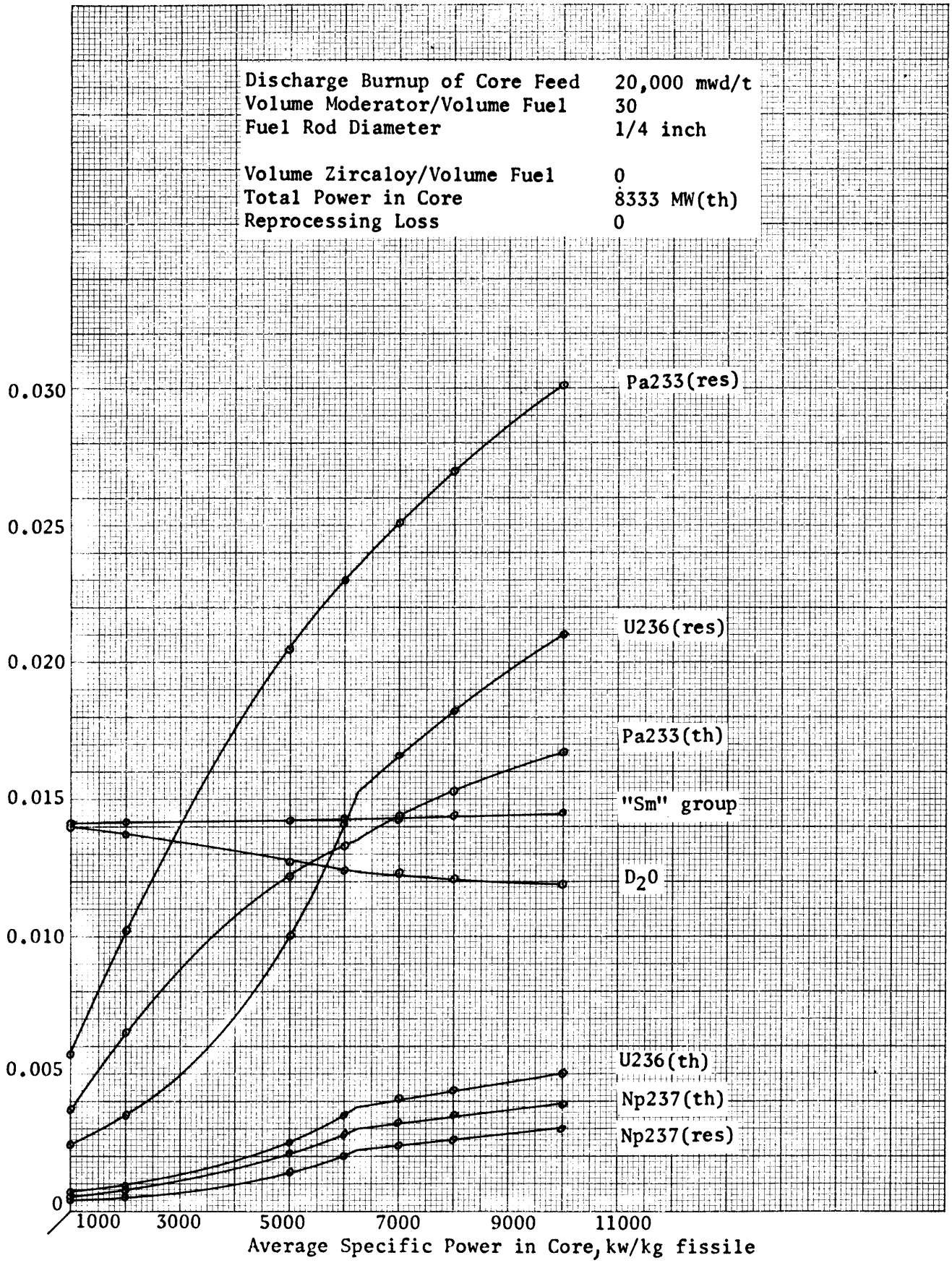

Figure 6.17: Absorptions by Pa233(th,res), U236(th,res), Np237(th,res), "Sm" group, D_2O vs. Average Specific Power in Core: 20,000 mwd/t Burnup

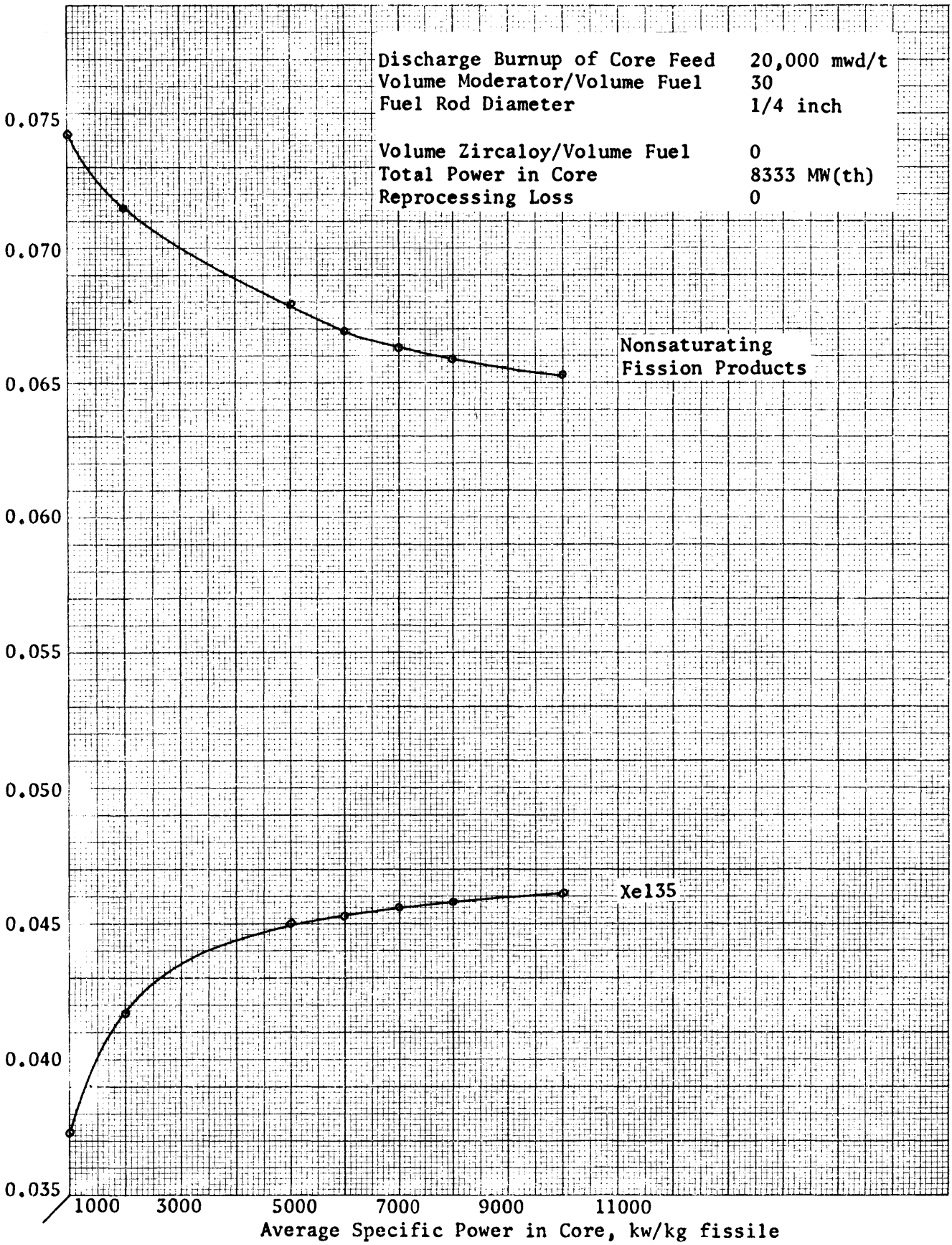

Figure 6.18: Absorptions by Xe135 and Nonsaturating Fission Products vs. Average Specific Power in Core: 20,000 mwd/t Burnup

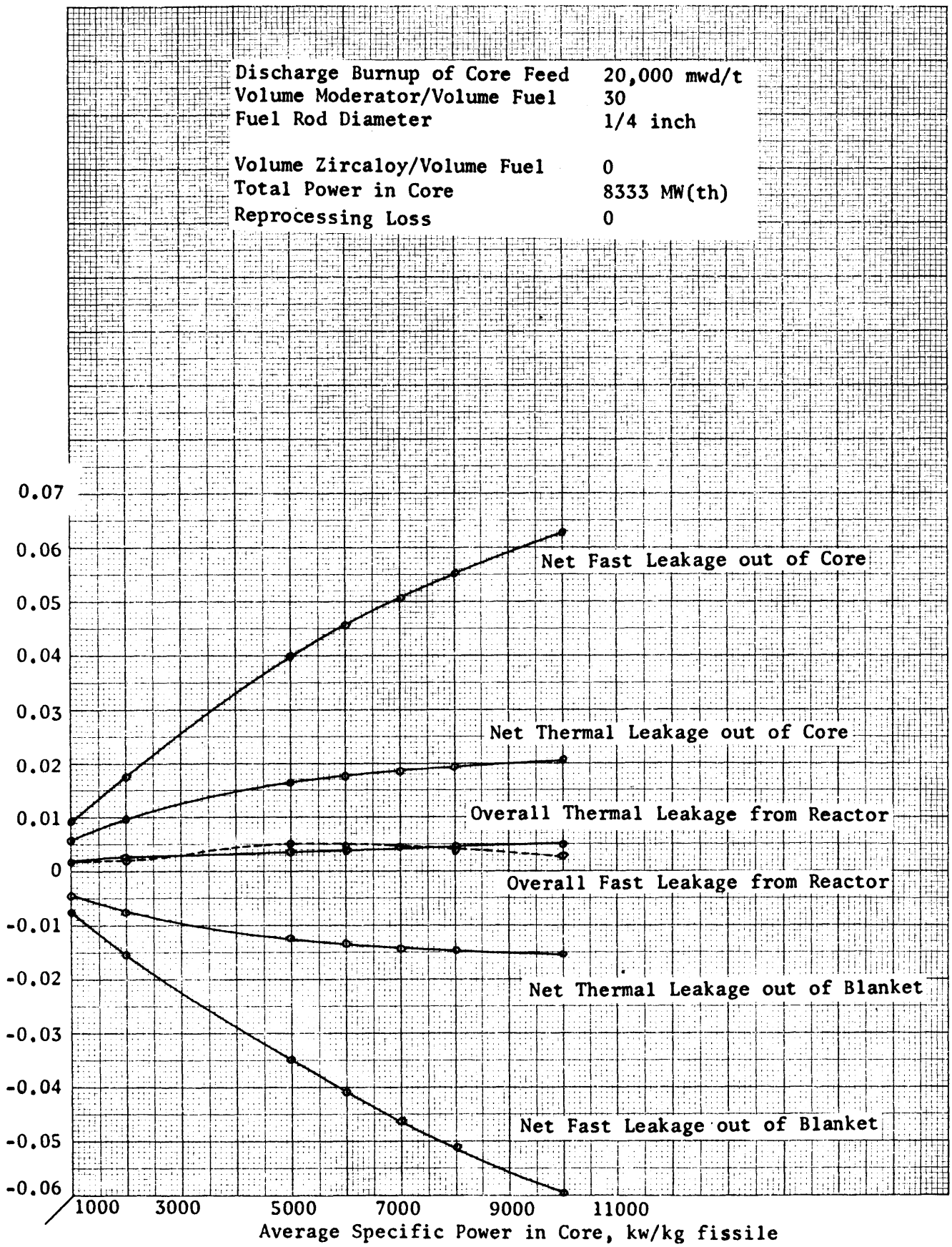

Figure 6.19: Fast and Thermal Leakages vs. Average Specific Power in Core: 20,000 mwd/t Burnup

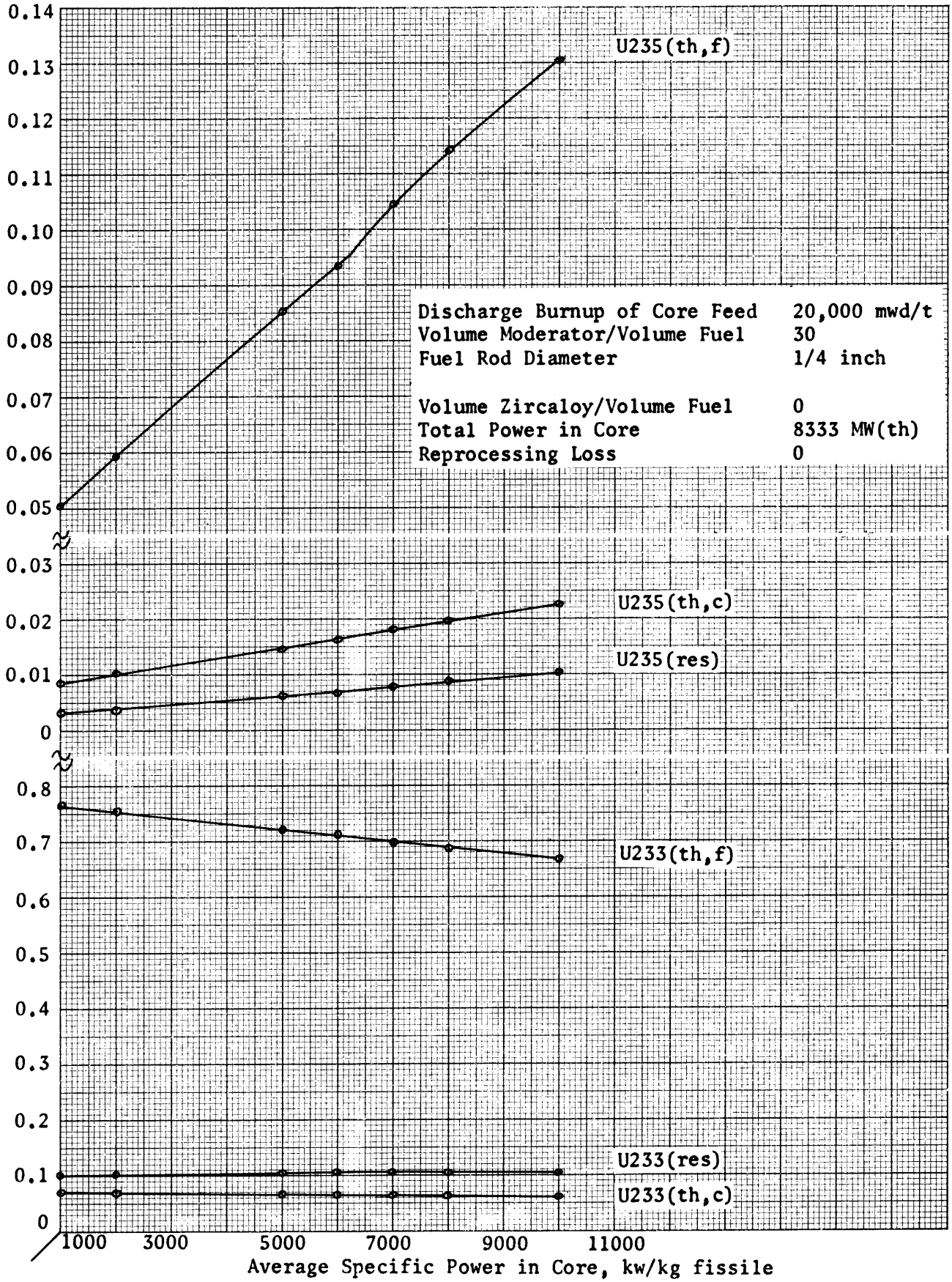

Figure 6.20: Absorptions by Fissile Nuclides vs. Average Specific Power in Core: 20,000 mwd/t Burnup

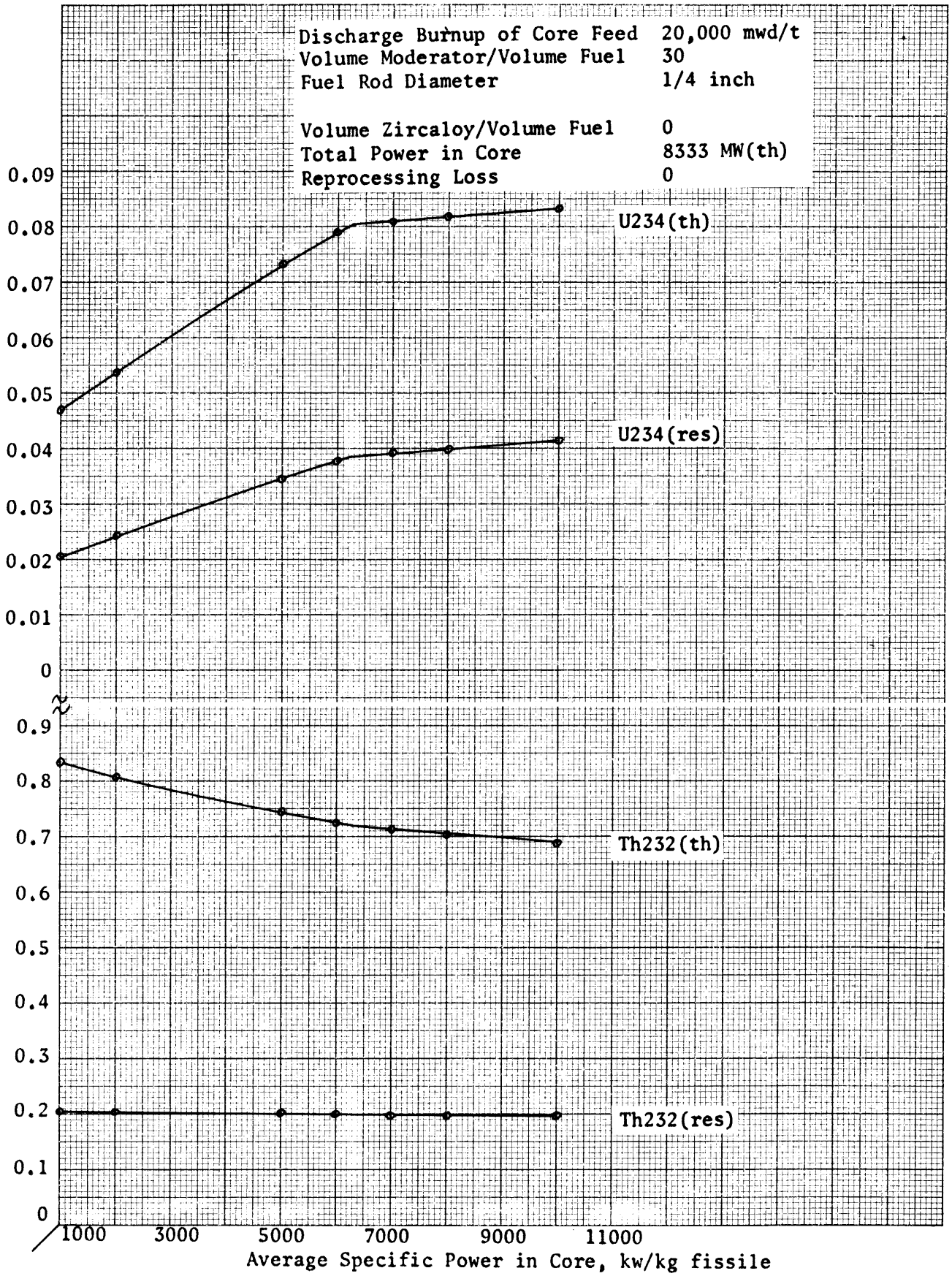

Figure 6.21: Absorptions by Fertile Nuclides vs. Average Specific Power in Core: 20,000 mwd/t Burnup

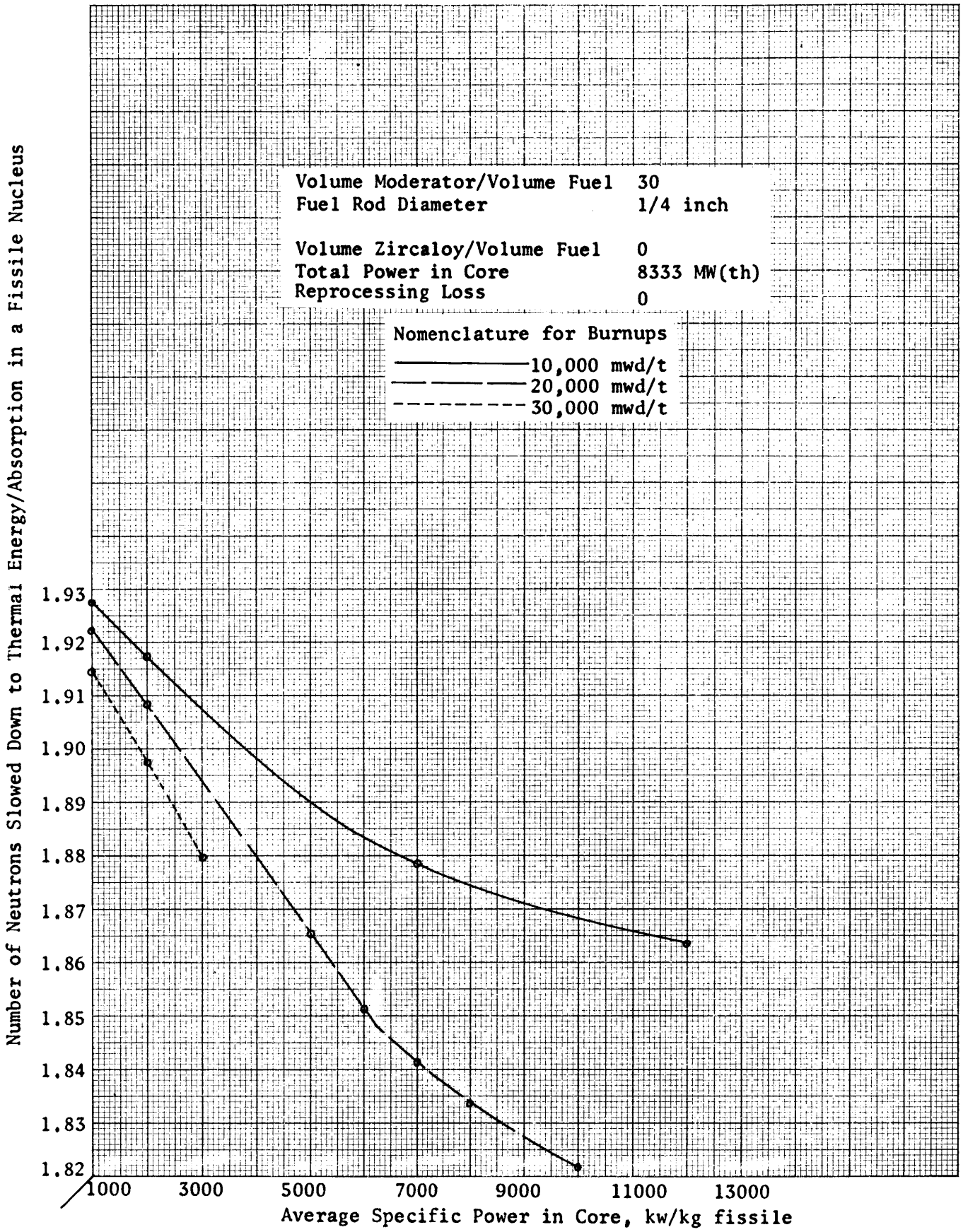

Figure 6.22: Number of Neutrons Slowed Down to Thermal Energy/Absorption in a Fissile Nucleus vs. Average Specific Power in Core: 10,000 mwd/t, 20,000 mwd/t, 30,000 mwd/t Burnups

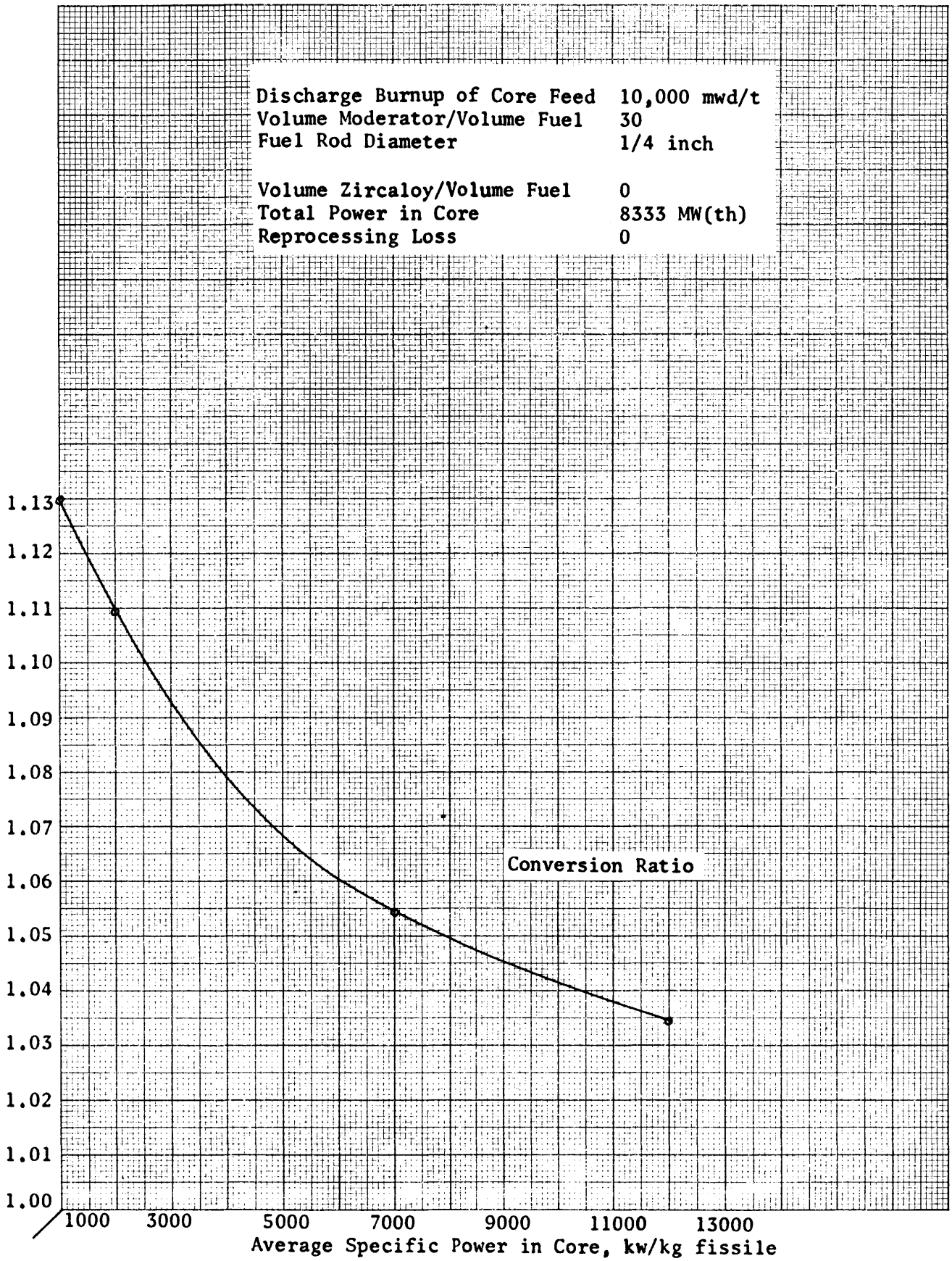

Figure 6.23: Conversion Ratio vs. Average Specific Power in Core: 10,000 mwd/t Burnup

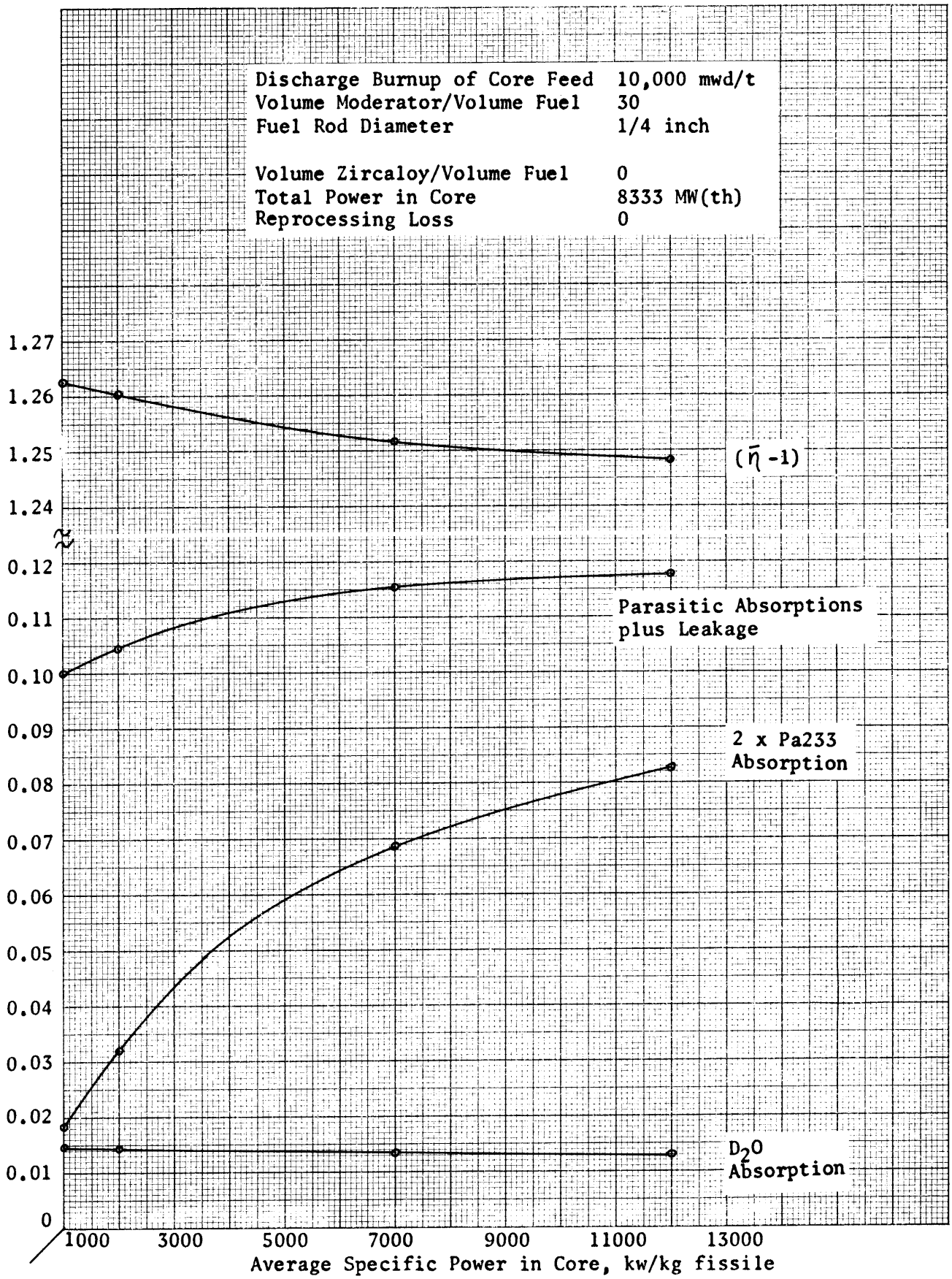

Figure 6.24: Components of the Conversion Ratio vs. Average Specific Power in Core: 10,000 mwd/t Burnup

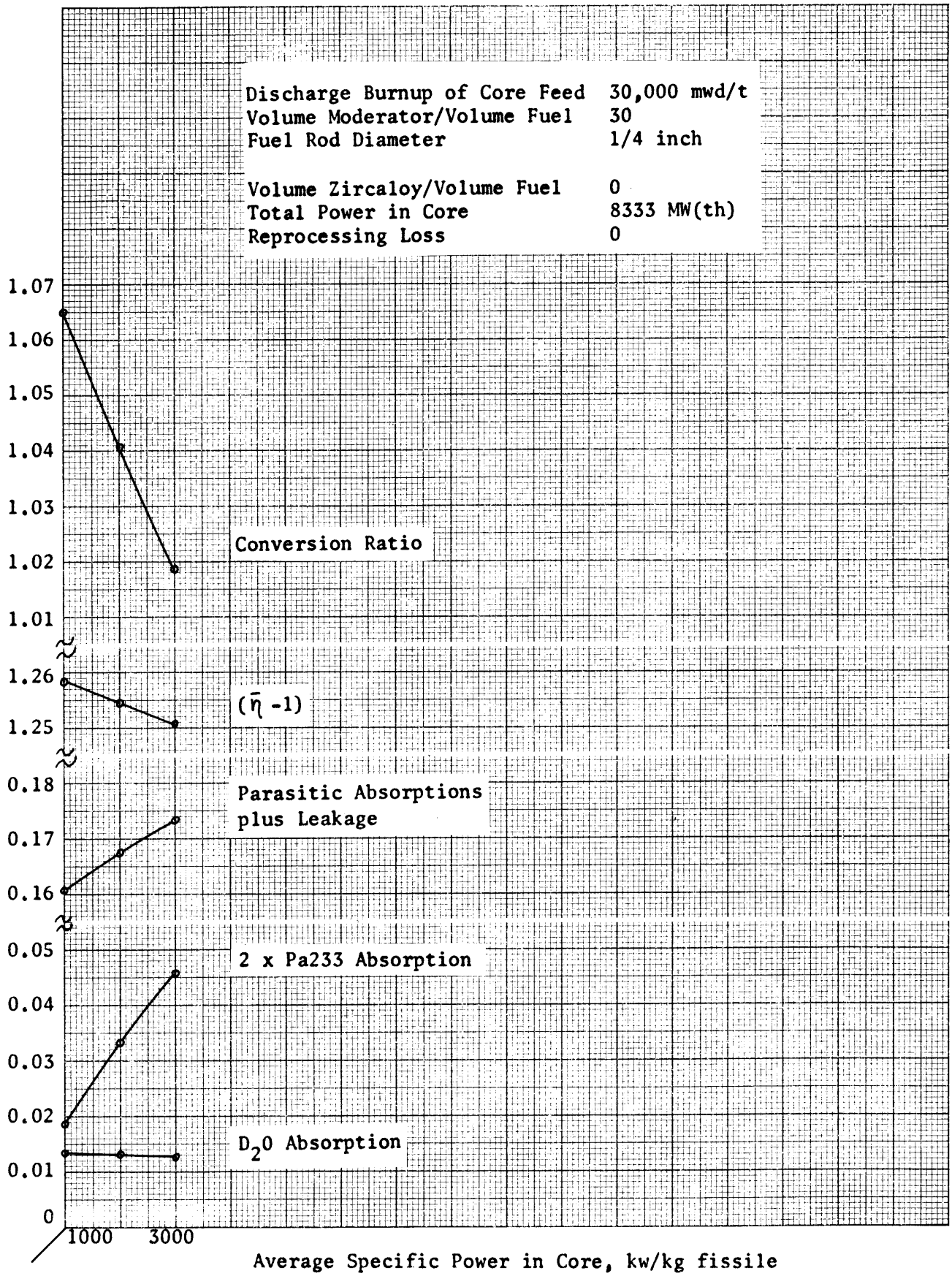

Figure 6.25: Conversion Ratio and its Components vs. Average Specific Power in Core: 30,000 mwd/t Burnup

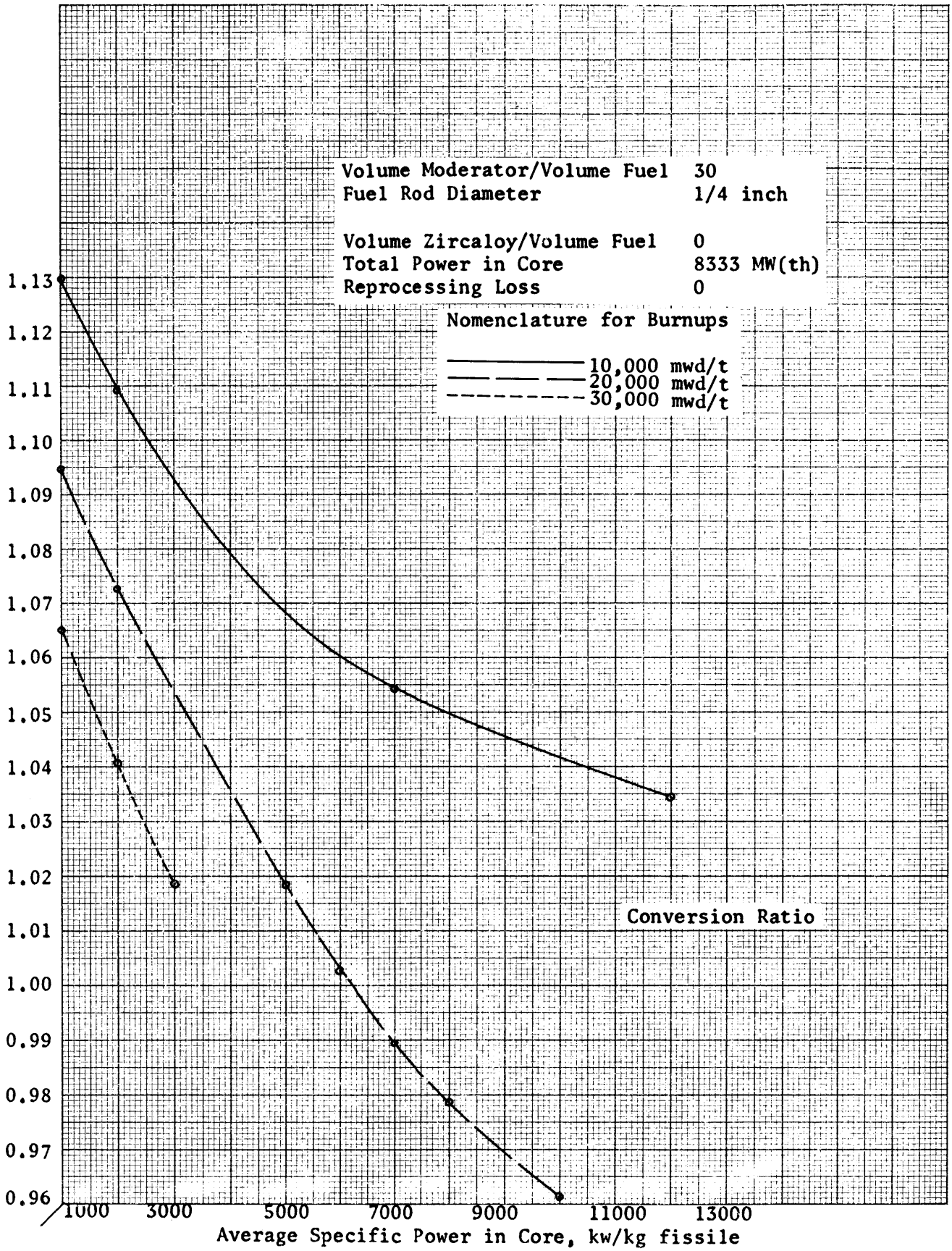

Figure 6.26: Conversion Ratio vs. Average Specific Power in Core: 10,000 mwd/t, 20,000 mwd/t, 30,000 mwd/t Burnups

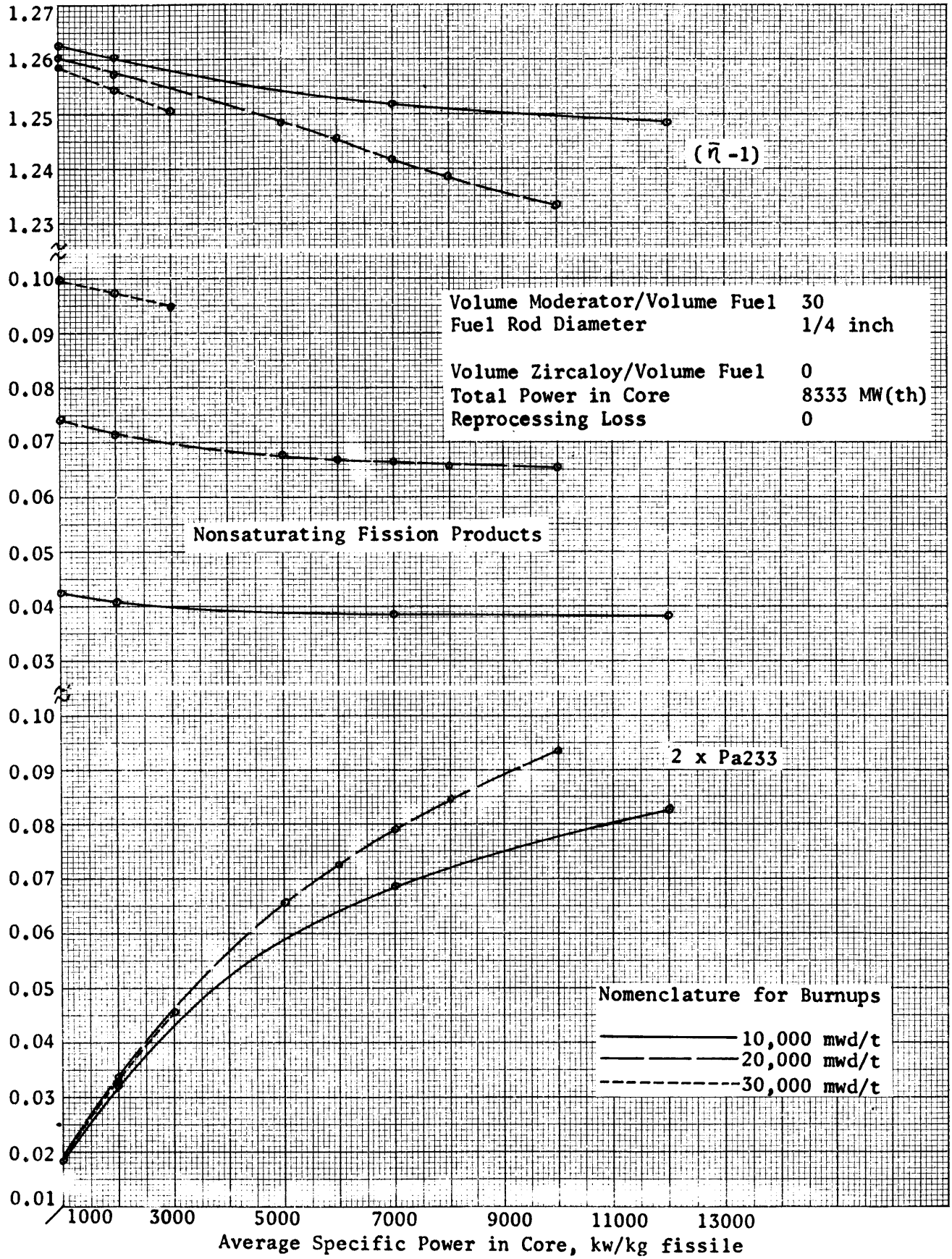

Figure 6.27: $(\bar{\eta} - 1)$, Nonsaturating Fission Product Absorptions, 2 x Pa233 Absorptions vs. Average Specific Power in Core: 10,000 mwd/t, 20,000 mwd/t, 30,000 mwd/t Burnups

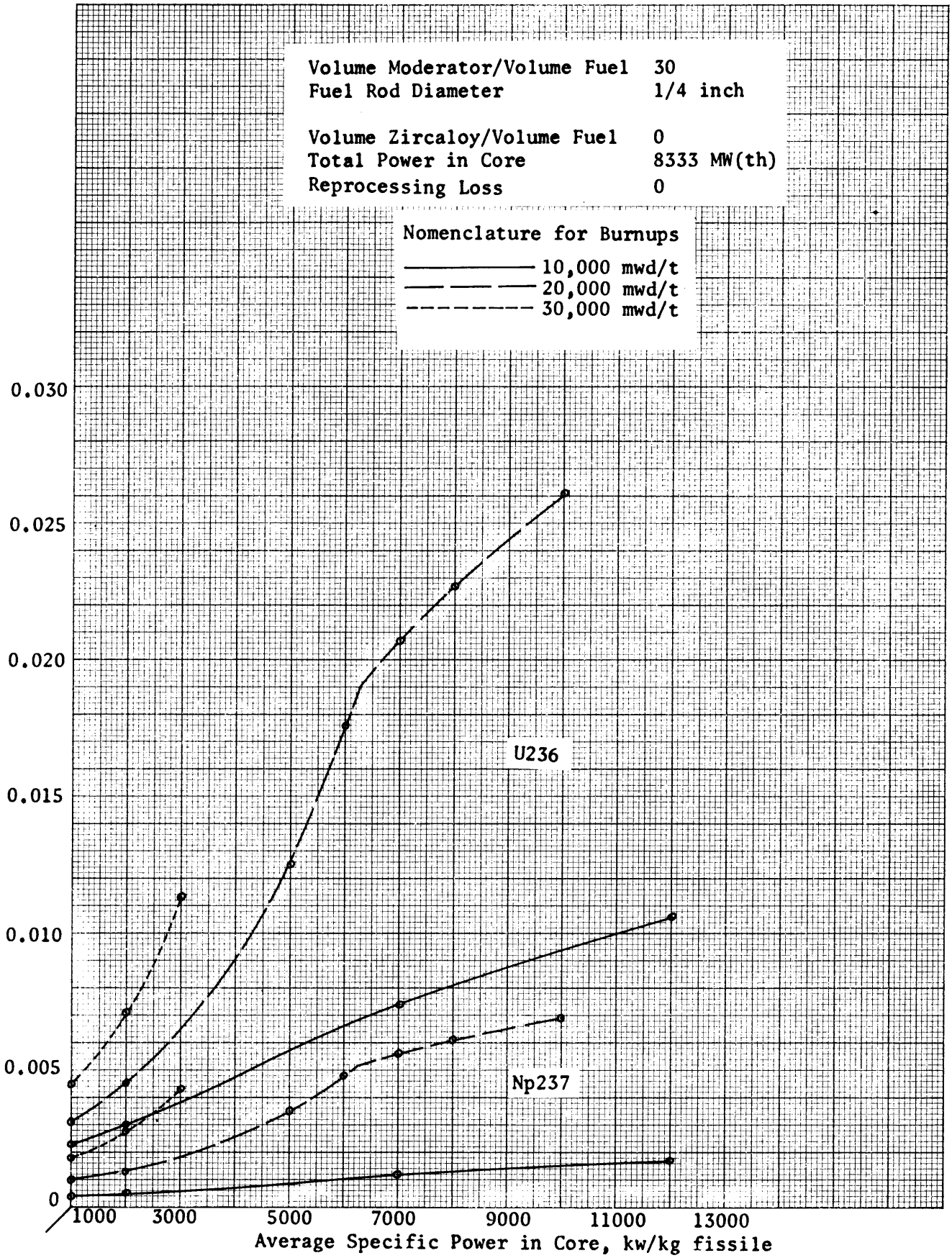

Figure 6.28: Absorptions by U236 and Np237 vs. Average Specific Power in Core: 10,000 mwd/t, 20,000 mwd/t, 30,000 mwd/t Burnups

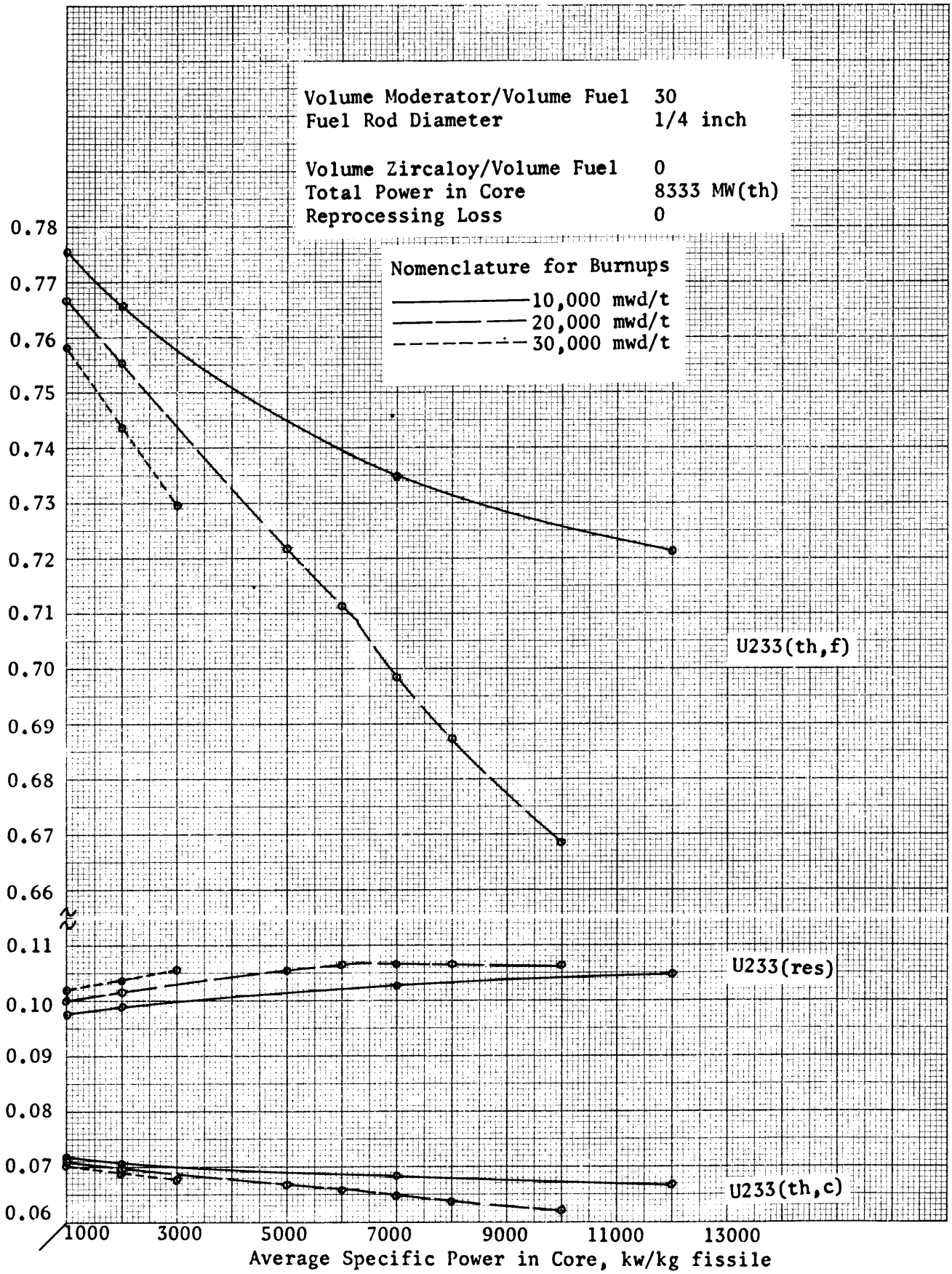

Figure 6.29: Absorptions by U233 vs. Average Specific Power in Core: 10,000 mwd/t, 20,000 mwd/t, 30,000 mwd/t Burnups

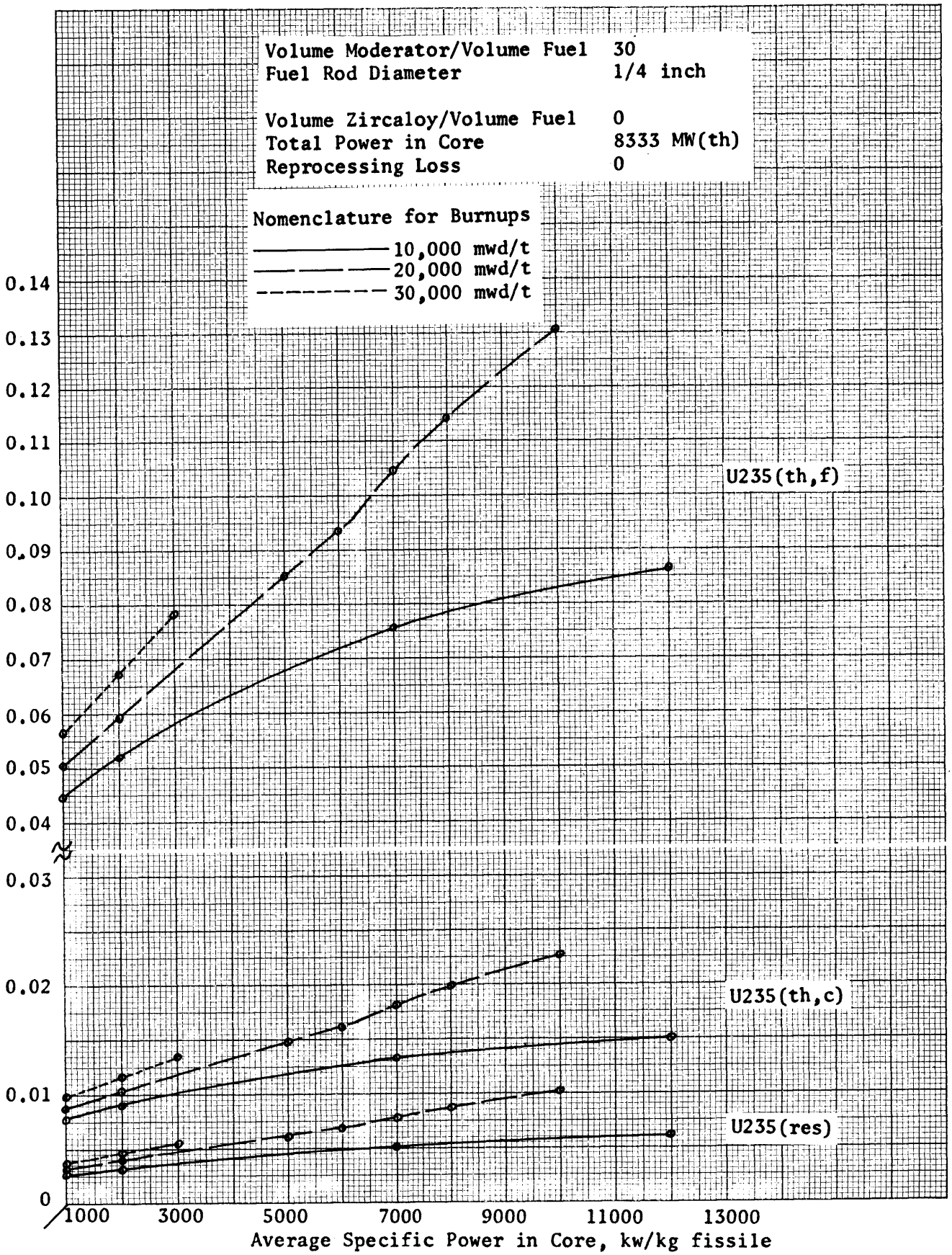

Figure 6.30: Absorptions by U235 vs. Average Specific Power in Core: 10,000 mwd/t, 20,000 mwd/t, 30,000 mwd/t Burnups

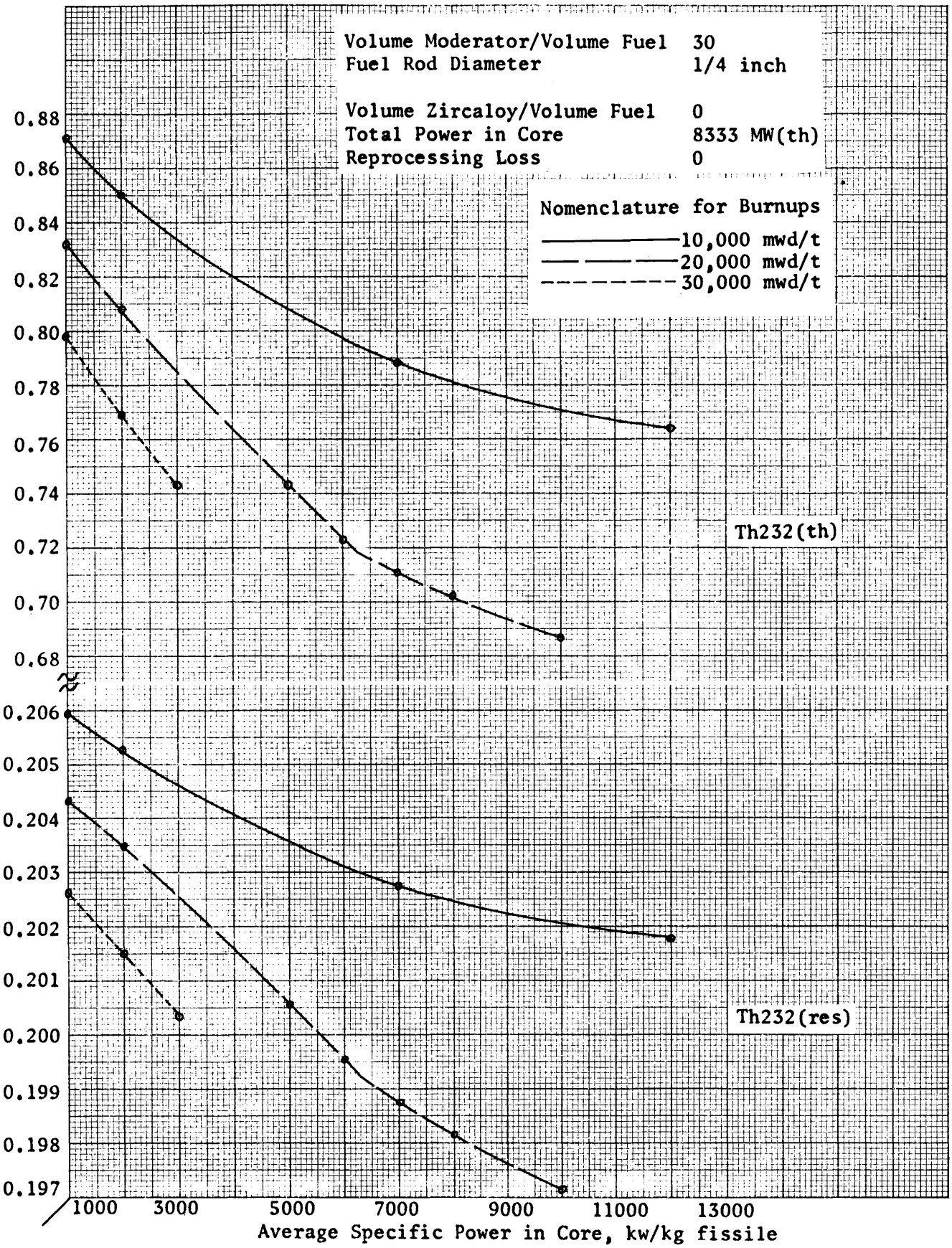

Figure 6.31: Absorptions by Th232 vs. Average Specific Power in Core: 10,000 mwd/t, 20,000 mwd/t, 30,000 mwd/t Burnups

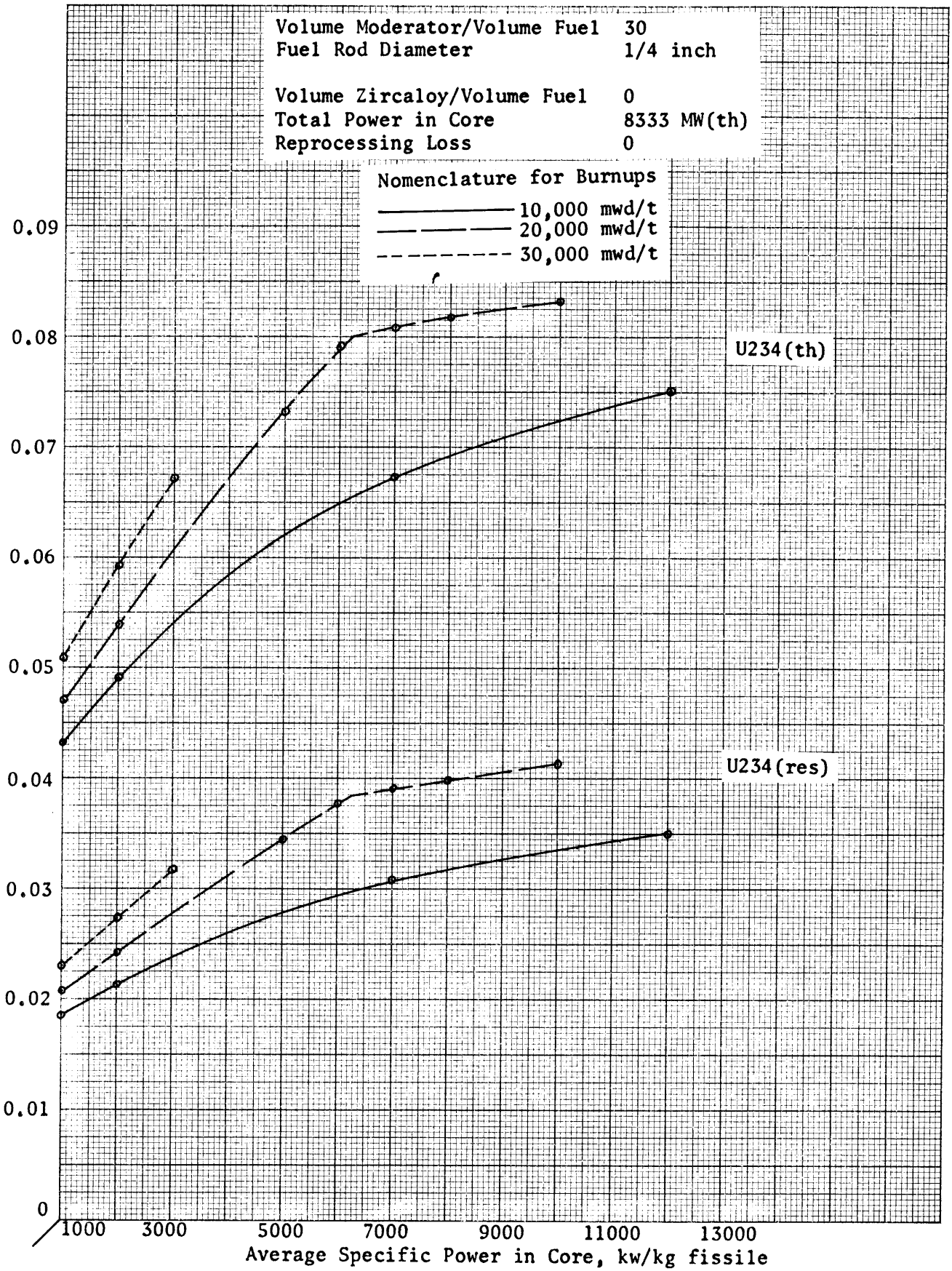

Figure 6.32: Absorptions by U234 vs. Average Specific Power in Core: 10,000 mwd/t, 20,000 mwd/t, 30,000 mwd/t Burnups

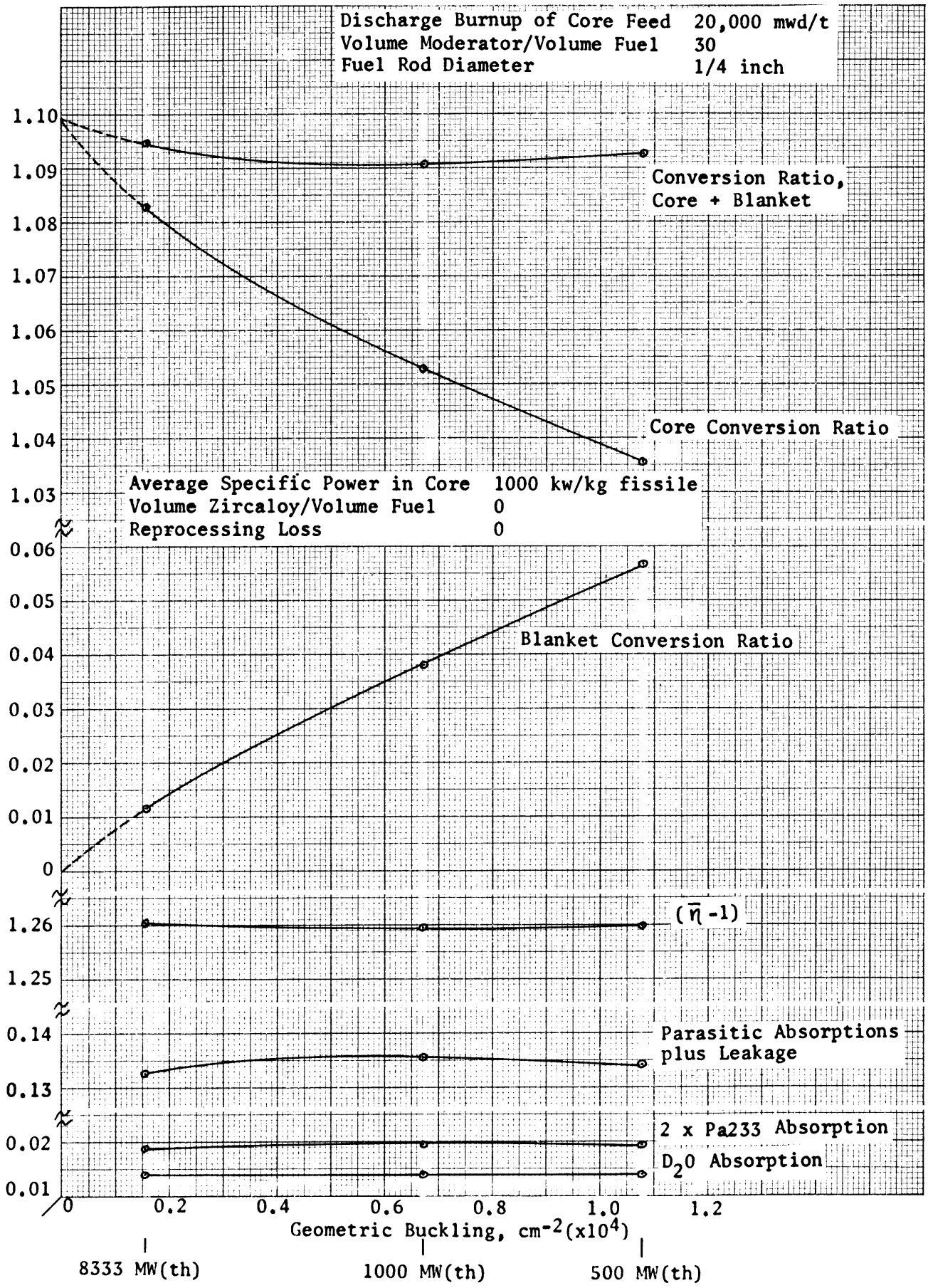

Figure 6.33: Conversion Ratio and its Components vs. Geometric Buckling: 20,000 mwd/t Burnup

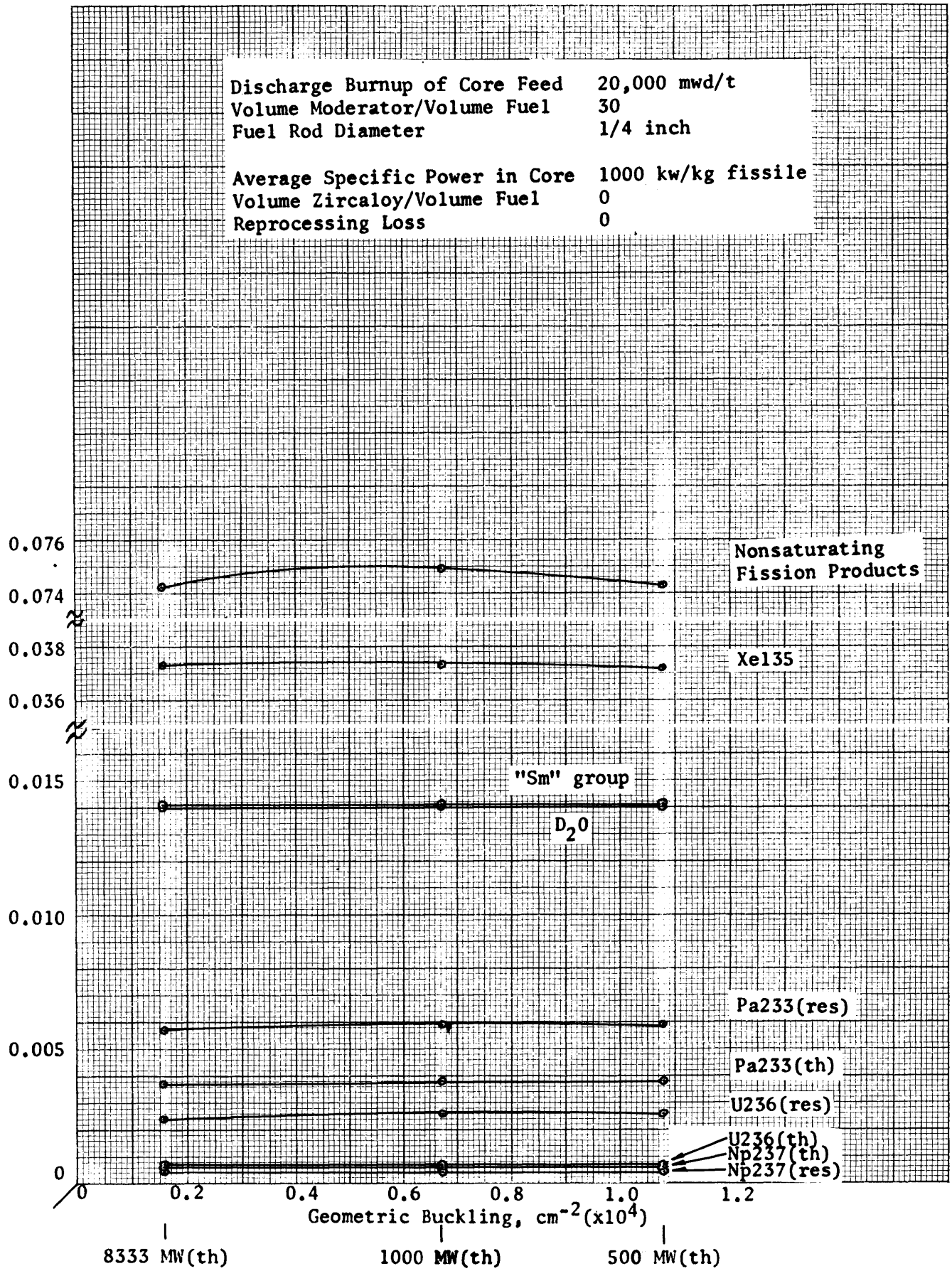

Figure 6.34: Absorptions by Pa233(th,res), U236(th,res), Np237(th,res), Xe 135, "Sm" group, Nonsaturating Fission Products, D_2O vs. Geometric Buckling: 20.000 mwd/t Burnup

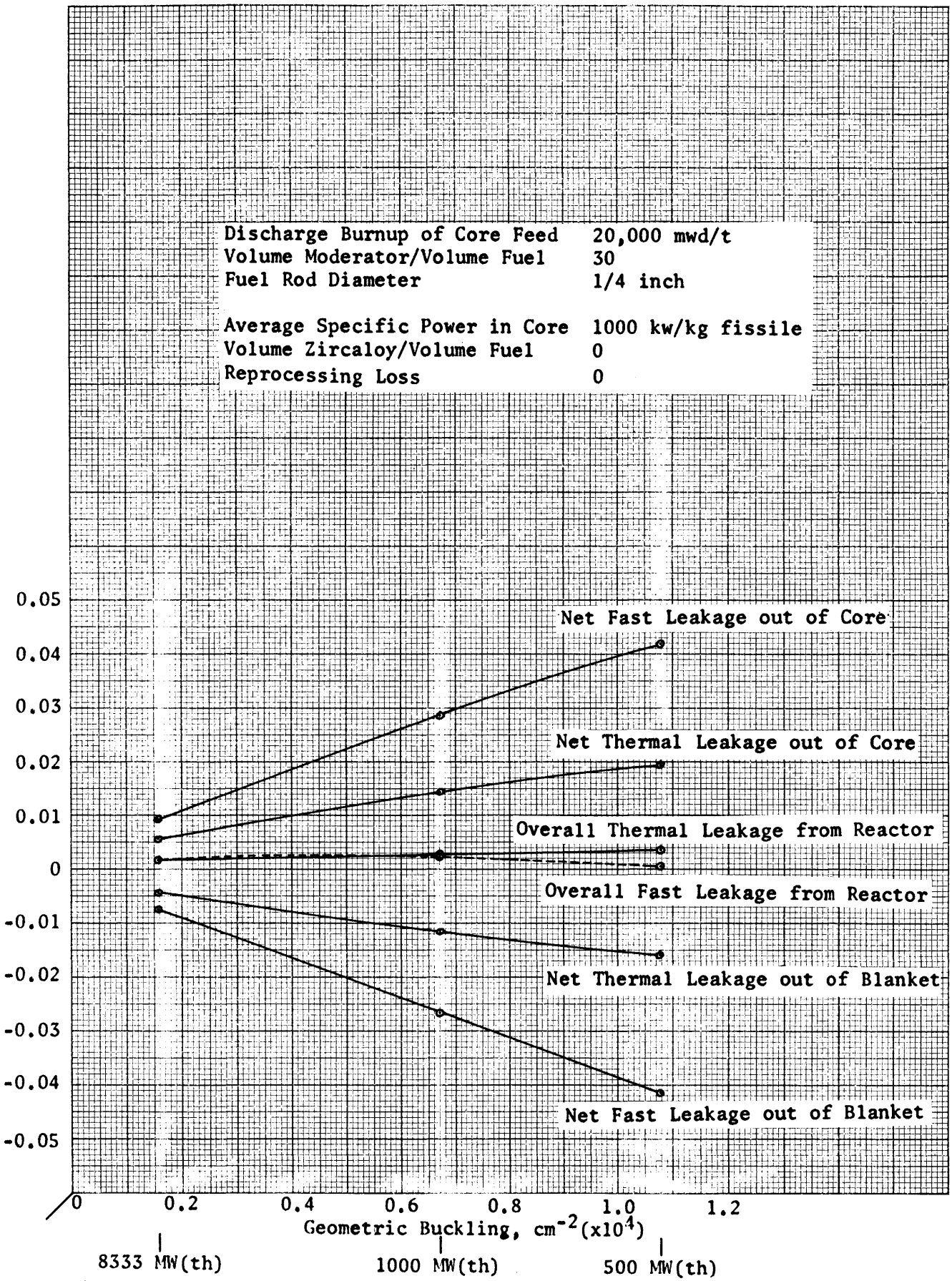

Figure 6.35: Fast and Thermal Leakages vs. Geometric Buckling: 20,000 mwd/t Burnup

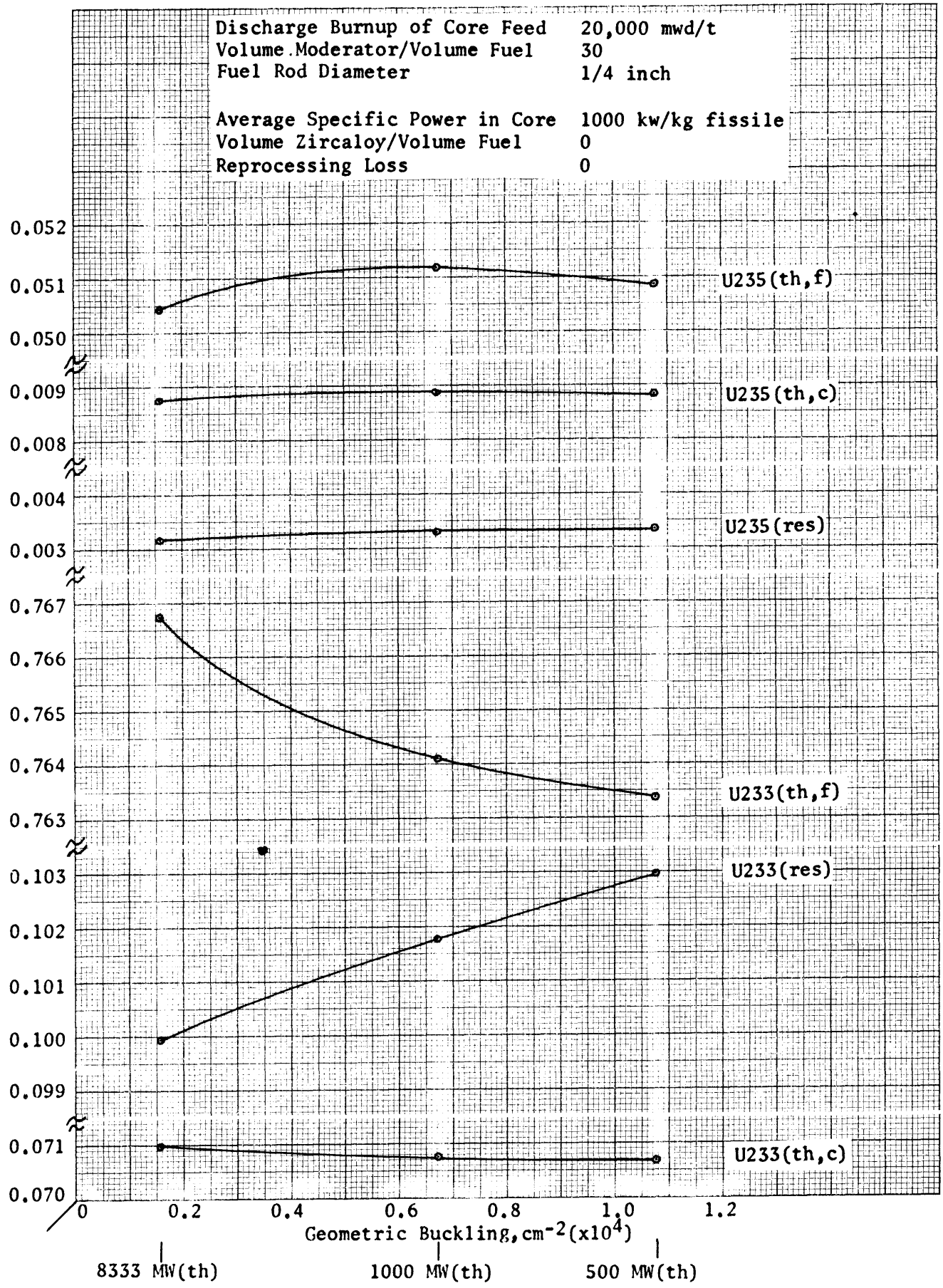

Figure 6.36: Absorptions by Fissile Nuclides vs. Geometric Buckling: 20,000 mwd/t Burnup

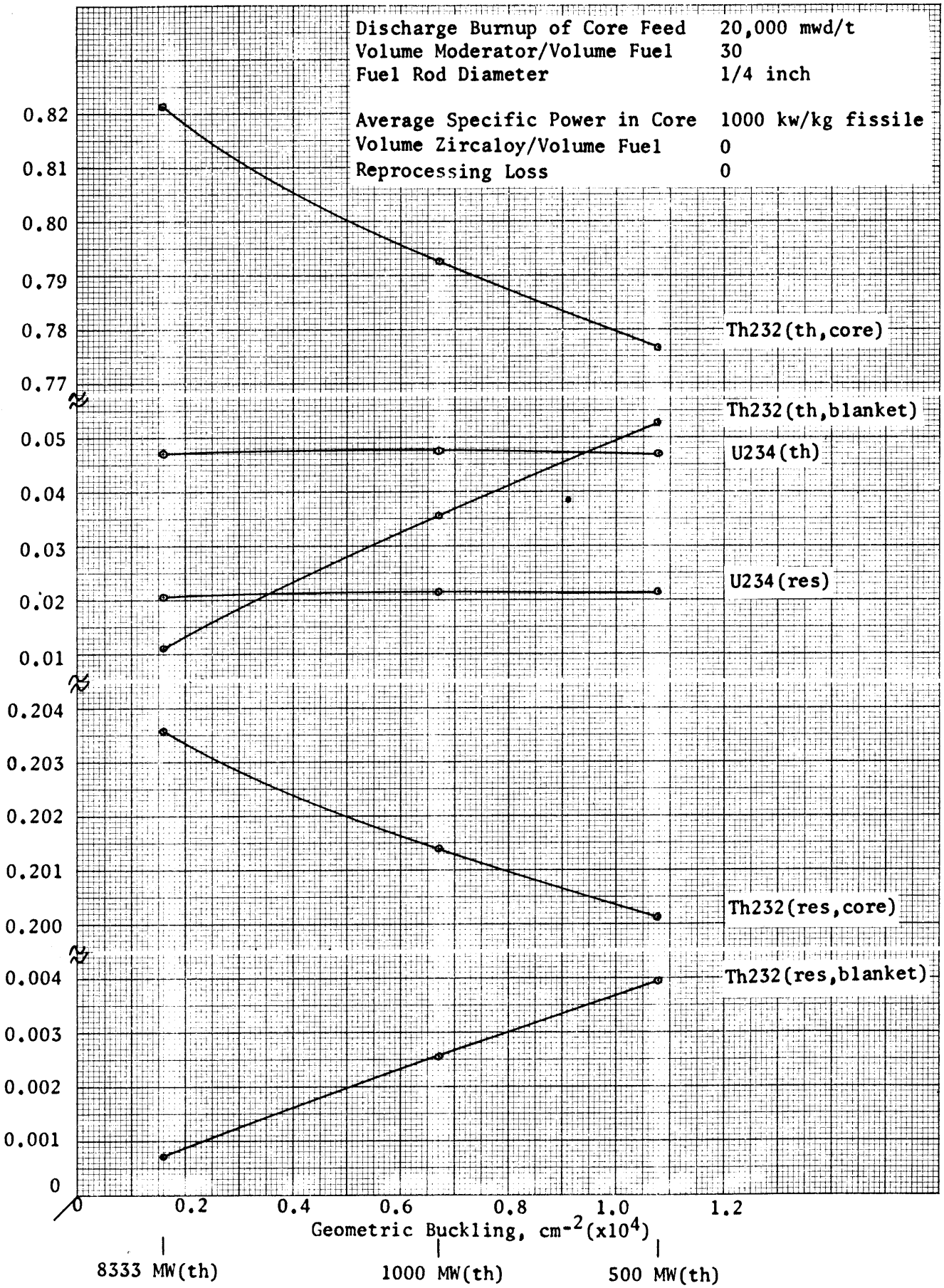

Figure 6.37: Absorptions by Fertile Nuclides vs. Geometric Buckling: 20,000 mwd/t Burnup

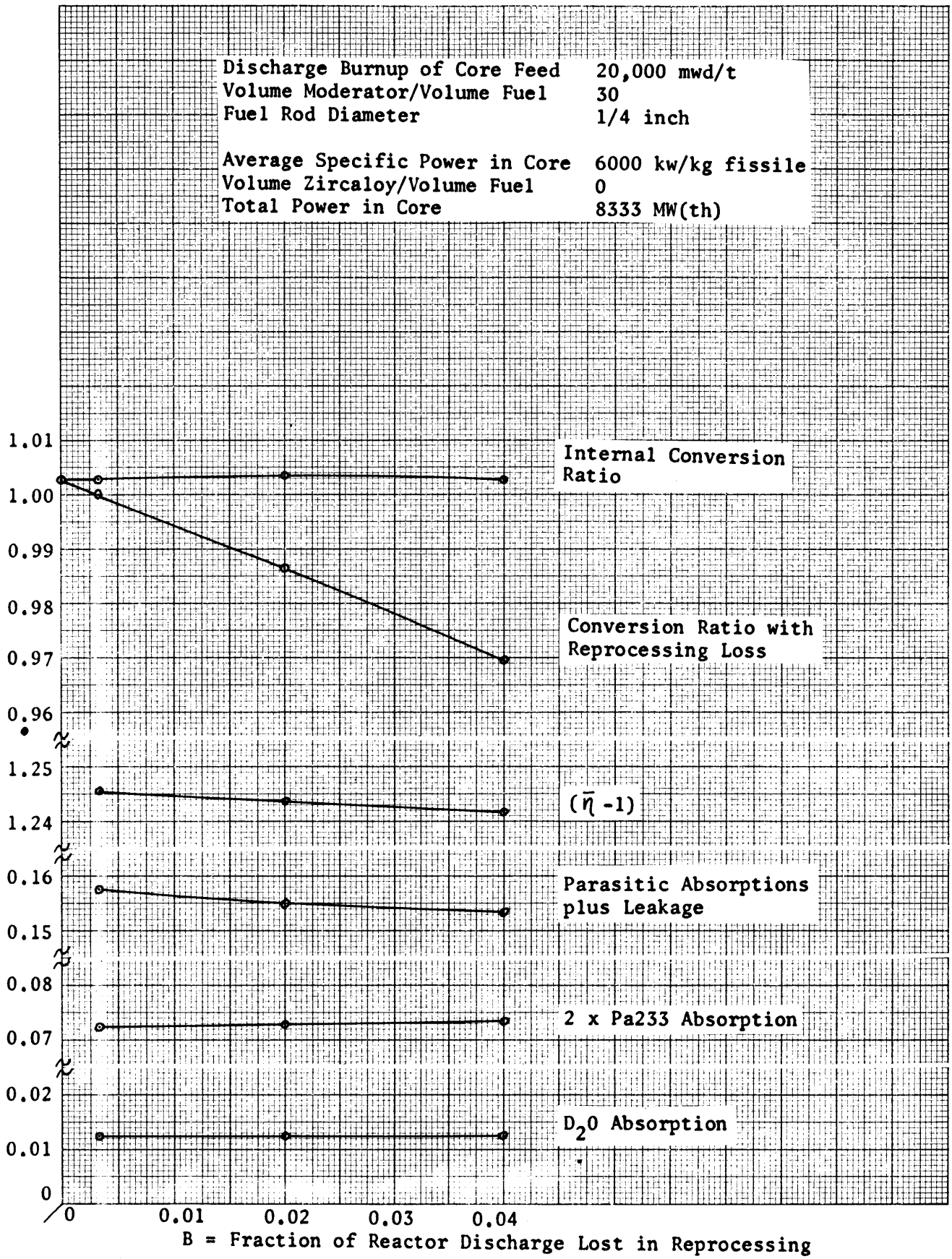

Figure 6.38: Conversion Ratio and its Components vs. Reprocessing Loss: 20,000 mwd/t Burnup

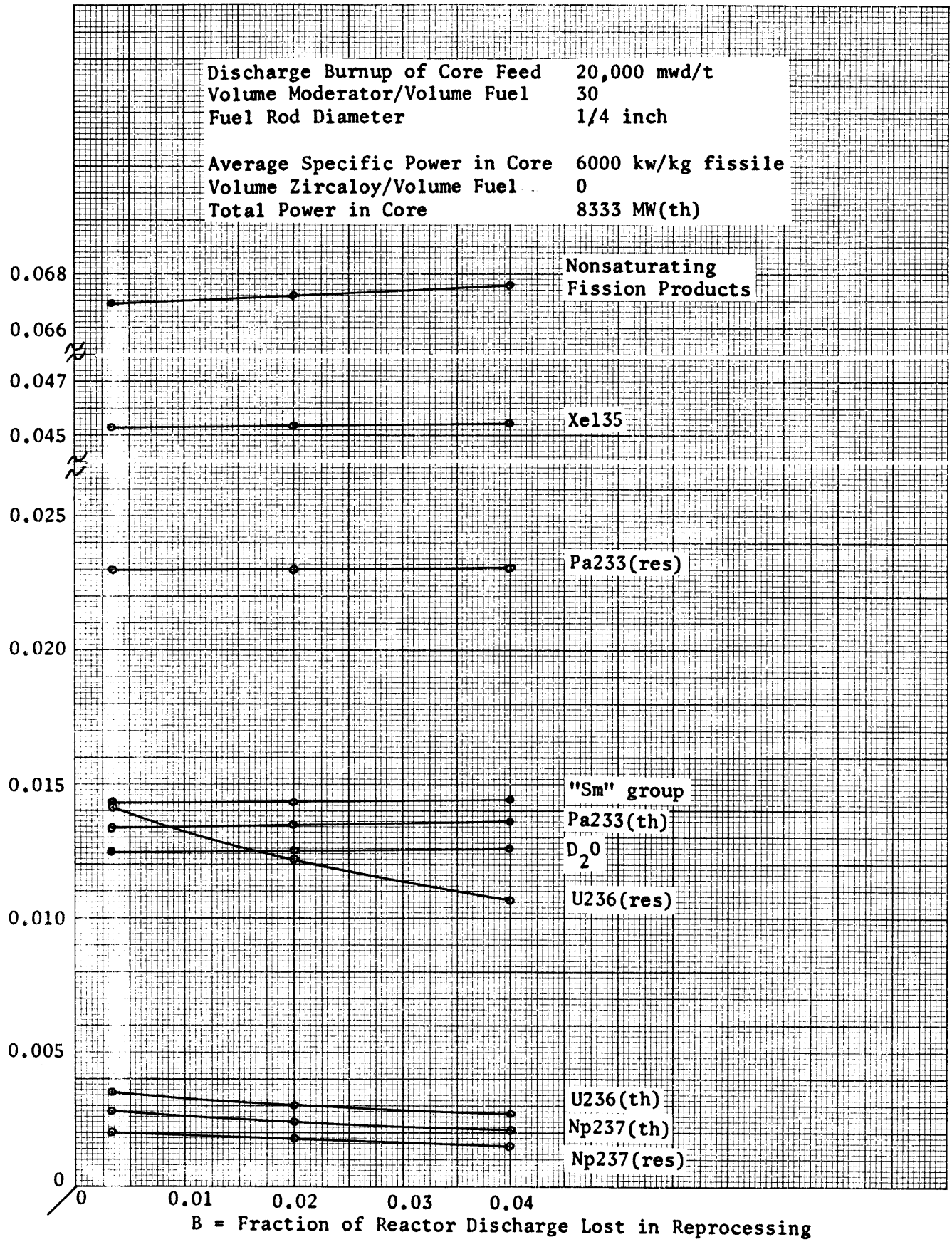

Figure 6.39: Absorptions by Pa233(th,res), U236(th,res), Np237(th,res), Xe135, "Sm" group, Nonsaturating Fission Products, D_2O vs. Reprocessing Loss: 20,000 mwd/t Burnup

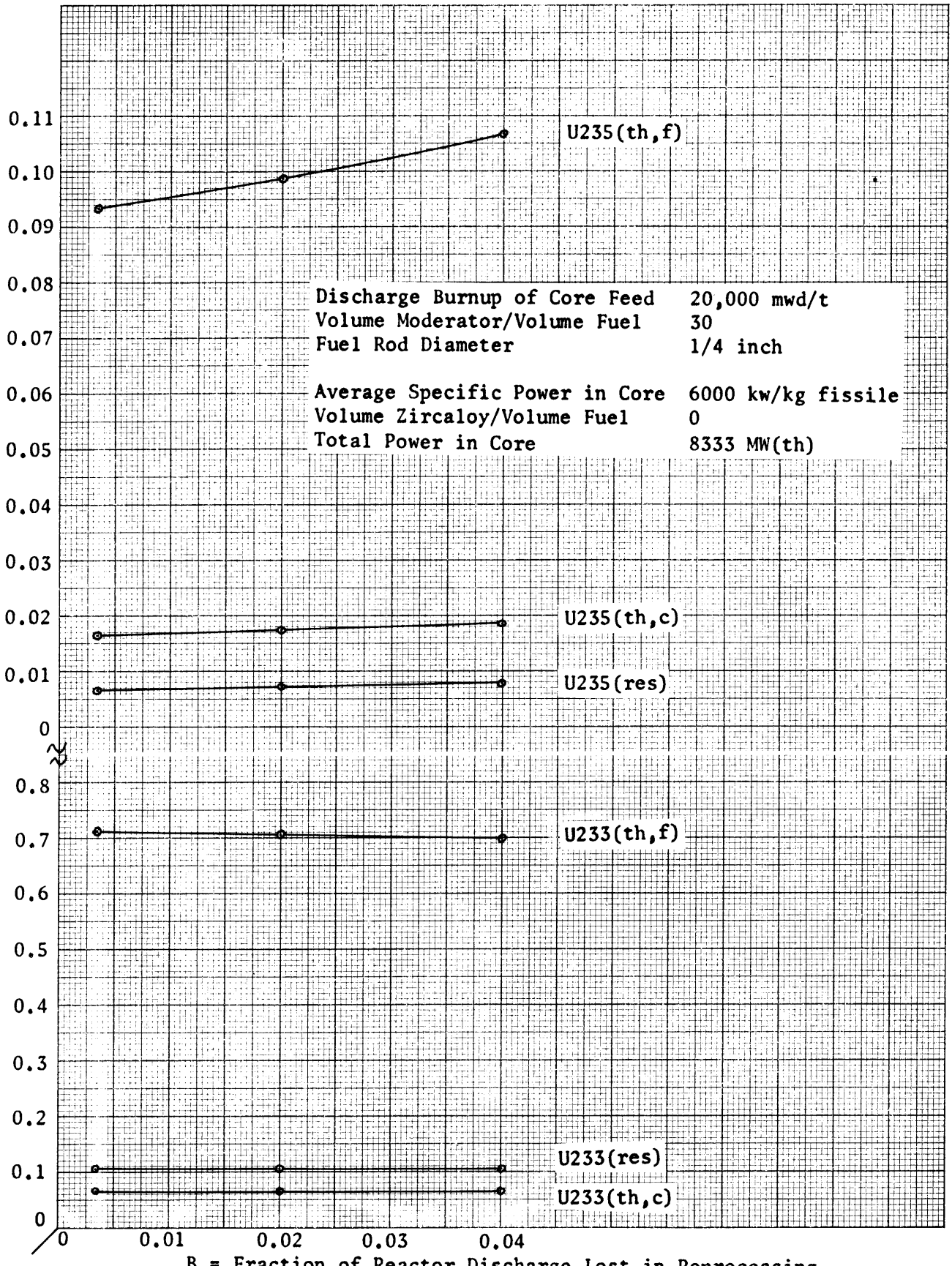

Figure 6.40: Absorptions by Fissile Nuclides vs. Reprocessing Loss: 20,000 mwd/t Burnup

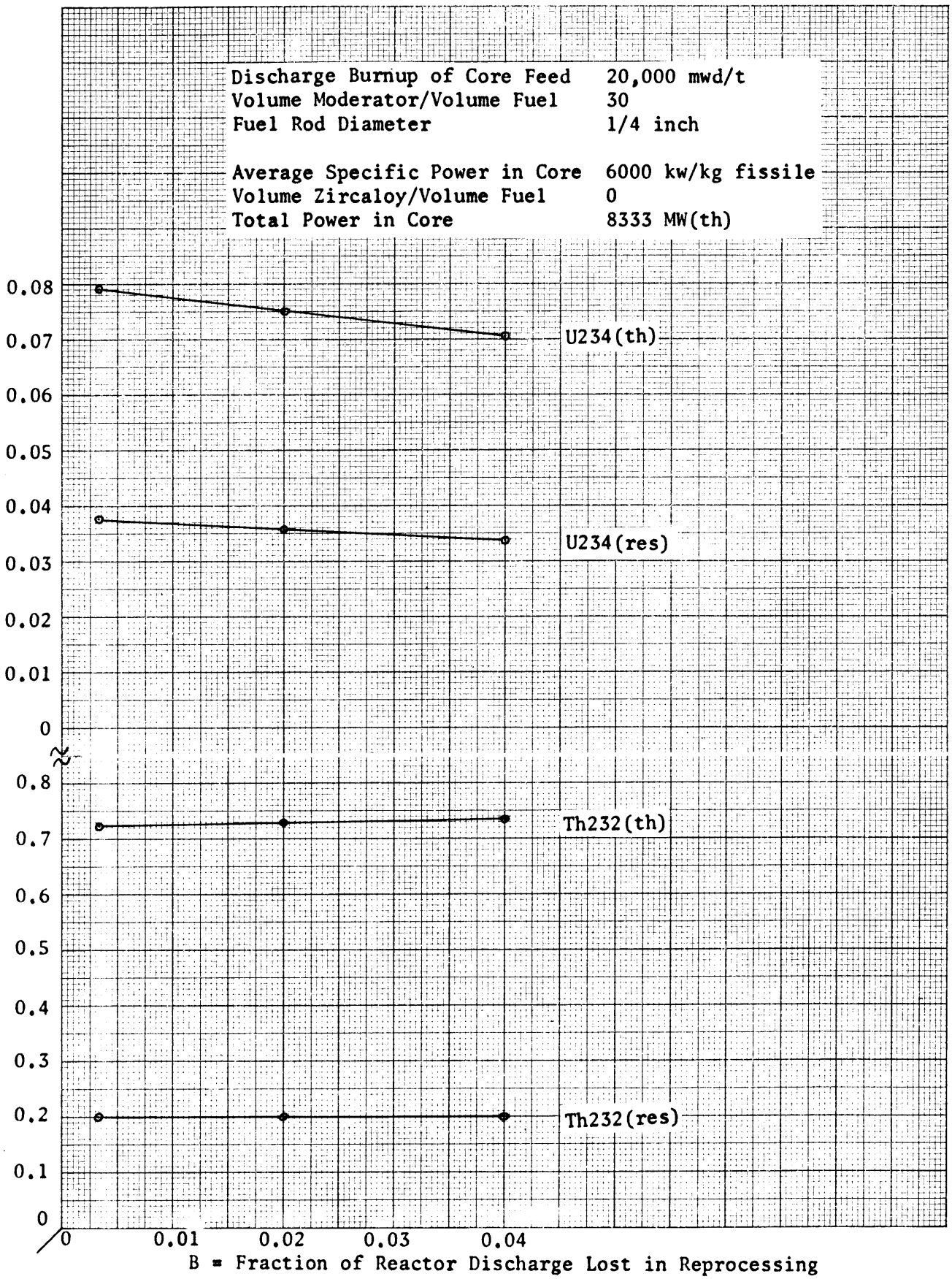

Figure 6.41: Absorptions by Fertile Nuclides vs. Reprocessing Loss: 20,000 mwd/t Burnup

CHAPTER VII

COMBINED EFFECT OF PRIMARY AND SECONDARY VARIABLES ON CONVERSION RATIO

A. Introduction

Chapter VI has described the effect of changes in each of the four secondary variables by itself on conversion ratio. Chapter VII considers the effect of changing all four secondary variables together on conversion ratio and develops approximate procedures for using the results of Chapters V and VI to estimate the conversion ratio for any combination of primary and secondary variables. First, a More Refined Approximate (MRA) procedure is described in section VIIB and is illustrated by an example problem. Second, a Less Refined Approximate (LRA) procedure is described in section VIIC. Finally, in section VIID, the conversion ratio is calculated for a reactor generally similar to one studied by the Oak Ridge National Laboratory (R1), to provide a comparison among results of estimates by the MRA and LRA procedures, an exact calculation by the computer code described in chapter IV, and Oak Ridge's calculated conversion ratio.

B. More Refined Approximate (MRA) procedure for estimating conversion ratios

1. Introduction

In chapter VI we have calculated the effect on the conversion ratio of changing individual secondary variables with the primary variables set at the values listed in the first column of numbers on the next page. In the present section VIIB, we will describe and illustrate with an example problem the More Refined Approximate (MRA) procedure for estimating the

effect on the conversion ratio of changing two or more of the secondary variables together starting from values of the primary variables possibly different from those employed in chapter VI. In the example to be given in this section the primary variables have the values listed in the second column of numbers below:

	Values of primary variables	
	Chapter VI	This section
Burnup, mwd/t	10,000, 20,000 or 30,000	20,000
Vol. moderator/vol. fuel	30	20
Fuel diameter, inches	1/4	1

In the example to be given in this section the secondary variables are to be changed from the values used in chapter V, which are in the first column of numbers below. These variables are to be changed one at a time in the order given to the values listed in the second column of numbers below:

	Secondary variables changed	
	from Chapter V	to This section
Average specific power, kw/kg fissile	1000	3000
Zircaloy absorption ratio	0	0.05
Reprocessing loss	0	0.02
Total power, MW(th)	8333	Anything over 500 MW(th)

The values of the secondary variables in the second column of numbers are typical of the CANDU reactor (A2,H2,S3).

2. Average specific power

The effect on the conversion ratio of changing the average specific power in the core is estimated first. This reduces to the task of estimating the effect of changing the average specific power on the following neutron balance items: $(\bar{\eta}-1)$; the parasitic absorptions by U236, Np237 and the nonsaturating fission products; the flux dependent items Xe135 absorption, 2 x Pa233 absorption and overall fast and thermal leakages from the reactor. The results of section VIC show that the absorptions by D_2O and the "Sm" group do not change significantly with increasing average specific power. The changes in absorptions by the fissile nuclides are reflected in the changes in $(\bar{\eta}-1)$. The changes in absorptions by the fertile nuclides are reflected in the changes in the conversion ratio itself.

The values of the neutron balance items for the initial values of the primary and secondary variables for the example problem are taken from table 5.1 and are listed in the first column of table 7.1. These neutron balance items may be lumped into three groups according to the

manner in which their values change with changing average specific power:

Group 1 includes those neutron balance items which do not change significantly with average specific power. Inspection of table 6.1 shows that absorptions by D_2O, the "Sm" group and zircaloy are of this character. Hence, these may be assumed to have the same value at all average specific powers as found in table 5.1 for an average specific power of 1000 kw/kg fissile, a burnup of 20,000 mwd/t, a moderator ratio of 20 and a fuel rod diameter of one inch.

Group 2 includes those neutron balance items whose rate of change with average specific power shows no discontinuity when U235 feed is started when the conversion ratio drops below unity. Inspection of table 6.1 shows that overall fast and thermal leakage from the reactor and absorptions by Xe135 are of this character. We assume that the change in these items with change in average specific power from 1000 kw/kg fissile found in table 6.1 for a burnup of 20,000 mwd/t, a moderator ratio of 30 and a fuel rod diameter of 1/4 inch may be applied to the value of these items at an average specific power of 1000 kw/kg fissile, a burnup of 20,000 mwd/t, a moderator ratio of 20 and a fuel rod diameter of 1 inch given in table 5.1. Figure 7.1 is a plot of the change in these items from their values at 1000 kw/kg fissile, taken from table 6.1.

Group 3 includes those neutron balance items whose rate of change with average specific power changes discontinuously when U235 feed is started when the conversion ratio drops below unity. In section VIC it has been shown that these items consist of $(\bar{\eta}-1)$; 2 x Pa233 absorptions; and absorptions by U236, Np237 and nonsaturating fission products considered together. On physical grounds, it is clear that the behavior of these

neutron balance items should change discontinuously when U235 feed is started. The solid lines of figure 7.2 show how these three items change with average specific power for the cases considered in table 6.1, with burnup of 20,000 mwd/t, moderator ratio of 30, and fuel rod diameter of 1/4 inch. For this combination of primary variables, the conversion ratio passes through unity at an average specific power of 6250 kw/kg fissile; see point A of figure 7.3 and figure 7.2. The curves from the calculated results of chapter VI will be called the "master" curves . The problem now is to estimate how these curves versus conversion ratio would look for the case of present interest, with a burnup of 20,000 mwd/t, moderator ratio of 20 and fuel rod diameter of 1 inch. For the case of present interest, the values of these items at an average specific power of 1000 kw/kg fissile are known from table 5.1, and have been plotted at point B on each of the curves.

It is assumed that each curve for the case of present interest will have the same shape as the corresponding master curve of figure 7.2, but that it will be displaced horizontally and vertically to meet the following conditions:

a. At an average specific power of 1000 kw/kg fissile, each curve should pass through point B at the correct initial value obtained from table 5.1.

b. Each curve should have its discontinuity in slope at the same average specific power.

c. At the average specific power at which the discontinuity in slope occurs, the conversion ratio calculated from these curves and the items of groups 1 and 2 should equal unity.

Determination of the average specific power to which the slope dis-

continuity in these curves should be moved requires a trial-and-error procedure, whose solution is illustrated in the second column of table 7.1 and the dashed curves of figure 7.2. Here it is seen that the assumption that the slope discontinuity should be moved to an average specific power of 5150 kw/kg fissile at points A' of figure 7.2 is consistent with a conversion ratio of 1.0000 at this average specific power, calculated in the second column of table 7.1.

After the proper location of the dashed curves has been found by the foregoing procedure, their contribution to the conversion ratio may be combined with group 2 items read from figure 7.1 and with group 1 items given in table 7.1 to give a curve of conversion ratio versus average specific power illustrated by the dashed line of figure 7.3. The "master curve" plotted from table 6.1 from which it was derived is given as the solid line of this figure. Point B is the conversion ratio for an average specific power of 1000 kw/kg fissile given in table 6.1. Points A and A' show the discontinuities in slope occurring at a conversion ratio of unity.

The required conversion ratio at an average specific power of 3000 kw/kg fissile may be read from the dashed curve of figure 7.3, or calculated with greater precision from the individual curves of figures 7.1 and 7.2 as illustrated in the third column of table 7.1. This shows that the required conversion ratio is 1.0375. The values of the individual items in the third column are used as the starting point for estimating the effect on the conversion ratio of increasing the zircaloy absorption ratio.

3. Absorption in zircaloy/absorption in a fissile nucleus

The effect on the conversion ratio of changing the zircaloy absorption

ratio is estimated next. The results of section VIB summarized in table 6.1 show that the only items in the neutron balance which change significantly with zircaloy absorption ratio are $(\bar{\eta} - 1)$ and parasitic absorptions by U236, Np237 and nonsaturating fission products. Items which do not change significantly with zircaloy absorption ratio are overall fast and thermal leakages from the reactor and absorptions by Xe135, the "Sm" group, Pa233 and D_2O. These are held constant at the values listed in the last column of table 7.1 and are listed in the first column of table 7.2.

The procedure for estimating the changes with increasing zircaloy absorption ratio of $(\bar{\eta} - 1)$ and absorptions by U236, Np237 and nonsaturating fission products is similar to that just described for increasing average specific power for the neutron balance items in group 3. The procedure for the zircaloy absorption ratio changes is illustrated in figure 7.4, where the nomenclature is similar to figures 7.1 and 7.2. The shapes of the master curves for these two items from the 20,000 mwd/t burnup case studied in section VIB are transferred in a trial and error procedure to the initial values listed in the first column of table 7.2 and plotted as points B in figure 7.4 until the zircaloy absorption ratio is found at which the conversion ratio equals 1.0. This value of the zircaloy absorption ratio turns out to be 0.027 as is shown if figure 7.4 on the curves of $(\bar{\eta} - 1)$ and absorptions by U236, Np237 and nonsaturating fission products. The values of the neutron balance items at this value of the zircaloy absorption ratio are listed in the second column of table 7.2. The resulting conversion ratio curve is shown at the top of figure 7.4.

The values of the neutron balance items and the conversion ratio for

a zircaloy absorption ratio of 0.05 are taken from the dashed curves in figure 7.4 and are listed in the last column of table 7.2. The value of the conversion ratio is about 0.965.

4. Reprocessing loss

The effect on the conversion ratio of increasing the reprocessing loss is estimated next. The effect of the reprocessing loss on the conversion ratio may be evaluated exactly from data given in tables 5.3 and 6.5 so long as the conversion ratio with reprocessing loss is above unity. In such cases, the reprocessing loss merely reduces the net surplus of fissile material produced by the reactor plus reprocessing plant without changing the material quantities entering or leaving the reactor. The effect of the reprocessing loss is illustrated on figure 7.5, which also gives the notation to be used in deriving the equation for the change it causes in the conversion ratio.

The internal conversion ratio CR_o of the reactor itself is defined in this thesis by

$$CR_o = \frac{Q_{13} - S_{13} + Q_{25}}{S_{23} + S_{25}} \qquad (7D1)$$

where

Q_{13} = rate of production of Pa233 by absorption of neutrons in Th232

S_{13} = rate of consumption of Pa233 by neutron absorption

Q_{25} = rate of production of U235 by absorption of neutrons in U234

S_{23} = rate of consumption of U233 by neutron absorption

S_{25} = rate of consumption of U235 by neutron absorption

Thus, $Q_{13} - S_{13}$ is the rate at which Th232 is converted eventually into U233 through the formation of Pa233 and its subsequent decay to U233.

The overall conversion ratio, taking into account the reprocessing loss representing B fraction of the reactor output, is defined in this thesis by

$$CR = \frac{Q_{13} - S_{13} + Q_{25}}{S_{23} + S_{25} + B\cdot(O_{13} + O_{23} + O_{25})} \qquad (7D2)$$

where

O_{13} = output flow rate of Pa233 from the reactor

O_{23} = the output flow rate of U233

O_{25} = output flow rate of U235

This differs from the internal conversion ratio by addition to the consumption rate term in the denominator the reprocessing loss of U233, U235 and Pa233 (which would decay to U233 if not lost). The numerator of (7D2) may be expressed in terms of the internal conversion ratio by (7D1):

$$CR = \frac{CR_o}{1 + B\cdot(O_{13} + O_{23} + O_{25})/(S_{23} + S_{25})} \qquad (7D3)$$

or, more concisely, by

$$CR = \frac{CR_o}{1 + B\cdot(O_R/S_R)} \qquad (7D4)$$

(O_R/S_R) is the ratio of the output rate of atoms of Pa233, U233 and U235, to the consumption rate of fissile atoms U233 and U235 in the reactor.

The ratio (O_R/S_R) has been given for each of the 56 cases studied in tables 5.3 and 6.3. These ratios may be used to calculate exactly the effect of the reprocessing loss on the conversion ratio, as long as the conversion ratio with reprocessing loss remains above unity, so that the flow sheet of figure 7.5 applies. When the reprocessing loss is great enough to cause the conversion ratio with reprocessing loss to drop below unity, the flowsheet is changed with addition of U235 makeup. In such a case, the values of CR_o and (O_R/S_R) in equation (7D4) will no longer have exactly the same values as calculated for cases with the conversion ratio with reprocessing loss greater than unity. The change in CR_o and (O_R/S_R) caused by an increase in B is not great, however, and the values given in tables 5.1, 5.3, 6.1 and 6.3 may be used to estimate the effect of reprocessing loss on the conversion ratio without significant error, so long as B is small.

So the estimation of the effect of the reprocessing loss on the conversion ratio for the example problem of this section reduces to the problem of estimating the value of O_R/S_R for the reactor with an average specific power of 3000 kw/kg fissile and a zircaloy absorption ratio of 0.05. The value of O_R/S_R for the example problem at the initial values of the primary and secondary variables is listed in table 5.3 and has a value of 0.632. Now the perturbations in O_R/S_R due to the increases in average specific power from 1000 kw/kg fissile to 3000 kw/kg fissile and zircaloy absorption ratio from zero to 0.05 must be estimated. These perturbations are assumed to be the same as for the 20,000 mwd/t cases studied in chapter VI in which the moderator ratio is 30 and the fuel rod diameter is 1/4 inch. Figure 7.6 shows the perturbations in O_R/S_R from its value at an average specific power of 1000 kw/kg fissile and a zircaloy absorption ratio of zero for the 20,000 mwd/t cases from

chapter VI as functions of both the average specific power and the zircaloy absorption ratio. An increase in the average specific power from 1000 to 3000 kw/kg fissile increases O_R/S_R by 0.094. Table 7.2 shows that in the example problem, the internal conversion ratio equals unity at a zircaloy absorption ratio of 0.027. Figure 7.4 shows that in the 20,000 mwd/t cases from chapter VI, from which the lower curve in figure 7.6 was derived, the conversion ratio equals unity at a zircaloy absorption ratio of 0.083. If the lower curve in figure 7.6 is shifted horizontally to the left by an amount (0.056) sufficient to place at a zircaloy absorption ratio of 0.027 the point in the curve at which the slopes become discontinuous, it is seen that the increase in O_R/S_R in the example problem for an increase in the zircaloy absorption ratio from zero to 0.05 is 0.062 - 0.030 = 0.032. We then have for the example problem at an average specific power of 3000 kw/kg fissile and a zircaloy absorption ratio of 0.05,

$$\frac{O_R}{S_R} = (0.632 + 0.094 + 0.032) = 0.758 \qquad (7D5)$$

Upon substituting into equation (7D4) the values of $CR_o = 0.965$ from table 7.2, $O_R/S_R = 0.758$ from equation (7D5) and B = 0.02, the following expression results:

$$CR = \frac{0.965}{1 + 0.02 \times 0.758} = 0.951 \qquad (7D6)$$

The conversion ratio with reprocessing loss for the example problem is therefore about 0.95.

5. Total power in the core

The results of section VIB show that as long as there is a blanket of fixed thickness surrounding the core to stop most of the neutrons leaking out of the core, the conversion ratio does not vary significantly with decreasing total power. Therefore the conversion ratio which results from increasing the other three secondary variables will be valid for any total thermal power greater than 500 MW(th).

6. Combined effect of changed variables

Figure 7.7 summarizes the conversion ratio results of increasing the average specific power, the zircaloy absorption ratio and the reprocessing loss for the example problem. The conversion ratio which results from the MRA procedure described in this section VIIB is about 0.95.

This value may be considered representative of the CANDU reactor if operated at feed enrichment which leads to a reactivity-limited burnup of 20,000 mwd/t.

7. Cases in which the value of average specific power for which the conversion ratio equals 1.0 cannot be found.

It has been shown in section VIIB that in order to make good estimates of the effect on the conversion ratio of increasing the average specific power and the zircaloy absorption ratio, one must be able to determine the values of these two secondary variables for which the conversion ratio equals unity for the particular case under consideration. This section suggests an approximate procedure when the conditions at which the conversion ratio equals unity are not known.

In the example problem of section VIIB, the values of these two

secondary variables for which the conversion ratio equals unity was determined by the shapes of the curves near a conversion ratio of unity of $(\bar{\eta}-1)$, absorptions by U236, Np237 and nonsaturating fission products considered together, and 2 x Pa233 absorptions versus the particular secondary variable for the 20,000 mwd/t burnup cases from chapter VI. Examination of the curves of conversion ratio versus zircaloy absorption ratio for burnups of 10,000, 20,000 and 30,000 mwd/t in figure 6.9 and the curves of conversion ratio versus average specific power for the three burnups in figure 6.26 shows that the only case in which it would be difficult to estimate the value of a secondary variable at which the conversion ratio equals unity would be the case in which the secondary variable is the average specific power and the burnup is 10,000 mwd/t. This is because for a burnup of 10,000 mwd/t, it would be difficult to estimate the shapes of the curves near a conversion ratio of unity of $(\bar{\eta}-1)$, absorption by U236, Np237 and nonsaturating fission products considered together, and 2 x Pa233 absorptions versus average specific power, as is shown in figures 6.27 and 6.28. In the case of an example problem using a burnup of 10,000 mwd/t, one can assume that the curves of $(\bar{\eta}-1)$, absorptions by U236, Np237 and nonsaturating fission products considered together, and 2 x Pa233 absorptions versus average specific power

a. pass through the correct values from table 5.1 at 1000 kw/kg fissile for the example problem, and

b. are parallel to the curves of the same items which can be derived from table 6.1.

C. Less Refined Approximate (LRA) procedure for estimating conversion ratios

The Less Refined Approximate (LRA) procedure for estimating the effect of the average specific power in the core and the zircaloy absorption ratio on the conversion ratio using the results of this thesis will now be described. Refer to the curves of conversion ratio versus average specific power in figure 7.3 and conversion ratio versus zircaloy absorption ratio in figure 7.4. It is seen that in both figures, the curves for the estimated cases (dashed curves) and for the "master" cases (solid curves) from chapter VI are similar in shape. In order to make an estimate of the change in the conversion ratio with increasing average specific power and zircaloy absorption ratio which is more rapid but less accurate than the estimate arrived it in section VIIB, one can merely sketch in the curves of conversion ratio versus average specific power and zircaloy absorption ratio, using as a guide the "master" conversion ratio curves for the particular burnup and secondary variable from chapter VI. An example problem in which the LRA procedure is used is given in section VIID3.

D. Comparison of results from the MRA and LRA procedures with a computer calculation and a conversion ratio calculated by the Oak Ridge National Laboratory.

1. Introduction

Although no other study has been made of the conversion ratios in thorium - U233 fueled heavy water moderated and cooled reactors for the same combinations of values of design variables as were used in this work, it is possible and instructive to compare conversion ratios obtained from this work with the conversion ratio of an

economically optimized design of a reactor of this general type calculated by the Oak Ridge National Laboratory (R1). Case G4 of the Oak Ridge study, with which the results of this thesis are to be compared, was similar to the reactors studied in this work in many respects, but had fuel elements consisting of three concentric tubes. Table 7.3 compares the general characteristics of the reactor considered in this study and the reactor of Oak Ridge Case G4 as well as the calculation methods used for each.

A principal effect on the conversion ratio of the fuel element design is through the effective resonance integral of ThO_2. The mean chord length, 1, of a lump of fuel is calculated by equation (7D7):

$$1 = \frac{4(\text{lump volume})}{(\text{lump surface})} \qquad (7D7)$$

For a cylindrical rod, 1 equals the rod diameter. For the three concentric tubes used in the Oak Ridge study, 1, calculated by equation (7D7), is about 1/2 inch. However, the "effective" lump surface for the three concentric tubes is less than the "actual" lump surface because the inner surfaces are shielded from resonance neutrons by the outer surfaces. This would make the mean chord length or fuel rod equivalent diameter greater than 1/2 inch. For purposes of the estimates of the conversion ratio to be made in this section VIID, it is assumed that a fuel rod diameter of one inch is equivalent to the three concentric tubes of the Oak Ridge case G4.

Table 7.4 lists values of the three primary variables and four secondary variables which have been selected as most nearly descriptive of Oak Ridge case G4. The reactor represented by these variables will

be referred to as Reactor "A." In the Oak Ridge case, no blanket was used, and neutron leakage from the core led to a loss of neutrons amounting to 0.025 times the consumption of neutrons by fissile material. Because of the two-foot thick blankets used in the present work, neutron leakage losses are much smaller than in the Oak Ridge case. This difference between the Oak Ridge reactor and the present one will be taken into account by estimating the neutron leakage loss for a blanketed 8333 MW(th) reactor and then estimating the effect of increasing the leakage loss to 0.025 on the conversion ratio of the blanketed reactor.

Since the Oak Ridge calculation did not consider reprocessing losses, these are taken to be zero for Reactor "A" and the conversion ratio used is the internal conversion ratio.

In section D.2, following, the conversion ratio of this Reactor "A" is estimated by the MRA procedure of section VIIB; in section D.3, the LRA procedure is used; and in section D.4 the conversion ratio is calculated in detail by the present computer code. Section D.5 compares these calculations of the conversion ratio with a value of 0.8255 obtained by Oak Ridge (R1).

2. More Refined Approximate procedure

The first step is to estimate, with the aid of table 5.1, the values of the various neutron balance items for the values of the primary variables listed in table 7.4 and the following secondary variables:

Average specific power in core, kw/kg fissile	1000
Zircaloy absorption ratio	0.0
Initial overall fast and thermal leakages from reactor (Because of the absence of a blanket in ORNL case G4, this variable replaces total thermal power in the core or B_g^2 as the related secondary variable.)	0.0034
Reprocessing loss	0.0

These values of average specific power in the core, zircaloy absorption ratio and reprocessing loss are the same as those used in table 5.1. The value of initial overall fast and thermal leakages from the reactor of 0.0034 is a result of the interpolation and extrapolation in table 5.1 and is consistent with a total power in the core of 8333 MW(th). The estimates of the values of the neutron balance items are listed in the first column of table 7.5. This table is of the same form as table 7.1. The values of the group 1 and group 2 neutron balance items are estimated by interpolation and extrapolation in table 5.1. The values of the group 3

neutron balance items are estimated with the use of figures 5.15, 5.16, 5.17 and 5.18 which were constructed from the data in table 5.1. The initial values of the group 3 neutron balance items are plotted as point B in figure 7.8, which is of the same form as figure 7.2.

The next step is to estimate the effect on the conversion ratio of changing the secondary variables from the above values to those of table 7.4. When estimating the effect on the conversion ratio of the average specific power, "master" curves of the group 3 neutron balance items for the appropriate burnup (28,800 mwd/t, in this case) should be used, as was done in section VIIB2. Likewise when estimating the effect on the conversion ratio of the zircaloy absorption ratio, "master" curves of $(\bar{\eta}-1)$ and U236, Np237 and nonsaturating fission products considered together for the appropriate burnup should be used, as was done in section VIIB3. However, no "master" curves for 28,800 mwd/t were calculated in chapter VI. The "master" curves from chapter VI for the closest burnup, i. e., 30,000 mwd/t, do not extend below a conversion ratio of 1.0, while the Oak Ridge case G4, with which the results of this section are to be compared, has a conversion ratio of 0.84. Since the objective of this section is to compare an estimated conversion ratio using the results of this thesis with the calculated conversion ratio of Oak Ridge case G4, the "master" curves for the 20,000 mwd/t results from chapter VI will be used. These curves extend below a conversion ratio of 1.0 and, therefore, require less of an extrapolation than do the 30,000 mwd/t curves to reach the neighborhood of the Oak Ridge case G4 conversion ratio of 0.84.

One then proceeds with the estimate of the effect on the conversion ratio of changing the average specific power and the zircaloy absorption

ratio using the MRA procedure as discussed in section VIIB. Table 7.6 and figure 7.9 summarize the effect on the conversion ratio and its components of the zircaloy absorption ratio. These are of the same form as table 7.2 and figure 7.4, respectively. The steps in the MRA estimating procedure are summarized in figure 7.10. The MRA procedure gives a conversion ratio of 0.897. The increase in the overall fast and thermal leakages from the reactor from 0.0055 (table 7.6) to 0.025 decreases the conversion ratio further by 0.019 to a final estimate of 0.878 as compared to the Oak Ridge value of 0.84, also plotted in figure 7.10.

3. Less Refined Approximate (LRA) procedure

The conversion ratio of Reactor "A" is now estimated using the LRA procedure of section VIIC.

As in the case of the MRA procedure, the first step in the LRA procedure is to estimate the conversion ratio for the values of the primary variables listed in table 7.4 and the values of the secondary variables listed at the beginning of section VIID2, the previous section. This value is 1.0419 as listed in the first column of table 7.5. This value is plotted as the initial estimate in figure 7.11.

The next step is to estimate the effect on the conversion ratio of changing the average specific power and the zircaloy absorption ratio from the values listed at the beginning of the previous section to the values of table 7.4. It was stated in section VIIC that the "master" conversion ratio curves for the particular burnup (28,800 mwd/t, in this case) and secondary variable from chapter VI should be used as guides in this procedure. However for the reasons stated in section VIID2, the "master" curves for a burnup of 20,000 mwd/t are used.

The steps in estimating the effect on the conversion ratio of changing the secondary variables to the values listed in table 7.4 are illustrated in figure 7.11. Appropriate portions of the "master" conversion ratio curves for the 20,000 mwd/t burnup cases from chapter VI are shown as solid lines. The "master" curve of conversion ratio vs. average specific power is from figure 6.15 and the "master" curve of conversion ratio vs. zircaloy absorption ratio is from figure 6.1.

The "master" curve of conversion ratio vs. average specific power is used as a guide in this example problem by shifting it horizontally to the left and insuring that

(1) the point at which the slope is discontinuous remains on the ordinate of conversion ratio = 1.0, and

(2) the curve passes through the initial value of the conversion ratio of 1.0419.

The conversion ratio resulting from the increase in average specific power from 1000 to 2700 kw/kg fissile is 1.012.

Next the "master" curve of conversion ratio vs. zircaloy absorption ratio is used as a guide in this example problem by shifting it horizontally to the left and insuring that

(1) the point at which the slope is discontinuous remains on the ordinate of conversion ratio = 1.0, and

(2) the curve passes through the conversion ratio of 1.012

The conversion ratio resulting from the increase in zircaloy absorption ratio from 0.0 to 0.07 is 0.906.

Finally, the overall fast and thermal leakages from the reactor are increased from 0.0034 to 0.025. This decreases the conversion ratio further to a value of 0.884. This compares with the Oak Ridge value of 0.8255.

4. Calculation by computer code

Table 7.7 gives the detailed results of computer calculations of the conversion ratio for Reactor "A," which is characterized by values of the primary and secondary variables of Table 7.4, with one exception. The neutron leakage fraction of 0.025 is replaced as a secondary variable by a thermal power of 8333 mw, with a two-foot blanket, because the computer code is designed for such a reactor. The conversion ratio calculated for this blanketed reactor is 0.8662. The calculated fractional leakage of fast and thermal neutrons is 0.0064. It is then estimated that if the fractional leakage had been 0.025, as attributed to the Oak Ridge case, the conversion ratio for the unblanketed reactor would have been $0.8662 - (0.025 - 0.0064) = 0.8476$.

Return now to the fact that the "master" curves used in both the MRA and LRA procedures in section VIID are for a burnup of 20,000 mwd/t while the actual burnup is 28,800 mwd/t. Referring to figure 6.26, it is seen that the curve of conversion ratio vs. average specific power for the 30,000 mwd/t case decreases more rapidly than for the 20,000 mwd/t case. Likewise it is seen in figure 6.9 that the curve of conversion ratio vs. zircaloy absorption ratio for the 30,000 mwd/t case decreases more rapidly than for the 20,000 mwd/t case. Therefore, the final conversion ratios for Reactor "A" estimated by the MRA procedure and the LRA procedure should be lower than the values plotted in figures 7.10 and 7.11, respectively. This decrease can be conservatively estimated

by rounding the estimated conversion ratios to the next lower two decimal places.

5. Comparison of conversion ratio estimates

Conversion ratios calculated in these different ways for Reactor "A," which is similar to Oak Ridge case G4, are compared below with Oak Ridge's calculation:

More Refined Approximate procedure	Less Refined Approximate procedure	MIT Computer calculation	Oak Ridge calculation
0.87	0.88	0.8476	0.8225

The agreement between the MIT and Oak Ridge computer calculations is as good as might have been expected, in view of the uncertainty introduced in representing the three concentric tubes of the Oak Ridge design by a solid rod of one inch equivalent diameter. The agreement among the MRA and LRA procedures and the computer calculations is considered to be good enough to confirm the utility of these approximate procedures in estimating conversion ratios in heavy-water-moderated thorium-fueled reactors with combinations of the principal design variables different from those studies in this report.

Table 7.1: Conversion Ratio and Its Components for Various Average Specific Powers

Primary variables	
Burnup	20,000 mwd/t
Moderator/fuel volume ratio	20
Fuel rod diameter	1 inch
Secondary variables	
Zircaloy absorption ratio	0
Reprocessing loss	0
Total power	8333 MW(th)

	Initial values (Table 5.1)	Conversion ratio = 1.0	Final specific power
Avg. spec. power, kw/kg fissile	1000	5150*	3000
Neutron balance items			
Group 1			
D_2O absorption	0.012105	0.0121	0.0121
"Sm" group absorption	0.013655	0.0137	0.0137
Group 2			
Overall fast leakage	0.001762		
Overall thermal leakage	0.001472		
Xe135 absorption	0.035579		
Total	0.038813	0.0388	0.0388
Change in fast leakage	0.0000	0.0033**	0.0013**
Change in thermal leakage	0.0000	0.0021**	0.0013**
Change in Xe135 absorption	0.0000	0.0078**	0.0063**
Group 3			
$(\bar{\eta} - 1)$	1.252747	1.2397***	1.2464***
Absorptions by			
2 x Pa233	0.022590	0.0620***	0.0458***
{U236, Np237, Nonsat. fission products}	0.086234	0.0999***	0.0896***
Conversion ratio, $(\bar{\eta} - 1)$ minus other items	1.079350	1.0000	1.0375

*Found by trial as described in text
**From figure 7.1
***From figure 7.2

Table 7.2: Conversion Ratio and Its Components for Various Values of the Zircaloy Absorption Ratio

Primary variables	
Burnup	20,000 mwd/t
Volume of moderator/volume of fuel	20
Fuel rod diameter	1 inch
Secondary variables	
Average specific power	3000 kw/kg fissile
Reprocessing loss	0
Total power	8333 MW(th)

	Initial values (Table 7.1)	Conversion ratio = 1.0	Final zircaloy ratio
Zircaloy absorption ratio	0.0000	0.0270	0.0500
Items independent of zircaloy abs.			
D_2O absorption	0.0121	0.0121	0.0121
Leakage plus Xe135 absorption	0.0477	0.0477	0.0477
2 x Pa233 absorption	0.0458	0.0458	0.0458
"Sm" group absorption	0.0137	0.0137	0.0137
Items dependent on zircaloy abs.			
Absorptions by {U236, Np237, Nonsat. fission products}	0.0896	0.0956*	0.1000*
$(\bar{\eta} - 1)$	1.2464	1.2419*	1.2345*
Conversion ratio, $(\bar{\eta} - 1)$ minus other items	1.0375	1.0000*	0.9652*

*From figure 7.4

Table 7.3: Comparisons between some characteristics of the ThO_2-UO_2 fueled D_2O moderated power reactors presented in chapter VII of this work and in ORNL 3686 (case G4)

Item	Chapter VII, this work	ORNL 3686 (case G4)
Nuclear model	Diffusion theory; 1 fast group; 1 thermal group; 2 dimensions in cylindrical coordinates	Diffusion theory; 20 fast groups; 4 thermal groups; zero dimensions
Fueling method	Continuous steady state bidirectional with recycle	Simulated bidirectional with recycle
Fuel element	ThO_2-UO_2 in a 1 inch diameter cylindrical rod; zircaloy cladding. Vibratory compacted and swaged to 92% of theoretical density	ThO_2-UO_2 in 3 concentric tubes: 0.22" - 0.30" fuel thickness; 3.80" - 1.31" outside diameters; 0.25" thick zircaloy cladding; zircaloy pressure tube and liners. Vibratory compacted and swaged to 92% of theoretical density
Nuclear data	Reference (G1,G2,G3)	Same
H_2O in D_2O	0.25% by weight	Same
D_2O temperature	80°C	Same
Fuel temperature	1200°C	Unknown
Radial and axial blankets	2 feet thick	None

Table 7.4: Primary and Secondary Variables for Reactor "A" Assumed Equivalent to Oak Ridge Case G4

Primary variables	
Feed burnup, mwd/t	28,800
Volume moderator/volume fuel	16.6
Assumed fuel rod equivalent diameter, inch	1
Secondary variables	
Average specific power in core, kw/kg fissile	2700
Zircaloy absorption ratio	0.07
Overall fast and thermal leakages from reactor (Because of the absence of a blanket, this replaces total thermal power in the core or B_g^2 as the related secondary variable.)	0.025
Reprocessing loss	0.0

Table 7.5: Conversion Ratio and Its Components for Various Average Specific Powers for Reactor "A"

Primary variables	
Burnup	28,800 mwd/t
Volume of moderator/volume of fuel	16.6
Assumed fuel rod equivalent diameter	1 inch
Secondary variables	
Zircaloy absorption ratio	0
Reprocessing loss	0
Initial overall fast and thermal leakage from reactor	0.0034

	Initial values (Interpolation and extrapolation in Table 5.1)	Conversion ratio = 1.0	Final specific power
Avg. spec. power, kw/kg fissile	1000	3080*	2700
Neutron balance items			
Group 1			
D_2O absorption	0.0091	0.0091	0.0091
"Sm" group absorption	0.0132	0.0132	0.0132
Group 2			
Overall fast leakage	0.0022		
Overall thermal leakage	0.0012		
Xe135 absorption	0.0342		
Total	0.0376	0.0376	0.0376
Change in fast leakage	0.0000	0.0014**	0.0010**
Change in thermal leakage	0.0000	0.0013**	0.0011**
Change in Xe135 absorption	0.0000	0.0064**	0.0058**
Group 3			
$(\bar{\eta}-1)$	1.2429	1.2360***	1.2373***
Absorptions by 2 x Pa233	0.0246	0.0402***	0.0380***
{U236, Np237, Nonsat. fission products}	0.1165	0.1268***	0.1244***
Conversion ratio, $(\bar{\eta}-1)$ minus other items	1.0419	1.0000	1.0071

*Found by trial as described in text, section VII B2
**From figure 7.1
***From figure 7.8

Table 7.6: Conversion Ratio and Its Components for Various Values of the Zircaloy Absorption Ratio for Reactor "A"

Primary variables	
Burnup	28,800 mwd/t
Volume of moderator/volume of fuel	16.6
Assumed fuel rod equivalent diameter	1 inch
Secondary variables	
Average specific power	2700 kw/kg fissile
Reprocessing loss	0
Overall fast and thermal leakages from reactor	0.0055*

	Initial values (Table 7.5)	Conversion ratio = 1.0	Final zircaloy ratio
Zircaloy absorption ratio	0.0000	0.0045**	0.0700
Items independent of zircaloy abs.			
D_2O absorption	0.0091	0.0091	0.0091
Leakage plus Xe135 absorption	0.0455	0.0455	0.0455
2 x Pa233 absorption	0.0380	0.0380	0.0380
"Sm" group absorption	0.0132	0.0132	0.0132
Items dependent on zircaloy abs.			
Absorptions by {U236, Np237, Nonsat. fission products}	0.1244	0.1262***	0.1418***
$(\bar{\eta}-1)$	1.2373	1.2365***	1.2150***
Conversion ratio, $(\bar{\eta}-1)$ minus other items	1.0071	1.0000	0.8974

*From table 7.5
**Found by trial as described in text, section VIIB3
***From figure 7.9

Table 7.7: Results of Computer Calculation for Reactor "A" Assumed Equivalent to Oak Ridge Case G4

Burnup	28,800 Mwd/t
Vol.mod./vol.fuel	16.6
Rod dia.	1.0 inch
Avg.spec.power	2700 kw/kg
Abs.ratio, Zr/fuel	0.0706
Vol.ratio, Zr/fuel	0.70
Reprocessing loss	0.00
Total power	8333 Mw(th)

Neutron Balance

Prod. of fast neutrons		Cons. of thermal neutrons	
Res. fission of U233	0.380520	Overall therm. leakage	0.001406
Res. fission of U235	0.048108	Abs. by Th232, core	0.464877
Thermal fiss. of U233	1.337332	Th232, blanket	0.037569
Thermal fiss. of U235	0.427951	Pa233	0.005401
Total ($\bar{\eta}$)	2.193911	U233 fission	0.534292
Net fast leakage out of		U233 capture	0.049818
Core	0.045364	U234	0.050325
Blanket	-0.040399	U235 fission	0.176112
Neuts.reach.res.energy	2.188946	U235 capture	0.030938
Resonance absorptions		U236	0.004382
Th232, Core	0.280999	Np237	0.006153
Th232, Blanket	0.005755	Xe135	0.038410
Pa233	0.021404	"Sm" group	0.013516
U233	0.178241	Non.sat.f.p.'s	0.081845
U234	0.052720	D_2O	0.005013
U235	0.030600	Zircaloy	0.070565
U236	0.037722		
Np237	0.010154		
Net prod. of thermal neutrons	1.571351	Total consumption of thermal neutrons	1.570622

Conversion ratio 0.866169

Material Quantities

	Inventory		Flow Rate, kg/day	
	Mass, kg	Mass Fraction	Input	Output
Core Th232	142350	0.957867	276.40	268.96
Pa233	267.39	0.001799	0	0.4515
U233	2338.8	0.015738	5.2655	4.3815
U234	1137.8	0.007656	2.1795	2.1787
U235	746.49	0.005023	2.2956	0.9358
U236	1690.8	0.011377	3.2073	3.2040
Np237	80.26	0.000540	0	0.2628
Total	148611.54	1.000000	289.3479	280.3743
Blanket Th232	85094	--	24996	24995
Pa233	4.800	--	0	0.3106
U233	4.695	--	0	0.1205
U234	0.009	--	0	0.0004

Core radius 12.75 ft.
Core height 23.52 ft.

$S_R = 2.5933 \times 10^{25}$ fissile atoms/day

$O_R = 1.6011 \times 10^{25}$ fissile atoms/day

$O_R/S_R = 0.6174$

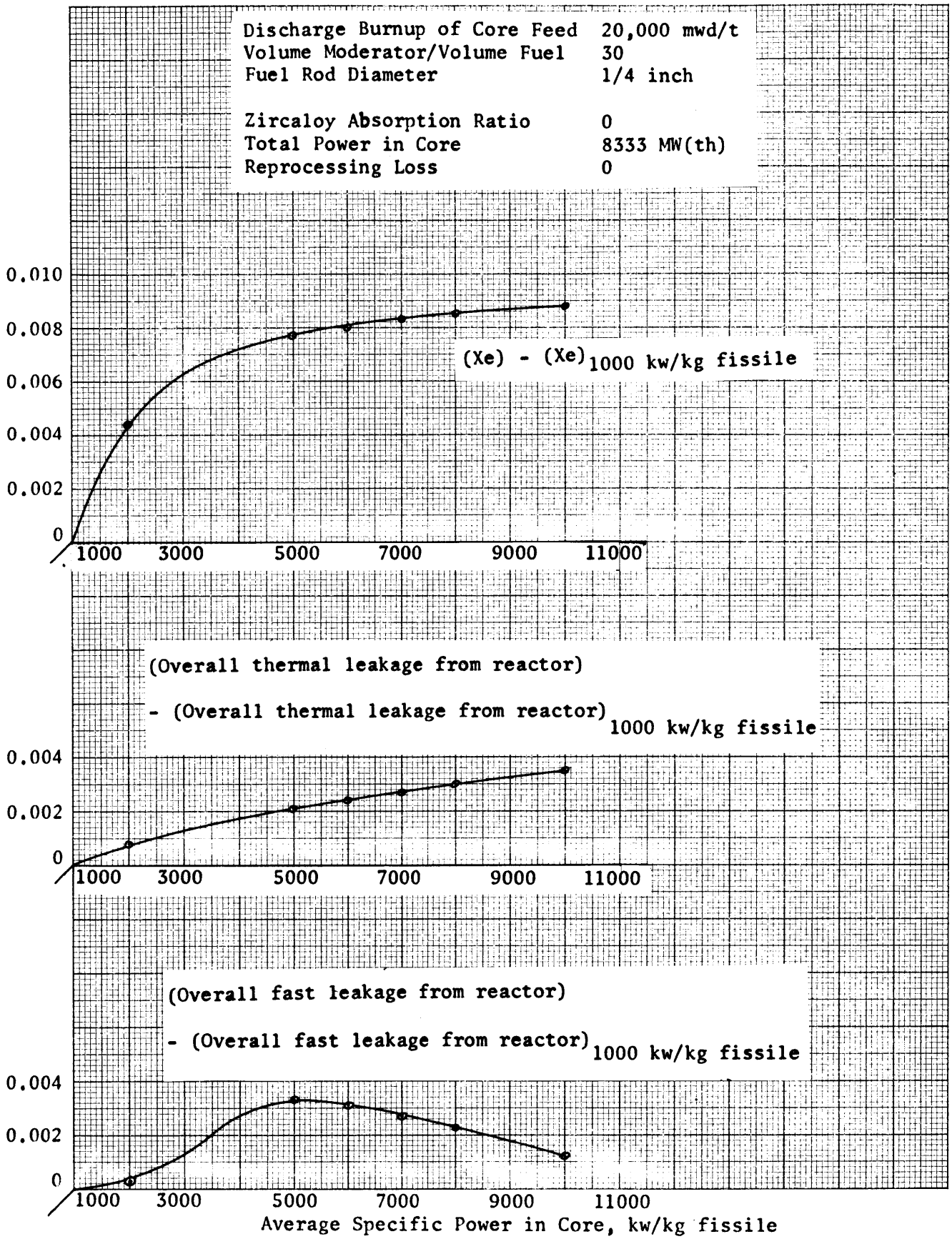

Figure 7.1: Change in Group 2 Neutron Balance Items with Average Specific Power in Core

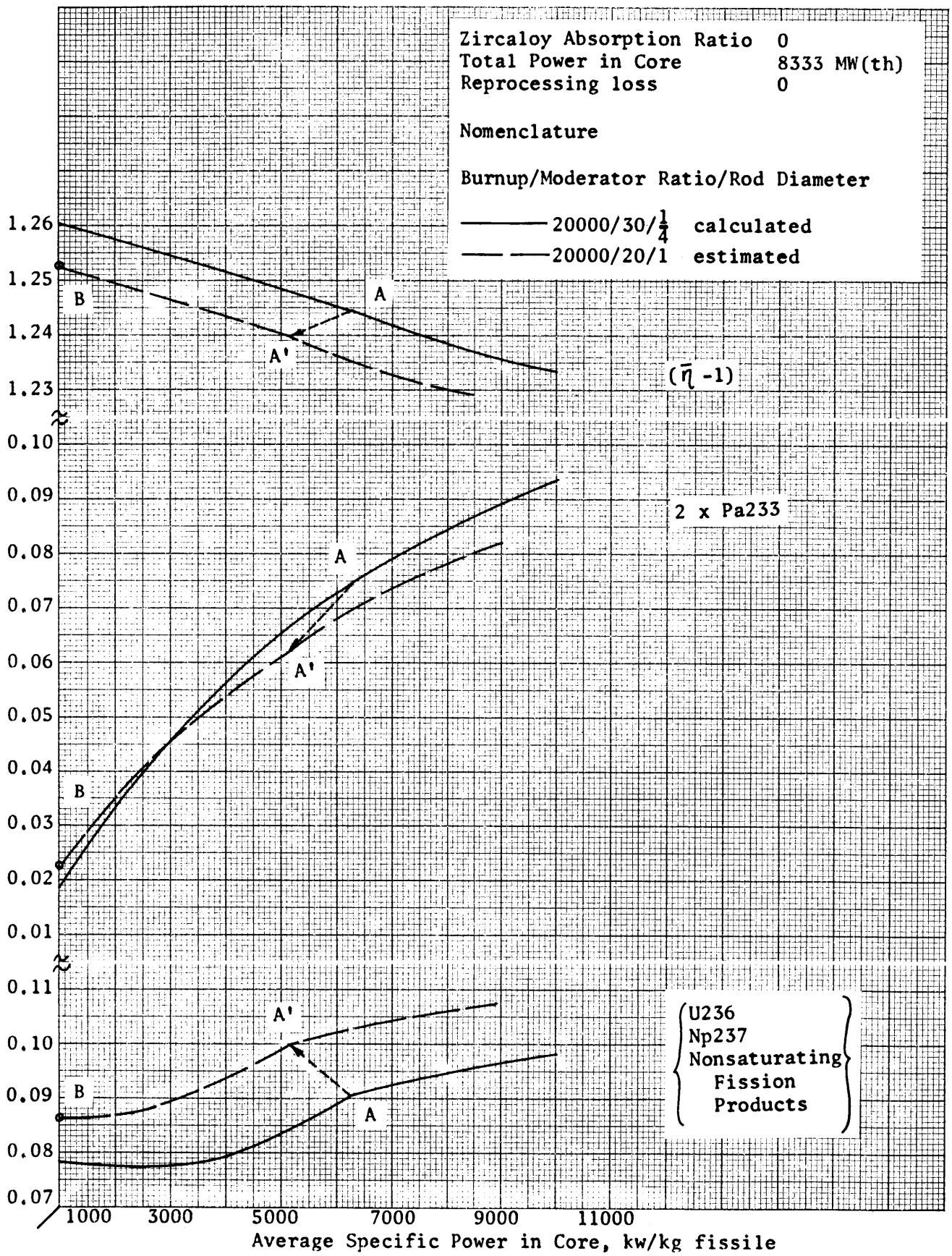

Figure 7.2: Change in Group 3 Neutron Balance Items with Average Specific Power in Core

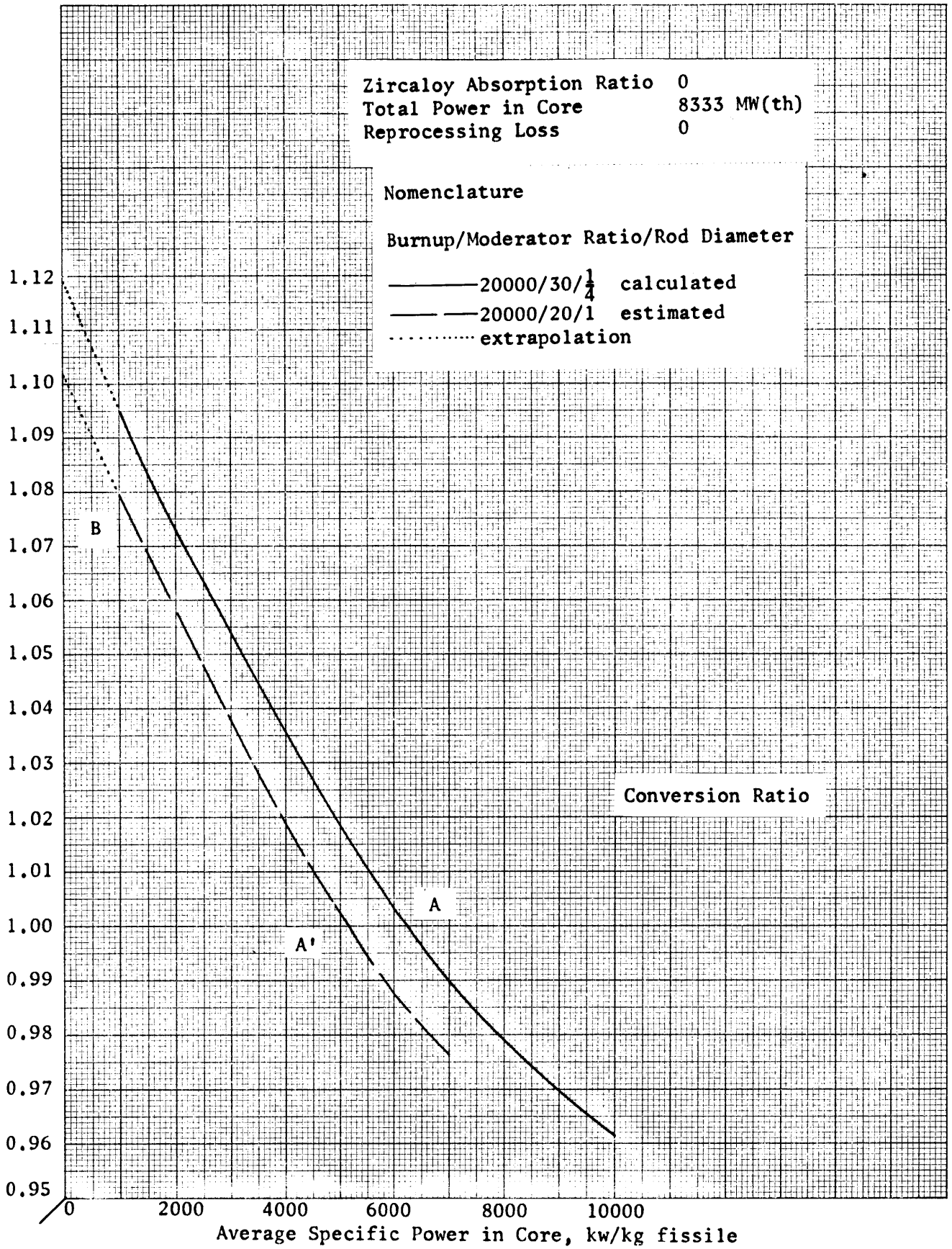

Figure 7.3: Effect of Average Specific Power in Core on Conversion Ratio

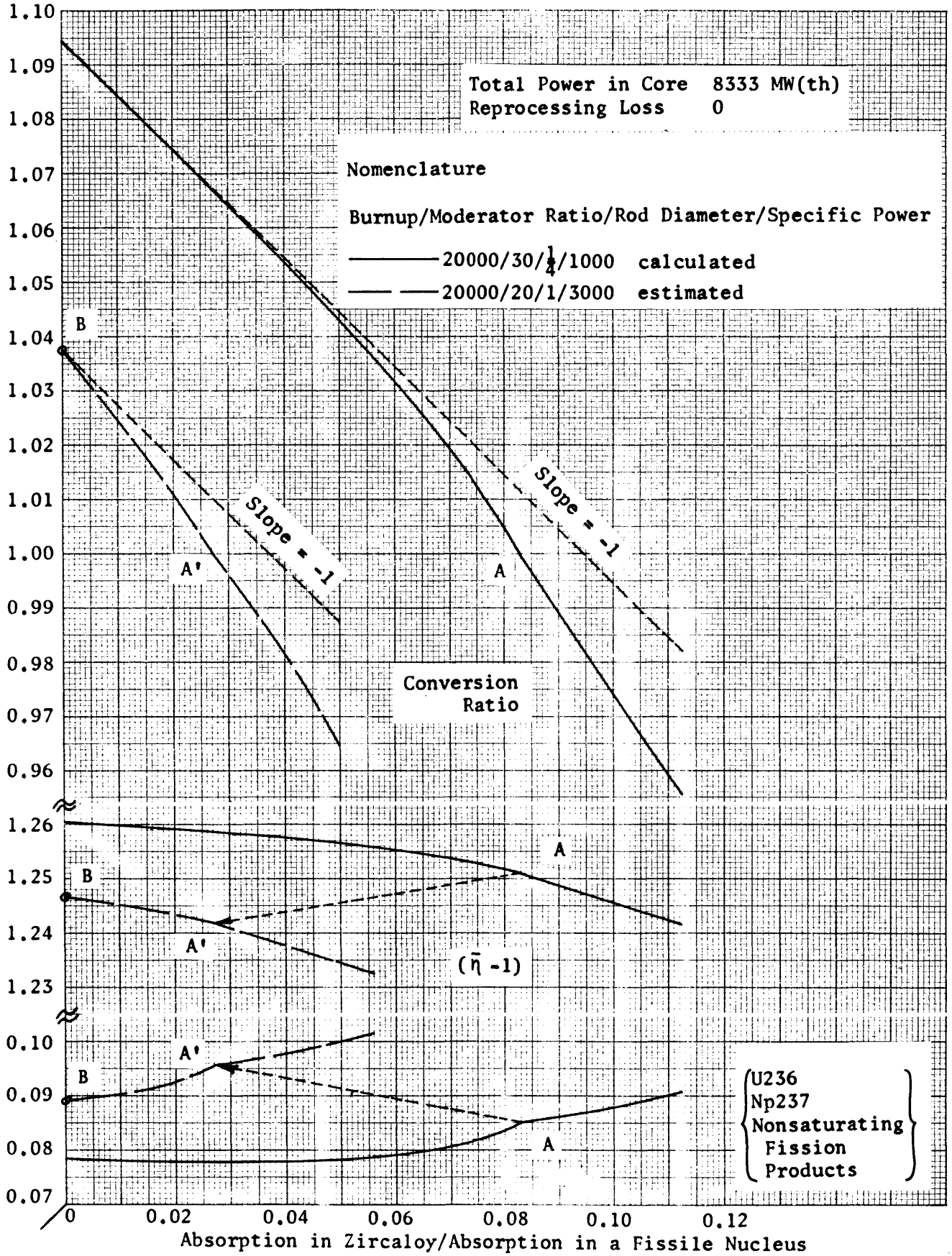

Figure 7.4: Effect of Zircaloy Absorption Ratio on Some Neutron Balance Items and the Conversion Ratio

(All rates refer to fissile material.)

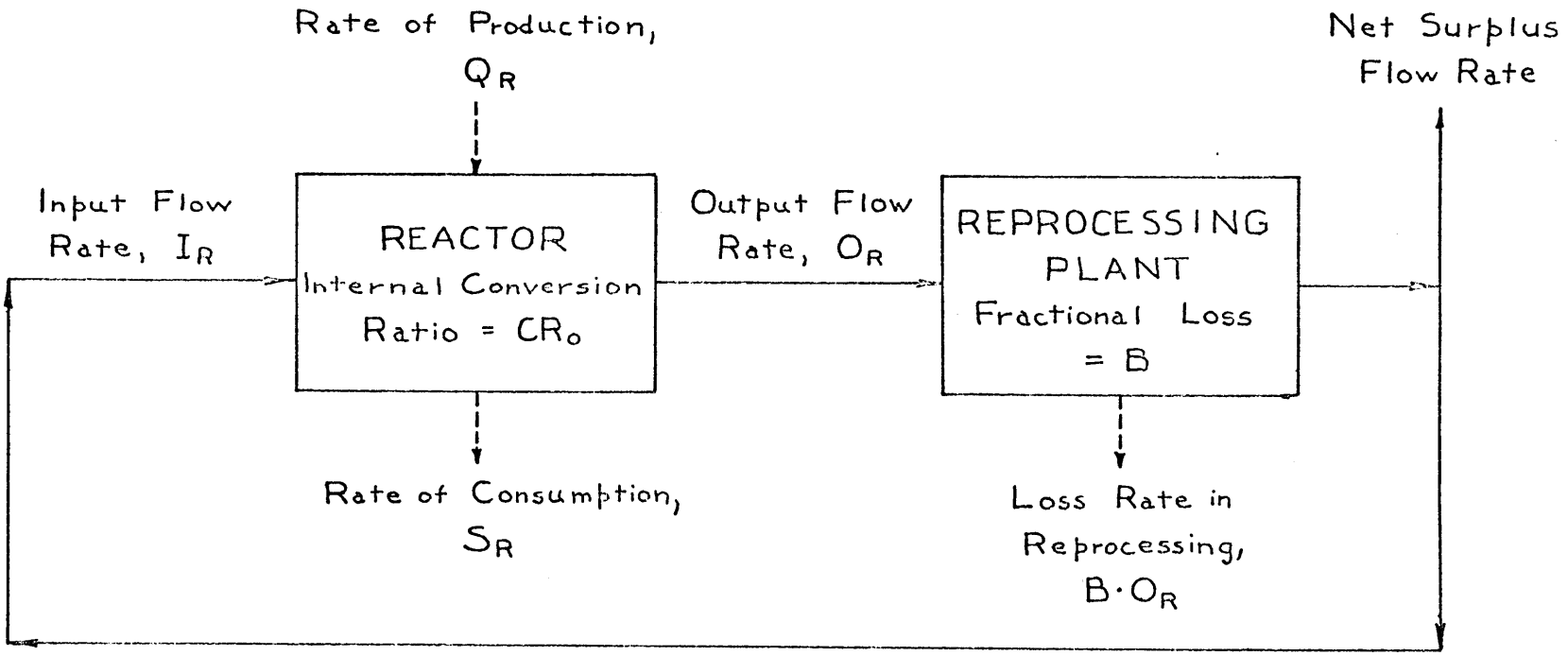

Figure 7.5: Effect of Reprocessing Loss on Conversion Ratio

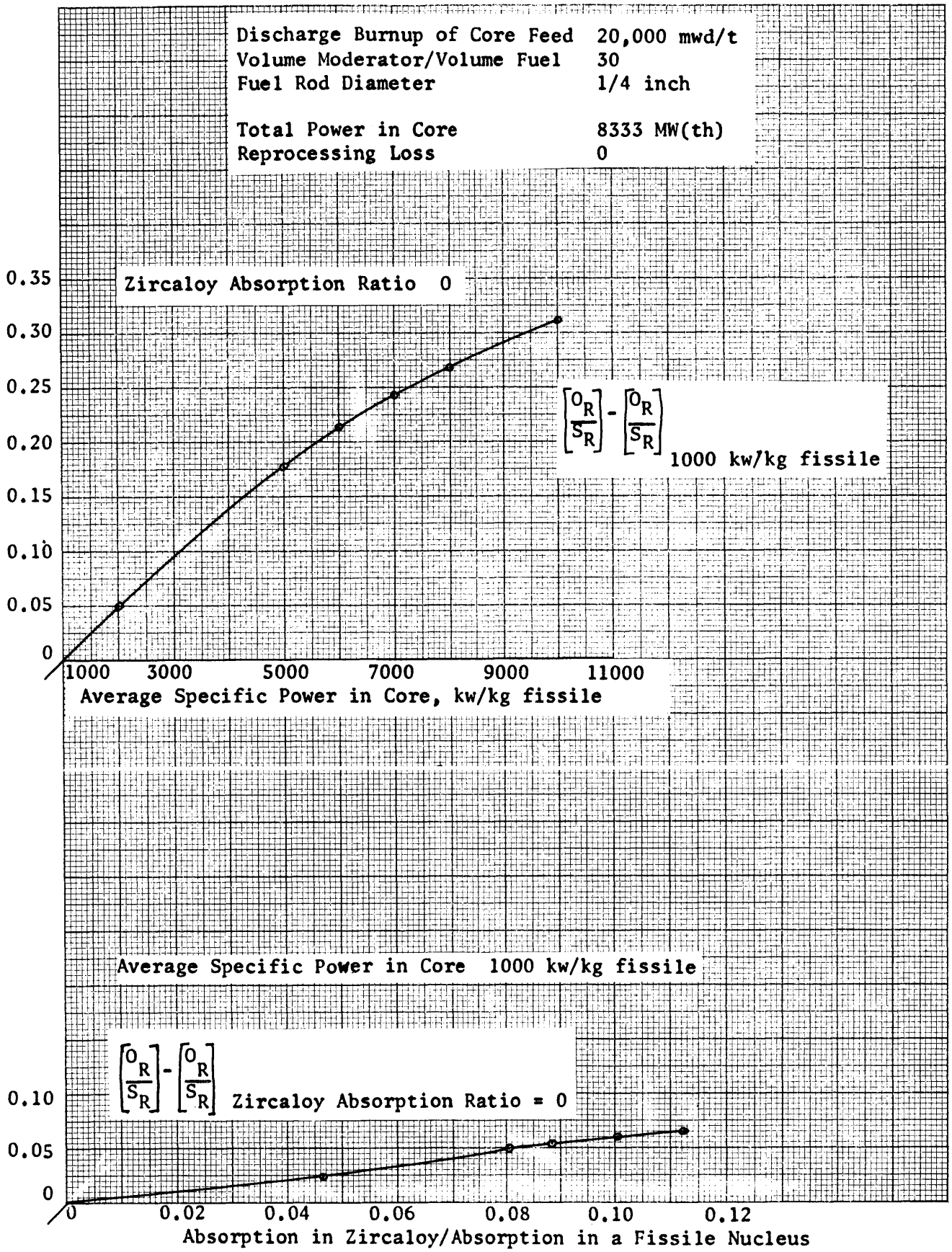

Figure 7.6: Perturbations in (O_R/S_R) vs. Average Specific Power in Core and Zircaloy Absorption Ratio for the 20,000 mwd/t Burnup Cases from Chapter VI

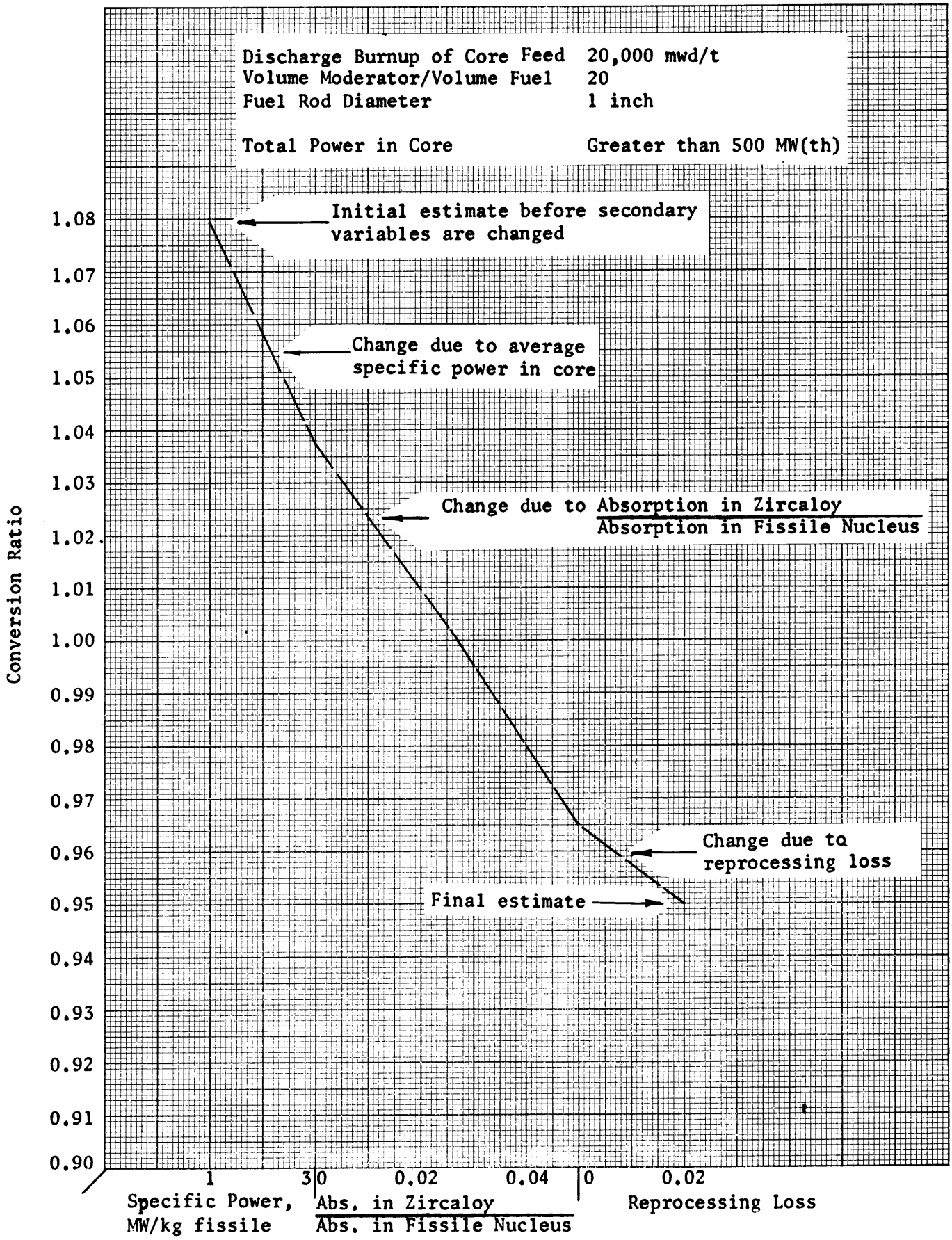

Figure 7.7 : Steps in Example of Estimate of Effect of Changing All Secondary Variables on Conversion Ratio

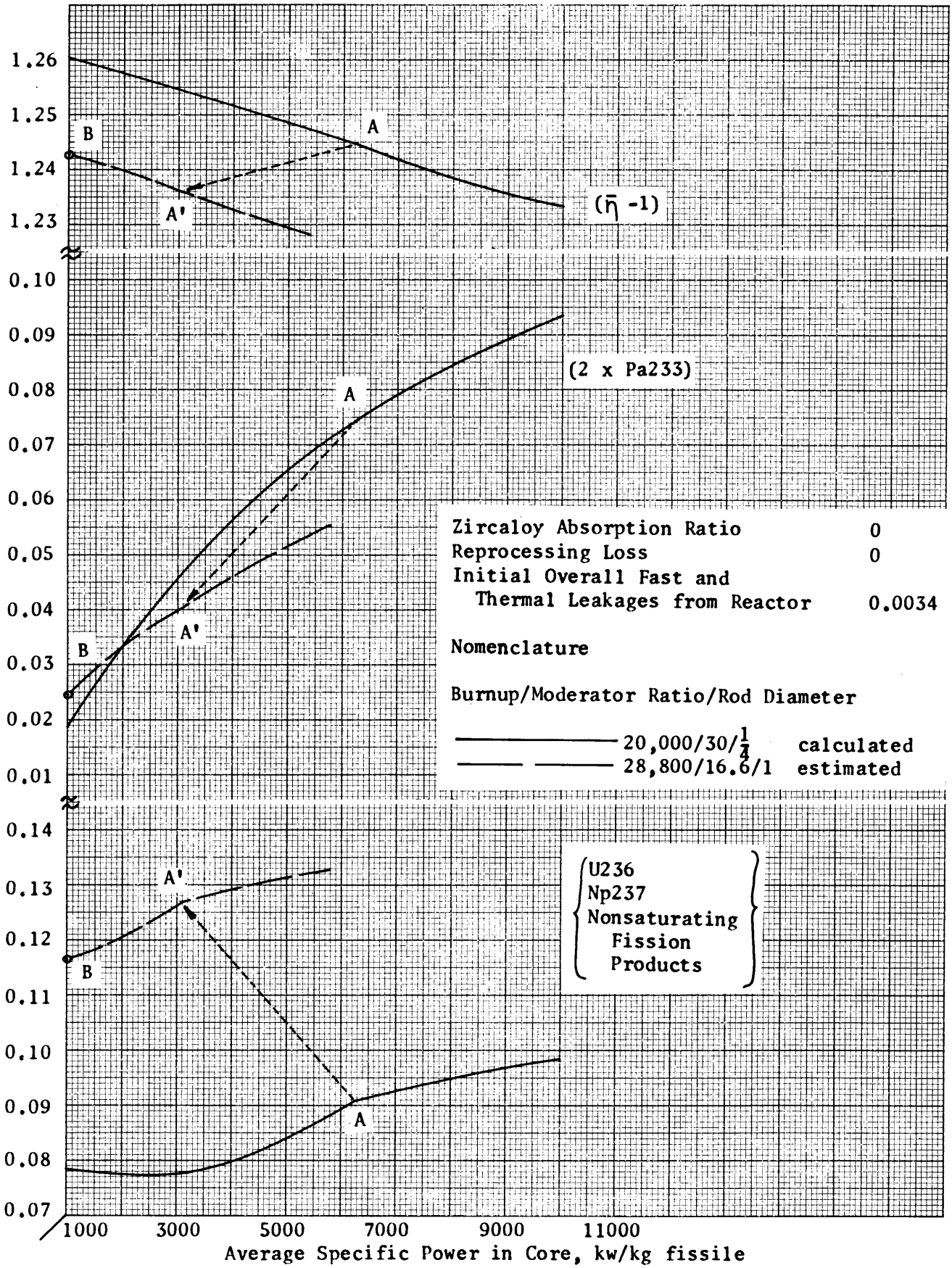

Figure 7.8: Change in Group 3 Neutron Balance Items with Average Specific Power in Core for Reactor "A"

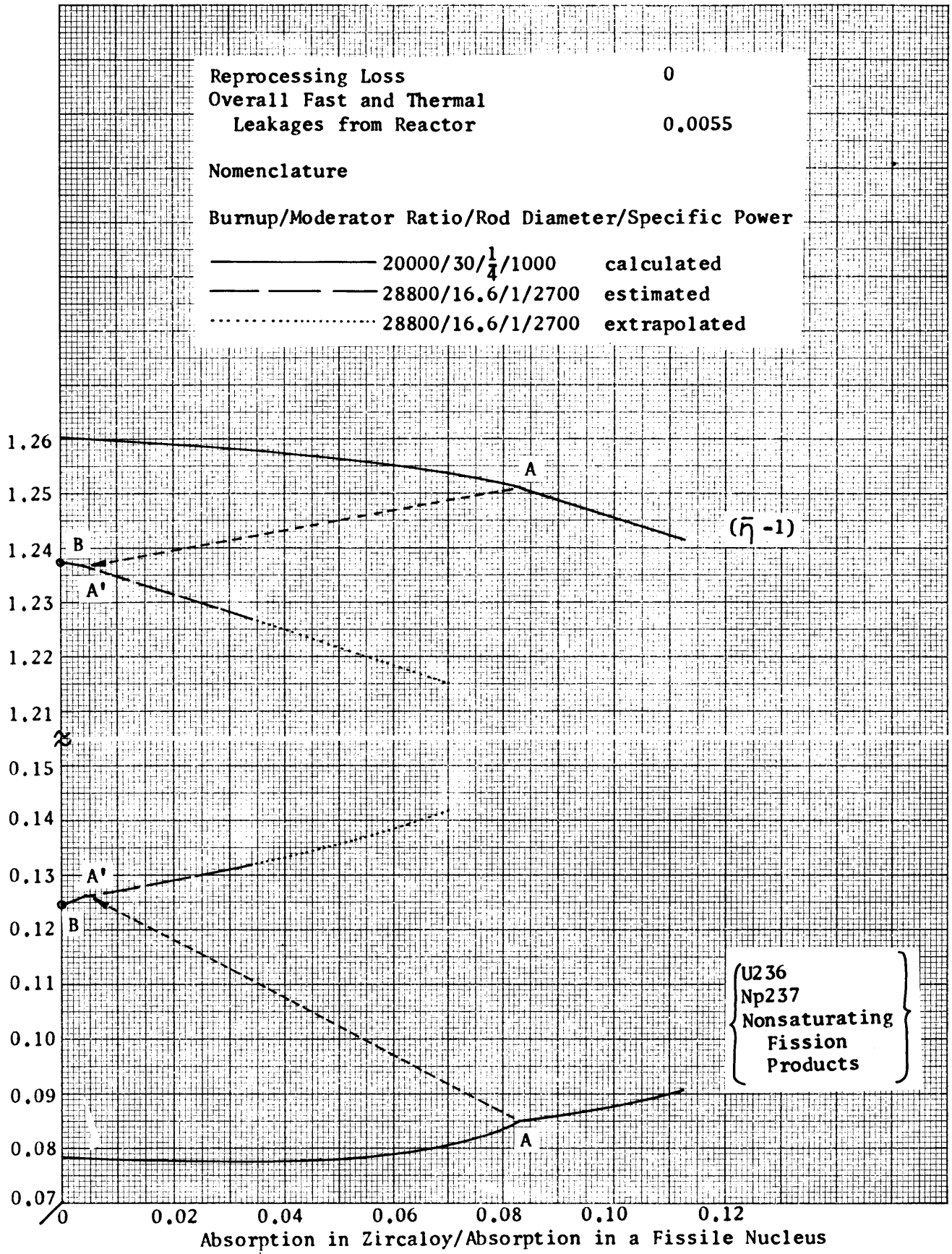

Figure 7.9: Effect of Zircaloy Absorption Ratio on some Neutron Balance Items for Reactor "A"

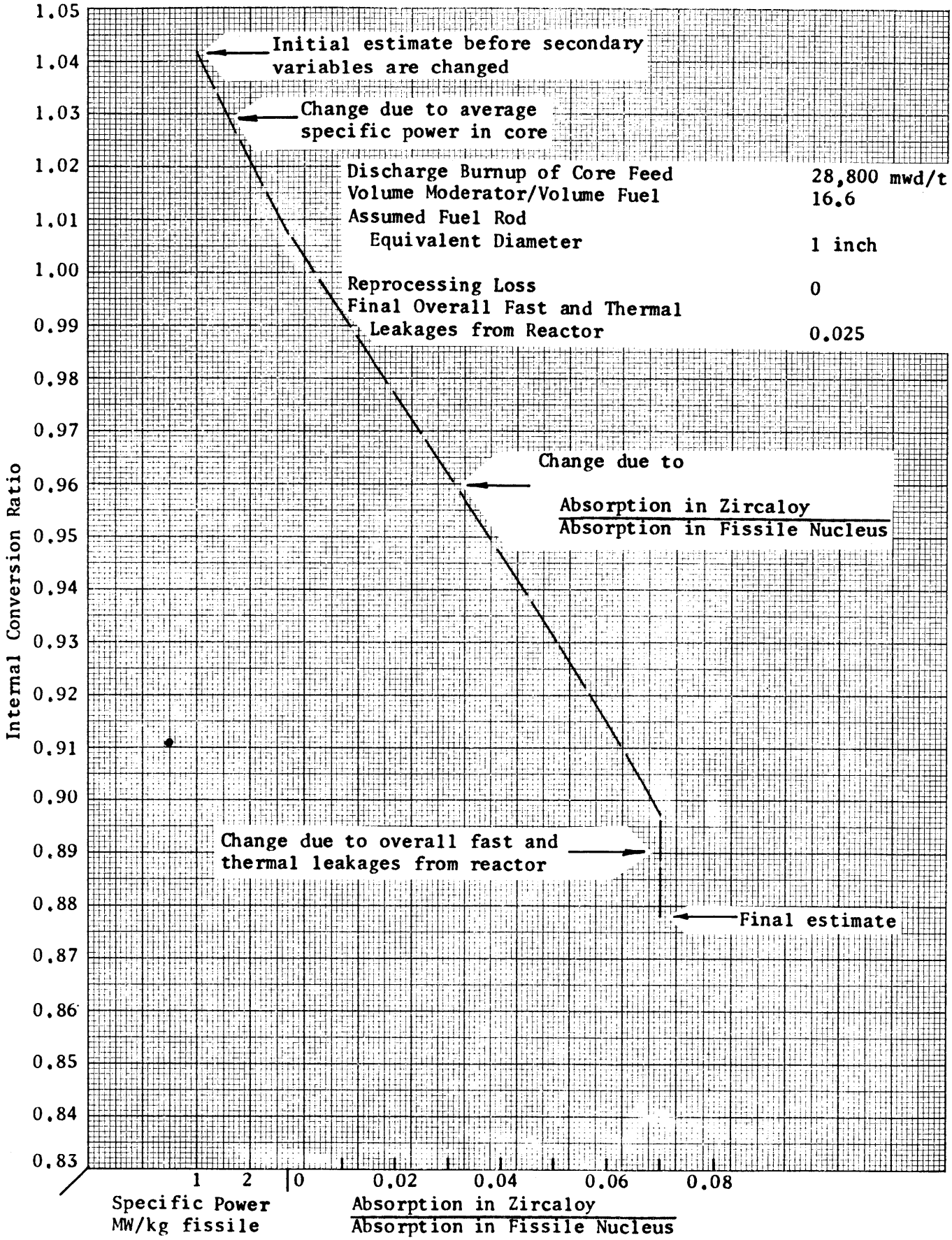

Figure 7.10: Steps in Example of Estimate of Effect of Changing All Secondary Variables on Internal Conversion Ratio using More Refined Approximate Procedure and Comparison with Reactor "A"

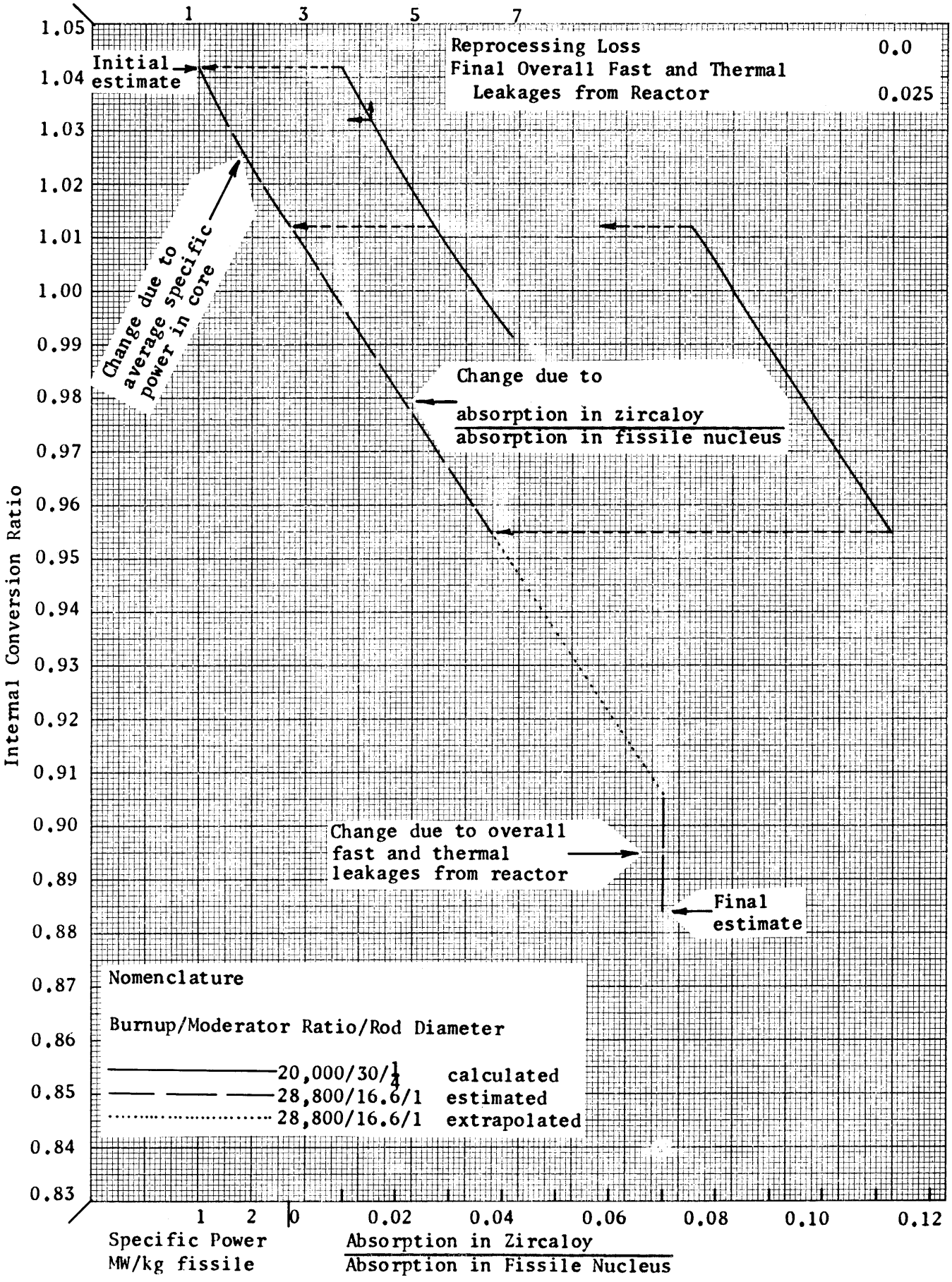

Figure 7.11: Steps in Example of Estimate of Effect of Changing All Secondary Variables on Internal Conversion Ratio using Less Refined Approximate Procedure and Comparison with Reactor "A"

CHAPTER VIII

CONCLUSIONS

The comparisons of the previous chapter have shown that the results of this work can be used to estimate the conversion ratios of reactors fueled with thorium and moderated by heavy water for widely varying values of the principal design variables.

This work has shown that one of the prime requirements for a high conversion ratio in the Th232-U233 system is that Th232 have a high effective resonance integral, such as that afforded by a small diameter fuel rod. If the fuel element designs commonly considered in D_2O reactor design studies, such as the concentric tubes of the Savannah River Laboratory or the fuel bundles of CANDU, are to be considered for a Th232 fueled, D_2O moderated reactor with a high conversion ratio, every effort should be made to insure that these fuel elements give a high effective resonance integral for Th232.

It is interesting to note that Sharma (S2), in a study of thermal converters fueled with U238-Pu239, found that in order to obtain a high conversion ratio in that system, one must use massive fuel elements in order to take advantage of the fast fission effect in U238. In this study of the Th232-U233 system, however, in which the fast fission effect of Th232 is neglected and would be very small in any event, it was found that the fuel elements should be of small dimensions to produce a high effective resonance integral in Th232 in order to obtain a high conversion ratio.

The reliability of the absolute values of the conversion ratios presented here has not been closely defined. However, the magnitudes

of the conversion ratios obtained for some of the cases studied are sufficiently high to suggest that it would be possible to design a heterogeneous, D_2O moderated, Th232-U233 fueled reactor which would breed. However, the Oak Ridge study (R1), which included economic optimization rather than optimization on the basis of conversion ratio, shows that the conversion ratio for combinations of design variables which represent economically attractive designs is around 0.85, far below unity. To obtain a conversion ratio over unity in an operable, but less economic reactor, the results of Chapter VI show that it would be necessary to use burnups under 20,000 mwd/t, to increase the moderator/fuel volume ratio to 30, to decrease the rod diameter to around 1/4 inch, to use specific powers under 1000 kw/kg fissile, and to use a zircaloy/fuel volume ratio under 0.9. All but the last of these lead to higher power costs than the Oak Ridge case.

Despite the fact that when designed for low-cost power this type of reactor will not breed, the Oak Ridge study shows that thorium fueled heavy water moderated converters would require less than one-third as much natural uranium makeup to produce power as would heavy water moderated converters using U238 as the fertile material. This result suggests that the thorium-fueled heavy water reactor may be useful in "holding the line" against rapid depletion of fissile resources during the time of an expanding nuclear power industry (D1) while the fast breeder technology is being developed. The results of the present report can be used in the design of such a reactor.

APPENDICES

APPENDIX A

DERIVATION OF THE WESTCOTT r FACTOR

In order to select from reference (W1, W2) the correct value of $\hat{\sigma}_{FP}(\theta_o)$, the effective 2200 m/s cross section for the nonsaturating fission products as a function of the 2200 m/s flux time θ_o, one must determine an approximate value of the Westcott r factor in the fuel. The derivation follows reference (M2). The following assumptions are made:

1. The entire resonance absorption in Th232 takes place at a higher neutron energy than any resonance absorption in any other nuclide. The resonance absorption in nuclides other than Th232 takes place close to thermal energy.

2. The flux per unit energy in the resonance region has a 1/E dependence.

3. The resonance flux is spatially constant throughout the fuel and moderator of the unit cell

4. The thermal neutron flux in the derivation of the Westcott r factor follows the Maxwell-Boltzmann distribution.

5. The thermal neutron flux actually calculated in this work and assumed to follow the Wilkins distribution $(n_w \bar{v}_w)$ is equal to the Maxwell-Boltzmann flux $(n_{MB}\bar{v}_{MB})$.

The Westcott r factor in the fuel is defined as follows:

$$r = \frac{\sqrt{\pi\mu}}{4} = \frac{n_{epi}^{fuel}}{n_{epi}^{fuel} + n_{MB}^{fuel}} \qquad (A1)$$

where

n_{epi} = density of neutrons in the epithermal energy group.

n_{MB} = density of neutrons following the Maxwell-Boltzmann distribution.

μ = 5. From the epithermal cutoff energy of μkT where T = modal temperature of the Maxwellian distribution of neutrons.

Using assumption 1, the slowing down density in the unit cell below the Th232 resonance energy and close to thermal energy is

$$q_{th} = q\, p_{02}\, P_1 \tag{A2}$$

where

q = fast source in the unit cell, $(\text{sec-cm}^3 \text{ of cell})^{-1}$.

p_{02} = resonance escape probability from Th232.

P_1 = fast neutron nonleakage probability.

Using assumption 2, the epithermal component of the total flux in the unit cell, corresponding to q_{th}, is

$$\left(\frac{d\phi^{cell}}{dE}\right)_{epi} = \frac{q_{th}}{\xi \Sigma_s V_m E} = \frac{q\, p_{02}\, P_1}{\xi \Sigma_s V_m E} \tag{A3}$$

where

$\xi\Sigma_s$ = slowing down power of the moderator, cm^{-1}.

V_m = volume fraction of the moderator in the unit cell.

The density of epithermal neutrons in the unit cell, corresponding to q_{th}, is

$$n_{epi}^{cell} = \int_{\mu KT}^{\infty} \frac{1}{v(E)} \left(\frac{d\phi^{cell}}{dE}\right)_{epi} dE = \frac{q \dot{P}_{02} P_i}{\xi \Sigma_s V_m} \sqrt{\frac{2m}{\mu KT}} \qquad (A4)$$

where

m = neutron mass

By assumption 3,

$$n_{epi}^{fuel} = n_{epi}^{cell} \qquad (A5)$$

By assumption 4,

$$n_{MB} = \phi_{MB} \sqrt{\frac{\pi m}{8KT}} \qquad (A6)$$

where

ϕ_{MB} = Maxwell-Boltzmann thermal flux = $(n_{MB}\bar{v}_{MB})$

By assumption 5,

$$n_{MB} = \phi \sqrt{\frac{\pi m}{8KT}} \qquad (A7)$$

where

ϕ = Wilkins thermal flux averaged over the unit cell = $(n_W \bar{v}_W)$

Inserting the thermal disadvantage factor,

$$n_{MB}^{fuel} = \phi \psi \sqrt{\frac{\pi m}{8KT}} \qquad (A8)$$

where

$$\Psi = \phi_{fuel} / \phi_{cell}$$

Inserting (A5) and (A8) into (A1), the final result reduces to

$$r = \frac{\frac{q/\phi \; p_{oz} P_1}{\xi \Sigma_s V_m} \sqrt{\frac{\pi}{8}}}{\frac{q/\phi \; p_{oz} P_1}{\xi \Sigma_s V_m} \sqrt{\frac{2}{\mu}} + \Psi \sqrt{\frac{\pi}{8}}} \qquad (A9)$$

APPENDIX B

DATA

1. Thermal data

The thermal cross sections used in this work are listed in table B1 as a function of $v/v_{E=0.414}$, where

v = neutron velocity of interest

$v_{E=0.414}$ = neutron velocity corresponding to the thermal cutoff energy of 0.414 ev

The thermal cross sections are for the following nuclides: absorption cross sections of Th232, Pa233, U233, U234, U235, U236, Np237, the "Sm" group and Xe135; fission cross sections of U233 and U235.

The "Sm" group cross sections are based on the following distribution of fissions among the fissile nuclides: U233, 85%; U235, 15%; Th232, 0%. As stated in section IVC1, it is not necessary that microscopic cross sections for the "Sm" group be used at all since it is a saturating fission product.

For $v/v_{E=0.414} = 0$, the cross section for each nuclide is given as 1.0. Any value could be used since $d\phi/dx = 0$ at $v/v_{E=0.414} = 0$, where $d\phi/dx$ is defined near equation (4C20).

The values of τ used in the thermal energy region are the same as at the lower end of the resonance region, listed in table B2.

2. Resonance data

The basic resonance data for the six dilute fuel nuclides are in table B2 and are from (G1). The nuclides are Pa233, U233, U234, U235, U236 and Np237. The data consist of the absorption cross sections versus

lethargy interval from 0.414 to 10^7 ev. In addition, the fission cross sections for U233 and U235 versus lethargy interval are included.

These absorption data are used as described in section VIC2 to determine the homogeneous effective absorption resonance integrals of these six nuclides as a function of σ_M, the moderator potential scattering cross section per absorber nucleus in a homogeneous mixture. The result for U233 is shown in figure 4.9. A fourth order polynomial is then fitted to the effective absorption resonance integral versus $\frac{1}{\sigma_M}$ for each fuel nuclide. The result is as follows:

$$I_{abs}^{eff} = I_{abs}^{\infty} + ax + bx^2 + cx^3 + dx^4 \qquad (B1)$$

where

I_{abs}^{eff} = effective absorption resonance integral, barns

I_{abs}^{∞} = infinitely dilute absorption resonance integral, barns

$x = \frac{1}{\sigma_M}$, $(\text{barns})^{-1}$

and

Nuclide	a	b	c	d
Pa233	-0.3874×10^{6}	0.1917×10^{9}	-0.6696×10^{11}	0.1045×10^{14}
U233	-0.3441×10^{6}	0.1923×10^{9}	-0.7672×10^{11}	0.1300×10^{14}
U234	-0.9989×10^{6}	0.1003×10^{10}	-0.4957×10^{12}	0.9233×10^{14}
U235	-0.4746×10^{5}	0.7105×10^{7}	-0.1119×10^{10}	0.1116×10^{12}
U236	-0.1927×10^{6}	0.1250×10^{9}	-0.4940×10^{11}	0.8164×10^{13}
Np237	-0.1037×10^{7}	0.7849×10^{9}	-0.3500×10^{12}	0.6228×10^{14}

These constants cover the range of σ_M from 500 barns to infinity.

The resonance data is also used to calculate the following items:

1. Fraction of the resonance absorption above 5 ev for Pa233, U233, U235, and Np237. See equation (4C41) and figure 4.10.

2. $\alpha^{\text{epithermal}}_{>5\text{ev}}$ for U233 and U235. See equation (4C39) and table B3.

3. $\alpha^{\text{epithermal}}_{<5\text{ev}}$ for U233 and U235. See equation (4C40) and table B3.

4. $\eta^{\text{epithermal}}_{>5\text{ev}}$ for U233 and U235. See equation (4C42) and table B3.

5. $\eta^{\text{epithermal}}_{<5\text{ev}}$ for U233 and U235. See equation (4C43) and table B3.

3. Miscellaneous data

Miscellaneous data and their references are listed in table B3.

The densities of ThO_2 and UO_2 are 92% of theoretical density due to fuel element fabrication by vibratory compaction and swaging. This is the fabrication method and theoretical density recommended by reference (R1).

The microscopic absorption cross section and Fermi age of heavy water are based on a H_2O content of 0.25% by weight. This weight percent of H_2O was suggested by reference (R1).

The yields of the "Sm" group are based on the following individual yields of the components of the "Sm" group (G3):

Fissile Nuclide	Components of "Sm" group					
	Sm149	Sm151	Rh105	Cd113	Eu155	Gd157
U233	0.0077	0.0035	0.005	0.0002	0.0002	6.35×10^{-5}
U235	0.0113	0.0044	0.009	0.00011	0.00033	7.8×10^{-5}

Table B1: Thermal Point Cross Sections of the Fuel Nuclides over the Range 0 to 0.414 ev (G1,G2,G3)

$v/v_{E=0,414}$	Th232	Pa233	U233(abs)	U233(fis)	U234	U235(abs)
0	1.0	1.0	1.0	1.0	1.0	1.0
0.021	91.0	517	6800	6550	1400	9900
0.042	45.0	257	3400	3240	680	4700
0.063	30.0	171	2260	2140	442	3000
0.083	23.3	128	1700	1600	329	2220
0.104	18.0	102	1360	1270	261	1740
0.125	15.0	85.0	1130	1050	215	1420
0.146	12.8	73.0	970	900	182	1200
0.167	11.2	63.5	850	790	159	1040
0.188	10.0	56.8	759	697	140	925
0.208	8.99	51.1	682	626	126	825
0.229	8.16	46.4	619	568	114	742
0.250	7.46	42.5	567	520	104	673
0.271	6.87	39.2	523	479	95.2	614
0.292	6.37	36.3	485	444	87.9	564
0.313	5.92	33.9	452	413	81.6	520
0.333	5.54	31.7	423	387	76.0	481
0.354	5.20	29.8	398	363	71.0	447
0.375	4.89	28.1	375	342	66.6	416
0.396	4.62	26.6	354	323	62.6	389
0.417	4.37	25.2	336	306	59.0	364
0.438	4.15	24.0	319	290	55.7	342
0.458	3.94	22.9	304	276	52.7	322
0.479	3.76	21.9	290	263	50.0	305
0.500	3.58	20.9	278	251	47.4	289
0.521	3.42	20.1	266	240	45.1	275
0.542	3.28	19.3	256	230	42.9	262
0.563	3.14	18.5	247	220	40.9	251
0.583	3.01	17.9	238	212	39.1	241
0.604	2.89	17.3	232	206	37.3	232
0.625	2.78	16.7	228	203	35.7	224
0.646	2.68	16.1	225	201	34.1	219
0.667	2.58	15.6	223	200	32.7	214
0.688	2.49	15.2	219	198	31.3	212
0.708	2.40	14.8	214	195	30.0	213
0.729	3.62	14.4	208	192	28.8	215
0.750	2.24	14.0	202	188	27.7	222
0.771	2.16	13.6	196	184	26.6	230
0.792	2.09	13.3	191	180	25.6	238
0.813	2.03	13.0	186	175	24.6	242
0.833	1.96	12.8	181	171	23.7	238
0.854	1.90	12.5	177	167	22.8	228
0.875	1.84	12.3	173	163	22.0	216
0.896	1.79	12.1	169	160	21.2	201
0.917	1.73	11.9	166	156	20.4	186
0.938	1.68	11.7	162	153	19.7	169
0.958	1.63	11.6	159	150	19.0	153
0.979	1.58	11.4	157	147	18.4	137
1.0	1.54	11.3	154	144	17.7	126

Table B1: (continued)

$v/v_{E=0.414}$	U235(fis)	U236	Np237	"Sm"	Xe
0	1.0	1.0	1.0	1.0	1.0
0.021	9000	71.0	2050	10.4×10^4	13.2×10^6
0.042	4200	35.3	1020	6.70	8.10
0.063	2670	23.6	680	5.22	6.20
0.083	1940	17.6	508	4.35	5.05
0.104	1520	14.2	408	3.80	4.35
0.125	1240	11.8	340	3.40	3.85
0.146	1040	10.2	289	3.09	3.45
0.167	900	8.90	253	2.84	3.15
0.188	789	7.93	224	2.63	2.90
0.208	704	7.13	202	2.48	2.78
0.229	633	6.47	183	2.37	2.69
0.250	574	5.93	168	2.32	2.64
0.271	523	5.47	155	2.30	2.63
0.292	480	5.08	144	2.33	2.65
0.313	442	4.73	134	2.41	2.68
0.333	408	4.43	126	2.55	2.72
0.354	379	4.17	119	2.77	2.80
0.375	353	3.93	112	3.09	2.86
0.396	329	3.72	106	3.52	2.90
0.417	309	3.53	101	4.10	2.88
0.438	290	3.36	96.1	4.78	2.79
0.458	273	3.20	91.7	5.40	2.63
0.479	258	3.06	87.7	5.52	2.40
0.500	245	2.93	84.0	5.15	2.12
0.521	233	2.81	80.7	4.40	1.82
0.542	222	2.70	77.6	3.38	1.53
0.563	212	2.60	74.7	2.40	1.26
0.583	204	2.50	72.0	1.76	1.03×10^6
0.604	196	2.41	69.6	1.30×10^4	8.28×10^5
0.625	189	2.33	67.2	9870	6.73
0.646	184	2.25	65.1	7740	5.53
0.667	179	2.18	63.0	6170	4.63
0.688	176	2.11	61.1	5000	3.88
0.708	175	2.05	59.3	4060	3.20
0.729	176	1.98	57.6	3360	2.64
0.750	180	1.93	56.0	2800	2.18
0.771	185	1.87	54.5	2360	1.82
0.792	190	1.82	53.1	2020	1.54
0.813	193	1.77	51.7	1770	1.32
0.833	191	1.73	50.4	1550	1.12×10^5
0.854	186	1.69	49.2	1370	9.57×10^4
0.875	178	1.64	48.0	1240	8.27
0.896	169	1.61	46.9	1130	7.17
0.917	157	1.57	45.8	1030	6.20
0.938	145	1.53	44.8	945	5.41
0.958	132	1.50	43.9	879	4.75
0.979	119	1.47	42.9	827	4.21
1.0	110	1.44	42.0	776	3.71×10^4

Table B2: Resonance Cross Sections of the Fuel Nuclides as a Function of Lethargy over the Range 0.414 to 10^7 ev (G1)

The resonance cross section data from reference (G1) consist of cross sections over each of 68 - 0.25 lethargy intervals from 0.414 to 10^7 ev for each of the six dilute fuel nuclides. The lethargies and energies (ev) at the bottom of each of these 68 lethargy intervals are given in this table, in addition to the cross section data themselves. Some of the 68 lethargy intervals for the various dilute fuel nuclides are further subdivided, as described in section IVC2a(I). The value of the lethargy at the bottom of each of the new subdivided intervals can be easily determined from the information for each of the six dilute fuel nuclides.

Table B2: (continued)

Interval	u (lower)	E (lower)	Interval	u(lower)	E(lower)
1	17.00	0.414	35	8.50	2.04×10^3
2	16.75	0.532	36	8.25	2.61
3	16.50	0.683	37	8.00	3.36
4	16.25	0.876	38	7.75	4.31
5	16.00	1.125	39	7.50	5.53
6	15.75	1.44	40	7.25	7.10
7	15.50	1.86	41	7.00	9.12×10^3
8	15.25	2.38	42	6.75	1.17×10^4
9	15.00	3.06	43	6.50	1.50
10	14.75	3.93	44	6.25	1.93
11	14.50	5.04	45	6.00	2.48
12	14.25	6.48	46	5.75	3.18
13	14.00	8.32	47	5.50	4.09
14	13.75	10.68	48	5.25	5.25
15	13.50	13.7	49	5.00	6.74
16	13.25	17.6	50	4.75	8.65×10^4
17	13.00	22.6	51	4.50	1.11×10^5
18	12.75	29.0	52	4.25	1.43
19	12.50	37.3	53	4.00	1.83
20	12.25	47.9	54	3.75	2.35
21	12.00	61.4	55	3.50	3.02
22	11.75	78.9	56	3.25	3.88
23	11.50	101	57	3.00	4.98
24	11.25	130	58	2.75	6.39
25	11.00	167	59	2.50	8.21×10^5
26	10.75	215	60	2.25	1.05×10^6
27	10.50	275	61	2.00	1.35
28	10.25	354	62	1.75	1.74
29	10.00	454	63	1.50	2.23
30	9.75	583	64	1.25	2.87
31	9.50	748	65	1.00	3.68
32	9.25	961	66	0.75	4.72
33	9.00	1230	67	0.50	6.07
34	8.75	1590	68	0.25	7.79×10^6

Table B2: (continued)

← Pa233 →				← U234 →			
I^{∞}_{abs} = 925 barns				I^{∞}_{abs} = 689 barns			
ΔU	σ_a	ΔU	σ_a	ΔU	σ_a	ΔU	σ_a
0.25	10.6	0.25	0.0921	0.25	21.0	0.25	8.58
	9.39		0.0812		18.5		7.14
	36.4		0.0717		16.0		5.40
	34.5		0.0633		13.3		4.10
	430		0.0558		10.8		3.23
	847		0.0493		8.20		2.76
	33.2		0.0435		6.00		2.26
	144		0.0384		4.00		1.92
	198		0.0339		3.00		1.63
	592		0.0299		2.50		1.38
	31.2		0.0264		2276		1.12
	30.8		0.0233		1.60		0.988
	374		0.0205		1.20		0.862
	30.2		0.0181		0.800		0.762
	30.0		0.0160		0.600		0.675
	264		0.0141		0.400		0.587
	29.6		0.0125		0.300		0.507
	29.4		0.100		98.8		0.443
	184		0.499		0.631		0.394
	29.1		0.639		51.8		0.300
	29.0		0.921	0.25	13.7		0.270
	128		1.02	0.0308	2.04		0.250
	28.8		1.12	0.2192	29.5		0.230
	88.8		1.15	0.0779	6.45		0.230
	28.7		1.21	0.1721	19.2		0.310
	10.6		1.24	0.0838	23.4		0.560
	0.413		1.30	0.0832	24.0		0.790
	0.364		1.34	0.0830	24.3		1.20
	0.321		1.37	0.0923	25.5		1.33
	0.284	0.25	1.37	0.0328	14.8		1.33
	0.250			0.1249	26.5		1.45
	0.221			0.25	2.83		1.54
	0.195			0.115	11.1		1.51
	0.172			0.135	11.0		1.55
	0.152			0.0390	11.5		1.56
	0.134			0.2110	18.5		1.50
	0.120			0.25	11.6		1.90
0.25	0.104			0.25	9.26	0.25	2.35

Table B2: (continued)

U236				Np237			
I^{∞}_{abs} = 311 barns				I^{∞}_{abs} = 1510 barns			
Δu	σ_a	Δu	σ_a	Δu	σ_a	Δu	σ_a
0.25	1.40	0.25	1.76	0.25	1843	0.25	5.62
	1.20		1.46		161		4.76
	1.00		1.29		233		4.01
	0.900		1.13		19.9		3.38
	0.800		0.981		375		2.84
	0.700		0.803		686		2.38
	0.600		0.734		84.9		1.99
	0.500		0.660		4.11		1.67
	0		0.602	0.25	280		1.40
	0		0.547	0.132	87.0		1.17
	893		0.485	0.118	90.0		0.980
	0		0.426	0.1891	511		0.824
	0		0.378	0.0609	67.2		0.694
	0		0.333	0.0512	5.17		0.588
	2.00		0.280	0.1988	81.4		0.501
	2.00		0.240	0.0688	81.8		0.429
0.25	2.00		0.210	0.0632	80.7		0.370
0.0909	17.5		0.180	0.1180	293		0.321
0.1591	60.5		0.150	0.25	496		0.284
0.25	91.2		0.140		93.3		0.254
	2.00		0.130		120		0.242
	50.2		0.140		259		0.275
0.25	36.1		0.210		104		0.443
0.2020	31.2		0.440		90.3		0.758
0.0480	10.7		0.710		97.8		1.13
0.25	5.85		0.790		79.9		1.55
	10.2		0.850		77.8		1.68
0.25	8.68		0.920		7.42		1.73
0.119	10.0		0.950		26.7		1.74
0.131	9.57		0.950		23.0		1.71
0.25	7.36		0.920		19.9		1.62
	4.31		1.60		17.1		1.49
	3.83	0.25	2.05		14.7		1.46
	3.45				12.6		1.90
	3.15				10.8	0.25	2.19
	2.91				9.18		
	2.52				7.81		
0.25	1.98			0.25	6.63		

Table B2: (continued)

U233

I^{∞}_{abs} = 1012b, I^{∞}_{fis} = 865b

ΔU	σ_a	σ_f	ν
0.25	145	135	2.503
	135	123	
	133	121	
	157	141	
0.25	250	236	
0.1567	363	671	
0.0933	1396		
0.25	565	458	
	103	75.0	
	142	125	
5ev →	101	96.2	
	110	99.7	
0.25	194	165	
0.0477	8.80	112	
0.2023	158		
0.25	137	117	
	108	83.5	
	160	112	
	92.0	79.5	
	75.7	54.6	
	32.7	25.6	
	53.4	40.4	
	46.3	34.1	
	43.0	32.4	
	42.4	36.0	
	26.7	22.8	
	27.7	18.5	
	26.0	22.5	
	24.6	21.5	
	18.6	15.7	
	17.9	13.3	
	19.4	15.4	
	17.1	13.9	
	14.2	12.5	
	12.6	9.05	
	10.4	8.17	
	9.59	8.20	
0.25	8.24	7.82	2.503

ΔU	σ_a	σ_f	ν
0.25	7.47	7.38	2.503
	6.80	6.70	2.503
	8.24	5.95	2.504
	8.00	5.50	
	5.80	5.09	
	5.40	4.76	
	4.90	4.42	2.504
	4.60	4.14	2.51
	4.35	3.91	
	4.00	3.60	
	3.66	3.30	
	3.42	3.08	
	3.10	2.80	
	2.88	2.61	
	2.65	2.40	2.51
	2.58	2.35	2.52
	2.52	2.30	2.52
	2.48	2.28	2.53
	2.47	2.28	2.53
	2.31	2.15	2.54
	2.13	2.00	2.55
	2.07	1.96	2.57
	2.02	1.95	2.58
	2.02	1.93	2.61
	2.01	1.91	2.63
	2.00	1.90	2.71
	1.98	1.88	2.80
	1.88	1.78	2.91
	1.77	1.67	3.06
	1.69	1.59	3.25
	2.14	2.04	3.50
0.25	2.34	2.24	3.81

Table B2: (continued)

U235

I^{∞}_{abs} = 483b, I^{∞}_{fis} = 315b

ΔU	σ_a	σ_f	ν	ΔU	σ_a	σ_f	ν
0.25	104	90.1	2.43	0.0278	52.1		2.43
	74.3	64.3		0.0199	52.1		
	62.8	55.8		0.0273	67.1		
	86.6	70.6		0.0176	69.3	48.9	
	56.8	44.5		0.0316	30.9		
	19.7	16.0		0.0108	10.5		
	21.5	16.1		0.0252	82.8		
0.25	17.4	13.3		0.0151	54.3		
0.150	28.2	32.4		0.0180	24.7		
0.100	80.0			0.0234	37.7		
0.25	23.2	6.13		0.0411	69.5	63.0	
0.0465	10.8			0.0412	86.8		
0.0355	7.39	30.0		0.0527	133		
0.0429	11.7			0.0736	180		
0.1251	138			0.0176	5.27		
0.25	40.6	24.4		0.0681	81.5	41.1	
0.1440	256			0.0487	102		
0.0413	35.5			0.0300	44.0		
0.0235	15.5	105		0.0405	72.0		
0.0248	18.9			0.0451	22.0		
0.0164	9.35			0.0451	164		
0.0824	143			0.0367	151		
0.1321	173	53.1		0.0455	29.0	61.9	
0.0024	0.407			0.0584	147		
0.0331	9.90			0.0359	66.6		
0.0491	26.2			0.0284	8.07		
0.0674	22.5			0.25	35.9	24.0	
0.0338	44.3	38.9			39.6	26.4	
0.0326	92.0				43.0	28.7	
0.0341	157				38.6	25.7	
0.0330	90.9				32.1	21.4	
0.0357	33.4				36.5	24.3	
0.0247	21.4				23.4	15.6	
0.1185	172	68.0			20.2	13.5	
0.0249	46.6				22.8	15.1	
0.0462	115				18.7	12.6	
0.0296	108				12.9	8.82	
0.0451	237		2.43	0.25	12.6	8.75	2.43

Table B2: (continued)

U235

ΔU	σ_a	σ_f	ν
0.25	10.7	7.54	2.43
	8.82	6.28	
	7.23	5.20	
	7.27	5.29	
	6.69	4.92	
	5.95	4.44	
	5.68	4.29	
	4.78	3.66	
	4.35	2.98	
	4.85	3.35	
	4.47	3.12	
	4.11	2.90	
	3.77	2.69	
	3.44	2.48	
	3.14	2.29	2.43
	2.84	2.11	2.44
	2.57	1.93	
	2.34	1.78	
	2.12	1.64	2.44
	1.94	1.52	2.45
	1.78	1.42	2.45
	1.67	1.36	2.46
	1.57	1.32	2.46
	1.47	1.27	2.47
	1.37	1.19	2.49
	1.32	1.16	2.50
	1.33	1.21	2.52
	1.33	1.23	2.55
	1.34	1.27	2.58
	1.37	1.31	2.63
	1.35	1.31	2.71
	1.29	1.25	2.82
	1.20	1.17	2.96
	1.17	1.15	3.13
	1.48	1.48	3.37
0.25	1.77	1.77	3.65

Table B3: Miscellaneous Data with References

	ρ $\frac{gm}{cm^3}$	τ, cm^2	T, °C	D_{fast}, cm	Y_{U235}	Y_{U233}
ThO_2	9.20/G6		1200/G5			
UO_2	10.09/G6					
"Sm"					0.0252/G3	0.0167/G3
Xe					0.0641/G3	0.0584/G3
Heavy water	1.0782/E1	124/K1	80/M3	1.24/K1		

	λ, sec^{-1}	σ_{2200}, barns	σ_s^{epi}, barns	σ_{tr}^{th}, barns	σ_{tr}^{epi}, barns	ξ
ThO_2			20/E1	22/E1	12.28/E1	0.0508/E1
Th		7.56/G1				
Pa	2.93×10^{-7}/H2	43/G1				
U233		574/G1				
U234		105/G1				
U235		682/G1				
U236		6/G1				
Xe	2.09×10^{-5}/H2					
Heavy water		0.0026/E1	6.2/E1	7.98/E1	6.15/E1	0.0220/E1

Table B3: (continued)

	σ_{zz00}, barns	σ_s^{epi}, barns	σ_{tr}^{th}, barns	σ_{tr}^{epi}, barns	ξ	
Zr	0.212/M3	10.59/E1	10.53/E1	8.14/E1	0.509/E1	
O_2		7.5/E1				
	N, $\frac{atom}{b\text{-}cm}$	$\alpha_{>5ev}^{epi}$	$\alpha_{<5ev}^{epi}$	$\eta_{>5ev}^{epi}$	$\eta_{<5ev}^{epi}$	Heat per fission, w-sec
U233		0.225/IV,G1	0.137/IV,G1	2.05/IV,G1	2.20/IV,G1	3.14×10^{-11}/M3
U235		0.665/IV,G1	0.259/IV,G1	1.47/IV,G1	1.93/IV,G1	3.14×10^{-11}/M3
Zr	0.0429/E1					

APPENDIX C

COMPUTER CODES

1. Chain-1

a. Logical flow diagram of MAIN

The basic FORTRAN computer code used in this work was written by Hofmann (H2,S3) but has been extensively revised in the course of this work. The theories behind the revisions are explained in detail in chapter IV. Due to the large requirement of fast memory storage in this work, the computations are divided into two codes: chain-1, which is basically Hofmann's code and chain-2, which performs all of the calculations for the detailed neutron balance as listed in table 5.1. Although the terms chain-1 and chain-2 are used, the actual CHAIN technique of the FORTRAN system is not used.

The logical flow diagram of the MAIN program for chain-1 is shown in figure C1. This figure is comparable to figure II.14, page 65 of Hofmann. The flow diagram is largely self explanatory and when studied in conjunction with Hofmann's explanation of his figure II.14, will become quite clear.

The only section of figure C1 which requires explanation here is steps 19 through 31. Consider the following situation: you are making your first computer run using a given set of input values and the initial estimates of these values, whether read in or calculated by the code, are very uncertain. That is, the initial estimates of the feed composition, core dimensions, axial velocity of the fuel in the core, thermal flux and fast flux are probably very poor. Refer now to the source terms for fast and thermal neutrons in table 4.1. It is seen that these source terms are made up of two parts: the fuel properties as calculated in subroutine

Figure C1: Logical Flow Diagram for Chain-1 MAIN Program

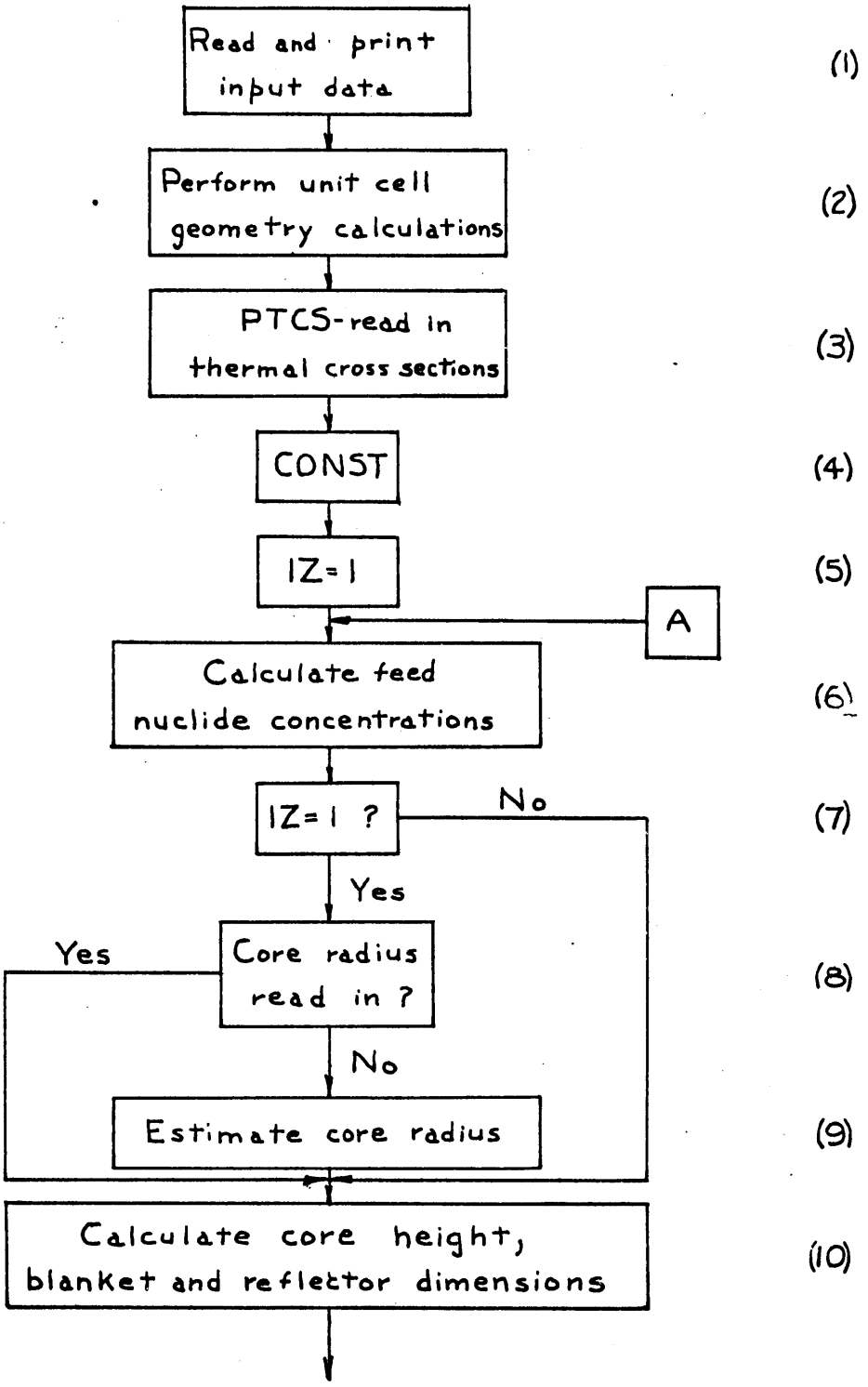

Figure C1: (continued)

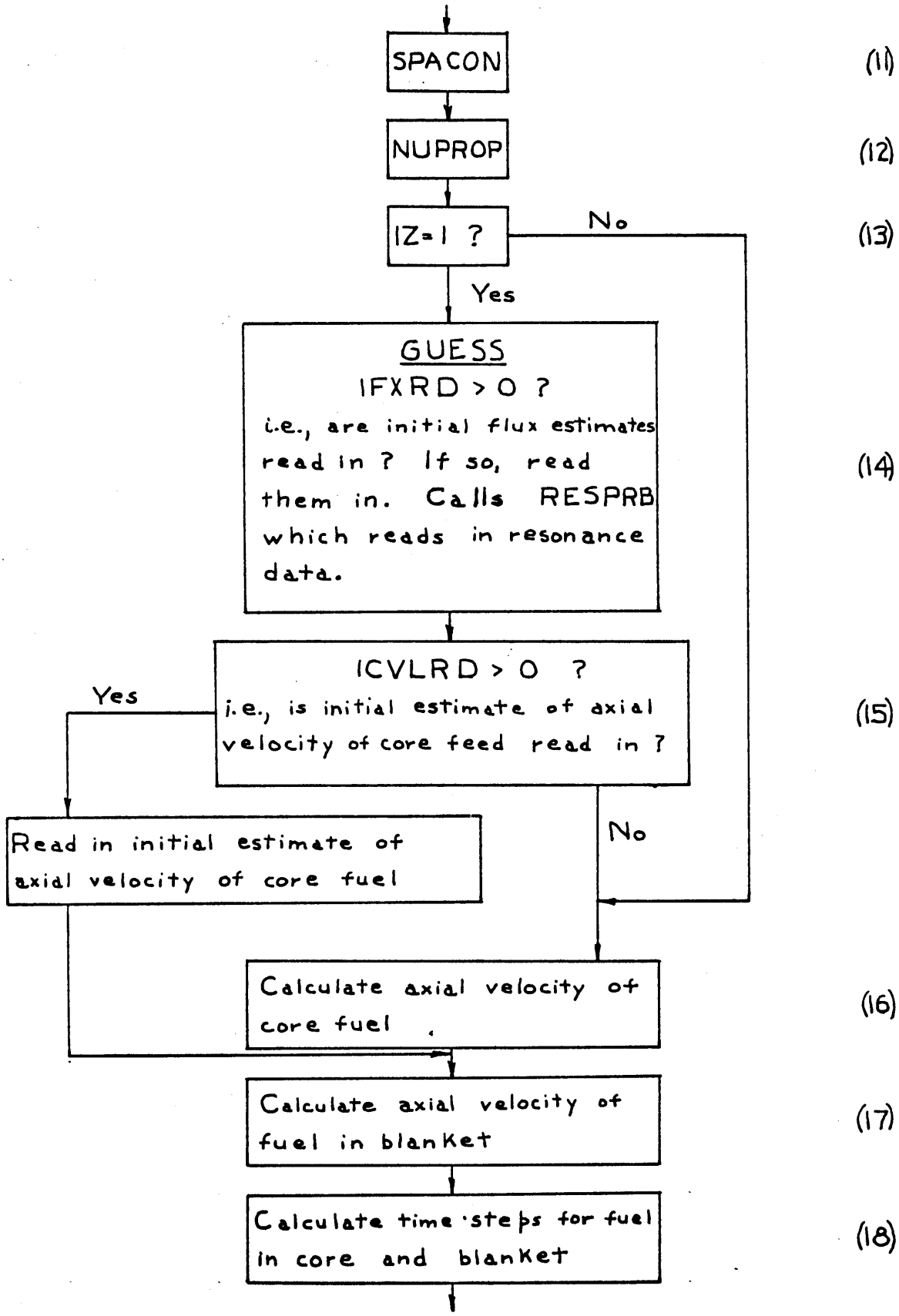

Figure C1: (continued)

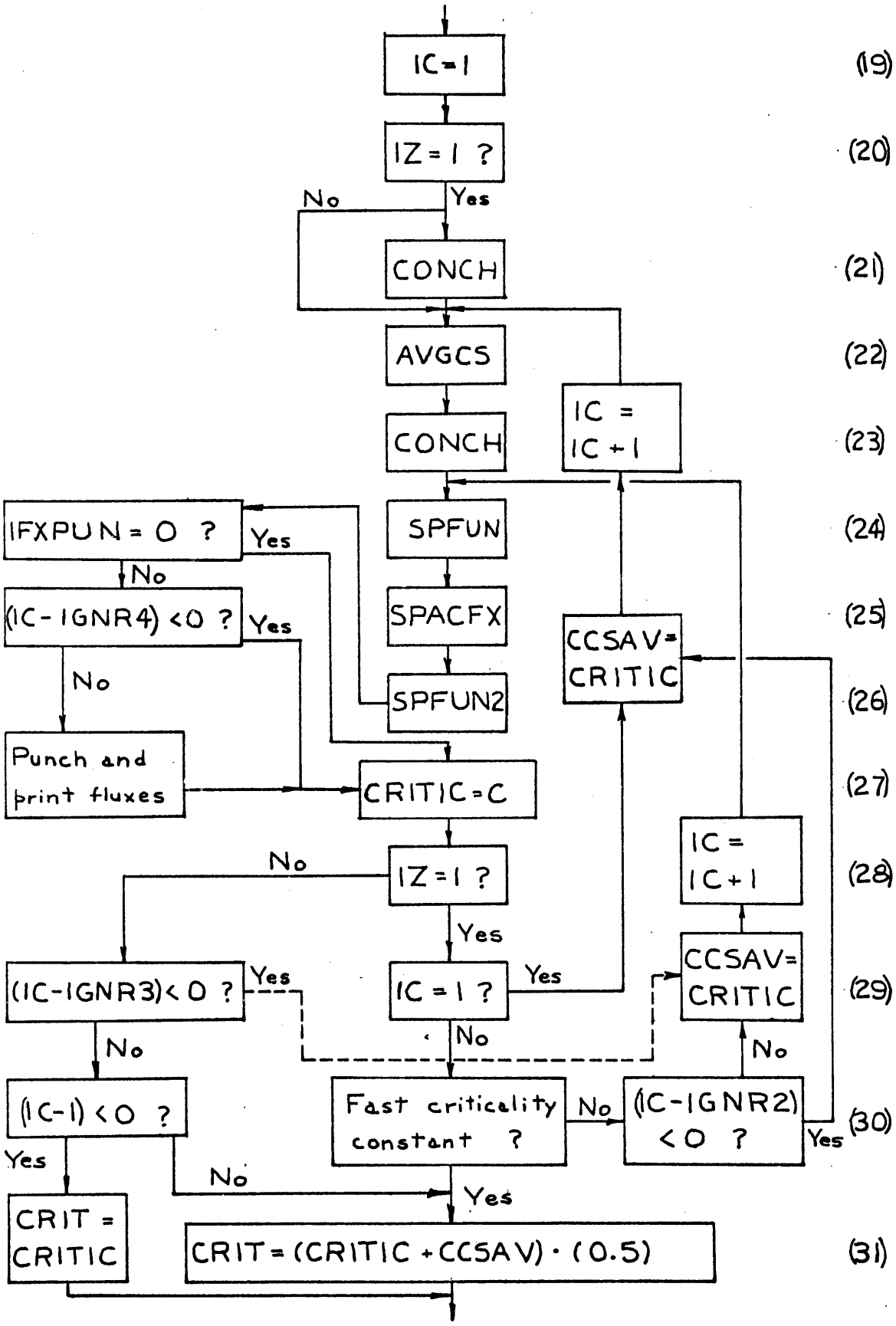

Figure C1: (continued)

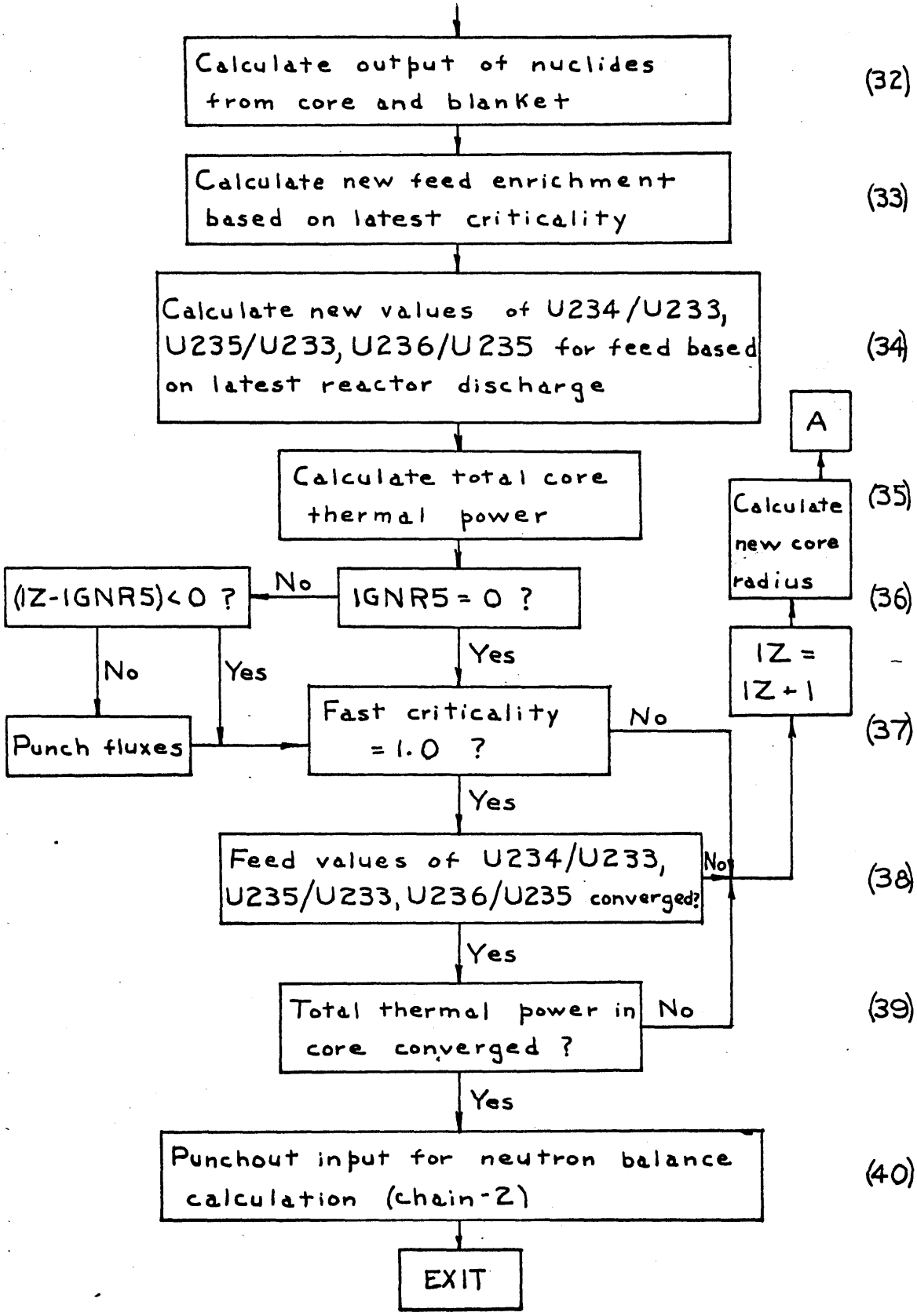

CONCH and the other flux. Experience has shown that for IZ=1 and for the very poor input values mentioned above, after two IC passes through CONCH in step 23, the change in the fuel properties with each succeeding IC pass through CONCH is completely overshadowed by the changes in the absolute values of the fast and thermal fluxes which are calculated in SPFUN, SPACFX and SPFUN2. Therefore for the first two or three computer runs on a problem, the following input variables are set at the given values:

CRDELI = 0.0. This causes the question in step 30 "Fast criticality constant?" to always be answered "No" and thus sends the logical flow back up through SPFUN, et cetera.

IGNR2 = 2. This controls the number of passes through CONCH in step 23 for IZ=1.

IFXPUN = 1, IGNR4 = 30 or so. This controls the number of IC passes (30 in this case) through SPFUN, et cetera before the program starts punching out the fluxes to be used in the succeeding run. See step 24.

After two or three computer runs like this, with each succeeding run using improved estimates of the input values of the feed enrichment, core dimensions, axial velocity of the fuel in the core, thermal flux and fast flux, these input values are pretty well established.

After obtaining the improved input values mentioned above, one sets the following input variables at the given values:

CRDELI = 0.003. This allows the question asked in step 30 to be answered "Yes" so the logical flow can proceed through step 31 and on.

IGNR2 = 2. This serves the same function as before.

IGNR3 = 2. This controls the number of IC passes through SPFUN, et cetera for each IZ > 1. Even at this stage, the fluxes in the source terms of table 4.1 vary slightly from IC loop to IC loop and two calculations of the fluxes with the same values of the fuel properties give improved values of the fluxes.

IGNR5 = 7. This controls the IZ loop on which the latest values of the fluxes are punched out in step 37. In case the problem does not run to completion on the current run, these fluxes can be used as input to the next run.

IFXPUN = 0, IGNR4 = 0. These are not needed for IZ > 1.

b. Input data to chain-1

Figure C2 shows the input data deck for chain-1.

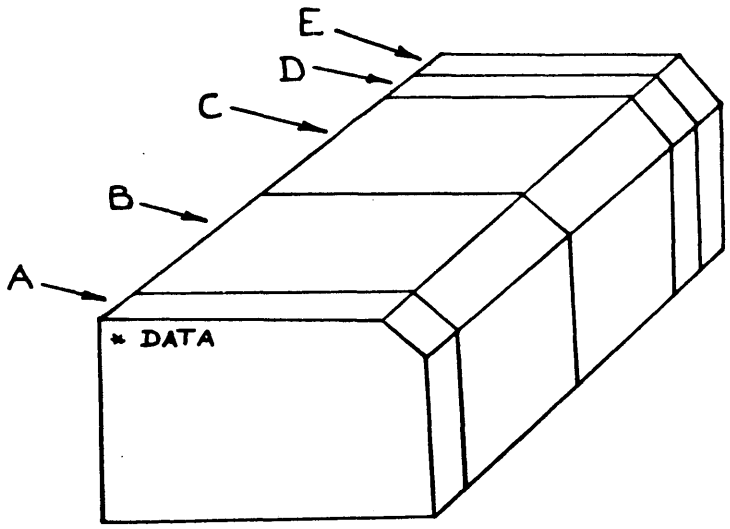

Figure C2: Input Data Deck for Chain-1

Section A: This is the basic input data which is listed and explained in table C1 where an example problem is also presented. Card 1 has a format of (72H). Cards 15, 16 and 17 have a format (2413). The other cards have formats of (6E12.5).

TABLE C1: BASIC INPUT DATA

Card	FORTRAN Symbol	Definition	Units	Example
1	-	Identification card. 72 spaces	-	-
2	BURNUP	Average burnup of fuel discharged from core	mwd/t	20000.0
	VHWVTH	Volume of moderator/volume of fuel	-	30.0
	RODDIA	Fuel rod diameter	inch	0.25
	CR	First estimate of core radius. If CR=0, the code of calculates a value.	feet	24.2
	BR	Blanket radius. Calculated by code.	-	0.0
	RR	Reflector radius. Calculated by code.	-	0.0
3	DELR	Radial extrapolation length	cm	2.0
	CH	Core height. Calculated by code.	-	0.0
	BH	Blanket height. Calculated by code.	-	0.0
	RH	Reflector height. Calculated by code.	-	0.0
	DELH	Axial extrapolation length	cm	2.0
	SPPTMX	Average thermal specific power in core	$\frac{kw}{kg\ fissile}$	1000.0
4	VZRVTH	Volume of zircaloy cladding/ volume of fuel	-	0.5
	ROSS	Fraction of reactor discharge lost in reprocessing	-	0.02
	ENA	Initial estimate of atom enrichment of feed	-	0.013
	ANIFRA(4)	Atom ratio U234/U233 in feed (initial guess)	-	0.30
	ANIFRA(5)	Atom ratio U235/U233 in feed (initial guess)	-	0.059

TABLE C1 (Cont.)

Card	FORTRAN Symbol	Definition	Units	Example
4	ANIFRA(6)	Atom ratio U236/U235 in feed (initial guess)	-	1.26
5	THETAB	Radial blanket discharge flux time	n/kb	0.05
	THETAX	Axial blanket discharge flux time	n/kb	0.001
	ROTHO2	Density of ThO_2	gm/cm^3	9.20
	ROUO2	Density of UO_2	gm/cm^3	10.09
	EVCUT	Cutoff energy between thermal region and resonance region	ev	0.414
	TD2O	D_2O and neutron temperature	^oC	80.0
6	ROD2O	Density of D_2O at TD2O	gm/cm^3	1.0782
	TAUR	Fermi age of $D_2O(0.25\%H_2O)$	cm^2	124.0
	D ASTR	Fast diffusion coefficient of D_2O	cm	1.24
	COLPRO	Unused	-	0.0
	PHI11	Initial estimate of the central thermal flux	$\frac{neut}{cm^2\text{-}sec}$	$0.5x10^{14}$
	FFOTFC	Initial estimate of fast flux/ thermal flux in core	-	1.0
7	FFOTFB	Initial estimate of fast flux/ thermal flux in blanket	-	0.3
	FFOTFR	Initial estimate of fast flux/ thermal flux in reflector	-	0.0
	TFUEL	Fuel temperature ($< 1227°C$)	°C	1200.0
	WESTR	Initial estimate of Westcott R factor	-	0.0446
	XA	Pseudo nonsaturating fission product cross section coefficient for U233 fission products corresponding to WESTR	barns	25.03

TABLE C1 (Cont.)

Card	FORTRAN Symbol	Definition	Units	Example
7	XB	Same as for XA	barns	39.67
8	XC	Same as for XA	barns	-2.42
	YA	Pseudo nonsaturating fission product cross section coefficient for U235 fission products corresponding to WESTR	barns	27.98
	YB	Same as for YA	barns	40.75
	YC	Same as for YA	barns	-4.16
	GF23	Unused	-	0.0
	GF25	Unused	-	0.0
9	SF23	Unused	-	0.0
	SF25	Unused	-	0.0
	FLIEB	Extrapolated Liebmann parameter (SPACFX)	-	1.5
	ERROR	Flux shape convergence criterion (SPACFX)	-	0.001
	TIGG	Maximum number of SPACFX loops	-	300.0
	CMPTIG	Unused	-	0.0
10	DCDE	Fast criticality iteration parameter	-	50.0
	CRDEL1	Fast criticality convergence criterion 1 (IZ=1)	-	0.002
	CRDEL2	Fast criticality convergence criterion 2 (IZ $\geq$ 1)	-	0.0005
	ANDEL	Convergence criterion for feed atom ratios	-	0.002
	EXTRAP(4)	Extrapolation parameter for feed atom ratio U234/U233	-	1.0

TABLE C1 (Cont.)

Card	FORTRAN Symbol	Definition	Units	Example
10	EXTRAP(5)	Extrapolation parameter for feed atom ratio U235/U233	-	1.0
11	EXTRAP(6)	Extrapolation parameter for feed atom ratio U236/U235	-	1.0
12	HOR	Core height/core radius	-	1.845
	RBTFT	Radial blanket thickness	feet	2.0
	ABTFT	Axial blanket thickness	feet	2.0
	RRTFT	Radial reflector thickness	feet	0.0
	ARTFT	Axial reflector thickness	feet	0.0
	CORPOW	Thermal power in core	MW	8333.0
13	RICALC(1)	Unused	-	0.0
	RICALC(2)	Unused	-	0.0
	RICALC(3)	Unused	-	0.0
	RICALC(4)	Unused	-	0.0
	RICALC(5)	Unused	-	0.0
	RICALC(6)	Unused	-	0.0
14	RICALC(7)	Unused	-	0.0
	SMOTH1	Unused but must=1.(CONCH)	-	1.0
	SMOTH2	Unused but must=1.(CONCH)	-	1.0
	DELPOW	Convergence criterion for core thermal power	-	0.0003
15	IRC	Number of radial mesh points in core (IRC $\leq$ IRB)	-	14
	IRB	Number of radial mesh points in core and blanket (IRB $\leq$ IRR)	-	16
	IRR	Total number of radial mesh points (core + blanket + reflector) (IRR $\leq$ 24)	-	16

TABLE C1 (Cont.)

Card	FORTRAN Symbol	Definition	Example
15	JZC	Number of axial mesh points in 1/2 of the core height (JZC $\leq$ JZB)	13
	JZB	Number of axial mesh points in 1/2 core height plus one axial blanket (JZB $\leq$ JZR)	15
	JZR	Total number of axial mesh points (1/2 core height+one blanket+one reflector) (JZR $\leq$ 20)	15
	IL	Number of points for solution of Wilkins equation. IL must be odd and less than 50	49
	IVELCO	Determines velocity distribution of fuel in core. 0 = radially uniform discharge burnup. 1 = radially uniform velocity	1
	ICVLRD	Determines if initial estimate of velocity of fuel in core is read in or calculated by code. 0 = calculated. 1 = read in. If IVELCO = 1, IRC values of velocity must be read in at the very end of the input data.	0
	IFXRD	Determines if initial flux estimates are read in GUESS. 0 = no. 1 = yes.	0
	IFXPUN	Determines if fluxes are punched out. 0 = no. 1 = yes.	0
	IPADEC	Determines if discharged Pa233 has an infinite or zero decay time before being fed back into core. 0 = zero. 1 = infinite.	1
16	IPRT1	Printout control parameter for SPFUN2	0
	IPRT2	Printout control parameter for SPACFX	0
	IPRT3	Printout control parameter for PTCS	0
	IPRT4	Printout control parameter for AVGCS	0
	IRPT5	Printout control parameter for SPFUN2	0
	IPRT6	Printout control parameter for CONCH	0

TABLE C1 (Cont.)

Card	FORTRAN Symbol	Definition	Example
16	IPRT7	Printout control parameter for SPACON	0
	IPRT8	Printout control parameter for CONCH	0
	IPRT9	Printout control parameter for SPFUN	0
	IPRT10	Unused	0
	IPRT11	Unused	0
	IPRT12	Unused	0
17	IGNR1	Unused	0
	IGNR2	IZ = 1. Number of IC passes through CONCH	2
	IGNR3	IZ > 1. Number of IC passes through SPFUN.	2
	IGNR4	IZ = 1, IFXPUN = 1, CRDEL1 = 0.0. Number of IC passes through SPFUN before punchout of fluxes is started.	0
	IGNR5	IZ > 1, IFXPUN = 0. Designates the IZ loop on which punchout of fluxes is to start.	5
	IGNR6-IGNR10	Unused	0

Section B: This is the thermal point cross section data. The data is presented in table B1. The first card in this section is an identification card on which arbitrary characters can be punched in the first 72 spaces. In the first 12 spaces on the first data card corresponding to a column in table B1, an arbitrary fixed point identification number is punched. In each succeeding group of 12 spaces on the first card and on succeeding cards, a cross section is punched as a floating point number until all of the numbers in a column have been punched. This process is repeated for each column in table B1. The cross sections are arranged in this section of input cards in the following order: Th232, Pa233, U233 absorption, U234, U235 absorption, U236, Np237, U233 fission, "Sm" group, Xe135. These data are read in in subroutine PTCS.

Section C: This section contains the initial estimates of the absolute values of the thermal and fast fluxes in that order. This section is supplied only for IFXRD = 1 and the data are read in in subroutine GUESS.

Section D: This section contains the resonance data for the dilute fuel nuclides from appendix B. The first card is an identification card as described above for the thermal data. The resonance data are read in for the dilute fuel nuclides in the following order: Pa233, U233, U234, U235, U236 and Np237. The three data cards for U233 are given below:

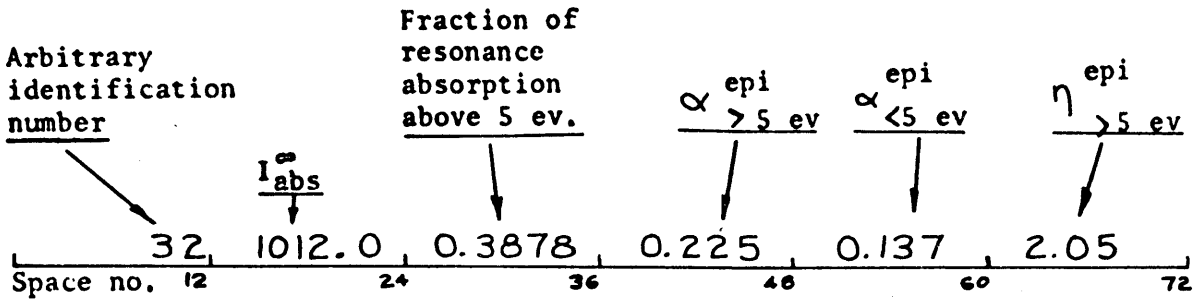

Coefficients for 4th order polynomial. See equation (B1).

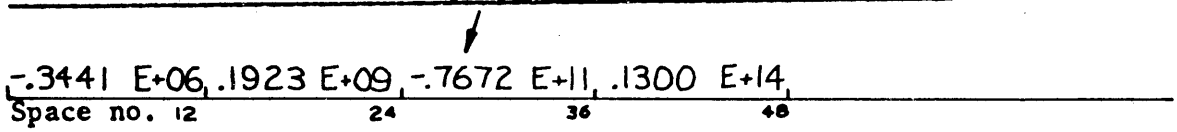

The data cards for the other dilute fuel nuclides are of identical form to those for U233 except that the second card is deleted for the nonfissionable nuclides and other individual items are deleted for nuclides for which they are not applicable.

The resonance data are read in in subroutine RESPRB which is called first by subroutine GUESS.

Section E: This section contains the initial estimates of the fuel axial velocity in the core at each radial mesh position. These cards are required only for ICVLRD = 1. The format is (6E12.5).

2. Chain-2

a. Logical flow diagram for MAIN

The purpose of chain-2 is to perform the calculations for the detailed neutron balance, examples of which are shown in table 5.1. The logical flow diagram for the MAIN program is shown in figure C3:

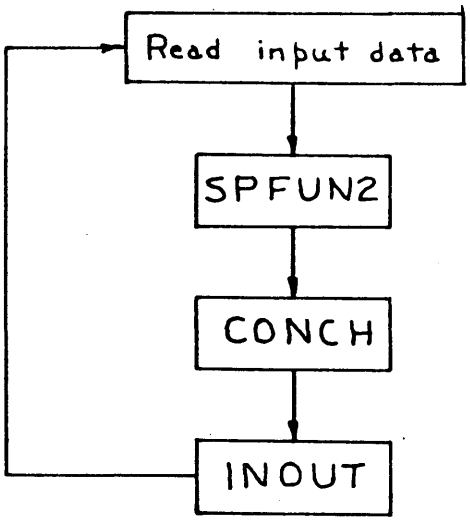

Figure C3: Logical Flow Diagram for Chain-2 MAIN Program

Subroutine SPFUN2 is called for the sole purpose of calculating the fast leakages, thermal leakages and fast nonleakage probability for each mesh point in the reactor. These items are not transferred from chain-1.

Subroutine CONCH calculates the fuel properties at each mesh point in the reactor and calls subroutine NUTBAL which calculates the detailed neutron balance.

Subroutine INOUT calculates feed input and discharge rates and other miscellaneous quantities.

b. Input data for chain-2

Figure C4 shows the input data deck for chain-2.

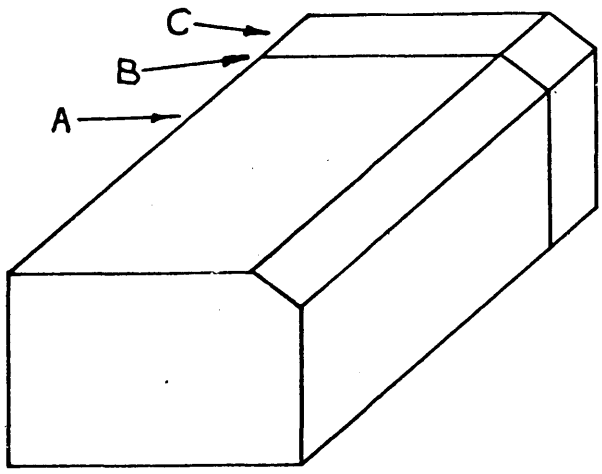

Figure C4: Input Data Deck for Chain-2

Section A: These input data are punched out at the end of chain-1 (step 40, figure C1).

Section B: This is a single card at the end of section A. It contains the following control parameters for printing:

IRESPT: Controls printout of the effective resonance integrals of the fuel nuclides along the innermost channel. 0 = no print. 1 = print.

IPRT1: Unused

IPRT5: Unused

IPRT6: Controls printout of CONCH

IPRT8: Controls printout of CONCH

Three spaces are allowed on the data card for each of these five fixed point variables.

Section C: This section contains the same resonance data as used in chain-1.

3. Availability of codes

FORTRAN decks and/or printouts of the two fuel cycle codes described in appendix C, i.e., chain-1 and chain-2, are available from the MIT Nuclear Engineering Department.

APPENDIX D

REFERENCES

A1. Argonne National Laboratory: Reactor Physics Constants, 2nd Edition ANL 5800, (July, 1963).

A2. Atomic Energy of Canada Limited: Douglas Point Nuclear Generating Station, AECL 1596, (January, 1963).

B1. Babcock, D. F. et al.: An Evaluation of Heavy Water Moderated Power Reactors. A Status Report as of March 1963, DP 830.

B2. Babcock, D. F., R. R. Hood and D. S. St. John: Thorium Fueled D_2O Moderated Power Reactors, DP 864, (December, 1963).

B3. Bechtel Corporation: Large Reactor Study for Sea Water Distillation, Appendix A, TID 19267 UNC(Revised), (July, 1963).

C1. Chernick, J. and R. Vernon: Some Refinements in the Calculation of Resonance Integrals, Nuclear Science and Engineering, 4, 649 (1958).

C2. "Civilian Nuclear Power, A Report to the President-1962", USAEC, (November, 1962).

C3. Clark, M., Jr. and K. F. Hansen: "Numerical Methods of Reactor Analysis", Academic Press, New York, London, 1964.

C4. Crowther, R. L.: Doppler Resonance Integral Coefficient of UO_2 and ThO_2, Transactions of the American Nuclear Society, 4, 18 (June, 1961).

D1. Dietrich, J. R.: Efficient Utilization of Nuclear Fuels, Power Reactor Technology, 6, 1 (Fall, 1963).

D2. Dresner, L.: "Resonance Absorption in Nuclear Reactors", Pergamon Press, New York, Oxford, London and Paris, 1963.

E1. Etherington, H., editor: "Nuclear Engineering Handbook", McGraw Hill Book Company, Inc., New York, Toronto, London, 1958.

G1. Gift, E. H.: Private communication of August 7, 1964 to E. A. Mason.

G2. Gift, E. H.: Private communication of September 14, 1964.

G3. Gift, E. H.: Private communication of January 6, 1965.

G4. Glasstone, S. and M. C. Edlund: "The Elements of Nuclear Reactor Theory", D. Van Nostrand Company, Inc., Princeton, N. J., Toronto, London, New York, 1952.

G5. Goellner, D. A.: Fuel Cycle Performance of Thorium Fueled Fast Breeder Reactors, Nuclear Engineer's Thesis, Department of Nuclear Engineering, MIT, September, 1964.

G6. Goldsmith, A., T. E. Waterman, and H. J. Hirschhorn: "Handbook of Thermophysical Properties of Solid Materials, Revised Edition, Volume III, Ceramics", Macmillan Company, New York, 1961.

G7. Goldstein, R. and E. R. Cohen: Theory of Resonance Absorption of Neutrons, Nuclear Science and Engineering, 13, 132 (1962).

G8. Goldstein, R. and H. Brooks: Intermediate Resonance Absorption in Nonhomogeneous Systems, Nuclear Science and Engineering, 20, 331 (1964).

H1. Hildebrand, F. B.: "Introduction to Numerical Analysis", McGraw-Hill Book Co., Inc., New York, Toronto, London 1956.

H2. Hofmann, F., Fuel Cycle Analysis in a Thorium Fueled Reactor Using Bidirectional Fuel Movement, MIT-2073-1 (MITNE-51), (June, 1964).

H3. Honeck, H. C. and J. L. Crandall: The Physics of Heavy Water Lattices, BNL 8253, (June, 1964)

H4. Hughes, D. J. and R. B. Schwartz: Neutron Cross Sections, 2nd edition, BNL 325, (July, 1958); Supplement No. 1, (January, 1960).

K1. Kaplan, I.: Course 22.21 class notes, MIT, 1960.

K2. Kelber, C. N.: Equivalence Factors for D_2O, Nuclear Science and Engineering, 3, 633 (1958).

L1. Leslie, D. C., J. G. Hill and A. Jonsson: Improvements to the Theory of Resonance Escape in Heterogeneous Fuel-I, Nuclear Science and Engineering, 22, 78 (May, 1965).

L2. Leslie, D. C. and A. Jonsson: Improvements to the Theory of Resonance Escape in Heterogeneous Fuel-II, Nuclear Science and Engineering, 23, 82 (September, 1965).

M1. Mason, E. A. and J. A. Larrimore: Effect of Specific Power on Fuel Reactivity and Costs in Thorium Fueled Reactors, Nuclear Science and Engineering, 9, 332 (March, 1961).

M2. Massachusetts Institute of Technology, Nuclear Engineering Department memo NT-282b (October, 1960).

M3. McLeod, N. B., M. Benedict et al.: The Effect of Fuel and Poison Management on Nuclear Power Systems, June 1959-September 1961, NYO 9715.

M4. Meghreblian, R. V. and D. K. Holmes: "Reactor Analysis," McGraw-Hill Book Company, New York, 1960.

N1. Neill, J. M.: Reactivity Lifetime and Cost Characteristics of a Thorium-Fueled Reactor, Master of Science Thesis, Department of Nuclear Engineering, MIT, February, 1961.

N2. Nordheim, L.W.: A Program of Research and Calculations of Resonance Absorptions, GA 2527.

R1. Rosenthal, M. W. et al.: A Comparative Evaluation of Advanced Converters, ORNL 3686, (January, 1965). Neutron balance for case G4 given in letter from A. M. Perry to M. Benedict, Dec. 23, 1966.

S1. Shanstrom, R. T., M. Benedict and C. T. McDaniel: Fuel Cycles in Nuclear Reactors, NYO 2131, (August, 1959).

S2. Sharma, S. G.: Plutonium Fueled Thermal Reactors with High Conversion Ratios, BNL 7355, (March, 1963).

S3. Stephen, J. D.: Fuel Cycle Analysis in a Thorium Fueled Reactor Using Bidirectional Fuel Movement, MIT-2073-4 (MITNE-61), (June, 1965).

T1. Trapp, D. L.: The Effects of Changing Economic Conditions on Energy Costs in Stainless-Steel Clad Pressurized Water Reactors, Master of Science Thesis, Department of Nuclear Engineering, MIT, September, 1962.

W1. Walker, W. H.: The Effect of New Data on Reactor Poisoning by Nonsaturating Fission Products, AECL 2111, (November, 1964).

W2. Walker, W. H.: Private communication of August 19, 1965.

W3. Weitman, J.: The Effective Resonance Integral of ThO_2 Rods, Nuclear Science and Engineering, 18, 246 (1964).

W4. Wigner, E. P.: Metallurgical Project Report C-4, January, 1942.

W5. Wigner, E. P. et al.: Resonance Absorption of Neutrons by Spheres, Journal of Applied Physics, 26, 260 (1955).

W6. Westcott, C. H.: Effective Cross Section Values of Well-moderated Thermal Reactor Spectra, AECL 1101, (November, 1960).

APPENDIX E

NOMENCLATURE FOR CHAPTER IV

This appendix summarizes the nomenclature for chapter IV, giving the first text reference for each symbol used. Only a few symbols are used in the other chapters, and they are defined where they are used.

Text symbol	Definition	Text reference
A(x)	Hardening parameter for Wilkins spectrum	(4C20)
B	Fraction of core discharge lost in reprocessing	(4E1)
b	Arbitrarily defined term in equivalence theorem	(4C30)
C	Normalization constant in SPACFX	(4E2)
$C_{7,i}$	Geometric term in difference approximation	(4B8)
$C_{8,j}$	"	(4B8)
$C152_i$	"	(4B3)
$C153_i$	"	(4B4)
$C15_j$	"	(4B5)
$C154_j$	"	(4B6)
$C151_{i,j}$	"	(4B7)
D	Thermal diffusion coefficient averaged over the unit cell	(4A2)
D_1	Fast diffusion coefficient averaged over the unit cell	(4A1)
$(D_1)_{cell}$	Same as D_1	(4C44)
$(D_1)_{D_2O}$	Fast diffusion coefficient for D_2O	(4C44)
D_{rod}	Fuel rod diameter	(4C35)
E	Neutron energy between 0 and 0.414	(4C20)
(E-1)	A measure of the extra absorptions in the moderator of the unit cell due to the rise of the moderator thermal flux above the thermal flux at the rod surface	(4C4)

Text symbol	Definition	Text reference
F	Thermal flux at rod surface/average thermal flux in rod	(4C2)
-	Extrapolated Liebmann parameter	(4D2)
f	Thermal utilization	(4C2)
f_i	Fraction of resonance absorption which occurs in nuclide i above 5 ev.	(4C41)
G_f	Grams of fissile material associated with each mesh point	(4E9)
g_i	Radial mesh spacing	Fig. 4.2
h_j	Axial mesh spacing	Fig. 4.2
I_{zr}^{∞}	Infinitely dilute resonance integral of zirconium	(4C15)
I_u	Effective resonance integral of a single resonance located at lethargy u in a given dilute absorber	(4C28)
I_{eff}^{i}	Effective resonance integral over the entire resonance region for nuclide i	(4C23)
I_{ThO_2}	Effective resonance integral of ThO_2	(4C36)
$(I/I_o)_{ThO_2}$	Effective resonance integral of ThO_2 at temperature T/effective resonance integral of ThO_2 at temperature T_o(20°C).	(4C38)
I_i^{∞}	Infinitely dilute resonance intergral of nuclide i	(4C41)
I_R	Fissile atoms entering the reactor	(4E1)
IRC	Outermost radial mesh point in core	Fig. 4.2
IRB	Outermost radial mesh point on blanket	Fig. 4.2
IRR	Outermost radial mesh point in reflector	Fig. 4.2
i	Usually the radial mesh point index	Fig. 4.2
JZC	Outermost axial mesh point in core	Fig. 4.2
JZB	Outermost axial mesh point in blanket	Fig. 4.2
JZR	Outermost axial mesh point in reflector	Fig. 4.2

Text symbol	Definition	Text reference
j	Usually the axial mesh point index	Fig. 4.2
K	Index of the axial mesh point of interest in calculating $\hat{\Sigma}_{FP}$.	(4D1)
kT_{mod}	Neutron temperature at moderator temperature T_{mod}	(4C20)
$\bar{l}$	Average chord length in lump	Section IVC 2a(I)(A)
M	Number of mesh points in 1/4 of the reactor	(4E2)
N	Concentration in the fuel of the absorber on interest	Section IVC 2a(I)(A)
-	Summation index used in calculating $\hat{\Sigma}_{FP}$.	(4D1)
N_{D_2O}	Concentration of D_2O	(4C1)
N_{FP}	Concentration of nonsaturating fission products in the fuel	(4C17)
N_i	Concentration of nuclide i in fuel. Includes all fuel nuclides.	(4C21)
-	Concentration of nuclide i in fuel. Includes only the seven resonance absorbers	(4C23)
-	Concentration of nuclide i in fuel. Includes all of the fuel nuclides	Section IVC4
N_{ThO_2}	Concentration of ThO_2 in pure ThO_2.	(4C1)
N_{zr}	Concentration of zircaloy	(4C1)
O_R	Fissile atoms leaving the reactor	(4E1)
P	Escape probability from a spatially uniform source in a lump	(4C24)
P_1	Fast nonleakage probability	Fig. 4.1
p	Total resonance escape probability. Equals p_{TOT} below.	(4A2)
p_i	Resonance escape probability for individual nuclides in various resonance regions. Nomenclature for i figure 4.1.	Fig. 4.1

Text symbol	Definition	Text reference
p_i	Resonance escape probability for nuclide i. Used only for defining resonance escape probability	(4C23)
p_{17}	$p_1p_2p_3p_4p_5$	Fig. 4.1
p_{174}	$p_{17}p_6p_7$	Fig. 4.1
p_{TOT}	$p_{174}p_8p_9p_{10}p_{11}$	Fig. 4.1
$\langle 1-p \rangle_i$	Resonance absorption probability for individual nuclides in various energy regions. Nomenclature for i in figure 4.1. See also figure 4.10	Fig. 4.1
$\langle 1-p \rangle_{zr}$	Resonance absorption probability for zircaloy	(4C15)
$\left(\frac{1-p}{1+\alpha}\right)$	Resonance fission probability	(4E7)
Q	Generalized fast or thermal neutron source	(4B1)
Q_R	Source of fissile atoms in the reactor	(4E1)
q	Source of fast neutrons averaged over the unit cell	(4A1)
R_i	Radius of interest	Fig. 4.2
r	Westcott r factor	(4C19)
r_o	Radius of cylindrical fuel rod	Fig. 4.3
r_z	Outer radius of zircaloy cladding	Fig. 4.3
r_1	Outer radius of unit cell	Fig. 4.3
S	Coefficient of the generalized fast or thermal neutron sink	(4B1)
S_R	Sink of fissile atoms in the reactor	(4E1)
SPPTMX	Average specific power in the core	(4E9)
(S/M_{ThO_2})	Surface area/mass of ThO_2 for calculating I_{ThO_2}	(4C36)
T	Moderator and neutron temperature	(4C19)
T_o	293°K	(4C19)

Text symbol	Definition	Text reference
(T/T_o)	Actual fuel temperature/fuel temperature for which I_{ThO_2} was calculated (20°C)	(4C38)
t	Time	Section IVC4
u	Lethargy	Section IVC 2a(I)(A)
V	Volume of fuel lump	(4C24)
V_o	Volume of fuel lump	Fig. 4.3
V_z	Volume of zircaloy	Fig. 4.3
V_l	Volume of moderator	Fig. 4.3
$\bar{v}_o$	Volume fraction of fuel lump	(4C1)
$\bar{v}_z$	Volume fraction of zircaloy	(4C1)
$\bar{v}_l$	Volume fraction of moderator	(4C1)
V_{fl}	Volume fraction of fuel	(4C47)
x	$\sqrt{\frac{E}{KT_{mod}}}$ = normalized velocity at energy E	(4C20)
Y	$\frac{d\Phi}{dx}$ = flux per unit velocity	(4C20)
y_{S2}	Yield of "Sm" group from U233 fission	(4C56)
y_{S3}	Yield of "Sm" group from U235 fission	(4C56)
y_{X2}	Yield of Xe135 from U233 fission	(4C57)
y_{X3}	Yield of Xe135 from U235 fission	(4C57)
α_j	Capture/fission for U233 and U235 above and below 5 ev. See figure 4.10	(4C50), (4C52)
$\alpha_{lower,i}$	Capture/fission for U233 or U235 below 5 ev.	(4C40)
$\alpha_{upper,i}$	Capture/fission for U233 or U235 above 5 ev.	(4C39)
Γ	Total resonance width at half maximum	(4C34)

Text symbol	Definition	Text reference
ΔN_{FP}	Nonsaturating fission products produced during time interval Δt_N	(4D1)
Δu	Finite lethargy interval	(4C32b)
ΔV	Volume element associated with each mesh point	(4E9)
2Δ	Practical width of resonance	(4C34)
δH	Axial extrapolation length	Fig. 4.2
δR	Radial extrapolation length	Fig. 4.2
ϵ	Fast fission factor for Th232	Fig. 4.1
$-$	Convergence criterion for flux shapes	(4E6)
η	Number of fast neutrons produced by fission per absorption in a fissile nucleus. A general definition.	
$\bar{\eta}$	Number of fast neutrons produced by fission per absorption (resonance plus thermal) in a fissile nucleus (U233 plus U235).	(4E2a)
$\bar{\bar{\eta}}_j$	Average number of fast neutrons produced by fission per resonance absorption in U233 or U235 above or below 5 ev. See figure 4.10.	Fig. 4.1
η_o	Number of fast neutrons produced by fission per fast absorption in Th232	Fig. 4.1
$\langle\bar{\bar{\eta}}(1-p)\rangle$	See equation (4A3) and figure 4.1	(4A3)
θ	Actual thermal flux time	(4C17)
θ_o	2200 m/s thermal flux time	(4C18)
κ_o	Inverse thermal diffusion length in fuel	(4C11)
κ_1	Inverse thermal diffusion length in moderator	(4C12)
λ_{Pa}	Decay constant of Pa233	(4C48)
λ_{Xe}	Decay constant of Xe135	(4C57)
$\lambda_{tr,1}$	Transport mean free path for fast neutrons	(4C44)

Text symbol	Definition	Text reference
ν	Average number of fission neutrons produced per thermal fission	(4A3)
-	Flux shape iteration loop number	(4E5)
ν_i	Number of fission neutrons produced per resonance fission by neutrons of various resonance energies.	(4C42)
$\nu\Sigma_f$	See equation (4A3) and figure 4.1	(4A3)
ν_3	Fission neutrons produced per thermal fission of U233	Fig. 4.1
ν_5	Fission neutrons produced per thermal fission of U235	Fig. 4.1
ξ	Lethargy gain per collision	(4C16)
$\xi\Sigma_s$	Slowing down power of unit cell	(4C20)
$\xi\Sigma_{s,nonfuel}$	Slowing down power of nonfuel region of unit cell	(4C15)
	Macroscopic cross section	
Σ_a	Thermal absorption homogenized, everything in unit cell, averaged over Wilkins spectrum	(4A2)
—	Resonance absorption, function of u, absorber of interest	(4C25)
Σ_a^H	Resonance absorption, function of u, heavy absorbers in lump other than absorber of interest	(4C25)
$\bar{\bar{\Sigma}}_{a,D_2O}$	Thermal absorption, D_2O, spectrum hardened	(4C13)
$\Sigma_{a,Zr}$	2200 m/s absorption, zircaloy	(4C2)
$\bar{\bar{\Sigma}}_{a,Zr}$	Thermal absorption, zircaloy, spectrum hardened	(4C13)
Σ_{a0}	2200 m/s absorption, fuel region	(4C2)
Σ_{a1}	2200 m/s absorption, moderator region	(4C2)
Σ_f	Thermal fission homogenized, averaged over Wilkins spectrum	(4E7)

Text symbol	Definition	Text reference
Σ_f^{TOT}	Resonance plus thermal fission homogenized, thermal portion averaged over Wilkins spectrum	(4E7)
$\Sigma_{f,3}$	Thermal fission homogenized, U233, averaged over Wilkins spectrum	Fig. 4.1
$\Sigma_{f,5}$	Thermal fission homogenized, U235, averaged over Wilkins spectrum	Fig. 4.1
$\hat{\Sigma}_{FP}$	Westcott effective 2200 m/s absorption, non-saturating fission products	(4C17)
$\bar{\Sigma}_{FP}$	Westcott hardened, nonsaturating fission products	(4C19)
Σ_m	Potential scattering, lump diluent	Section IVC 2a(I)(A)
Σ_{s,O_2}	Scattering, O_2 in fuel lump	(4C35)
Σ_{tr}	Thermal transport, unit cell	(4C1)
$\Sigma_{tr,1}$	Fast transport	(4C44)
Σ_1	Fast removal, unit cell	(4A1)
	Microscopic cross section	
σ_a	Resonance absorption, function of u, absorber of interest	(4C29)
$\bar{\sigma}_a$	General thermal absorption, averaged over Wilkins spectrum	Section IVC
-	Thermal absorption, averaged over Wilkins spectrum. See section IVC4 for subscripts	Section IVC4
σ_a^M	Resonance absorption, function of u, macroscopic of heavy absorbers in lump other than absorber of interest per atom of absorber of interest	(4C29)
$\sigma_{a,i}$	Resonance absorption, function of u, six dilute fuel nuclides	(4C39)
$\sigma_{ai}(x)$	Thermal absorption, function of x, all nuclides in the unit cell	(4C21)

Text symbol	Microscopic cross section	Text reference
$\bar{\sigma}_{a,Th}$	Thermal absorption, Th232, averaged over Wilkins spectrum	(4C13)
$\sigma_{a,2200}$	2200 m/s absorption	(4C13)
$\bar{\sigma}_f$	General thermal fission, averaged over Wilkins spectrum	Section IVC
–	Thermal fission, averaged over Wilkins spectrum. See section IVC4 for subscripts	Section IVC4
$\sigma_{f,i}$	Resonance absorption, function of u, U233 and U235	(4C39)
$\hat{\sigma}_{FP}$	Westcott effective 2200 m/s absorption, non-saturating fission products	(4C17)
$\bar{\sigma}_i$	Thermal absorption and fission, averaged over Wilkins spectrum, all fuel nuclides except nonsaturating fission products	(4C22)
$\sigma_i(x)$	Thermal absorption and fission, function of x, all fuel nuclides except nonsaturating fission products	(4C22)
σ_M	Potential scattering, homogeneous mixture, macroscopic of moderator per atom of absorber of interest.	Section IVC 2a(I)(A)
σ_m	Potential scattering, heterogeneous, macroscopic of lump diluent of low atomic weight per atom of absorber of interest	Section IVC 2a(I)(A)
σ_p	Potential scattering, resonance absorber	(4C34)
$\sigma_{s,epi}$	Epithermal scattering	(4C16)
σ_{tr}	Thermal transport	(4C1)
σ_o	Resonance peak	(4C34)
	Definition	
τ_{cell}	Fermi age averaged over the unit cell	(4C45)
τ_{D_2O}	Fermi age of D_2O	(4C46)
ϕ	Thermal flux averaged over the unit cell	(4A2)
–	Average thermal flux in fuel	Section IVC4

Text symbol	Definition	Text reference
Φ_1	Fast flux averaged over the unit cell	(4A1)
$\bar{\Phi}_0$	Average thermal flux in fuel. Used in derivation of thermal disadvantage factors	Fig. 4.3
Φ_Z	Thermal flux at surface of rod. Used in derivation of thermal disadvantage factors	Fig. 4.3
$\bar{\Phi}_1$	Average thermal flux in moderator. Used in derivation of thermal disadvantage factors	Fig. 4.3
$\bar{\Phi}_{cell}$	Average thermal flux in unit cell. Used in derivation of thermal disadvantage factors	(4C6)
$\Phi(u)$	Resonance flux per unit lethargy	Section IVC 2a(I)(A)
Ψ_0	Thermal disadvantage factor in fuel	(4C1a)
Ψ_1	Thermal disadvantage factor in moderator	(4C1a)
Ψ_Z	Thermal disadvantage factor in zircaloy	(4C1a)